



Instituto de Investigación y Formación Agraria y
Pesquera
CONSEJERÍA DE AGRICULTURA, PESCA Y DESARROLLO
RURAL



University of Córdoba
*Andalusian Institute for Agricultural and Fisheries
Research and Training (IFAPA)*
Department of Natural Resources
PhD Dissertation

Water monitoring in vegetation covers through multi-
scale energy balance modelling using time series of
remotely sensed data.

PhD Student: Ana Andreu Méndez
Supervisor: María P. González-Dugo
Supervisor: María J. Polo Gómez

Córdoba, November 2014



TITULO: *Evolución del estado hídrico de la vegetación mediante un modelo multiescala de balance de energía usando series temporales de imágenes por satélite.*

AUTOR: *Ana Andreu Mendez*

© Edita: Servicio de Publicaciones de la Universidad de Córdoba. 2014
Campus de Rabanales
Ctra. Nacional IV, Km. 396 A
14071 Córdoba

www.uco.es/publicaciones
publicaciones@uco.es



TÍTULO DE LA TESIS: Water monitoring in vegetation covers through multi-scale energy balance modelling using time series of remotely sensed data

DOCTORANDO/A: Ana Andreu Méndez

INFORME RAZONADO DEL/DE LOS DIRECTOR/ES DE LA TESIS

(se hará mención a la evolución y desarrollo de la tesis, así como a trabajos y publicaciones derivados de la misma).

María Patrocinio González Dugo, investigadora del IFAPA y María José Polo Gómez, profesora del Departamento de Agronomía de la Universidad de Córdoba, como directoras de la tesis doctoral de la alumna del Programa de Doctorado “*Dinámica de Flujos Biogeoquímicos y su Aplicación*” Ana Andreu Méndez,

INFORMAN,

Que la doctoranda ha cubierto los objetivos propuestos en la tesis, y ha abordado la integración de sensores remotos en el modelado del balance de energía a distintas escalas para el seguimiento del uso del agua en cubiertas mediterráneas; para ello, ha combinado distintas metodologías que le han permitido desarrollar y aplicar a escala puntual, de parcela y regional, un modelo de estimación de la evapotranspiración, profundizando en la separación de la transpiración de la planta y la evaporación desde el suelo. Los resultados permiten concluir con suficiente significación cuales son los factores que en mayor medida condicionan el intercambio de energía entre la cubierta y la atmósfera en estos ecosistemas adaptados, mediante distintas estrategias, a la escasez de agua, así como los aspectos operativos a tener en cuenta en el desarrollo de una herramienta multiescala de seguimiento el uso del agua y del estado hídrico de la vegetación. Se ha realizado la difusión de estos resultados en 3 comunicaciones a congresos nacionales y 5 internacionales. Se ha publicado un artículo en la revista *Acta Geophysica* y otro se encuentra en revisión en la misma publicación. Dos artículos se encuentran en elaboración en estos momentos.

Por todo ello, se autoriza la presentación de la tesis doctoral

Córdoba, 12 de noviembre de 2014

Firma del/de los director/es

Fdo.: M^o Pat. González Dugo

Fdo.: M^o Jose Polo Gómez

Acknowledgments

Al Instituto de Formación Agraria y Pesquera de Andalucía (IFAPA), por la oportunidad que me ha brindado mediante la financiación de este trabajo, apoyado al 80% por el Programa Operativo del Fondo Social Europeo 2007-2013, en el ámbito de actuación prioritario del Eje 3 (Aumento y mejora del capital humano).

A mis directoras de tesis, M^º Pat González Dugo, por guiarme, acompañarme y enseñarme, por mostrarme un camino que me gusta y con el que disfruto, y a M^º José Polo Gómez, por sus revisiones críticas, por su apoyo y su animo en todas las etapas de este trabajo, especialmente en la recta final.

A Jesús Ayuso, a los propietarios de la finca, a Pablo y a Antonio...por darnos la oportunidad de tener una zona de experimentación tan preciosa como es Santa Clotilde. Gracias por echarnos una y varias manos cada vez que han sido necesarias. A Arnaud Carrara y al equipo de la torre de Las Majadas del Tiétar, gracias por los datos y sobretodo, por la ayuda. A toda la gente que me ha aportado sus consejos, que ha respondido a mis constantes dudas, que me ha permitido saber cada día un poquito más y desenvolverme mejor – como Luca, Isidro y José. I would like to say thank you especially to Bill Kustas. It's been a pleasure to share this process with you. Thanks for your feedbacks, that have always opened new ways for me. Gracias Wim!! Gracias for being a colleague and most important, a friend. It was very nice to work with you, hand to hand, sharing the good moments and also the stressful ones...and of course the beers. I also would like to thank Alex Graf, who was with me in the first steps of our eddy tower installation, and without which the setting up would not be the same.

A mis compañeros/as de trabajo (y este término es muy amplio), y en especial a las personas que han tenido que aguantar mis cambios de humor y mis ladridos de los últimos días. Me ha encantado compartir con vosotros mi vida, dentro y fuera del centro.

A toda mi familia Cordobesa, que con vuestro cariño habéis hecho que esta sea mi casa. Y os quiero con locura.

A mi madre, a mi padre y a mi hermana. Porque siempre os siento cerca. Porque siempre lo estáis.

Gracias a las personas que habéis hecho que llegue hasta este momento. Y gracias a las que hacéis que continúe desde aquí.

Table of contents

List of figures.....	11
List of tables.....	15
List of symbols.....	17
Acronyms.....	17
Symbols.....	18
Abstract.....	23
Chapter 1: Introduction and objectives.....	29
1.1 INTRODUCTION.....	29
1.1.1 Evapotranspiration: concept, measurement methods and estimation models.....	33
1.1.1.1 Energy-balance and micrometeorological methods.....	34
1.1.1.2 Measurement methods based on the soil-water balance.....	40
1.1.1.3 Plant physiology approaches.....	42
1.1.2 Modelling evapotranspiration by means of remote sensing.....	43
1.1.2.1 Earth Observation (EO) technology.....	44
1.1.3 Mediterranean woody ecosystems.....	49
1.2 OBJECTIVES AND DOCUMENT SCHEMA.....	52
1.3 REFERENCES.....	53
Chapter 2: Modelling surface energy fluxes over a dehesa (oak savanna) ecosystem using a thermal based two-source energy balance model (TSEB).....	65
2.1 INTRODUCTION.....	66
2.2 MATERIALS AND METHODS.....	68
2.2.1 Study areas and ground-truth measurements.....	68
2.2.1.1 Santa Clotilde.....	68
2.2.1.2 Las Majadas del Tietar.....	77
2.2.2 Description of the model and the modified wind speed profile versions.....	79
2.2.2.1 Two source energy balance model (TSEB).....	80
Radiation scheme.....	83
Soil heat flux.....	84
Sensible heat flux.....	84
Resistances and wind-speed profile scheme.....	85
Latent heat flux.....	89
Green fraction (fg).....	89
Priestly-Taylor coefficient.....	90
2.2.2.2 Wind speed profile modification and TSEB versions.....	92
2.3 RESULTS AND DISCUSSION.....	99
2.3.1 Evaluation of the energy surface fluxes measured at the ECT sites.....	99
2.3.2 Oak tree clumping factor $\Omega(0)$	107
2.3.3 Oak and understorey LAI variation over the year.....	108
2.3.4 Green fraction estimation.....	111
2.3.5 Roughness length and zero displacement plane assessment.....	113
2.3.6 Wind profile analysis.....	117
2.3.7 Priestly-Taylor coefficient analysis.....	120
P-T bulk coefficient estimation with the equilibrium ET and its relationship with vapor pressure deficit (VPD).....	123
2.3.8 Detail-scale evaluation of TSEB integrating the parameter analysis (ZOM/d0 and P-T coefficient) and the wind profile modifications (TSEB G, TSEB M, TSEB Gp, TSEB Mp, TSEB ef).....	125

2.5. SUMMARY AND CONCLUSIONS.....	128
2.6. REFERENCES.....	132
Chapter 3: Application and evaluation of TSEB over a dehesa ecosystem integrating remote sensing information from medium and low spatial resolution sensors.....	141
3.1 INTRODUCTION.....	142
3.2. MATERIALS AND METHODS.....	143
3.2.1 Remote sensing data: surface radiometric temperature and vegetation indexes.....	146
3.2.2 Derivation of the oak LAI and total ecosystem LAI from remote-sensing data.....	149
3.2.3 Footprint analysis.....	149
3.2.4 Daily evapotranspiration estimation.....	150
3.2.5 Distributed evaluation of energy fluxes over Andalusian dehesas.....	151
3.3 RESULTS AND DISCUSSION.....	153
3.3.1 Comparison between MODIS estimated and measured LAI. Derivation of the oak constant LAI.....	153
3.3.2 Distributed application using MODIS images over Las Majadas and Santa Clotilde.....	154
3.3.3 Distributed application using LANDSAT images over Santa Clotilde area.....	156
3.3.4. Temporal evaluation of daily ET.....	159
3.3.5 Evaluation of distributed energy fluxes over Andalusian dehesas.....	161
3.4. SUMMARY AND CONCLUSIONS.....	171
3.5. REFERENCES.....	173
Chapter 4: Influence of thermal component derivation for dual source energy flux estimates over a drip-irrigated vineyard using TSEB.....	177
4.1 INTRODUCTION.....	178
4.2 MATERIALS AND METHODS.....	180
4.2.1. Description of the two source energy balance model.....	180
4.2.1.1. Single-angle model.....	181
4.2.1.2. Dual-angle model.....	185
Dual-angle iteration approach.....	185
Dual-angle component approach.....	186
4.2.2. Methodology.....	186
4.2.3. Observations and data processing.....	188
4.2.3.1. REFLEX 2012 Campaign.....	188
Ground-truth data.....	188
Remote sensing data.....	191
4.2.3.2. EODIX 2011 Campaign.....	191
Ground-truth data.....	191
Remote-sensing data.....	192
4.3 RESULTS AND DISCUSSION.....	193
4.3.1 Validation of single-angle model over Barrax (REFLEX 2012 Campaign).....	193
4.3.2. Comparison between single-angle and dual-angle model (EODIX 2011 Campaign).....	196
4.3.2.1. Soil and canopy component temperatures.....	196
4.3.2.2. Single-angle (TSEB1) and dual-angle iteration approach (TSEB2I).....	197
4.3.2.3. Single-angle (TSEB1) and dual-angle component approach (TSEB2D).....	200
4.4 SUMMARY AND CONCLUSIONS.....	204
4.5 REFERENCES.....	206
Chapter 5: Conclusions and future research lines.....	211

Annexe I: Correction of Landsat images.....	215
REFERENCES of Annexe I.....	218

List of figures

Figure 1.1: Surface energy balance fluxes scheme.....	34
Figure 1.2: a) Scintillometer and b) an eddy covariance tower (ECT) system located in Las Tiasas experimental farm (Source: REFLEX training course supported by the FP7-funded EUFAR and Cost Action-funded by ES0903 EUROSPEC, Barrax, Albacete, Spain).....	35
Figure 1.3: Eddy covariance tower system scheme.....	36
Figure 1.4: Footprint contribution area scheme (Figure based on Burba et al., 2005).....	37
Figure 1.5: Distribution of tower sites in the global network of networks. (From FLUXNET, Integrating worldwide CO ₂ , water and energy flux measurements, http://fluxnet.ornl.gov)...	39
Figure 1.6: Lysimeter system located in Las Tiasas experimental farm, outside and inside equipment (Source: Instituto Técnico Agronómico Provincial, ITAP, Barrax, Albacete, Spain. During REFLEX training course).....	41
Figure 1.7: EO scheme for gathering and processing information.....	43
Figure 1.8: Atmospheric windows for the satellites (Figure adapted from Casey et al., 2012)..	44
Figure 1.9: Different satellite orbits, polar orbit with different speed than the Earth, and geostationary orbit with the same speed than the Earth.....	45
Figure 1.10: Spatial, spectral and temporal resolution (Source: Jensen, J. R. , 2000).....	47
Figure 1.11: Dehesa landscape evolution over a) 2013 and b) 2014 in Santa Clotilde.....	50
Figure 2.1: Location of site 1, Santa Clotilde study area and areas of dehesa system (in green) in Andalucía.....	67
Figure 2.2: a) Measurements of height of the herbaceous layer in the Santa Clotilde study area. b) Example of oak leaves size and c) measurements of leaf area index over the area....	68
Figure 2.3: Spectral information measurements over Santa Clotilde.....	70
Figure 2.4: ECT installed in Santa Clotilde study area. CSAT 3D, KH20 and net radiometer over the grass.....	71
Figure 2.5: Grazing exclusion areas over Santa Clotilde, a) EA1 and b) EA2.....	72
Figure 2.6: Porcine livestock in Santa Clotilde.....	73
Figure 2.7: Soil humidity probes installed in Santa Clotilde study area.....	73
Figure 2.8: Wind components fetch of Santa Clotilde study area.....	75
Figure 2.9: a) FOV of the SI111 installed over the oak and b) pyranometer installed in EA1.....	76
Figure 2.10: Location of site 2, Las Majadas study area and areas of dehesa system (in green), in Extremadura.....	77
Figure 2.11: Scheme of the TSEB series version. Variables are described in this section (Figure adapted from Norman et al., 1995).....	79
Figure 2.12: Modified Goudriaan (1977) wind speed profile for the different canopy layers....	94
Figure 2.13 compares the available energy of the ecosystem and the turbulent flux measurements for both sites.....	98
Figure 2.13: Closure balance for a) Santa Clotilde and b) Las Majadas ground-ECT measurements.....	99
Figure 2.14: a) Annual mean fluxes and b) precipitation for Santa Clotilde study area.....	99
Figure 2.15: Annual mean fluxes and precipitation for Las Majadas study area.....	100
Figure 2.16: Contributing percentage of the wind speed direction for a) Santa Clotilde and b) Las Majadas.....	101

Figure 2.17: Maximum contribution to the energy fluxes measured in the ECT (Schuepp et al., 1990) for a) Santa Clotilde and b) Las Majadas.....	101
Figure 2.18: Example of the remote information spatial resolution.....	102
Figure 2.19: Typical measured daily fluxes for Santa Clotilde for a) spring, b) summer, c) autumn and d) winter.....	103
Figure 2.20: a) Incoming solar radiation and b) maximum, average and minimum air temperatures for Santa Clotilde and Las Majadas sites.....	105
Figure 2.21: a) Canopy measured temperature vs. air temperature over Santa Clotilde.....	106
Figure 2.22: Local LAI measured in the field for Santa Clotilde and Las Majadas.....	107
Figure 2.23: a) Oak and b) herbaceous layer spectral information measured in the field. The blue band is marked with blue, the red band in orange and NIR band in red.....	108
Figure 2.24: Spectrum information for oak leaves measured in the laboratory. The blue band is marked in blue, the RED band in orange and the NIR band in red.....	109
Figure 2.25: Monthly fg parameter estimated from MODIS satellite for a) year 2013 and b) 2014 over Santa Clotilde.....	112
Figure 2.26: RA, RS and RX monthly values with ZOM values ranging from 0.1 to 1.....	114
Figure 2.27: a) Sensible and b) latent heat flux RMSD [Wm^{-2}] at Las Majadas, obtained for a range of roughness lengths during the year.....	115
Figure 2.28: a) Wind speed estimated and measured at 9 meters on Las Majadas site and b) in relation to the fetch.....	117
Figure 2.29: a) Wind speed estimated and measured at 5 m over Las Majadas. b) Wind speed estimates following Goudriaan related to the different seasons.....	117
Figure 2.30: Wind speed estimated and measured at 5 meters over Las Majadas using the modified wind profile.....	118
Figure 2.31: Latent heat flux RMSD [Wm^{-2}] modifying the Priestley-Taylor coefficient from 0.5 to 1.5 with a) constant fg and b) variable fg, for Las Majadas.....	120
Figure 2.32: Average RMSD [Wm^{-2}] for LE and H, modifying the Priestley-Taylor coefficient from 0.5 to 1.5 with a) constant fg and b) variable one, at Las Majadas.....	121
Figure 2.33: Leeq and LE [Wm^{-2}] measured over Las Majadas for 2007-2011 period.....	122
Figure 2.34: α_{PT} bulk estimations vs. VPD over Las Majadas for 2007-2011 period.....	123
Figure 2.35. Estimated values for LE, H, G and Rn for TSEB and the different version using TRAD derived from the ECTs vs. the observed values measured in the ECTs.....	126
Figure 3.1: Dehesa-type ecosystem located over Andalusia (in green) and Natural Parks of the region (marked in grey).....	143
Figure 3.2: Comparison between NDVI derived from reflectance MODIS product and NDVI from MOD13Q1 product.....	146
Figure 3.3: Location of the regional meteorological stations selected.....	149
Figure 3.4: Location of selected meteorological stations form RIA network (Source: IFAPA, Consejería de Agricultura, Pesca y Desarrollo Rural).....	151
Figure 3.5: Comparison between effective LAI observed in the field (following the ecosystem structure with a constant f_c for trees and grasses) and MODIS-estimated LAI.....	152
Figure 3.6: TSEB-MODIS estimated values and ECT observed values of energy fluxes over Las Majadas site during 2008 and 2011.....	154
Figure 3.7: TSEB-MODIS estimated values and ECT observed values of energy fluxes over Santa Clotilde site during 2012- 2014.....	154

Figure 3.8: TSEB-Landsat estimated values and ECT observed values of energy fluxes over Santa Clotilde site during 2012- 2013.....	155
Figure 3.9: TSEB-Landsat energy fluxes distributed estimations for Santa Clotilde experimental site.....	156
Figure 3.10: TSEB-MODIS daily estimated ET and daily measured ET (ECTs) and ETO for Las Majadas (2008 and 2011).....	158
Figure 3.11: TSEB-MODIS daily estimated ET and daily measured ET (ECTs) and ETO for Santa Clotilde (2012-2014).....	158
Figure 3.12: Example of the meteorological maps used as an input for TSEB-MODIS dehesa application.....	159
Figure 3.13: MODIS-estimated fractional cover for Andalusian dehesa for the a) wet and b) dry seasons.....	160
Figure 3.14: Annual mean values for temperature and precipitation for a) the entire Andalusian region and b) the zones 2 & 3.....	161
Figure 3.15: Stability classes (A-very unstable, B-unstable, C-near-neutral, D-stable, E-very stable) derived from air-surface temperatures gradient, wind speed and solar incoming radiation for a) wet and b) dry season.....	162
Figure 3.16: TSEB-MODIS estimated LE distributed over Andalusian dehesa for 2014. Other landuses different of dehesa were masked (white area).....	164
Figure 3.17: TSEB-MODIS estimated H distributed over Andalusian dehesa for 2014. Other landuses different of dehesa were masked (white area).....	165
Figure 3.18: TSEB-MODIS estimated G distributed over Andalusian dehesa for 2014. Other landuses different of dehesa were masked (white area).....	166
Figure 3.19: TSEB-MODIS estimated Rn distributed over Andalusian dehesa for 2014. Other landuses different of dehesa were masked (white area).....	167
Figure 3.20: Example of the gaps caused in the TSEB-MODIS LE estimates by the cloud coverage, for March 21st (DOY 80) and April 7th (DOY 97).....	168
Figure 4.1: Site overview with reference stations and flux tower sites. The zoom shows details of the vineyard site with a W-NW to E-SE crop row orientation, and lysimeter and flux tower positions.....	187
Figure 4.2: Observed versus estimated fluxes with the TSEB model over the Barrax site for 25th July 2012 (REFLEX campaign).....	192
Figure 4.3: Observed versus estimated component temperatures for 12th, June 2011.....	195
Figure 4.4: Turbulent fluxes from TSEB1 vs. TSEB2I, left panel for sensible heat flux, right panel for latent heat flux.....	196
Figure 4.5: Component turbulent fluxes from TSEB1 vs. TSEB2I, left panel for the canopy, right panel for soil.....	196
Figure 4.6: Left panel RS, right panel TAC.....	198
Figure 4.7: Turbulent fluxes from TSEB1 versus TSEB2D, left panel for H, right panel for LE...	199
Figure 4.8: Component turbulent fluxes from TSEB1 versus TSEB2D, left panel for canopy, right panel for soil.....	199
Figure A.1: Landsat correction process (Image based on the report “Corrección de Imágenes Landsat” from Rafael Pimentel and Javier Herrero, 2012).....	214

List of tables

Table 2.1: formulation for d_0 – ZOM and the wind-speed profile used for TSEB, TSEB G, TSEB M, TSEB Gp, TSEB Mp and TSEB eff.....	95
Table 2.2: Monthly closure balance for Santa Clotilde and Las Majadas ground ECT measurements.....	97
Table 2.3: Accumulate precipitation [mm] and ET [mm] for Las Majadas site.....	103
Table 2.4: Local LAI observed in the field and estimated with Landsat and MODIS distribution functions.....	109
Table 2.5: f_g estimated from field spectra using MODIS bands functions and f_g estimated from MODIS products.....	110
Table 2.6: MAE between measured and estimated values of wind speed at 12, 7 and 3 meters over Santa Clotilde.....	118
Table 2.7: RMSD for R_n , G, H and LE from the application of TSEB and the different versions with TRAD derived from the 4-way radiometer (ECT).....	124
Table 3.1: MODIS selected dates for Santa Clotilde and Las Majadas study sites.....	144
Table 3.2: MODIS and Landsat-7 ETM+ and -8 OLI wavelengths intervals for Blue, Red, NIR and TIR bands.....	144
Table 3.3: TSEB-MODIS RMSD of the surface energy fluxes for Las Majadas and Santa Clotilde.	152
Table 4.1. Site characteristics.....	186
Table 4.2. Difference statistics for the four observation sites.....	191
Table 4.3. Model output statistics for TSEB1 and TSEB2I: mean (\bar{x}) and standard deviation (σ).	195
Table 4.4: LE model results for TSEB1, TSEB2I and TSEB2D versus the lysimeter observation.	201

List of symbols

Acronyms

<i>AHS</i>	<i>Airborne Hyperspectral Scanner</i>
<i>ALEXI</i>	<i>Atmosphere – Land Exchange Inverse model</i>
<i>BC</i>	<i>Balance closure</i>
<i>BD</i>	<i>Bulk density</i>
<i>BREB</i>	<i>Bowen ratio energy balance</i>
<i>CW</i>	<i>Crown width</i>
<i>DBH</i>	<i>Diameter breast height</i>
<i>DEM</i>	<i>Digital Elevation Model</i>
<i>EA1</i>	<i>Grazing exclusion area 1</i>
<i>EA2</i>	<i>Grazing exclusion area 2</i>
<i>EB</i>	<i>Energy Balance</i>
<i>ECT</i>	<i>Eddy covariance tower</i>
<i>EO</i>	<i>Earth Observation</i>
<i>ET</i>	<i>Evapotranspiration</i>
<i>EVI</i>	<i>Enhanced Vegetation Index</i>
<i>FAI</i>	<i>Frontal area index</i>
<i>FBH</i>	<i>First branch height</i>
<i>FOV</i>	<i>Field of view</i>
<i>IFAPA</i>	<i>Instituto de Formación e Investigación Agraria y Pesquera de Andalucía.</i>
<i>IFOV</i>	<i>Instantaneous field of view</i>
<i>INTA</i>	<i>Instituto Nacional de Técnica Aeroespacial</i>
<i>LAI</i>	<i>Leaf area index</i>
<i>MA</i>	<i>Mean value</i>
<i>MAD</i>	<i>Mean absolute difference</i>
<i>MAE</i>	<i>Mean absolute error</i>
<i>MD</i>	<i>Mean absolute difference</i>
<i>MODIS</i>	<i>Moderate-Resolution Imaging Spectroradiometer</i>
<i>MOST</i>	<i>Monin-Obhukov similarity theory</i>
<i>NDVI</i>	<i>Normalized Difference Vegetation Index</i>
<i>PAR</i>	<i>Photosynthetically active radiation</i>
<i>PET</i>	<i>Evapotranspiration potential value</i>
<i>RMSD</i>	<i>Root mean square difference</i>

SEBAL	Surface Energy Balance Algorithm for Land
SEBS	Surface Energy Balance System
SWAT	Soil Water Assessment Tool
TSEB	Two Source Energy Balance Model
TSEB ef	TSEB with Goudriaan (1977) wind-speed profile with weighted parameters
TSEB G	TSEB with Goudriaan (1977) wind-speed profile
TSEB G	TSEB with Goudriaan (1977) wind-speed profile with separately oak-grass extinction coefficients
TSEB M	TSEB with Massman (1987) wind-speed profile
TSEB M	TSEB with Massman (1987) wind-speed profile with separately oak-grass extinction coefficients
TSEB1	TSEB using one T_{RAD} observation
TSEB2D	Dual-angle TSEB without Priestley-Taylor iteration process
TSEB2I	Dual-angle TSEB with Priestley-Taylor iteration process
VI	Vegetation indexes
VIC	Variable Infiltration Capacity
VPD	Vapor pressure deficit
WiMMed	Watershed Integrated Model in Mediterranean Environments

Symbols

A	Maximum value of the ratio G/Rn_s
a	Goudriaan (1977) extinction coefficient for the wind-speed
a''	Vertical leaf area density
a'	R_s calculation constant
$A(0)$	Amplitude of the temperature wave at the surface
a_1	Constant to define Raupach (1994) d_o and Z_{OM}
a_2	Constant to define Raupach (1994) d_o and Z_{OM}
a_3	Constant to define Raupach (1994) d_o and Z_{OM}
A_f	Frontal area
B	Soil heat flux calculation constant
b'	R_s calculation constant
b_2	Constant to define Raupach (1994) d_o and Z_{OM}
b_3	Constant to define Raupach (1994) d_o and Z_{OM}
C	Upward contribution from the water table
C	Peak in time position
c	Soil specific heat

C'	Constant to define R_x
C_1	Coefficient of the aerosol resistance term to define EVI
c_1	Constant to define Massman (1997) d_0 and Z_{OM}
c_2	Constant to define Massman (1997) d_0 and Z_{OM}
C_2	Constant to define Raupach (1994) d_0 and Z_{OM}
C_2	Coefficient of the aerosol resistance term to define EVI
c_3	Constant to define Massman (1997) d_0 and Z_{OM}
C_3	Constant to define Raupach (1994) d_0 and Z_{OM}
C_c	Lalic (2003) parameter to defined $u(z)$
C_d	Drag coefficient of the foliage elements
c_g	Parameter that relates Rn_s to G
C_p	Specific heat at constant pressure
C_s	Calorific capacity of the soil
D	Deep percolation
d_0	is the zero-displacement plane
d_2	Constant to define Raupach (1994) d_0 and Z_{OM}
d_3	Constant to define Raupach (1994) d_0 and Z_{OM}
D_{dd}	Damping depth
D_p	Plant height to the width ratio
D_{th}	Soil heat flux plate depth
E	Evaporation rate
E_{eq}	Equilibrium evaporation rate
ET_0	Reference evapotranspiration
F	Photosynthesis
f_2	Constant to define Raupach (1994) d_0 and Z_{OM}
f_c	Fractional ground cover
F_{evap}	Evaporative fraction
f_g	Green vegetation fraction
$F_{x'}$	Relative contribution per running meter along the wind direction
$F_{x'y'}$	Source strength for the footprint model
G	Soil heat flux
H	Sensible heat flux
h_c	Canopy height
H_c	Canopy sensible heat flux
H_s	Soil sensible heat flux
I	Irrigation
k	Leaf angle distribution function

k'	<i>Damping coefficient</i>
K_{cb}	<i>Crop coefficient</i>
k_L	<i>Extinction coefficient in the long-wave</i>
K_{vk}	<i>is the Von Karman constant</i>
L	<i>Vaporization latent heat of liquid water,</i>
L'	<i>Canopy background adjustment factor</i>
LE	<i>Latent heat flux</i>
LEc	<i>Canopy latent heat flux</i>
LEs	<i>Soil latent heat flux</i>
Ln	<i>Long wave radiation</i>
Lnc	<i>Soil long-wave radiation</i>
Lns	<i>Canopy long-wave radiation</i>
n	<i>Sample size.</i>
NIR	<i>Near infrared</i>
p'	<i>Empirical parameter defined to computed clumping factor at solar angle $\Omega(\varphi)$</i>
P_{mv}	<i>Momentum shelter factor</i>
P_R	<i>Precipitation</i>
q'	<i>instantaneous fluctuations of the specific air humidity</i>
R	<i>Surface runoff</i>
R_a	<i>is the aerodynamic resistance calculated from the stability-corrected temperature profile equations</i>
Rn	<i>Net radiation</i>
Rnc	<i>Net radiation reaching the canopy</i>
Rns	<i>Net radiation reaching the soil</i>
R_s	<i>is the resistance to the heat flow in the boundary layer above the soil</i>
R_S	<i>Incoming solar radiation.</i>
R_x	<i>is the resistance to heat flow of the vegetation leaf boundary layer</i>
S	<i>Energy storage within the biomass</i>
s	<i>Leaf size</i>
s'	<i>Instantaneous fluctuations of the state variable</i>
S_g	<i>Energy stored in the soil layer above the soil heat flux plates</i>
Sn	<i>Short-wave radiation</i>
SnC	<i>Canopy short-wave radiation</i>
SnS	<i>Soil short-wave radiation</i>
S_{ROW}	<i>Mean row spacing of the crops</i>
$SWIR$	<i>Medium-infrared part of the spectrum</i>
t	<i>Time interval</i>

T'	<i>instantaneous fluctuations of the air temperature</i>
T_0	<i>Aerodynamical temperature</i>
T_{AC}	<i>Air temperature in the canopy – air space</i>
T_{air}	<i>Air temperature above the canopy.</i>
T_C	<i>Canopy temperature</i>
T_i	<i>Actual temperature</i>
T_{i-1}	<i>Temperature at the previous moment</i>
TIR	<i>Thermal part of the spectrum</i>
T_{RAD}	<i>Radiometric surface temperature</i>
T_S	<i>Soil temperature</i>
t_s	<i>time in seconds relative to solar noon</i>
$u(z)$	<i>Wind speed at height z</i>
u_C	<i>Wind speed at the top of the canopy</i>
$u_{C(grass)}$	<i>Wind speed at the top of the grass</i>
$u_{C(oak)}$	<i>Wind speed at the top of the oak</i>
$u_{d_0+z_{OM}}$	<i>Wind- speed at height $d_0 + Z_{OM}$</i>
u_S	<i>Wind speed just above the soil surface</i>
u_{star}	<i>Friction velocity</i>
VIS	<i>Visible part of the spectrum</i>
w'	<i>Instantaneous fluctuations of the vertical wind speed</i>
w_V	<i>Vegetation clump width</i>
x'	<i>Wind direction</i>
X_i	<i>i_{th} observed variable</i>
Y_i	<i>i_{th} measured variable</i>
Z_d	<i>Crown bottom height</i>
Z_{OM}	<i>is the roughness length for momentum transfer</i>
Z_S	<i>Height above the soil where the effect of soil surface roughness becomes negligible</i>
Z_T	<i>Measurement heights for temperature</i>
Z_u	<i>Measurement heights for wind speed</i>
α_C	<i>Canopy albedo</i>
α_{PT}	<i>Priestley-Taylor coefficient</i>
$\alpha_{PT-BULK}$	<i>Priestley-Taylor coefficient for the bulk system</i>
α_S	<i>Soil albedo</i>
α_{star}	<i>Massman (1987) coefficient for the wind-speed</i>
$\alpha_{y'}$	<i>Cross-wind spread in the direction y'</i>
β	<i>Massman (1987) extinction coefficient for the wind-speed</i>
γ	<i>Psychrometric constant</i>

Δ	<i>Slope of the saturation vapor pressure versus temperature</i>
Δt	<i>Selected time interval</i>
ΔW	<i>Net water amount accumulated in the soil plant system during Δt</i>
ε'	<i>Atmospheric emissivity</i>
ε_c	<i>Canopy emissivity</i>
ε_s	<i>Soil emissivity</i>
$\zeta (h_c)$	<i>Generalization of $C_d LAI$</i>
λ	<i>Soil thermal conductivity</i>
ρ_a	<i>mean air density</i>
σ	<i>Stefan-Boltzmann constant</i>
ϕ	<i>Viewing angle</i>
Ψ_H	<i>Atmospheric stability function for heat transfer</i>
Ψ_M	<i>Atmospheric stability function for momentum transfer</i>
Ω	<i>Clumping factor</i>
ω	<i>Period of the soil heat flux</i>

Abstract

This work has addressed the modelling of the energy balance, integrating thermal infrared data into the Two Source Energy Balance model (TSEB, *Norman et al., 1995; Kustas and Norman, 1999*), over two extended and valuable Mediterranean ecosystems, as the *dehesa* and the vineyard. Throughout the Mediterranean region, particularly in Southern Spain, the main river basins suffer an imbalance between the supply and demand for water, largely due to the variable climatic conditions and human activities. Dealing with the water scarcity situation must rely on the ability to improve management with timely and accurate information about the water status of the ecosystems, that would improved predictions of resource availability and reduced the uncertainty in decision-making processes. The integration of remote sensing data in energy balance modelling can provide this information at different spatio-temporal scales.

In water-controlled ecosystems there are many interrelationships between climate, soil and vegetation, with evapotranspiration (ET) as a key variable connecting energy and water budgets. ET has been exhaustively studied in cropped systems and different models for estimating ET at medium-large spatial scales have been developed, based on both soil water balance and surface energy balance. Energy balance (EB) models based on thermal remote sensing data enable updated diagnoses of the actual surface water condition. In general, these models do not require precipitation or soil properties inputs and are mostly conditioned by surface radiometric temperature (T_{RAD}) observations. The methodology that best accounts for the effects of a non-homogeneous partial canopy cover is the two-source approach (*Shuttleworth and Wallace, 1985; Norman et al., 1995; Kustas and Norman, 1999*), in particular the TSEB, in which surface fluxes are divided into soil and canopy components. Previous studies (*Timmermans et al., 2007; González-Dugo et al., 2009*) demonstrated the advantages of such

models compared to single-source versions. This partition into soil/substrate and vegetation contributions to the radiative and turbulent fluxes, provides an estimation of vegetation transpiration. This is of great importance for many applications, due to the difference between the fraction of the water evaporated from the soil and the one consumed by crops/natural vegetation in the form of transpiration, directly related to CO₂ assimilation (Scott *et al.* 2006).

The TSEB model has been validated to a great extent over agricultural areas, with variable ground fractional cover and under various climate conditions (Kustas and Norman, 1997; French *et al.*, 2005; Timmermans *et al.*, 2007; González-Dugo *et al.*, 2009), but mostly over homogeneously distributed canopies. Meanwhile, studies covering woody natural vegetation and woody crops are fewer (Cammalleri *et al.*, 2010; Morillas *et al.*, 2013; Guzinski *et al.*, 2013). Mediterranean ecosystems often present heterogeneous canopy mosaics with complex structures, disperse vegetation (generally evergreen sclerophyll trees) and large areas of grasses, scrubs and soil, all of which greatly influence turbulent and radiative exchanges. Thus, the ecosystem cannot be considered as a single, spatially uniform layer for water and energy flux exchanges. Furthermore, the vegetation of these arid and semi-arid regions is adapted to the climatic variability, with control mechanisms to face long periods of water scarcity, which need to be integrated into the models. For these reasons, the application of EB models over these landscapes is still a challenge.

To evaluate the ability of the TSEB to model energy fluxes over woody ecosystems under arid/semi-arid conditions, we selected two typical Mediterranean ecosystems; a vineyard and an oak savanna, known as *dehesa* in Spain. The first one is an agriculture ecosystem of great socioeconomic importance in the Mediterranean region, while the second is an agro-forestry system that plays a fundamental role in the rural development of the Iberian peninsula (Grove and Rackham, 2003; Papanastasis, 2004). A better understanding of the hydrological, atmospheric and physiological processes that drive these ecosystem functions could help to improve its management and conservation, being the dynamics of the ET a key indicator of the health of the system (Moran *et al.*, 2004), especially in such water-scarce environments.

That context have been taken into account for the regional estimation of ET with the TSEB model, analyzing some aspects affecting the EB. In particular, over the *dehesa* we have studied the co-existence of two vegetation layers and their effect over the wind-speed profile, the structure of the vegetation and its impact on the overall balance, the tree/vegetation separate leaf area index behavior

and its variability along the year, and the oak evaporative control. Over the vineyard, where the partition between soil and canopy is especially important, we analyzed separately the TSEB component turbulent fluxes estimations.

The accuracy on the estimates of the energy fluxes for a natural woody cover such as *dehesa* by means of TSEB model, with an adjusted Priestley-Taylor coefficient reflecting the relatively conservative water-use tendencies of this undomesticated semi-arid vegetation and a roughness length formulation which takes into account the tree structure and the low fractional covers, is adequate and encourages future applications. Mapping ET on a regional scale has been possible integrating earth observation techniques and meteorological distributed information into TSEB model, better representing the ecosystem heterogeneity and local meteorological conditions. Instantaneous latent heat values and the associated daily ET values were derived using *Moderate-Resolution Imaging Spectroradiometer* (MODIS) images, with 1 km spatial resolution and daily temporal frequency (depending on the cloud coverage) for both study sites (Las Majadas and Santa Clotilde), and later compared with ground-truth measurements. The difference between estimated and observed values is consistent with typical uncertainties derived for the flux measurement system, being sufficiently accurate to be employed in a distributed way and on a more regular basis. TSEB was also evaluated using a higher spatial resolution satellite (30/120 m), Landsat-7 ETM+ and Landsat-8 OLI for the Santa Clotilde site with similar accuracy. Distributed latent heat flux over Andalusian *dehesa* was mapped as a first approach to monitor the ecosystem status on a regular basis with the objective of assessing a future extension of the study.

The partition of the turbulent fluxes into soil and canopy components, provided by TSEB, produces an estimation of the vegetation transpiration. It has been studied in this work over a vineyard system, by means of directional T_{RAD} observations at different viewing-angles that allows direct estimates of soil and canopy temperatures and therefore, of the separate component turbulent fluxes. Values obtained with dual-angle TSEB model indicated some degree of stress over the vegetation stands, which was not confirmed by the results of TSEB, where the crop was transpiring always potentially.

The results presented here have been organized in chapters following the different steps in the study, which corresponded to the different papers produced, with an introduction describing the context and the work's framework. Up to the date, the paper in chapter 4 "Andreu, A., Timmermans, W., Skokovic, D., 2014. Influence of thermal-component derivation for dual source energy flux estimates over a drip-

irrigated vineyard” has already been submitted and is now under revision in Acta Geophysica journal. The rest of Chapters are in the final editing state for their submission. Complete work have been published in SPIE Conference Proceedings following a peer review process: “Andreu, A., Kustas, W. P., Polo, M. J., Anderson, M. C., González-Dugo, M. P., 2013. Modelling surface energy fluxes over a *dehesa* ecosystem using a two-source energy balance model and medium resolution satellite data. Proc. SPIE 8887, Remote Sensing for Agriculture, Ecosystems, and Hydrology XV, 888717 (16 October 2013)”,

This work was funded by the Andalusian Institute for Agricultural and Fisheries Research and Training (IFAPA, Consejería de Agricultura, Pesca y Desarrollo Rural de la Junta de Andalucía) and the European Social Fund Operational Programme 2007-2013, in the field of priority Axis 3 (Improving human capital), in an 80%.

REFERENCES

- Cammalleri, C., Anderson, M.C., Ciruolo, G., D'Urso, G., Kustas, W.P., La Loggia, G., & Minacapilli, M. (2010). The impact of in-canopy wind profile formulations on heat flux estimation in an open orchard using the remote sensing-based two-source model. *Hydrol. Earth Syst. Sci.*, 14, 2643-2659
- French, A.N., Jacob, F., Anderson, M.C., Kustas, W.P., Timmermans, W., Gieske, A., Su, Z., Su, H., McCabe, M.F., Li, F., Prueger, J., & Brunsell, N. (2005). Surface energy fluxes with the Advanced Spaceborne Thermal Emission and Reflection radiometer (ASTER) at the Iowa 2002 SMACEX site (USA). *Remote Sensing of Environment*, 99, 55-65
- Gonzalez-Dugo, M.P., Neale, C.M.U., Mateos, L., Kustas, W.P., Prueger, J.H., Anderson, M.C., & Li, F. (2009). A comparison of operational remote sensing-based models for estimating crop evapotranspiration. *Agricultural and Forest Meteorology*, 149, 1843-1853
- Grove, A.T., & Rackham, O. (2003). *The Nature of Mediterranean Europe. An Ecological History*. New Haven: Yale University Press
- Guzinski, R., Anderson, M.C., Kustas, W.P., Nieto, H., & Sandholt, I. (2013). Using a thermal-based two source energy balance model with time-differencing to estimate surface energy fluxes with day-night MODIS observations. *Hydrol. Earth Syst. Sci.*, 17, 2809-2825
- Kustas, W.P., & Norman, J.M. (1997). A two-source approach for estimating turbulent fluxes using multiple angle thermal infrared observations. *Water Resources Research*, 33, 1495-1508
- Kustas, W.P., & Norman, J.M. (1999). Evaluation of soil and vegetation heat flux predictions using a simple two-source model with radiometric temperatures for partial canopy cover. *Agricultural and Forest Meteorology*, 94, 13-29
- Moran, M.S., Peters-Lidard, C.D., Watts, J.M., & McElroy, S. (2004). Estimating soil moisture at the watershed

scale with satellite-based radar and land surface models. *Canadian Journal of Remote Sensing*, 30, 805-826

- Morillas, L., Garcia, M., Nieto, H., Villagarcia, L., Sandholt, I., Gonzalez-Dugo, M.P., Zarco-Tejada, P.J., & Domingo, F. (2013). Using radiometric surface temperature for surface energy flux estimation in Mediterranean drylands from a two-source perspective. *Remote Sensing of Environment*, 136, 234-246
- Norman, J.M., Kustas, W.P., & Humes, K.S. (1995). A two - source approach for estimating soil and vegetation energy fluxes in observations of directional radiometric surface temperature. *Agricultural and Forest Meteorology*, 77, 263-293
- Papanastasis, V.P. (2004). *Vegetation degradation and land use changes in agrosilvopastoral systems*. Catena Verlag, Reiskirchen, Germany: Advances in GeoEcology
- Scott, R.L., Huxman, T.E., Cable, W.L., & Emmerich, W.E. (2006). Partitioning of evapotranspiration and its relation to carbon dioxide exchange in a Chihuahuan Desert shrubland. *Hydrological Processes*, 20, 3227-3243
- Shuttleworth, W., & Wallace, J. (1985). Evaporation from sparse crops: an energy combination theory. *Q. J. R. Meteorol. Soc.*, 111, 1143-1162
- Timmermans, W.J., Kustas, W.P., Anderson, M.C., & French, A.N. (2007). An intercomparison of the Surface Energy Balance Algorithm for Land (SEBAL) and the Two-Source Energy Balance (TSEB) modelling schemes. *Remote Sensing of Environment*, 108, 369-384

Chapter 1: Introduction and objectives

1.1 INTRODUCTION

Throughout the Mediterranean region, particularly in Southern Spain, the main river basins suffer an imbalance between the supply and demand for water, largely due to climatic conditions and human activities that over-exploit water resources. Due to the difficulty of increasing water storage, dealing with water scarcity must rely on the ability to improve management. The existence of timely and accurate information about water use and the water status of the ecosystem would enable more precise water accounting, improving predictions of resource availability and reducing the uncertainty in decision-making processes.

In water-controlled ecosystems there are many interrelationships between climate, soil and vegetation, with evapotranspiration (ET) as a key variable connecting energy and water budgets. ET is used to predict water demands and to monitor drought and climate change (*Bastiaanssen et al., 2002; Chandrapala and Wimalasuriya, 2003; Anderson et al., 2007*), for estimating water consumption over irrigated areas and for planning irrigation schedules (*Garatuza-Payan and Watts, 2005; Rossi et al., 2010; Gonzalez-Dugo et al., 2013*), for analyzing irrigation and productivity performance indicators (*Bastiaanssen et al., 1999; Akbari et al., 2007; Gonzalez-Dugo and Mateos, 2008*), and for determining moisture stress, often quantified as the deviance of actual ET from its potential value (PET; *Jackson et al., 1981*). The integration of spatially distributed remotely sensed data in models for estimating and mapping ET allows studies to expand in scale from detail to regional and continental areas, generally more useful for management purposes, as they provide a better representation of vegetation

heterogeneity and account to some degree for local meteorological conditions.

ET has been exhaustively studied in cropped systems; for management purposes, estimating ET losses for a given crop at different time scales is a need for the selection of irrigation systems, irrigation schedules, the monitoring of crop water stress, etc. Different models for estimating ET at medium-large spatial scales have been developed, based on both soil water balance and surface energy balance. The first approach includes models such as VIC (Variable Infiltration Capacity; *Wood et al., 1992; Liang et al., 1996*), or ET formulations being incorporated in the hydrological calculations (as a fraction of PET regulated from some control state variables) that perform on a semi-distributed or distributed way, such as SWAT (Soil Water Assessment Tool; *Arnold et al., 1998*) or WiMMed (Watershed Integrated Model in Mediterranean Environments, *Egüen et al., 2009; Polo et al., 2009; Herrero et al., 2010*), respectively, among a wide group of models. They require spatially distributed inputs, such as maps of land use, vegetation/crops and soil characteristics (e.g. texture, soil depth, hydraulic conductivity); topographic information (e.g. Digital Elevation Model, DEM) and superficial network indicators of the river basin; precipitation and irrigation information; and meteorological variables. These ET models are regulated by the soil water content, which is dependent on the precipitation input data and on hydraulic soil properties, which are difficult to determine on a regional or continental scale (*Beljaars et al., 1996*). They usually produce continuous estimates that allow for water use monitoring on different time-scales. However, cumulative errors may develop in the absence of regular corrections being implemented (*Betts et al., 1997*).

A second approach can be found in energy balance (EB) models based on thermal remote sensing data that enable updated diagnoses of the actual surface water condition to be provided. In general, these models do not require precipitation or soil properties inputs and are mostly conditioned by surface radiometric temperature (T_{RAD}) observations. Other information required is a characterization of the canopy coverage, along with common meteorological data such as air temperature, humidity and wind speed. Some examples of these models in current use are: Surface Energy Balance Algorithm for Land (SEBAL; *Bastiaanssen et al., 1998*), Surface Energy Balance System (SEBS; *Su, 1999*), the triangulation method for temperature/NDVI (Normalized Difference Vegetation Index; *Gillies et al., 1997*), the Two-Source Energy Balance model (*Norman et al., 1995; Kustas and Norman, 1999*), and the ALEXI model (Atmosphere – Land Exchange Inverse model; *Anderson et al., 1997*). One of the main disadvantages of these approaches is, besides the complexity of the formulation, the potential input gaps caused by the availability of thermal data at a given spatial scale and the cloud coverage, which may distort the final

images.

In these models, the energy balance is applied over the surface by using T_{RAD} derived from thermal data (8–14 μm) to calculate the sensible heat flux, and then obtaining the latent heat flux as the residual of the balance (e.g., Moran et al., 1994; Kustas and Norman, 1996; Gillies et al., 1997; Bastiaanssen et al., 1998). This approach has to take into account the difference between T_{RAD} and the aerodynamic temperature (T_0), required to compute sensible heat, particularly for surfaces partly covered with vegetation (Kustas and Daughtry, 1990). Several schemes of various levels of complexity and input requirements have been set up to solve this problem. Some of these employ empirical or semiempirical relationships to adjust T_{RAD} to T_0 (e.g., Kustas et al., 1989; Lhomme et al., 1994; Chehbouni et al., 1996; Mahrt and Vickers, 2004). When calibration is performed using field data, these methods provide accurate results (Chavez et al., 2005). Another option to avoid the determination of T_0 involves applying an internal calibration to the surface temperature (Bastiaanssen et al., 1998). This procedure also reduces the need for atmospheric correction of T_{RAD} , which is a cumbersome process that may introduce additional errors.

The methodology that best accounts for the effects of a non-homogeneous partial canopy cover is the two-source approach (Shuttleworth and Wallace, 1985; Norman et al., 1995; Kustas and Norman, 1999), in particular the two-source energy balance model (TSEB) of Norman et al., (1995) and Kustas and Norman (1999), in which surface fluxes are divided into soil and canopy components. Previous studies (Timmermans et al., 2007; González-Dugo et al., 2009) demonstrated the advantages of such models compared to single-source versions. This partition into soil/substrate and vegetation contributions to the radiative and turbulent fluxes, provides an estimation of vegetation transpiration. This is of great importance for many applications, due to the difference between the fraction of the water evaporated from the soil and the one consumed by crops/natural vegetation in the form of transpiration, directly related to CO_2 assimilation (Scott et al. 2006).

The ET models described above have been validated to a great extent over agricultural areas, with variable ground fractional cover and under various climate conditions (Kustas and Norman, 1997; French et al., 2005; Timmermans et al., 2007; González-Dugo et al., 2009), but mostly over homogeneously distributed canopies. Meanwhile, studies covering woody natural vegetation and woody crops are fewer (Cammalleri et al., 2010; Morillas et al., 2013; Guzinski et al., 2013). Natural ecosystems are generally heterogeneous, and their regime strongly relies on the physical

environmental conditions (temperature, wetness, insolation...). In many regions, the most densely monitored areas correspond to agricultural uses, which may limit the availability of detailed weather datasets elsewhere in practice. Moreover, the topographic gradients in non-cropped systems often require a distributed approach for an adequate characterization of the weather variable. EB models constitute a promising and powerful tool to overpass these constraints. Mediterranean ecosystems often present heterogeneous canopy mosaics with complex structures, disperse vegetation (generally evergreen sclerophyll trees) and large areas of grasses, scrubs and soil, all of which greatly influence turbulent and radiative exchanges. Understanding the functioning of these ecosystems necessitates partitioning the system between the vegetation layers with different phenologies and functions and the soil. While the trees are evergreen and probably have access to water sources throughout the year (David *et al.*, 2004; Campos *et al.*, 2010) by using deep sinker roots, the herbaceous layer which dries out before the summer depends on topsoil moisture (Joffre and Rambal, 1993; Baldocchi *et al.*, 2004). Thus, the ecosystem cannot be considered as a single, spatially uniform layer for water and energy flux exchanges. Furthermore, the vegetation of these arid and semi-arid regions is adapted to the climatic variability, with control mechanisms to face long periods of water scarcity, which need to be integrated into the models. For these reasons, the application of EB models over these landscapes is still a challenge.

To evaluate the ability of the TSEB model to model energy fluxes over woody ecosystems under arid/semi-arid conditions, we selected two typical Mediterranean ecosystems; a vineyard and an oak savanna, known as *dehesa* in Spain. The first of these is an agriculture ecosystem of great socioeconomic importance in the Mediterranean region, while the second is an agro-forestry system that plays a fundamental role in the rural development of the Iberian peninsula (Grove and Rackham, 2003; Papanastasis, 2004). *Dehesa* consists of widely spaced trees (oaks) combined with crops, grass and shrubs (Diaz *et al.*, 1997; Plieninger and Wilbrand, 2001). Vine (*Vitis Vinifera L.*) is a woody species native to the Mediterranean region, a liana with alternate leaves and a berry fruit (the grape). Even though Iberian oak species have been defined as “regulatory” in terms of water use (Rambal, 1993) and vineyards are usually irrigated and not directly influenced by the water shortages, water dynamics play an important role in both ecosystems, determining the depletion of the woodland (Brasier, 1993; Gallego *et al.*, 1999; Sánchez *et al.*, 2002) in one case, and controlling the production and quality of the crop in the other.

A better understanding of the hydrological, atmospheric and physiological processes that drive

ecosystem functions could help to improve its management and conservation. The dynamics of the ET can be a key indicator of the health of the system (*Moran et al., 2004*), especially in such water-scarce environments. The integration of remotely sensed data into these models offers a tool for timely and accurate ET monitoring over large areas, providing a better knowledge of the water status of soil and vegetation, helping to assess drought impacts and designing appropriate management actions aimed at reducing the economic and environmental vulnerability of these systems.

1.1.1 Evapotranspiration: concept, measurement methods and estimation models

From the physical perspective, evapotranspiration is divided into two processes: evaporation and transpiration. The water exchanged from liquid to vapor between the surface and the atmosphere is evaporation, while the liquid water vaporization from plant tissue to the atmosphere is known as canopy transpiration. In practice it is difficult to distinguish between the amount of water evaporated directly from bare soil and the amount transpired by vegetation cover in an area of land surface, as both processes are affected by the structure of the vegetation. The change of state requires energy, supplied basically by solar radiation and to a lesser extent by the air surrounding the evaporative surface. The water and energy balance equations over a given system are coupled by the ET term, with L , the vaporization latent heat of liquid water, changing the evaporation flux ET [mm] into the latent heat flux (associated to both evaporation from the soil and transpiration) LE [Wm^{-2}]. When the surrounding air is saturated with water vapor, the net vaporization-condensation rate through the water-air interface is zero. Besides solar radiation, the meteorological factors that influence the process are wind speed, air temperature and humidity (*Penman, 1948*).

Plants lose water through their stomata, which are little openings on the leaf surface and to a lesser degree on the cuticle, through which water vapor and other gases (CO_2 and O_2) circulate. Only a small proportion of the water absorbed by the roots (5%) contributes to the formation of new canopy cells in the apex (growing areas) or are consumed in metabolic processes and hydrolytic reactions, while the rest is transpired to the atmosphere. Transpiration depends on the opening of the stomata, on the energy available for changes of state, on soil's moisture and salt content, and on the vapor pressure gradient between the saturated air of the intercellular space and the atmosphere, which is the force that drives the water vapor through the stomata (*Brutsaert, 1984*). Interactions between the wind and the surface also influence this process, which has a thermo-regulatory objective, as the heat consumed

chills the leaves, maintaining the temperature within certain optimal limits for biomass production. It is primarily responsible for the circulation of water and salts through the plant (*Sharma and Daniel, 1985*).

The processes of evaporation and transpiration take place simultaneously, and their relative proportions vary according to the growth state of the canopy and soil-water status. In the first phases of an annual grass, for example, the evaporation process will prevail, because the soil is mostly exposed and barely covered by vegetation. While the canopy is developing it will gradually cover the soil until it reaches a maximum value at grass maturity, with water losses basically then due to transpiration. It is not easy to measure ET directly with field instrumentation. Using indirect methods, it can be quantified by considering its relationship with other physical parameters that can be measured directly. Both direct and indirect methods are based on two types of factors (*Rana and Katerji, 2000*) that affect the soil or the atmosphere. The first are related to the soil-water content and the surface characteristics (albedo, canopy density and height, and surface roughness). The second type includes meteorological factors such as solar radiation, wind speed and the thermodynamic characteristics of the atmosphere over the surface. *Rana and Katerji (2000)*, following *Rose and Sharma (1984)*, presented a classification of measurement methods based on their approaches following the concepts of hydrology, micrometeorology and plant physiology.

1.1.1.1 Energy-balance and micrometeorological methods

In these methods, water and energy exchanges between the vegetation system and the soil and the atmosphere are assessed. Water and energy exchanges are defined by the net flux (mass/energy per unit of time and unit cross section) of every component in their balance equations. The energy associated with the water vapor exchanged between the surface and the atmosphere (vaporization latent heat), LE, is one of the most important energy fluxes, often limited by the available energy for the process. Due to this limitation it is possible to quantify LE by applying the law of energy conservation (Fig. 1). For the simplified system (Fig. 1.1), the instantaneous energy balance equation can be expressed as:

$$R_n = G + LE + H + F + dS/dt \quad (1.1)$$

where R_n is the net radiation flux which reaches the system [Wm^{-2}]; G is the soil heat-flux by

conduction between the surface and the soil [Wm^{-2}]; LE is the latent heat flux [Wm^{-2}], the energy flux associated with the water-vapor flux ET [$\text{kg m}^{-2} \text{s}^{-1}$] by means of the vaporization heat L [J kg^{-1}], H is the sensible heat flux, the energy in the form of heat exchange by convection between the surface and the atmosphere [Wm^{-2}]. F is the photosynthesis energy flux [Wm^{-2}]; and S is the energy stored within the system. Equation (1.1) is usually simplified; for example, F, which represents 2-3% of the net radiation is ignored. S is also usually not considered (Hillel, 1998; Wilson et al., 2002; Meyers and Hollinger, 2004), however, in forest ecosystems with tall vegetation, the energy storage within the biomass could be important (McCaughey, 1985; Foken et al., 2006), and this requires further study.

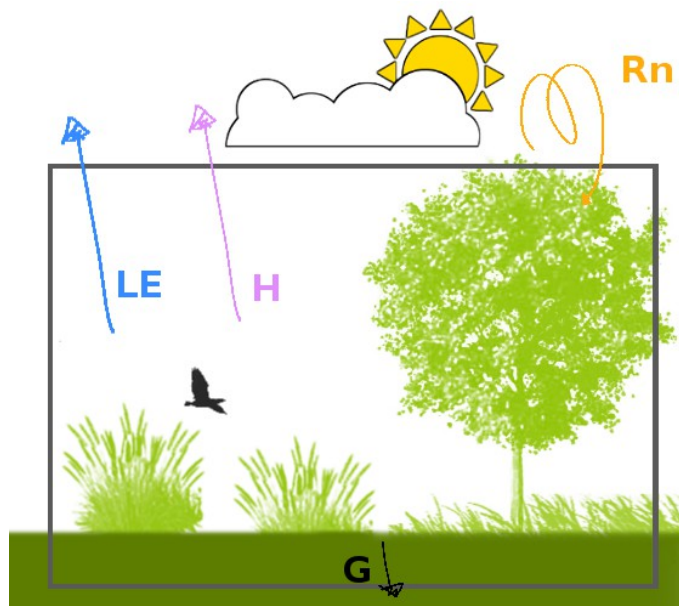


Figure 1.1: Surface energy balance fluxes scheme.

In Eq. (1.1) only vertical gradients are considered, and the net rate of energy transferred horizontally by wind advection is not taken into account. ET measuring systems using this approach include Bowen ratio, scintillometry, and eddy covariance methods. The Bowen ratio (ratio between H and LE) energy balance (BREB) is an indirect micrometeorological method (Bowen, 1926) that solves the energy balance equation by measuring air temperature and vapor pressure gradients in the near-surface layer above the evaporating surface. It is simple to apply since it does not require information about the aerodynamic characteristic of the canopies, but it may result in ET values without physical meaning when the Bowen ratio is close to -1. The Bowen ratio has been used in a variety of landscapes, and has proved to be an accurate method in semi-arid environments and tall crops (e.g. Dugas et al., 1991;

Cellier and Brunet, 1992; Frangi et al., 1996).

A scintillometer (Fig. 1.2a) is an optical device that measures small fluctuations of the air refractive index caused by temperature, humidity, and pressure-induced variations in density. Current scintillometers measure sensible heat flux, and to obtain ET, measurements of the net radiation (R_n) and soil heat (G) fluxes are also required (descriptions are available in Meijninger and De Bruin 2000; Meijninger et al. 2002; Hartogensis et al. 2003; De Bruin 2008).

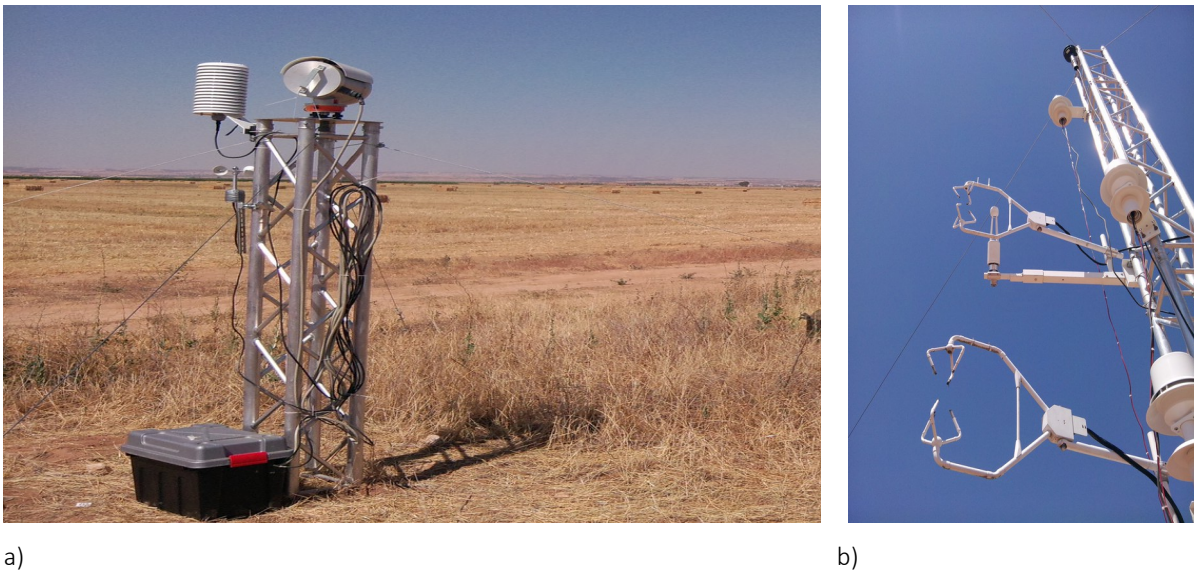


Figure 1.2: a) Scintillometer and b) an eddy covariance tower (ECT) system located in *Las Tiesas* experimental farm (Source: REFLEX training course supported by the FP7-funded EUFAR and Cost Action-funded by ES0903 EUROSPEC, Barrax, Albacete, Spain)

Eddy covariance systems (ECT, Fig. 1.2b) measure sensible and latent heat fluxes, momentum flux, and CO_2 or other fluxes, depending on their configuration. The method is based on the covariance between fluctuations in temperature and humidity (the concentration of interest), and upward and downward turbulent eddies (Fig. 1.3). Because these fluctuations are very fast, measurements of temperature, wind velocity, and humidity changes have to be made at high rates, with frequencies ranging between 5 and 20 Hz, and very accurately (Lee et al., 2004).

In a turbulent air flow, assuming that the air density fluctuations and the mean vertical flow are negligible, the associated energy fluxes can be represented as the product between the mean air

density (ρ_a) and the mean covariance between the instantaneous fluctuations (differences between the instantaneous value and the average value over a given time period) of the vertical wind speed (w') and a state variable (s'):

$$F \approx \overline{\rho_a w' s'} \quad (1.2)$$

The latent heat flux, LE , is computed from the covariance between w' and the instantaneous fluctuations of the specific air humidity (q').

$$LE = L \overline{\rho_a w' q'} \quad (1.3)$$

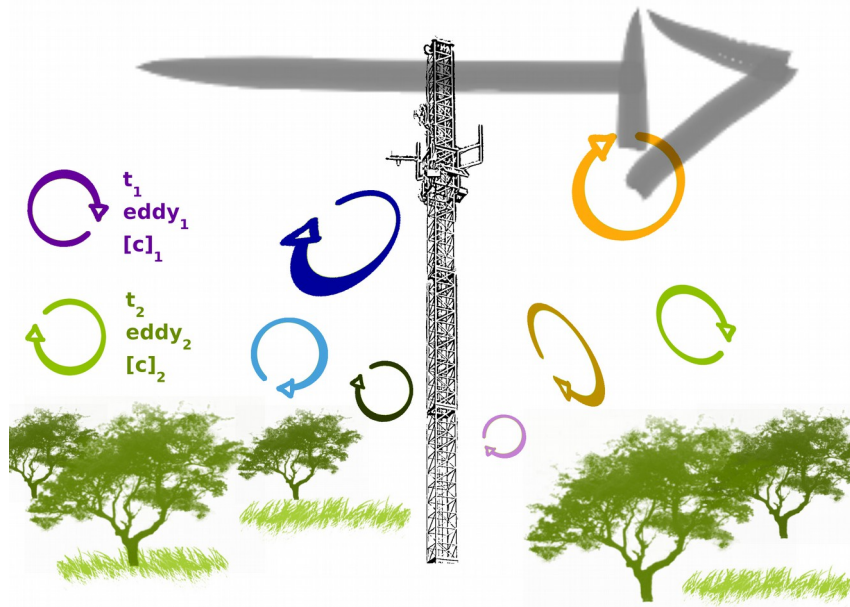


Figure 1.3: Eddy covariance tower system scheme.

By analogy, the sensible heat flux, H , is computed from the covariance between w' and the instantaneous fluctuations of the air temperature (T'), following equation (1.4).

$$H = \rho_a C_p \overline{w' T'} \quad (1.4)$$

where C_p is the air specific heat at constant pressure.

The major assumptions made by this method are that: (a) the measurements at one point can represent an upwind area and are assumed to be made within the boundary layer of interest, (b) the fluxes measured come from the area of interest, (c) the air flow is fully turbulent, and (d) the terrain is horizontal and uniform. This implies that field sites for these measurements need to fulfill certain conditions, such as being almost flat with an extensive footprint (area supplying the fluxes to be measured), and presenting a uniform and homogeneous landscape. The height at which the sensors must be placed depends on the height of the vegetation, the frequency response of the instruments and the extent of the footprint and the fetch.

The flux footprint (Fig. 1.4) is the area upwind the tower where the fluxes registered are generated, and this needs to be known to ensure the correct characterization of the measurements. The mentioned concept fetch, refers to the distance from the tower to the end of the measuring area. The footprint depends on the measurement height (footprint increases when height increases), the surface roughness (footprint decreases with increasing roughness) and the thermal stability (for the same measurement height and roughness, changes in atmospheric stability can expand the footprint several times). Thus, a sufficient fetch with undisturbed area around the instruments is required for these measurements to be representative. Most of the contribution usually comes from the area located between the underneath of the tower and the end of the fetch, and a number of models to evaluate the footprint contribution are available (*Schuepp et al., 1990; Kormann and Meixer, 2001; Soegaard et al., 2003*).

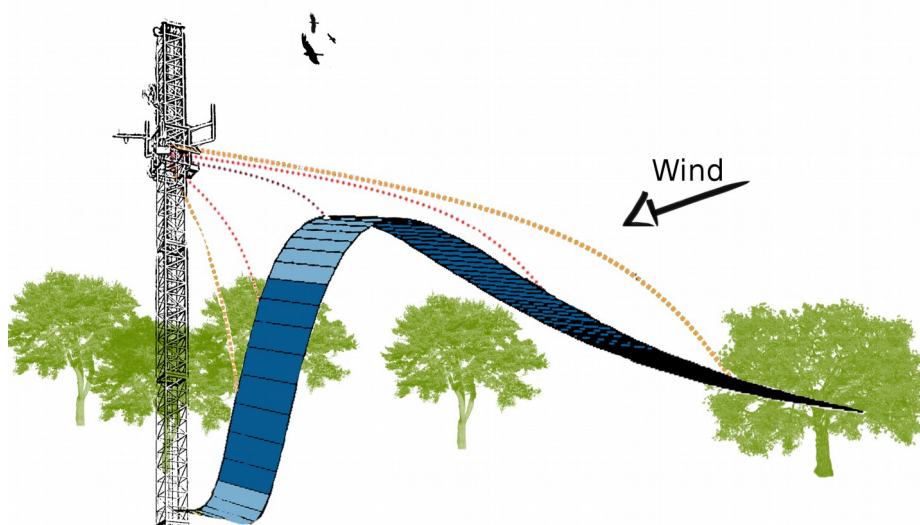


Figure 1.4: Footprint contribution area scheme (Figure based on *Burba et al., 2005*).

The instrumentation installed to provide the data is relatively fragile and expensive, requiring regular maintenance, but the methodology is highly reliable (*Burba and Anderson, 2005*). The vertical (and horizontal) wind component is generally measured by a sonic anemometer, which registers wind speed by means of the speed of sound in air, using a short burst of ultrasound transmitted from one transducer to another. The “travel time” between transducers is directly related to the wind speed along the sonic transducer axis, and the speed of sound is directly related to air density, temperature and humidity (*Campbell Scientific, Inc. 2010; Burba and Anderson, 2005*). Air temperature is measured by using ultrafine wire thermocouples, it can be also determined sonically and be corrected later for the effects of humidity (*Munger and Loescher, 2008*). Rain, dew, snow and frost on the sonic transducer may change the path length, causing errors in the measurements.

Specific humidity is measured by means of quick-response hygrometers (*Buck, 1976; Campbell and Tanner, 1985; Tanner, 1988*), which use a krypton lamp that emits two absorption lines that are absorbed by water vapor, and to a certain extent also by oxygen, so that the water vapor fluctuations need to be corrected for oxygen concentration. To measure CO₂ flux, gas analyzers are used: non-dispersive infrared (NDIR) sensor (LI-COR), narrow-band or single line LASER-analyzer. To characterize the same eddy scales, the measurements with the anemometer and the hygrometer must be made at the same point, or at least in very close vicinity, because the spatial separation underestimate the true covariance aimed to be measured between the wind speed and the fluctuations in humidity. For tall vegetation with high measurements heights, the size of the eddies increases, with the separation between the sensors having less influence on the accuracy of the relative measurements (*Kaimal and Finnigan, 1994; Lee et al., 2004; Foken et al., 2006*). Corrections are therefore required because of instrument separation, different frequency response, coordinate rotation, and the type of hygrometer employed (*Tanner et al., 1993; Villalobos, 1997; Aubinet et al., 2000; Horst, 2000; Massman, 2000, 2001; Paw et al., 2000; Twine et al., 2000; Rannik, 2001; Sakai et al., 2001; Wilson et al., 2002; Moncrieff et al., 2010; Mauder and Foken, 2013*). Various software packages are available for processing and correcting raw data from ECT devices (*EdiRE, Clement, 1999; ECPack, Van Dijk et al., 2004; EddySoft, Kolle and Rebmann, 2007; TK3, Mauder and Foken, 2013*).

Using this system turbulent heat fluxes often appear to be underestimated when their sum is compared to the available energy, $R_n - G$ (closure of the energy balance equation; see Eq. 1.1). Average closure errors are around 20% to 30% (*Twine et al., 2000; Wilson et al., 2002; Foken, 2008; Franssen et al., 2010*). Possible reasons can be found in the influence of the horizontal advection, the storage of

written as:

$$ET = \Delta W + P_R + I + C - R - D \quad (1.5)$$

where ΔW is the net water amount accumulated in the soil plant system during the selected time interval (Δt), the water inputs during (Δt) are precipitation (P_R), irrigation (I) in the case of irrigated crops, and the upward contribution from the water table (C), and the water outputs are evapotranspiration (ET), surface runoff (R), and deep percolation (D). In areas with high slopes, inputs and outputs due to subsurface fluxes should be also taken into account, although this component is usually neglected. In arid and semi-arid areas with low slopes, the runoff term R may be neglected (*Holmes, 1984*). This water exchange at the soil surface layer is conditioned by the physical properties of the soil, the vegetation characteristics, and the climate pattern shown by the distribution of dry and wet periods.

Lysimeters (Fig. 1.6) are isolated soil tanks, generally with a canopy of growths similar to the surrounding area. They are located in the field in order to be representative of natural conditions, and are used to determine the ET of a grown crop, reference vegetation cover or soil (*Aboukhaled et al., 1986*). Lysimetry was developed specifically for obtaining direct measurements of ET , calculating it as the water weight gain or loss of the soil contained in the instrument during a give time period (*Sharma and Daniel, 1985*). Because the root area is isolated from the environment, lateral fluxes, percolation and capillary rise are null. The rest terms of the balance can be accurately determined. The water loss or gain is given by the mass change over time, obtained by continuously weighting the soil tank. For the lysimeter measures to be representative of the whole field conditions, the density of the inside vegetation and the height and soil characteristics need to be similar to the surrounding area (*Grevet and Cuenca, 1991*).



Figure 1.6: Lysimeter system located in Las Tiasas experimental farm, outside and inside equipment (Source: Instituto Técnico Agronómico Provincial, ITAP, Barrax, Albacete, Spain. During REFLEX training course).

1.1.1.3 Plant physiology approaches

These methods analyze the water behavior of individual plants based on their physiology. The chamber system (*Reicosky and Peters, 1977; Wagner and Reicosky, 1996*) and sap flow method (*Cohen et al., 1988*) are the most widely used (*Rana and Katerji, 2000*).

The sap flow method is based on the assumption that this flow is related to the canopy transpiration rate. Applications at canopy scale require individual measurements to be extrapolated to the scale of interest, which is possible when the structure of the canopy and the spatial variability (density, height and leaf area index: LAI) are known. The effect of evaporation from the soil does not influence this measurement and it is not assessed. In Mediterranean climates with low fractional covers, evaporation from soil can be a very important fraction of the ET (up to 20%), which means that an additional measurement system is required in combination with sap flow to estimate total ET.

Chambers for measuring ET were described for the first time by *Reicosky and Peters (1977)*. These consist of a plastic chamber in which the air is mixed continuously. Vapor density is measured with infrared analyzers, and CO₂ flux can be also evaluated. The chambers are suitable for research studies on orchard crops such as vines and olive trees (*Katerji et al., 1994, Pérez-Priego et al., 2014*).

1.1.2 Modelling evapotranspiration by means of remote sensing

Due to the difficulties of ground ET measurement, along with the cost, maintenance of instrumentation and the punctual nature of the data, significant research efforts have been put into estimating ET by using models with different physical foundations. These can be broadly classified into analytical and empirical models (*Rana and Katerji, 2000*). The integration of remotely sensed data into evapotranspiration models has widened its area of application from point to basin and regional scales.

There are basically two research lines devoted to ET estimation using remotely sensed information. The first approach uses the vegetation indexes (VI) derived from airborne or satellite measured surface reflectance, to determine crop growth and to estimate the basal crop coefficient (K_{cb}) (*Bausch and Neale, 1989*). Together with data coming from meteorological stations to compute the reference ET (ET_0) that accounts for the atmospheric demand, it can be used to determine the crop actual ET (*Allen et al., 1998*). The second approach uses the surface radiometric temperature derived from the thermal bands of remote sensors to estimate ET as latent heat flux. LE is computed in these methods as the residual of the energy balance (e.g., *Moran et al., 1994; Kustas and Norman, 1996; Gillies et al., 1997; Bastiaanssen et al., 1998*).

The second approach requires the aerodynamical temperature (T_0) to be obtained. This is defined as the extrapolation of the air temperature profile down to an effective height within the canopy at which the vegetation component of sensible heat flux arises (*Kalma and Jupp, 1990*), which is not equivalent to the T_{RAD} given by the sensor. As mentioned previously several schemes have been formulated with different degrees of complexity and requirements for input parameters to solve this problem. For regional estimations, considering the effects of a partial vegetation cover, TSEB (*Norman et al., 1995; Kustas and Norman, 1999*) is of great interest, because it formulates separately the flux energy exchange between the atmosphere and the soil, and between the atmosphere and the vegetation. Moreover, it has a stronger physical basis than other models and allows for adaptation to the specific characteristics of each ecosystem, modifying some aspects of the energy balance to account for the particular physiological, phenological and meteorological conditions.

1.1.2.1 Earth Observation (EO) technology

Nowadays, remote sensing information has become an essential tool for research and management applications in many fields, such as agriculture, forestry, weather forecasting, land-use policy and cartography. EO technology refers to any method of remote observation of the surface of the Earth that acquires information from airborne or space sensors. The advantages of using these techniques are the global coverage of the Earth with various frequency and spatial resolutions, the non-destructive observation of ground cover, immediate information transmission, and the availability of data in digital format. Between the surface and the sensor there is an energy interaction, either due to the solar energy reflectance (VIS/NIR), an artificial energy beam reflectance (radar systems), or by self-emission of the surface (thermal/microwave). The signals are transmitted through the atmosphere and captured by the sensors and are finally available for further processing in digital format (Fig. 1.7).

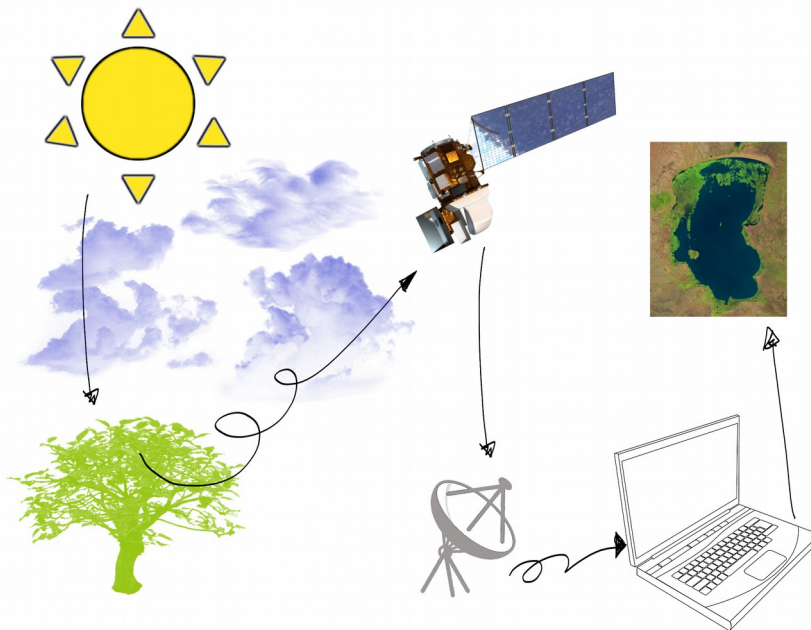


Figure 1.7: EO scheme for gathering and processing information.

The energy flux between the surface and the sensor takes the form of electromagnetic radiation and it is defined by its wavelength and frequency. Although the electromagnetic spectrum is continuous, the detectors need to divide it into a number of bands within which the radiation shows similar behavior. The most frequently used regions in remote sensing are the visible part of the spectrum (VIS, $0.4\mu\text{m} - 0.7\mu\text{m}$); the near-infrared (NIR, $0.7\mu\text{m} - 1.3\mu\text{m}$), useful for discriminating canopy masses and

humidity; medium-infrared (SWIR, $1.3\mu\text{m} - 3\mu\text{m}$), where reflectance of solar energy and emissivity from the surface are shown together; thermal (TIR, $3\mu\text{m} - 100\mu\text{m}$), which includes the emissivity portion of the spectrum in terms of ground cover temperature; and microwave bands ($1\text{ mm} - 1\text{m}$), radiation that can penetrate the clouds. The reflectance is the proportion of the incident energy reflected by a surface, a dimensionless magnitude that ranges between 0 and 1. For a given surface, it varies depending on the wavelength, and the curve representing this variation is called the spectral signature. This spectrum is characteristic of each surface and state, and enables land uses, materials, canopy growth status, etc., to be discriminated and classified (Richards and Jia, 2006).

When the electromagnetic radiation passes through the atmosphere it is attenuated by absorption and dispersion processes. The absorption is defined as the transformation that the energy undergoes when it passes through a medium. A fraction of the energy is absorbed by the atmospheric components (O_2 , CO_2 , O_3 and water vapor) and emitted at different wavelengths. Satellites used in remote sensing are designed to operate outside the regions where absorption effects are greatest, in what are called atmospheric windows (Fig. 1.8). The dispersion process produces a change in the direction of a portion of the incidence radiation in relation to the original one, due to the interaction between the energy and the suspended atmospheric particles. To avoid the effects of these processes in the analysis it is necessary to correct the original data acquired by the sensor using various methods, according to the part of the spectrum of interest (Gordon and Morel, 1983; Saunders and Kriebel, 1988; Asrar, 1989; Lenoble, 1993; Kaufman and Sendra, 1998).

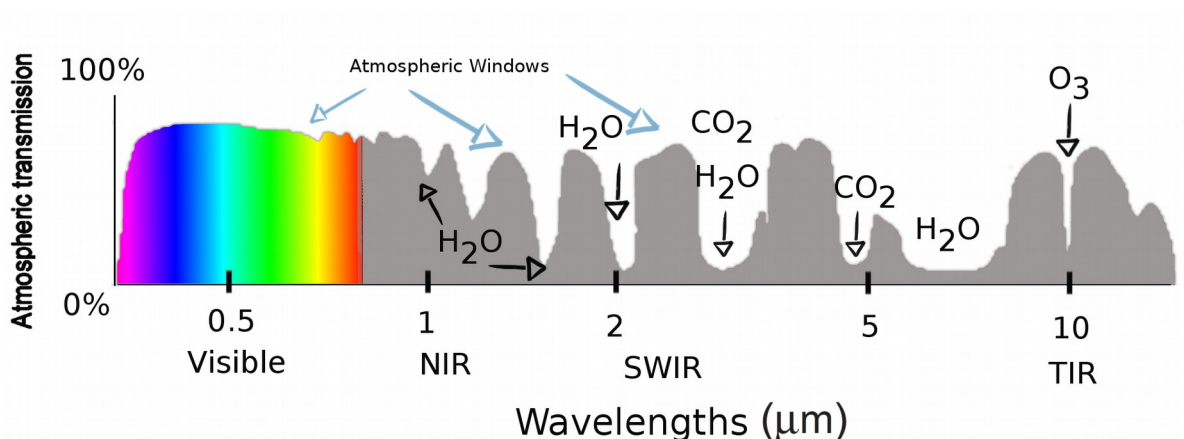


Figure 1.8: Atmospheric windows for the satellites (Figure adapted from Casey *et al.*, 2012).

Sensors mounted on satellites follow an orbit around the Earth depending on the objectives and characteristics of their mission. In general, orbits are defined by their height, orientation, and rotation relative to the Earth. Geostationary orbits are located at altitudes of around 36000 km, always seeing the same portion of the globe because they replicate the angular speed of the Earth (e.g. meteorological satellites such as METEOSAT or GOES). Most of the satellites are in polar orbit, covering the same portion of the surface at a fixed daily time, thus ensuring similar light conditions in the information they acquire (Fig. 1.9). In their movement around the Earth the satellites cover a given area of the surface, with the swath width depending on the satellite's field of view (FOV) and the pixel size on the sensor's instantaneous field of view (IFOV).

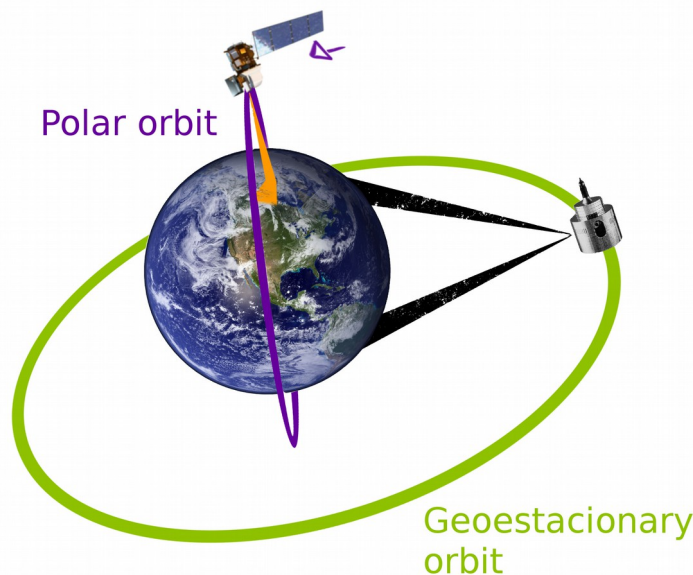


Figure 1.9: Different satellite orbits, polar orbit with different speed than the Earth, and geostationary orbit with the same speed than the Earth.

The resolution of a sensor is given by its ability to register and discriminate information, and it is dependent on the combined effect of a number of criteria, such as its spatial, spectral, radiometric and temporal resolutions (Fig. 1.10). The spatial resolution is determined by the IFOV, the height of the platform and the sensor viewing angle. It is defined as the angular section in radians observed at a particular time. It is usually referred to the distance corresponding to this angle over the surface. Thus, this distance will be the minimum size of the information registered: the pixel or picture element. The smaller the size of the pixel, the higher will be the spatial resolution that the sensor can provide; i.e. it

will be able to discriminate a larger number of surface objects. The spectral resolution of a sensor is the number, wavelength center and width of spectral bands that it can discriminate and register, depending on the optical filter installed. Radiometric resolution is defined as the minimum quantity of energy that is needed to increase the pixel value by one digital number. It is referred to as the sensor sensitivity. The temporal resolution is the time interval between two successive image acquisitions of the same part of the surface, depending on the orbital and sensor characteristics. Generally speaking, meteorological satellites (e.g. NOAA, METEOSAT) have lower spatial resolution ($\sim 10^3$ m) and high temporal resolution (daily), and natural resources-monitoring satellites (such as Landsat, SPOT, IRS, etc.) lower temporal and higher spatial resolution ($\sim 10-10^2$ m).

From remote sensing information it is possible to derive biophysical parameters that describe the soil and canopy state and dynamics, such as albedo, surface radiometric temperature, fractional cover (f_c) and LAI (Moran *et al.*, 1997; Glenn *et al.*, 2008; Chuvieco and Huete, 2010). Using simple numerical combinations of spectral information measured at different wavelength, mostly the visible and near infrared regions of the spectrum, it is possible to extract information about the state and structure of the vegetation, minimizing the perturbation caused by soil and atmospheric conditions (Huete, 1988). Such combinations are called vegetation indices (VI), and some of the most widely used are the Normalized Difference Vegetation Index (NDVI) and the EVI (Enhanced Vegetation Index), computed from the Blue (0.4 – 0.5 nm), Red (0.6-0.7 nm) and Near-InfraRed (NIR) (0.7 – 1.1 nm) regions of the spectrum (Asrar *et al.*, 1985; Choudhury *et al.*, 1994; Wittich and Hansing, 1995; Huete *et al.*, 2002; Chuvieco and Huete, 2010).

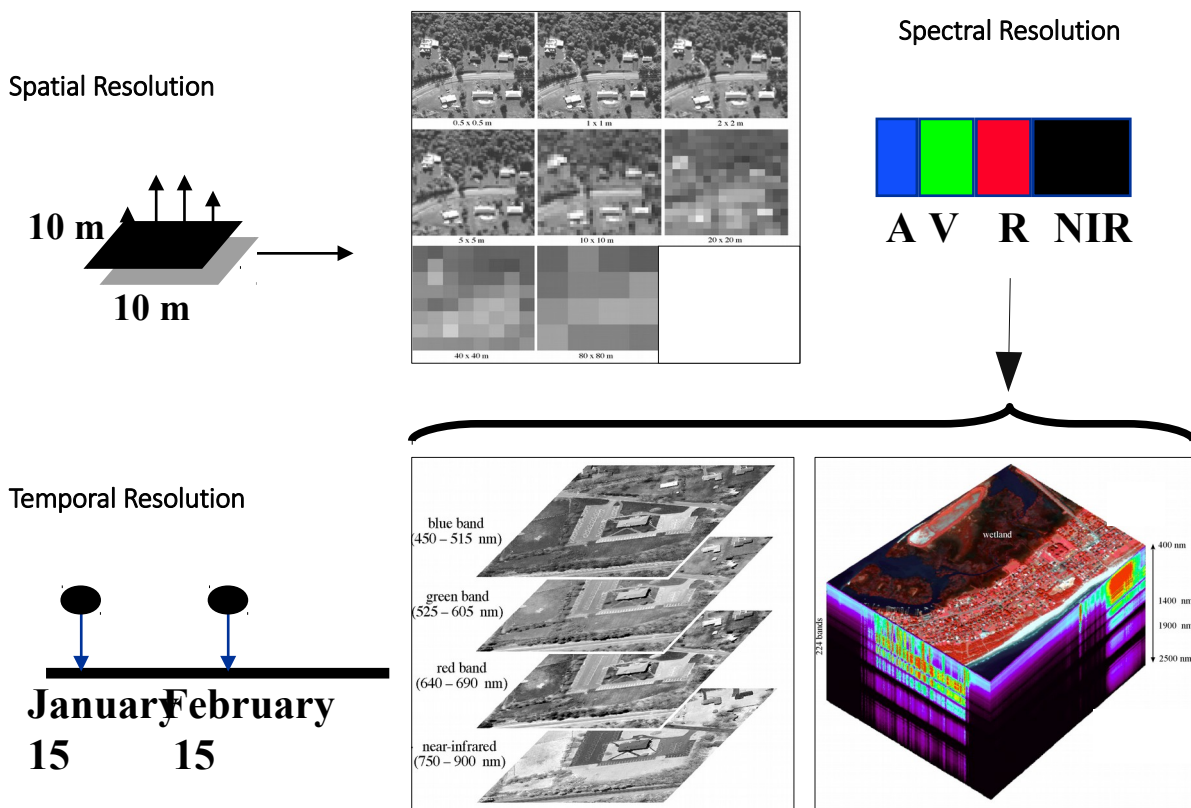


Figure 1.10: Spatial, spectral and temporal resolution (Source: Jensen, J. R. , 2000).

Early and late stages of plant water stress can be detected by means of the thermal portion of the spectrum, due to the direct link between the transpiration process and the vegetation thermal response (e.g. water evaporation from the leaves to the atmosphere cools the plant) (Idso and Baker, 1967). Transpiration strongly affects the proper functioning of these systems, and a reduction in the vegetation water content has an impact on the growth of plants and their physiological functions (Hatfield, 1997). Thus, with the launch of satellite-based thermal sensors, TIR information, capable of continuous distributed monitoring of the health of ecosystems, is available.

As mentioned above, important efforts have been put into refining and validating methods that integrate TIR measurements for estimating evapotranspiration [see review by Kustas and Norman, 1996] using sensors' surface radiometric temperature observations as an input. T_{RAD} was defined by Norman et al. (1995) as the "aggregate temperature of all objects comprising the surface", function of the canopy and soil temperature weighted by the fraction occupied by each component (Kustas et al., 1990). Nevertheless, the use of space-based thermal sensor data (as well as handheld and airborne sensor data) need to take into account the sun/sensor/viewing geometry (e.g. Lagouarde et al., 1995)

and the atmospheric effects described in this section, on temperature measurements (e.g. Perry and Moran, 1994).

1.1.3 Mediterranean woody ecosystems

Evergreen sclerophyll trees and shrubs with deep roots, which maintain green leaves during the summer period (e.g. oaks, olives); semi-deciduous shrubs (vines); and annual herbs with annual cycles completed before summer, dominate in Mediterranean environments (Ehleringer and Mooney, 1983). These ecosystems exist under extremely high air temperatures (30 – 40 °C), large vapor pressure deficits (exceeding 4 kPa), extremely low leaf-water potentials (3 – 7 MPa), and high radiation rates (>30 MJm⁻²day⁻¹) (Infante et al., 1997; Infante et al., 2003; Baldocchi and Xu, 2007). Due to these conditions, canopy temperature usually exceeds air temperature in the dry period, reaching the upper limit of the canopy temperature range (0 – 39 °C), outside which enzymatic activity is inhibited (Bjorkman, 1980). Precipitation in these areas is around 600 – 800 mm per year, not all of it available for the trees, due to runoff, deep infiltration, water interception (Joffre and Rambal, 1993; Lewis et al., 2000), and the water understorey canopy use (20 – 40%) (Baldocchi et al., 2004).

In these regions, with wet and cold winters and dry and hot summers, there is an imbalance between water supply (precipitation) and water demand (evapotranspiration) (Joffre and Rambal, 1993; Baldocchi and Xu, 2007). Mediterranean natural vegetation has adapted to these conditions by developing structural and physiological capabilities for survival in water-limited environments. As Baldocchi and Xu (2007) detailed, this could be achieved by different strategies: (1) constraining the ecosystem leaf area index with low dense widely-spaced tree landscapes (Joffre and Rambal, 1993, Carreiras et al., 2006), e.g. oak savanna such as *dehesa*; (2) decreasing their transpiring canopy leaf area (Ogaya and Peñuelas, 2006; Limousin et al., 2009; Ripullone et al., 2009); e.g. evergreen Mediterranean oak trees modify their shoot allometry (Villar-Salvador et al., 1997), changing the allocation rules (Pereira and Chaves, 1993), changing their leaf structure and biochemistry (Castro-Diez et al., 1997), modifying leaf phenology (Castro-Diez and Monserrat-Martí, 1998; Limousin et al., 2012) and the leaf life span (Mediavilla and Escudero, 2003; Ogaya and Peñuelas, 2006); (3) reducing the size of their leaves; e.g. Mediterranean oaks have leaves much smaller than temperate climate oaks (Taylor, 1975; Pavlik et al., 1991); (4) regulating water use by regulating physiological characteristics; e.g. stomatal or hydraulic conductance (Xu and Baldocchi, 2003; David et al., 2004); (5) accessing

shallow- and deep-water reservoirs, e.g. vines (Pavlik et al., 1991; David et al., 2004; Lewis and Burgy, 1964); and (6) by adopting a deciduous life form, that does not transpire during the summer months (Mooney, 1970).

Stomatal closure is a plant response to water stress (e.g. Mediterranean trees: Martínez-Ferri et al., 2000; Gulías et al., 2002; Mediavilla and Escudero, 2003; Galmés et al., 2007d; Gallé and Feller, 2007; Gallé et al., 2007), and it is usually considered to be the key factor controlling transpiration during water-scarce periods. For example, it has been established (Infante et al., 2003; Paço et al., 2009) that the high resilience of *Quercus ilex* to severe droughts is due to strong stomatal regulation. Oaks regulate their stomata by turgor and osmotic adjustment (Matzner et al., 2003), by altering their hydraulic conductance (David et al., 2004) or by the reallocation of leaf nitrogen, reducing photosynthetic capacity (Xu and Baldocchi, 2003). Smaller leaves have ecological advantages in semi-arid climates because their thinner leaf boundary layer allows the sensible heat flux to be convected outside the plant more effectively, enabling them to avoid reaching upper canopy temperature limits (Parkhurst and Loucks, 1972; Gates, 1980).

As it mentioned previously, for this study two typical Mediterranean ecosystems have been selected, vineyard and *dehesa*. An agricultural system and an agricultural/forestry and livestock farming form of land exploitation. Both exist under arid or semi-arid climatic conditions, with low fractional covers and complex canopy structures, and the possibility of a sub-canopy herbaceous layer. *Dehesa* combined the understorey layer with widely-spaced oak trees, mostly *Quercus ilex*, *Quercus suber*, *Quercus pyrenaica* and *Quercus rotundifolia*. Direct measurements of annual evaporation from oak woodlands in Mediterranean climates are scarce (Baldocchi and Xu, 2007), but it generally lied between 350 and 600 mm per year. During periods of drought, annual evapotranspiration may even drop below 300 mm per year (Joffre and Rambal, 1993; Lewis et al., 2000; Infante et al., 2003). A deeper understanding of the processes driving the functioning of such ecosystems would improve their conservation, avoiding the tendency to oak woodland depletion of the past several years (Montoya, 1998; Sánchez et al., 2002; Coelho et al., 2004; Schnabel and Ferreira, 2004; Pulido and Díaz, 2005). Vines are a woody crop with a heterogeneous/multidimensional structure, growing in bare soil, sometimes surrounded by an annual herbaceous layer. The vine is a deciduous climbing shrub, whose growth period coincides with the summer season, with a latent period during the winter. It is a perennial species, with a longevity of 20 – 30 years. Its perennial habit allows the roots to explore large volumes of soil and access underground water during dry periods. Estimates of water demand by the crop, place it as the irrigated

crop with fewer ratios per surface unit, along with other typical Mediterranean woody species like olives-trees and almonds-trees (López-Urrea, 2004).

Global warming may well significantly affect these ecosystems located over rainfall transition areas, which currently receive just enough water to scarcely support the canopy (Woodward, 1987). An in-depth analysis of the climatic and soil conditions and the biotic and abiotic factors that control ET by Mediterranean woody crops and natural lands is needed in order to evaluate how this process affects the water balance at different scales. To do so, it is necessary to gain insight into the structure and function of this ecosystem (e.g. radiation, energy and water fluxes), that requires the partitioning of the system between the vegetation layers with different seasonal cycles (Fig. 1.11a and 1.11b), not considering the ecosystem as a single homogeneous layer for the water and energy budgets.

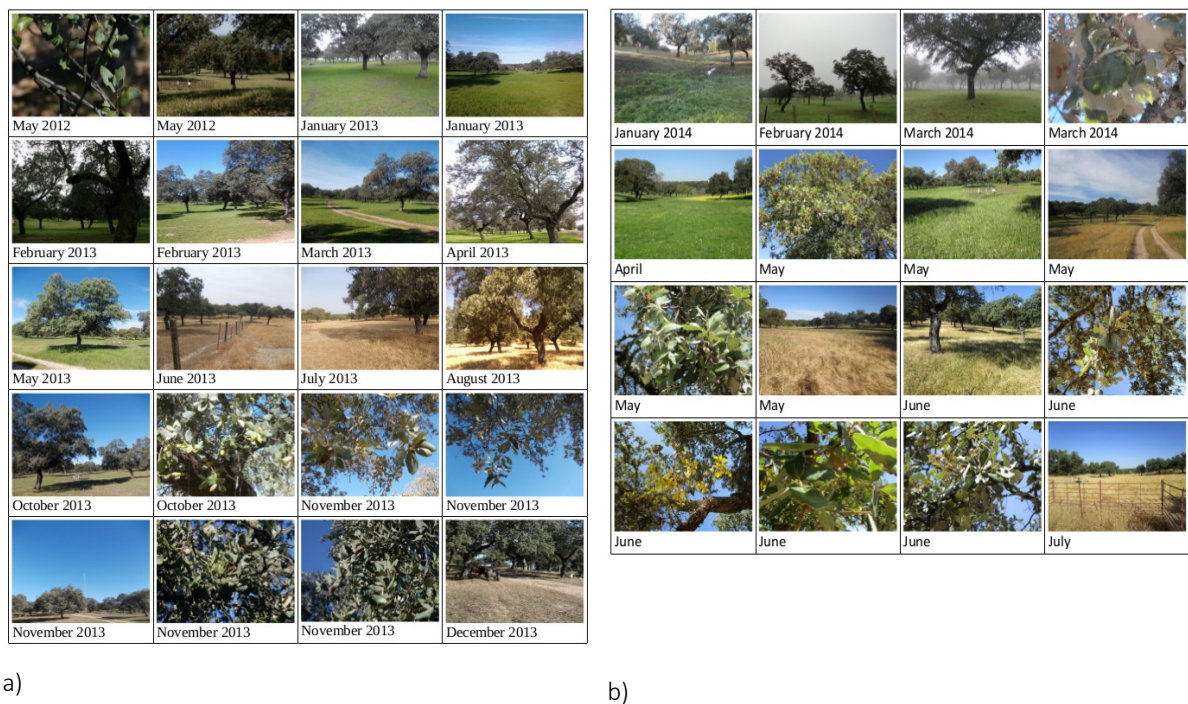


Figure 1.11: *Dehesa* landscape evolution over a) 2013 and b) 2014 in Santa Clotilde.

1.2 OBJECTIVES AND DOCUMENT SCHEMA

The overarching objective of this thesis is to model evapotranspiration using thermal infrared (TIR) remote sensing in Mediterranean woody ecosystems, as an indicator of ecosystem health and water status. A two-source surface energy balance model (TSEB) has been revisited, adapting the formulation to the structure and physiology of this pattern of vegetation, from detail to regional scales into account, and analyzing the partition of turbulent fluxes between the transpiration and evaporation components.

To achieve this objective, the study was divided into three specific sub-goals:

1) Analysis of the influence of complex vegetation structures with low fractional cover and soil/substrate, grass and tree layers, typical of Mediterranean woody ecosystems, into exchange modelling of the radiative and turbulent fluxes. Adaptation of the two-source surface energy balance model (TSEB) formulation to take these effects into account using data from two experimental sites located in a *dehesa* landscape. Evaluation of the general model behavior and specific key parameters, such as the Priestley-Taylor coefficient, roughness length, energy storage within the biomass, and wind speed profile. This work is described in Chapter 2.

2) Estimation of ET on a regional scale, with the integration of optical and thermal remote-sensing (Landsat 7 ETM+, Landsat 8 OLI and MODIS) and meteorological data into the TSEB model. Evaluation and validation of the results using ground-truth measurements corresponding to the experimental *dehesa* sites. Evaluation of a distributed application of TSEB over the entire Andalusian *dehesas*. This work is summarized in Chapter 3.

3) Evaluation of the separation of soil and canopy surface energy fluxes components produced by the TSEB model over vineyards, using data from two airborne campaigns that provided directional radiometric surface-temperature observations at two different viewing-angles, thus permitting direct estimates of soil and canopy temperatures to be made. This analysis is presented in Chapter 4.

1.3 REFERENCES

- Aboukhaled, A.A., Alfaro, A., & Smith, M. (1986). *Los lisímetros*. Roma: FAO
- Akbari, M., Toomanian, N., Droogers, P., Bastiaanssen, W., & Gieske, A. (2007). Monitoring irrigation performance in Esfahan, Iran, using NOAA satellite imagery. *Agricultural Water Management*, 88, 99-109
- Allen, R.G., Pereira, L., Raes, D., & Smith, M. (1998). *Crop evapotranspiration, guidelines for computing crop water requirements*. Rome
- Allen, R.G., Pruitt, W.O., Businger, J.A., Fritschen, L.J., Jensen, M.E., & F.H.Quinn (Eds.) (1996). *Evaporation and transpiration*. New York
- Anderson, M.C., Kustas, W.P., & Norman, J.M. (2007). *Upscaling flux observations from local to continental scales using thermal remote sensing*. Madison, WI, ETATS-UNIS: American Society of Agronomy
- Anderson, M.C., Norman, J.M., Diak, G.R., Kustas, W.P., & Mecikalski, J.R. (1997). A two-source time-integrated model for estimating surface fluxes using thermal infrared remote sensing. *Remote Sensing of Environment*, 60, 195-216
- Arnold, J.G., Srinivasan, R., Muttiah, R.S., & Williams, J.R. (1998). Large area hydrologic modelling and assessment part I: model development 1. *JAWRA Journal of the American Water Resources Association*, 34, 73-89
- Asrar, G. (1989). *Theory and Applications of Optical Remote Sensing (Wiley Series in Remote Sensing and Image Processing)*
- Asrar, G., Kanemasu, E.T., & Yoshida, M. (1985). Estimates of leaf area index from spectral reflectance of wheat under different cultural practices and solar angle. *Remote Sensing of Environment*, 17, 1-11
- Aubinet, M., Moncrieff, J., & Clement, R.C. (2000). Estimates of the annual net carbon and water exchange of forests: the EUROFLUX methodology. *Advances in Ecological Research*, 30, 113-175
- Baldocchi, D., Falge, E., Gu, L., Olson, R., Hollinger, D., Running, S., Anthoni, P., Bernhofer, C., Davis, K., Evans, R., Fuentes, J., Goldstein, A., Katul, G., Law, B., Lee, X., Malhi, Y., Meyers, T., Munger, W., Oechel, W., Paw, K.T., Pilegaard, K., Schmid, H.P., Valentini, R., Verma, S., Vesala, T., Wilson, K., & Wofsy, S. (2001). FLUXNET: A New Tool to Study the Temporal and Spatial Variability of Ecosystemâ€ˆScale Carbon Dioxide, Water Vapor, and Energy Flux Densities. In, *Bulletin of the American Meteorological Society* (pp. 2415-2434): American Meteorological Society
- Baldocchi, D.D., & Xu, L. (2007). What limits evaporation from Mediterranean oak woodlands - " The supply of moisture in the soil, physiological control by plants or the demand by the atmosphere? *Advances in Water Resources*, 30, 2113-2122
- Baldocchi, D.D., Xu, L., & Kiang, N. (2004). How plant functional-type, weather, seasonal drought, and soil physical properties alter water and energy fluxes of an oak grass savanna and an annual grassland. *Agricultural and Forest Meteorology*, 123, 13-39
- Bastiaanssen, W.G.M., Ahmad, M.-u.-D., & Chemin, Y. (2002). Satellite surveillance of evaporative depletion

- across the Indus Basin. *Water Resources Research*, 38, 1273
- Bastiaanssen, W.G.M., Pelgrum, H., Wang, J., Ma, Y., Moreno, J.F., Roerink, G.J., & van der Wal, T. (1998). A remote sensing surface energy balance algorithm for land (SEBAL): Part 2: Validation. *Journal of Hydrology*, 212-213, 213-229
- Bastiaanssen, W.G.M., Thiruvengadachari, S., Sakthivadivel, R., & Molden, D.J. (1999). Satellite Remote Sensing for Estimating Productivities of Land and Water. *International Journal of Water Resources Development*, 15, 181-194
- Bausch, W.C., & Neale, C.M.U. (1989). Spectral inputs improve corn crop coefficient and irrigation scheduling. *Transactions of the ASAE*, 32, 1901-1908
- Beljaars, A.C.M., Viterbo, P., Miller, M.J., & Betts, A.K. (1996). The Anomalous Rainfall over the United States during July 1993: Sensitivity to Land Surface Parameterization and Soil Moisture Anomalies. In, *Monthly Weather Review* (pp. 362-383): American Meteorological Society
- Betts, A.K., Chen, F., Mitchell, K.E., & JanjiÄš, Z.a.l. (1997). Assessment of the Land Surface and Boundary Layer Models in Two Operational Versions of the NCEP Eta Model Using FIFE Data. In, *Monthly Weather Review* (pp. 2896-2916): American Meteorological Society
- Bjorkman, O. (1980). *The response of photosynthesis to temperature*. Oxford, UK: Blackwell
- Bowen, I.S. (1926). The ratio of heat losses by conduction and by evaporation from any water surface. *Physics Review*, 27, 779-787
- Brasier, C.M. (1993). Phytophthora cinnamomi as a contributory factor on European oak declines. In A.V. N Luisi (Ed.), *Recent advances in Studies on Oak Decline*. (pp. 49-58)
- Brutsaert, W. (1984). *Evaporation into the Atmosphere: Theory, History and Applications*. Dordrecht/Boston/Lancaster: D. Reidel Publishing Company
- Buck, A.L. (1976). The Variable-Path Lyman-Alpha Hygrometer and Its Operating Characteristics. In, *Bulletin of the American Meteorological Society* (pp. 1113-1118): American Meteorological Society
- Burba, G., & Anderson, D. (2005). *A Brief Practical Guide to Eddy Covariance Flux Measurements: Principles and Workflow Examples for Scientific and Industrial Applications*
- Cammalleri, C., Anderson, M.C., Ciruolo, G., D'Urso, G., Kustas, W.P., La Loggia, G., & Minacapilli, M. (2010). The impact of in-canopy wind profile formulations on heat flux estimation in an open orchard using the remote sensing-based two-source model. *Hydrol. Earth Syst. Sci.*, 14, 2643-2659
- Campbell, G.S., & Tanner, B.D. (1985). *A krypton hygrometer for measurement of atmospheric water vapor concentration*. NC, USA
- Campbell Scientific., I. (2010). CSAT3 Three Dimensional Sonic Anemometer. In. Logan, Utah, United States: Campbell Scientific, Inc.
- Campos, I., Neale, C.M.U., Calera, A., Balbontin, C., & Gonzalez-Piqueras, J. (2010). Assessing satellite-based basal crop coefficients for irrigated grapes (*Vitis vinifera* L.). *Agricultural Water Management*, 98, 45-54
- Carreiras, J.M.B., Pereira, J.M.C., & Pereira, J.S. (2006). Estimation of tree canopy cover in evergreen oak

- woodlands using remote sensing. *Forest Ecology and Management*, 223, 45-53
- Casey, K.A., Kaab, A., & Benn, D.I. (2012). Geochemical characterization of supraglacial debris via in situ and optical remote sensing methods: a case study in Khumbu Himalaya, Nepal. *The Cryosphere*, 6, 85-100
- Castro-Díez, P., & Montserrat-Martí, G. (1998). Phenological pattern of fifteen Mediterranean phanerophytes from shape *Quercus ilex* communities of NE-Spain. *Plant Ecology*, 139, 103-112
- Castro-Díez, P., Villar-Salvador, P., Pétez-Rontomé, C., Maestro-Martínez, M., & Montserrat-Martí, G. (1997). Leaf morphology and leaf chemical composition in three *Quercus* (Fagaceae) species along a rainfall gradient in NE Spain. *Trees*, 11, 127-134
- Cellier, P., & Brunet, Y. (1992). Flux-gradient relationships above tall plant canopies. *Agricultural and Forest Meteorology*, 58, 93-117
- Clement, R. (1999). *EdiRe Data Software 1.5.0.10*. Edinburgh, England
- Coelho, C.O.A., Ferreira, A.J.D., Laouina, A., Hamza, A., Chaker, M., Naafa, R., Regaya, K., Boulet, A.K., Keizer, J.J., & Carvalho, T.M.M. (2004). *Changes in land use and land management practices affecting land degradation within forest and grazing ecosystems in the Western Mediterranean*. Catena Verlag, Reiskirchen, Germany: Advances in GeoEcology
- Cohen, Y., Fuchs, M., Falkenflug, V., & Moreshet, S. (1988). Calibrated Heat Pulse Method for Determining Water Uptake in Cotton. *Agron. J.*, 80, 398-402
- Chandrapala, L., & Wimalasuriya, M. (2003). Satellite measurements supplemented with meteorological data to operationally estimate evaporation in Sri Lanka. *Agricultural Water Management*, 58, 89-107
- Chavez, J., Neale, C.M.U., Hips, L.E., Prueger, J.H., & Kustas, W.P. (2005). Comparing Aircraft-Based Remotely Sensed Energy Balance Fluxes with Eddy Covariance Tower Data Using Heat Flux Source Area Functions. *Journal of Hydrometeorology*, 6, 923-940
- Chehbouni, A., Lo Seen, D., Njoku, E.G., & Monteny, B.M. (1996). Examination of the difference between radiative and aerodynamic surface temperatures over sparsely vegetated surfaces. *Remote Sensing of Environment*, 58, 177-186
- Choudhury, B.J., Ahmed, N.U., Idso, S.B., Reginato, R.J., & Daughtry, C.S.T. (1994). Relations between evaporation coefficients and vegetation indices studied by model simulations. *Remote Sensing of Environment*, 50, 1-17
- Chuvieco, E., & Huete, A. (2010). *Fundamentals of satellite remote sensing*. London
- David, T.S., Ferreira, M.I., Cohen, S., Pereira, J.S., & David, J.S. (2004). Constraints on transpiration from an evergreen oak tree in southern Portugal. *Agricultural and Forest Meteorology*, 122, 193-205
- De Bruin, H.A.R. (2008). *Theory and application of large aperture scintillometers*. In: Scintec Corp.
- Diaz, M., Campos, P., & Pulido, F.J. (1997). *The Spanish dehesas: a diversity in land-use and wildlife*. San Diego: Pain, D. J. and Pienkowsky, M. W.
- Dugas, W.A., Fritschen, L.J., Gay, L.W., Held, A.A., Matthias, A.D., Reicosky, D.C., Steduto, P., & Steiner, J.L. (1991). Bowen ratio, eddy correlation, and portable chamber measurements of sensible and latent heat flux over

irrigated spring wheat. *Agricultural and Forest Meteorology*, 56, 1-20

- Egüen, M., Aguilar, C., Polo, M. J., Herrero, J., Millares, A., Losada, M.A., (2009). "WiMMed, a distribute physically-based watershed model(II): Application examples". In: Environmental Hydraulics: Theoretical, Experimental & Computational Solutions, López-Jiménez et al. (eds.), Taylor&Francis, London, pp.229-231
- Ehleringer, J., & Mooney, H.A. (1983). *Productivity of dessert and Mediterranean-climate plants*. Berlin, Germany: Springer-Berlag
- Foken, T. (2008). The Energy Balance Closure Problem: an overview. *Ecological Applications*, 18, 1351-1367
- Foken, T., Wimmer, F., Mauder, M., Thomas, C., & Liebethal, C. (2006). Some aspects of the energy balance closure problem. *Atmos. Chem. Phys.*, 6, 4395-4402
- Frangi, J.P., Garrigues, C., Haberstock, H., & Forest, F. (1996). Evapotranspiration and stress indicator through Bowen ratio method. In S.E. Camp CR, Yoder RE (Ed.), *Evapotranspiration and irrigation scheduling international conference*. (pp. 800-805). San Antonio, Texas
- Franssen, H.J.H., Stockli, R., Lehner, I., Rotenberg, E., & Seneviratne, S.I. (2010). Energy balance closure of eddy-covariance data: A multisite analysis for European FLUXNET stations. *Agricultural and Forest Meteorology*, 150, 1553-1567
- French, A.N., Schmugge, T.J., Kustas, W.P., Brubaker, K.L., & Prueger, J. (2003). Surface energy fluxes over El Reno, Oklahoma, using high-resolution remotely sensed data. *Water Resour. Res.*, 39, 1164
- Galmés, J., Medrano, H., & Flexas, J. (2007d). Photosynthetic limitations in response to water stress and recovery in Mediterranean plants with different growth forms. *New Phytologist*, 175, 81-93
- Gallé, A., & Feller, U. (2007). Changes of photosynthetic traits in beech saplings (*Fagus sylvatica*) under severe drought stress and during recovery. *Physiologia Plantarum*, 131, 412-421
- Gallé, A., Haldimann, P., & Feller, U. (2007). Photosynthetic performance and water relations in young pubescent oak (*Quercus pubescens*) trees during drought stress and recovery. *New Phytologist*, 174, 799-810
- Gallego, F.J., de Algaba, A.P., & Fernandez-Escobar, R. (1999). Etiology of oak decline in Spain. *European Journal of Forest Pathology*, 29, 17-27
- Garatuza-Payan, J., & Watts, C. (2005). The use of remote sensing for estimating ET of irrigated wheat and cotton in Northwest Mexico. *Irrigation and Drainage Systems*, 19, 301-320
- Gates, D.M. (1980). *Biophysical Ecology*. Dover, Mineola, NY
- Gillies, R.R., Kustas, W.P., & Humes, K.S. (1997). A verification of the 'triangle' method for obtaining surface soil water content and energy fluxes from remote measurements of the Normalized Difference Vegetation Index (NDVI) and surface e. *International Journal of Remote Sensing*, 18, 3145-3166
- Glenn, E., Huete, A., Nagler, P., & Nelson, S. (2008). Relationship Between Remotely-sensed Vegetation Indices, Canopy Attributes and Plant Physiological Processes: What Vegetation Indices Can and Cannot Tell Us About the Landscape. *Sensors*, 8, 2136-2160
- Gonzalez-Dugo, M.P., Escuin, S., Cano, F., Cifuentes, V., Padilla, F.L.M., Tirado, J.L., Oyonarte, N., Fernandez, P., & Mateos, L. (2013). Monitoring evapotranspiration of irrigated crops using crop coefficients derived from

- time series of satellite images. II. Application on basin scale. In (pp. 92-104)
- Gonzalez-Dugo, M.P., & Mateos, L. (2008). Spectral vegetation indices for benchmarking water productivity of irrigated cotton and sugarbeet crops. *Agricultural Water Management*, 95, 48-58
- Gonzalez-Dugo, M.P., Neale, C.M.U., Mateos, L., Kustas, W.P., Prueger, J.H., Anderson, M.C., & Li, F. (2009). A comparison of operational remote sensing-based models for estimating crop evapotranspiration. *Agricultural and Forest Meteorology*, 149, 1843-1853
- Gordon, H.R., & Morel, A.Y. (1983). *Remote Assessment of Ocean Color for Interpretation of Satellite Visible Imagery: A review*. New York: John Wiley & Sons, Ltd
- Grebet, P., & Cuenca, R.H. (1991). History of lysimeter design and effects of environmental disturbances. In R.G.H. Allen, T.A.; Pruitt, W.O.; Walter, I.A.; Jensen, M.E. (Ed.), *Lysimeter for evapotranspiration and environmental measurements*. (pp. 11-18). New York: American Society of Civil Engineers
- Grove, A.T., & Rackham, O. (2003). *The Nature of Mediterranean Europe. An Ecological History*. New Haven: Yale University Press
- Gulías, J., Flexas, J., Abadía Bayona, A., & Medrano Gil, H. (2002). Photosynthetic responses to water deficit in six Mediterranean sclerophyll species: possible factors explaining the declining distribution of *Rhamnus ludovici-salvatoris*, an endemic Balearic species. *Tree Physiol.*, 22, 687-769
- Guzinski, R., Anderson, M.C., Kustas, W.P., Nieto, H., & Sandholt, I. (2013). Using a thermal-based two source energy balance model with time-differencing to estimate surface energy fluxes with day-night MODIS observations. *Hydrol. Earth Syst. Sci.*, 17, 2809-2825
- Hartogensis, O.K., Watts, C.J., Rodriguez, J.C., & De Bruin, H.A.R. (2003). Derivation of an Effective Height for Scintillometers: La Poza Experiment in Northwest Mexico. In *Journal of Hydrometeorology* (pp. 915-928): American Meteorological Society
- Hatfield, J.L. (1997). Plant-water interactions, Chapter 3. In C.L. Publishers (Ed.), *Plants for Environmental Studies* (pp. 81-103). New York
- Herrero, J., Aguilar, C., Egüen, M., Carpintero, M., Polo, M. J., Losada, M. A, (2010). [WiMMed. *Manual de usuario v1.1*], Grupo de Dinámica de Flujos Ambientales (Universidad de Granada) and Grupo de Hidrología e Hidráulica Agrícola (Universidad de Córdoba), España.
- Hillel, D. (1998). *Evaporation from bare soil and wind erosion*. San Diego: Academic Press
- Holmes, J.W. (1984). Measuring evapotranspiration by hydrological methods. *Agricultural Water Management*, 8, 29-40
- Horst, T.W. (2000). On Frequency Response Corrections for Eddy Covariance Flux Measurements. *Boundary-Layer Meteorology*, 94, 517-520
- Huete, A., Didan, K., Miura, T., Rodriguez, E.P., Gao, X., & Ferreira, L.G. (2002). Overview of the radiometric and biophysical performance of the MODIS vegetation indices. *Remote Sensing of Environment*, 83, 195-213
- Huete, A.R. (1988). A soil-adjusted vegetation index (SAVI). *Remote Sensing of Environment*, 25, 295-309
- Idso, S.B., & Baker, D.G. (1967). Relative importance of radiation, convection and transpiration in heat transfer

from plants. *Plant Physiology*, 42, 631-640

Infante, J.M., Domingo, F., Fernandez Alos, R., Joffre, R., & Rambal, S. (2003). Quercus ilex Transpiration as Affected by a Prolonged Drought Period. *Biologia Plantarum*, 46, 49-55

Infante, J.M., Rambal, S., & Joffre, R. (1997). Modelling transpiration in holm-oak savannah: scaling up from the leaf to the tree scale. *Agricultural and Forest Meteorology*, 87, 273-289

Jackson, R.D., Idso, S.B., Reginato, R.J., & Pinter, P.J. (1981). Canopy temperature as a crop water stress indicator. *Water Resources Research*, 17, 1133-1138

Jensen, J.R. (2000). *Remote Sensing of the Environment: An Earth Resource Perspective, 2000*. New Jersey

Joffre, R., & Rambal, S. (1993). How Tree Cover Influences the Water Balance of Mediterranean Rangelands. *Ecology*, 74, 570-582

Kaimal, J.C., & Finnigan, J.J. (1994). *Atmospheric boundary layer flows: Their structure and measurement*. New York

Kalma, J.D., & Jupp, D.L.B. (1990). Estimating evaporation from pasture using infrared thermometry: evaluation of a one-layer resistance model. *Agricultural and Forest Meteorology*, 51, 223-246

Katerji, N., Daudet, F.A., Carbonneau, A., & Ollat, N. (1994). Photosynthesis and transpiration studies with traditionally and lyre-trained vines. *Vitis*, 33, 197-203

Kaufman, Y.J., & Sendra, C. (1988). Algorithm for automatic atmospheric corrections to visible and near-IR satellite imagery. *International Journal of Remote Sensing*, 9, 1357-1381

Kolle, O., & Reibmann, C. (2007). *EddySoft. Documentation of a Software Package to Acquire and Process Eddy Covariance Data. Technical Reports*

Kormann, R., & Meixner, F. (2001). An Analytical Footprint Model For Non-Neutral Stratification. *Boundary-Layer Meteorology*, 99, 207-224

Kustas, W.P., Choudhury, B.J., Moran, M.S., Reginato, R.J., Jackson, R.D., Gay, L.W., & Weaver, H.L. (1989). Determination of sensible heat flux over sparse canopy using thermal infrared data. *Agricultural and Forest Meteorology*, 44, 197-216

Kustas, W.P., & Daughtry, C.S.T. (1990). Estimation of the soil heat flux/net radiation ratio from spectral data. *Agricultural and Forest Meteorology*, 49, 205-223

Kustas, W.P., & Norman, J.M. (1996). Use of remote sensing for evapotranspiration monitoring over land surfaces. *Hydrological Sciences Journal*, 41, 495 - 516

Kustas, W.P., & Norman, J.M. (1997). A two-source approach for estimating turbulent fluxes using multiple angle thermal infrared observations. *Water Resources Research*, 33, 1495-1508

Kustas, W.P., & Norman, J.M. (1999). Evaluation of soil and vegetation heat flux predictions using a simple two-source model with radiometric temperatures for partial canopy cover. *Agricultural and Forest Meteorology*, 94, 13-29

Lagouarde, J.P., Kerr, Y.H., & Brunet, Y. (1995). An experimental study of angular effects on surface temperature for various plant canopies and bare soils. *Agricultural and Forest Meteorology*, 77, 167-190

- Lee, X., Massman, W.J., & Law, B. (2004). *Handbook of Micrometeorology: A Guide for Surface Flux Measurement and Analysis*.
- Lenoble, J. (1993). *Atmospheric Radiative Transfer*. Hampton, Virginia
- Lewis, D., Singer, M.J., Dahlgren, R.A., & Tate, K.W. (2000). Hydrology in a California oak woodland watershed: a 17-year study. *Journal of Hydrology*, 240, 106-117
- Lewis, D.C., & Burgoyne, R.H. (1964). The Relationship between oak tree roots and groundwater in fractured rock as determined by tritium tracing. *Journal of Geophysical Research*, 69, 2579-2588
- Lhomme, J.P., Monteny, B., & Amadou, M. (1994). Estimating sensible heat flux from radiometric temperature over sparse millet. *Agricultural and Forest Meteorology*, 68, 77-91
- Liang, X., Wood, E.F., & Lettenmaier, D.P. (1996). Surface soil moisture parameterization of the VIC-2L model: Evaluation and modification. *Global and Planetary Change*, 13, 195-206
- Limousin, J.-M., Rambal, S., Ourcival, J.-M., Rodriguez-Calcerrada, J., Perez-Ramos, I.M., Rodriguez-Cortina, R., Misson, L., & Joffre, R. (2012). Morphological and phenological shoot plasticity in a Mediterranean evergreen oak facing long-term increased drought. *Oecologia*, 169, 565-577
- Limousin, J.M., Rambal, S., Ourcival, J.M., Rocheteau, A., Joffre, R., & Rodriguez-Cortina, R. (2009). Long-term transpiration change with rainfall decline in a Mediterranean Quercus ilex forest. *Global Change Biology*, 15, 2163-2175
- López-Urrea, R. (2004). *Evapotranspiración de referencia: Métodos de cálculo y medición directa en una estación lisimétrica en ambientes semiáridos*. Tesis Doctoral. Universidad de Castilla-La Mancha, Albacete.
- Mahrt, L., & Vickers, D. (2004). Bulk Formulation of the Surface Heat Flux. *Boundary-Layer Meteorology*, 110, 357-379
- Martínez-Ferri, E., Balaguer, L., Valladares, F., Chico, J.M., & Manrique, E. (2000). Energy dissipation in drought-avoiding and drought-tolerant tree species at midday during the Mediterranean summer. *Tree Physiol.*, 20, 131-138
- Massman, W.J. (2000). A simple method for estimating frequency response corrections for eddy covariance systems. *Agricultural and Forest Meteorology*, 104, 185-198
- Massman, W.J. (2001). Reply to comment by Rannik on "A simple method for estimating frequency response corrections for eddy covariance systems" *Agricultural and Forest Meteorology*, 107, 247-251
- Matzner, S., Rice, K., & Richards, J. (2003). Patterns of stomatal conductance among blue oak (*Quercus douglasii*) size classes and populations: implications for seedling establishment. *Tree Physiology*, 23, 777-784
- Mauder, M., & Foken, T. (2013). *Documentation and Instruction Manual of the Eddy-Covariance Software Package TK3*: Universitaet Bayreuth
- McCaughey, J.H. (1985). Energy balance storage terms in a mature mixed forest at Petawawa, Ontario "A case study. *Boundary-Layer Meteorology*, 31, 89-101
- Mediavilla, S., & Escudero, A. (2003). Stomatal responses to drought at a Mediterranean site: a comparative study of co-occurring woody species differing in leaf longevity. *Tree Physiology*, 23, 987-996

- Meijninger, W.M.L., & de Bruin, H.A.R. (2000). The sensible heat fluxes over irrigated areas in western Turkey determined with a large aperture scintillometer. *Journal of Hydrology*, 229, 42-49
- Meijninger, W.M.L., Hartogensis, O.K., Kohsiek, W., Hoedjes, J.C.B., Zuurbier, R.M., & De Bruin, H.A.R. (2002). Determination of Area-Averaged Sensible Heat Fluxes with a Large Aperture Scintillometer over a Heterogeneous Surface - Flevoland Field Experiment. *Boundary-Layer Meteorology*, 105, 37-62
- Meyers, T.P., & Hollinger, S.E. (2004). An assessment of storage terms in the surface energy balance of maize and soybean. *Agricultural and Forest Meteorology*, 125, 105-115
- Moncrieff, J.B., Clement, R., Finnigan, J., & Meyers, T. (2010). Averaging, detrending, and filtering of eddy covariance time series. Chapter 2. In X. Lee, Massman, W., Law, B. (Ed.), *Handbook of Micrometeorology: A Guide for Surface Flux Measurement and Analysis*. (pp. 7–31). Dordrecht: Kluwer Academic Publishers
- Montoya, J.M. (1998). *Método de ordenación silvopastoral. La dehesa, aprovechamiento sostenible de los recursos naturales*. Madrid: Editorial Agrícola Española
- Mooney, H., & Dunn, E.L. (1970). Photosynthetic systems of Mediterranean climate shrubs and trees of California and Chile. *American Naturalist*, 104
- Moran, M.S. (2003). Thermal infrared measurement as an indicator of plant ecosystem health. In D.A.Q.a.J. Luvall (Ed.), *Thermal Remote Sensing in Land Surface Processes* (pp. 257-282). Philadelphia, Pa: Taylor and Francis
- Moran, M.S., Clarke, T.R., Inoue, Y., & Vidal, A. (1994). Estimating crop water deficit using the relation between surface-air temperature and spectral vegetation index. *Remote Sensing of Environment*, 49, 246-263
- Moran, M.S., Inoue, Y., & Barnes, E.M. (1997). Opportunities and limitations for image-based remote sensing in precision crop management. *Remote Sensing of Environment*, 61, 319-346
- Moran, M.S., Peters-Lidard, C.D., Watts, J.M., & McElroy, S. (2004). Estimating soil moisture at the watershed scale with satellite-based radar and land surface models. *Canadian Journal of Remote Sensing*, 30, 805-826
- Morillas, L., Garcia, M., Nieto, H., Villagarcia, L., Sandholt, I., Gonzalez-Dugo, M.P., Zarco-Tejada, P.J., & Domingo, F. (2013). Using radiometric surface temperature for surface energy flux estimation in Mediterranean drylands from a two-source perspective. *Remote Sensing of Environment*, 136, 234-246
- Munger, J.W., & Loescher, H.W. (2008). *Ameriflux Guidelines for Making Eddy Covariance Flux Measurements*. Ameriflux
- Norman, J.M., Kustas, W.P., & Humes, K.S. (1995). A two - source approach for estimating soil and vegetation energy fluxes in observations of directional radiometric surface temperature. *Agricultural and Forest Meteorology*, 77, 263-293
- Ogaya, R., & Penuelas, J. (2006). Contrasting foliar responses to drought in *Quercus ilex* and *Phillyrea latifolia*. *Biologia Plantarum*, 50, 373-382
- Paço, T.A., David, T.S., Henriques, M.O., Pereira, J.S., Valente, F., Banza, J., Pereira, F.L., Pinto, C., & David, J.S. (2009). Evapotranspiration from a Mediterranean evergreen oak savannah: The role of trees and pasture.

Journal of Hydrology, 369, 98-106

- Papanastasis, V.P. (2004). *Vegetation degradation and land use changes in agrosilvopastoral systems*. Catena Verlag, Reiskirchen, Germany: Advances in GeoEcology
- Parkhurst, D.F., & Loucks, O.L. (1972). Optimal Leaf Size in Relation to Environment. *Journal of Ecology*, 60, 505-537
- Pavlik, B.M., Muick, P.C., Johnson, S.G., & Popper, M. (1991). *Oaks of California*. Los Olivos, CA: Cachuma Press
- Paw U, K., Baldocchi, D., Meyers, T., & Wilson, K. (2000). Correction Of Eddy-Covariance Measurements Incorporating Both Advective Effects And Density Fluxes. *Boundary-Layer Meteorology*, 97, 487-511
- Penman, H.L. (1948). Natural Evaporation from Open Water, Bare Soil and Grass. *Proceedings of the Royal Society of London. Series A. Mathematical and Physical Sciences*, 193, 120-145
- Pereira, J.S., & Chaves, M.M. (1993). *Plant water deficits in Mediterranean ecosystems*. Oxford: Bios Scientific Publishers
- Pérez-Priego, O., Testi, L., Kowalski, A.S., Villalobos, F.J., & Orgaz, F. (2014). Aboveground respiratory CO₂ effluxes from olive trees (*Olea europaea* L.). *Agroforestry Systems*, 88, 245-255
- Perry, E.M., & Moran, M.S. (1994). An evaluation of atmospheric corrections of radiometric surface temperatures for a semiarid rangeland watershed. *Water Resour. Res.*, 30, 1261-1269
- Plieninger, T., & Wilbrand, C. (2001). Land use, biodiversity conservation, and rural development in the dehesas of Cuatro Lugares, Spain. *Agroforestry Systems*, 51, 23-34
- Polo, M. J., Herrero, J., Aguilar, C., Millares, A., Moñino, A., Nieto, S., Losada, M. A.,(2009). WiMMed, a distributed physically-based watershed model (I): Description and validation. *Environmental Hydraulics: Theoretical, Experimental & Computational Solutions*.225-228 (2009).
- Pulido, F.J., & Diaz, M. (2005). Regeneration of a Mediterranean oak: a whole cycle approach. *Ecoscience*, 12, 92-102
- Rambal, S. (1993). The differential role of mechanisms for drought resistance in a Mediterranean evergreen shrub: a simulation approach. *Plant, Cell & Environment*, 16, 35-44
- Rana, G., & Katerji, N. (2000). Measurement and estimation of actual evapotranspiration in the field under Mediterranean climate: a review. *Eur. J. Agron.*, 13, 125-153
- Rannik, Ü. (2001). A comment on the paper by W.J. Massman "A simple method for estimating frequency response corrections for eddy covariance systems". *Agricultural and Forest Meteorology*, 107, 241-245
- Reicosky, D.C., & Peters, D.B. (1977). A portable chamber for rapid evapotranspiration measurements on field plots *Agronomy journal.*, 69, 729-732
- Richards, J.A., & Jia, X. (2006). *Remote Sensing Digital Image Analysis: An Introduction*
- Ripullone, F., Borghetti, M., Raddi, S., Vicinelli, E., Baraldi, R., Guerrieri, M., Noa , A., & Magnani, F. (2009). Physiological and structural changes in response to altered precipitation regimes in a Mediterranean macchia ecosystem. *Trees*, 23, 823-834
- Rose, C.W., & Sharma, M.L. (1984). Summary and recommendations of the workshop on evapotranspiration of

- plant communities. *Agricultural Water Management*, 8, 328-342
- Rossi, S., Rampini, A., Bocchi, S., & Boschetti, M. (2010). Operational Monitoring of Daily Crop Water Requirements at the Regional Scale with Time Series of Satellite Data. *Journal of Irrigation and Drainage Engineering*, 136, 225-231
- Sakai, R.K., Fitzjarrald, D.R., & Moore, K.E. (2001). Importance of Low-Frequency Contributions to Eddy Fluxes Observed over Rough Surfaces. In, *Journal of Applied Meteorology* (pp. 2178-2192): American Meteorological Society
- Sánchez, M.E., Caetano, P., Ferraz, J., & Trapero, A. (2002). Phytophthora disease of Quercus ilex in south-western Spain. *Forest Pathology*, 32, 5-18
- Saunders, R.W., & Kriebel, K.T. (1988). An improved method for detecting clear sky and cloudy radiances from AVHRR data. *International Journal of Remote Sensing*, 9, 123-150
- Scott, R.L., Huxman, T.E., Cable, W.L., & Emmerich, W.E. (2006). Partitioning of evapotranspiration and its relation to carbon dioxide exchange in a Chihuahuan Desert shrubland. *Hydrological Processes*, 20, 3227-3243
- Schnabel, S., & Ferreira, A. (2004). *Prologue*. Catena Verlag, Reiskirchen, Germany: Advances in GeoEcology
- Schuepp, P.H., Leclerc, M.Y., MacPherson, J.I., & Desjardins, R.L. (1990). Footprint prediction of scalar fluxes from analytical solutions of the diffusion equation. *Boundary-Layer Meteorology*, 50, 355-373
- Sette, D. (1977). *Elementi di Fisica*: Patron
- Sharma, M.L., & Daniel, H. (1985). Estimating Evapotranspiration. *Advances in Irrigation* (pp. 213-281): Elsevier
- Shuttleworth, W., & Wallace, J. (1985). Evaporation from sparse crops: an energy combination theory. *Q. J. R. Meteorol. Soc.*, 111, 1143-1162
- Soegaard, H., Jensen, N.O., Boegh, E., Hasager, C.B., Schelde, K., & Thomsen, A. (2003). Carbon dioxide exchange over agricultural landscape using eddy correlation and footprint modelling. *Agricultural and Forest Meteorology*, 114, 153-173
- Su, Z. (1999). The Surface Energy Balance System (SEBS) for estimation of turbulent heat fluxes. *Hydrol. Earth Syst. Sci.*, 6, 85-100
- Tanner, B.D. (1988). Use requirements for Bowen ratio and eddy correlation determination of evapotranspiration. . In D.R. Hay (Ed.), *Planning Now for Irrigation and Drainage in the 21st Century, Proc., Irrig. and Drain. Div, Conf. ASCE* (pp. 605–616). Lincoln, NE, USA: Hay, D.R.
- Tanner, B.D., Swiatek, E., & Green, J.P. (1993). Density fluctuations and use of the krypton hygrometer in surface flux measurements. In R.G.a.N. Allen, C. M. U. American Society of Civil Engineers (Ed.), *Management of Irrigation and Drainage Systems: Integrated Perspectives. National Conference on Irrigation and Drainage Engineering*. (pp. 105-112). Park City, UT. ASCE, New York
- Taylor, S. (1975). *Optimal leaf form*. New York: Springer-Verlag;
- Timmermans, W.J., Kustas, W.P., Anderson, M.C., & French, A.N. (2007). An intercomparison of the Surface Energy Balance Algorithm for Land (SEBAL) and the Two-Source Energy Balance (TSEB) modelling schemes. *Remote Sensing of Environment*, 108, 369-384

- Twine, T.E., Kustas, W.P., Norman, J.M., Cook, D.R., Houser, P.R., Meyers, T.P., Prueger, J.H., Starks, P.J., Wesely, M.L. (2000). Correcting eddy-covariance flux underestimates over a grassland. *Agric. For. Meteorol.*, 103, 279–300
- van Dijk, A., Moene, A., & De Bruin, H.A.R. (2004). The principles of surface flux physics: theory, practice and description of the ECPACK library. In M.a.A.Q. Group (Ed.), *Internal Report 2004/1* (p. 99). Wageningen, the Netherlands: Wageningen University
- Villalobos, F.J. (1997). Correction of eddy covariance water vapor flux using additional measurements of temperature. *Agricultural and Forest Meteorology*, 88, 77-83
- Villar-Salvador, P., Ocaña, L., Peñuelas, J.L., Carrasco, I., & Domínguez, S. (1997). Efecto de diferentes niveles de endurecimiento por estrés hídrico en el contenido de nutrientes y la resistencia a la desecación en *Pinus halepensis*. In Mill (Ed.), *Actas del I Congreso Forestal Hispano-Luso* (pp. 673-678)
- Wagner, S.W., & Reicosky, D.C. (1996). Mobile research gas exchange machine-MRGEM instrumentation update. In E.J. Camp, C.R. Sandler, Yoder, R.E. (Ed.), *Evapotranspiration and irrigation scheduling*. (pp. 781-786). San Antonio TX
- Wilson, K., Goldstein, A., Falge, E., Aubinet, M., Baldocchi, D., Berbigier, P., Bernhofer, C., Ceulemans, R., Dolman, H., Field, C., Grelle, A., Ibrom, A., Law, B.E., Kowalski, A., Meyers, T., Moncrieff, J., Monson, R., Oechel, W., Tenhunen, J., Verma, S., & Valentini, R. (2002). Energy Balance Closure at FLUXNET Sites. *Agric. For. Meteorol.*, 113, 223-243
- Wittich, K.P., & Hansing, O. (1995). Area-averaged vegetative cover fraction estimated from satellite data. *International Journal of Biometeorology*, 38, 209-215
- Wood, E.F., Lettenmaier, D.P., & Zartarian, V.G. (1992). A land-surface hydrology parameterization with subgrid variability for general circulation models. *Journal of Geophysical Research: Atmospheres*, 97, 2717-2728
- Woodward, F.I. (1987). *Climate and plant distribution*. . Cambridge:: Cambridge University Press
- Xu, L., & Baldocchi, D.D. (2003). Seasonal trends in photosynthetic parameters and stomatal conductance of blue oak (*Quercus douglasii*) under prolonged summer drought and high temperature. *Tree Physiology*, 23, 865-877

Chapter 2: Modelling surface energy fluxes over a *dehesa* (oak savanna) ecosystem using a thermal based two-source energy balance model (TSEB)

The main results of this chapter are been prepared for publication in a peer review journal. Partial results have been previously presented at:

Andreu, A., Kustas, W. P., Polo, M. J., Anderson, M. C., González-Dugo, M. P., 2013. Modelling surface energy fluxes over a *dehesa* ecosystem using a two-source energy balance model and medium resolution satellite data. Proc. SPIE 8887, Remote Sensing for Agriculture, Ecosystems, and Hydrology XV, 888717 (16 October 2013); doi: [10.1117/12.2029235](https://doi.org/10.1117/12.2029235)

Andreu, A., W. P. Kustas, M. C. Anderson, A. Carrara and M. P. González-Dugo. *Seguimiento de los flujos de energía en superficie en una dehesa integrando datos térmicos en un modelo de doble fuente. (Monitoring surface energy fluxes in a dehesa with the integration of thermal data in a two-source model.* Asociación Española de Teledetección, Madrid, 2013.

Andreu, A., Kustas, W. P., Anderson, M. C., Carrara, A. and González-Dugo, M. P. 2013. *Modelling surface energy fluxes over a Dehesa ecosystem using a two-source energy balance model.* Geophysical Research Abstracts, Vol. 15, EGU2013-977, 2013, EGU General Assembly 2013.

Andreu, A., Graff, A., Polo, M. J., González-Dugo, M. P., 20. Medida de flujos de energía en superficie en un sistema adehesado y análisis de su distribución espacial con vistas a la integración con sensores remotos. Estudios en la Zona No Saturada del Suelo. Vol. XI ZNS'13. Lugo, 6-8 Noviembre 2013.

2.1 INTRODUCTION

Thermal-based energy balance techniques that distinguish between soil/substrate and vegetation contributions to radiative temperature and radiation/turbulent fluxes have been shown to be reliable for semi-arid sparse canopy-cover ecosystems. In particular the two-source energy balance (TSEB) model of *Norman et al. (1995)* and *Kustas and Norman (1999)* has been shown to be robust in partially-vegetated landscapes (*Timmermans, 2007; González-Dugo, 2009*). However, there are few studies of the application of these models over Mediterranean woody ecosystems (*Cammalleri et al., 2010; Morillas et al., 2013*), a challenging issue due to the complex canopy structure. These ecosystems comprise heterogeneous canopy mosaics with very sparse (~20%) tall vegetation cover (generally evergreen sclerophyll trees) and large areas of understorey scrub, grass and bare soil, highly influencing the turbulent and radiative exchanges. They exist under arid or semi-arid conditions, which together with the large variability in precipitation (*Baldocchi and Xu, 2007*) lead to severe and frequent droughts; the vegetation is adapted to the surrounding conditions via mechanisms to face water scarcity that need to be integrated into the models.

Because they are located over rainfall transition areas and receive scarcely-enough water to support the canopy (*Woodward, 1987; Brasier, 1993*), climate change will affect their status. An in depth analysis of the climatic and soil conditions and the biotic and abiotic factors that control ET from Mediterranean woody crops and natural lands is needed to assess how this process will affect the regional water balance in next few years. To do so, we need to gain insight into ecosystem structure and functions (e.g. radiation, energy and water fluxes), that require the partitioning of the system between vegetation layers that differ in phenology and functioning, and the soil. While the trees are evergreen and may have access to sources of water all the year round (*David et al., 2004; Campos et al., 2013*), the herbaceous layer which dries out before the summer months depends on top soil moisture (*Joffre and Rambal, 1993; Baldocchi et al., 2004*). The ecosystem therefore cannot be considered as a single, spatially uniform layer for water and energy flux exchanges.

An example of one such complex landscape is *dehesa*, a combination of an agricultural and a naturally vegetated ecosystem, consisting of widely-spaced oak trees (mostly *Quercus ilex* and *Quercus suber*) combined with a sub-canopy comprised by herbaceous vegetation and scrubs. This ecosystem covers more than 3 million hectares between the Iberian Peninsula and Greece (*Grove and Rackham, 2003*;

Papanastasis, 2004). It is a Habitat of Community Interest (*Annex 1 of the EU habitat directive, council directive 92/43/EEC*) supporting a large number of species and diversity, and due to its importance in rural economy and development (*Diaz et al., 1997; Plieninger and Wilbrand, 2001*). Although Iberian oaks have been defined as “regulatory” species in terms of water use (*Rambal, 1993*), with physiological mechanisms against water stress, soil water dynamics play a central role in the reduction of these woodlands (*Sánchez et al., 2002*). In the course of the past few decades, the *dehesa* has been exposed to various threats derived from socio-economic changes and intensive agricultural use (*Pulido and Díaz, 2005*), which have led to the degradation of the ecosystem: reduction in tree density due to lack of regeneration (*Diaz et al., 1997; Plieninger and Wilbrand, 2001; Plieninger and Schaar, 2008*), soil degradation (*Shakesby et al., 2002*) such as compaction and erosion (*Montoya, 1998; Coelho et al., 2004; Schnabel and Ferreira, 2004; Pulido and Díaz, 2005*) and a reduction in plant establishment (*Basset et al., 2005*) and herbaceous diversity (*Godefroid and Koedam, 2004*). Understanding the processes that drive ecosystem functioning will improve the management and the conservation of this system, given that transpiration rate is a primary indicator of the forest health (*Moran et al., 2004*), particularly in this water-scarce environment.

In order to integrate this complex vegetation structure, a revision of the TSEB formulation has addressed the following main issues: 1) energy storage within the biomass, 2) roughness length and zero displacement plane 3) and 4) wind speed profile modelling. The first was estimated via a simple approach (*Stewart and Thom, 1973; Stewart, 1978*) due to the difficulties of obtaining representative ground-truth measurements. The Priestley-Taylor coefficient was evaluated by means of a statistical model application (*Agam et al., 2010*). For the wind speed profile two approaches have been proposed to incorporate the canopy layers (trees and grasses): a modification in the wind profile and a "weighted average" of the canopy parameters involved in the estimation of the ET (including height, roughness length, leaf area index, leaf angle distribution and leaf size). Velocity profile and roughness length modelling have been evaluated using wind profile measurements at different heights, using different formulations (*Goudriaan, 1977; Massman, 1987; Lalic et al., 2003; Nakai et al., 2008*).

2.2 MATERIALS AND METHODS

Data from two different *dehesa* sites equipped with energy flux measurement systems were used to evaluate TSEB; one was installed in Southern Spain (Santa Clotilde, *Andalucía*, 39°56' N; 5°46' W, 736 m a.s.l) with a 1 km homogeneous fetch along the principal wind direction (SW) and the other in Southwestern Spain (Boyal de Majadas del Tiétar, Extremadura, ES-LMa, 39°56' N; 5°46' W, 260 m a.s.l) within the Fluxnet network, with a 1.5 km fetch on the NE wind direction and 2 km on the SW.

2.2.1 Study areas and ground-truth measurements.

2.2.1.1 Santa Clotilde

This site is part of the Natural Park *Sierra de Cardeña y Montoro*, in *Sierra Morena* (Fig. 2.1). It is a homogeneous landscape with smooth topography, gentle slopes (<10%) and a predominance of oaks (mostly *Quercus Ilex. L.*), sparse shrub vegetation (*Cistus ladanifer L. and C. albidus L.*) (Alameda *et al.*, 2010), and extensive livestock (pigs and cattle). The estimated mean age in years of the trees is 170 ($\sigma = 40$) (Alameda, 2010).

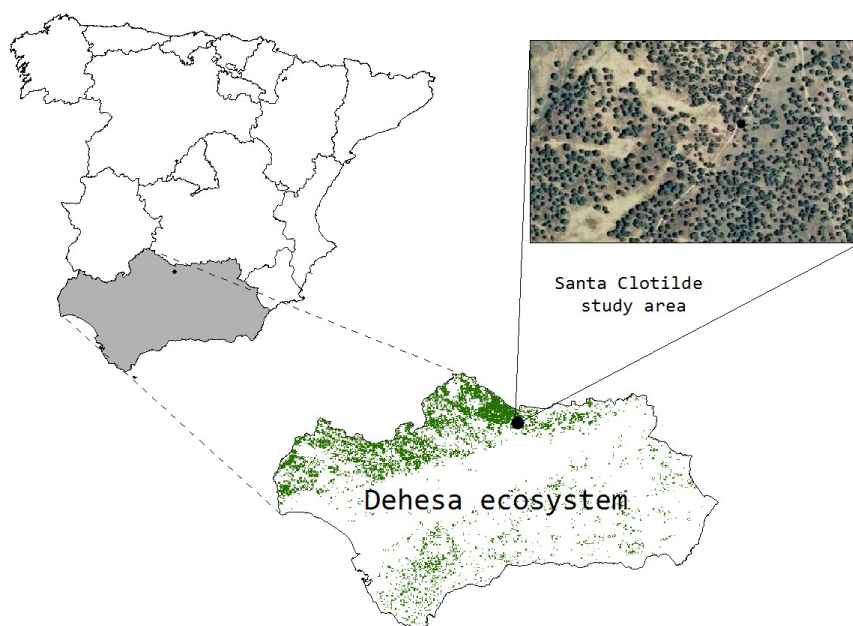


Figure 2.1: Location of site 1, Santa Clotilde study area and areas of dehesa system (in green) in Andalucía.

The continental Mediterranean climate in this area is characterized by an average annual rainfall of 720 mm, with cold winters, long dry summers and severe periodic droughts, the principal climatic characteristic being the annual variability and irregularity of rainfall. One km from the study area a maximum value of annual rainfall of 1800 mm was registered in 1960, and a minimum value of less than 300 mm in 1953. The average annual temperature is 15.3° C, with January the coldest month, with averages of 7° C and July the hottest, with 25.4° C on average. Soils are regosols mainly composed of sand with acid granitic bedrock (Quero *et al.*, 2007; Quero and Villar, 2009), with a maximum depth of 1.5 m, and 0.6 m on average. Bulk density (BD) was measured with a metallic cylinder of known height and diameter, being equal to 1.57 g/cm³. Alameda (2010) found a similar value for the first 2-7 soil centimeters and 1.77 for the portion between 9 and 14 cm.

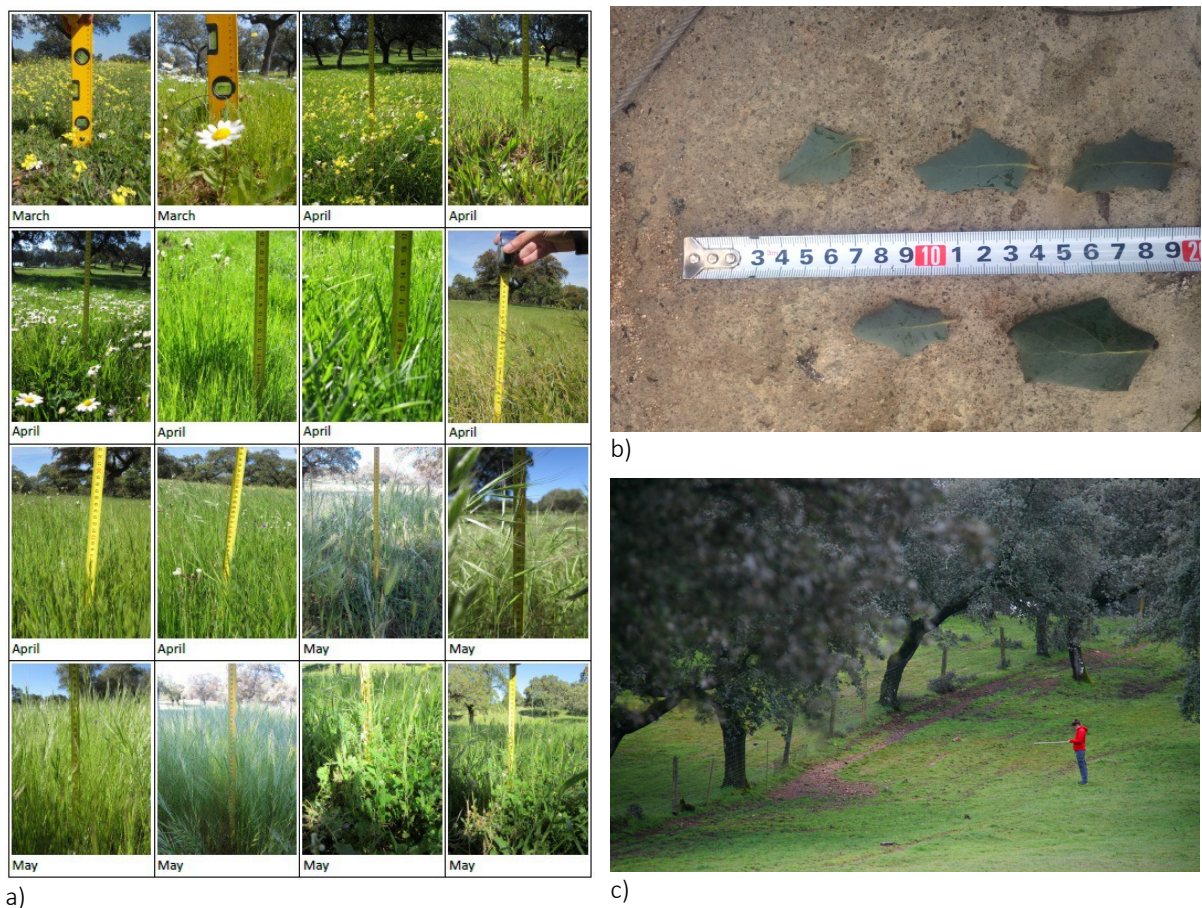


Figure 2.2: a) Measurements of height of the herbaceous layer in the Santa Clotilde study area. b) Example of oak leaves size and c) measurements of leaf area index over the area.

The fractional ground cover of the oaks (f_c) was calculated using image analysis techniques over a color orthophotography from 2007 (Source: *Sistema Cartográfico de Andalucía, Red de Información Ambiental de Andalucía*), which gave a value of ~ 0.20 for tree canopy cover. Water mass was masked, as were roads, paths or covers that could distort the estimation. Such low f_c values makes it difficult to monitor tree canopy cover with remote sensing data. As *Carreiras et al. (2006)* suggested, we selected a period with maximum spectral contrast between the overstorey and the understorey, in this case the dry summer, to estimate f_c . Significant parameters for the description of canopy structure were determined in the field (Fig. 2.2a,b), such as oak leaf size ($s = 0.02$ m), canopy height (h_c , with constant mean tree height of 8.5 m, and a seasonal variation for the grass layer, with a maximum height of 0.7 m in April/May and dry in the summer and winter periods), average height of the first branch (FBH = 2 m), average diameter of the trees measured at breast height located at 1.3 m (DBH = 1.52 m) and crown width estimated with high spatial resolution images (CW = 7m).

Leaf area index (LAI) measurements were made over the field using a linear Ceptometer AccuPAR (model LP-80, Decagon Devices) following the distribution of the ecosystem, integrating the relatively constant oak LAI along with the herbaceous layer LAI, with high seasonal variation (Fig. 2.2c). Only measurements on clear days, without cloud coverage and at nadir solar position (about 12 hours GMT) were made. Oak LAI data from another campaign were also evaluated (*Fernandez-Rebollo et al., 2009*).

Measurements of oak and grass spectral responses were made in the field during each growth state using a portable system to study the seasonal variability of the vegetation (Fig. 2.3). In addition, a number of leaves were collected and their spectral responses were measured in the laboratory (*Fernandez-Rebollo et al., 2009*). Reflectivity measurements were made using the ASD FieldSpec 3 (ASD Inc.) spectroradiometer, which registers radiance data in the range 350 – 2500 nm, for which a reference panel calibrated in a laboratory was used (Spectralon, Labsphere, North Sutton, NH) to measure incident radiation for calibration purposes. Measurements over this surface were made every 5 minutes (if atmospheric conditions over the field were very variable, between each target measurement).

Spectral measurements over the field were made without clouds and under stable weather conditions, between 11:00 – 13:00 GMT, in order to minimize the effects of shadowing and solar zenith changes. Around 20 samples with a bare fiber (FOV = 25°) were taken over different trees and regenerated

canopy, at 0.5 m height from the leaves, resulting in a circle with a diameter of 0.46 m. The understorey was more variable, with different species, canopy heights, fractional cover and green fractions. Fifty measurements were taken in the periods when the grass was not dry, at 1 m height above the soil, with a diameter of 0.93 m. The sampling strategy for leaf spectrum gathering is described in (Fernandez-Rebollo *et al.*, 2009).



Figure 2.3: Spectral information measurements over Santa Clotilde.

All energy balance components, R_n , G , H and LE , were measured directly over the field during the study period (15th April 2012 to 31th July 2014) and the system is still in operation (November 2014). Turbulent fluxes were measured by an eddy covariance system (ECT), based on the statistical covariance between the concentration of interest (temperature and water vapor) and vertical velocity of the turbulent eddies (Fig. 2.4). The equipment is installed at the top of an 18 m tower, due to the average canopy height, the slope and the homogeneous canopy cover. For turbulent components of surface energy balance, wind speed was measured with a CSAT 3D sonic anemometer (Campbell Scientific, Logan, UT), and specific humidity with a fast response hygrometer (KH20, Campbell

Scientific, Logan, UT). Temperature was determined sonically by the CSAT, and was corrected for moisture effects (Schotanus *et al.*, 1983). The anemometer was oriented in the prevailing wind direction (Southwest). The separation between the sensors was 20 cm, in accordance with the manufacturer's recommendations and the height of the tower. These measurements were recorded in a datalogger (CR1000, Campbell Scientific) at 10 Hz. For processing the data at high frequency, temperature and humidity were measured independently using a probe (HMP155, Vaisala, Helsinki, Finland,). A net radiometer (NR-Lite, Kipp & Zonen, Delft, The Netherlands) located in the tower measured net solar radiation, with no interference from the other instruments, and was corrected for wind speed measured with the sonic anemometer, in accordance with the manufacturer's recommendations (Campbell Scientific).



Figure 2.4: ECT installed in Santa Clotilde study area. CSAT 3D, KH20 and net radiometer over the grass.

Turbulent flux data require a post-processing that involves the removal of anomalies (Vickers and Mahrt, 1997), coordinate system transformations to prevent errors resulting from equipment alignment (Wilczak *et al.*, 2001), air-density fluctuation corrections (Webb *et al.*, 1980), a

correction for the oxygen absorption of the hygrometer (Tanner et al., 1993) and finally, the correction due to the separation of the sensors (Moore et al., 1986). For high vegetation and high measurement heights, the influence of the separation in the results is smaller, due to the larger eddies. (Kaimal and Finnigan, 1994; Lee et al., 2004; Foken et al., 2006). This process employed TK3 application (Mauder and Foken, 2013), which includes the necessary corrections and footprint analysis if required. After processing, half-hourly average values of the turbulent energy balance components were obtained. Soil heat flux was determined by ground heat flux plates (model HFP01, Hukseflux Thermal Sensors) installed in two grazing exclusion areas to take the heterogeneity of the area into account (Fig. 2.5), one located over open grass (EA1) and other under an oak (EA2), at a depth of 0.08 m, with two thermocouples buried at 0.02 and 0.06 m (Fuchs and Tanner, 1967). Although we made this attempt to characterize heterogeneity, a better distributed installation of the soil sensors over the area was hindered by the presence of rooting livestock (pigs) which would uproot the sensors if they were not set inside enclosures (Fig. 2.6).



Figure 2.5: Grazing exclusion areas over Santa Clotilde, a) EA1 and b) EA2.

Half-hour averages of the measurements taken every 5 seconds were recorded by another CR1000 datalogger. Heat flux on the ground was calculated by adding to the direct measurement of the soil heat fluxes at a particular depth, the energy stored in the layer above the flux plates (S_g). Changes in the calorific capacity and temperature soil over time are necessary for estimating energy storage:

$$S_g = \frac{(T_i - T_{i-1}) C_s D_{th}}{t} \quad (2.6)$$

where T_i is the actual temperature, T_{i-1} the temperature at the previous moment, D_{th} the soil heat flux plate depth [m], C_s the calorific capacity of the soil [$Jm^{-3}C^{-1}$] and t the time interval in seconds. For computing C_s , the soil density, the water content and specific heat of dry soil need to be known.



Figure 2.6: Porcine livestock in Santa Clotilde.

The soil water content was measured during the first study period (2012) as the difference between the wet and dry weights of five random samples, taken at intervals of 10 -15 days of frequency extracted every 30 cm until the maximum depth. For the rest of the period, five humidity soil probes (EnviroSCAN, Sentek Technologies, Stepney, Australia) measuring continuously at depths of 10, 30 and 50 cm, were installed inside the grazing exclusion areas (Fig. 2.7).

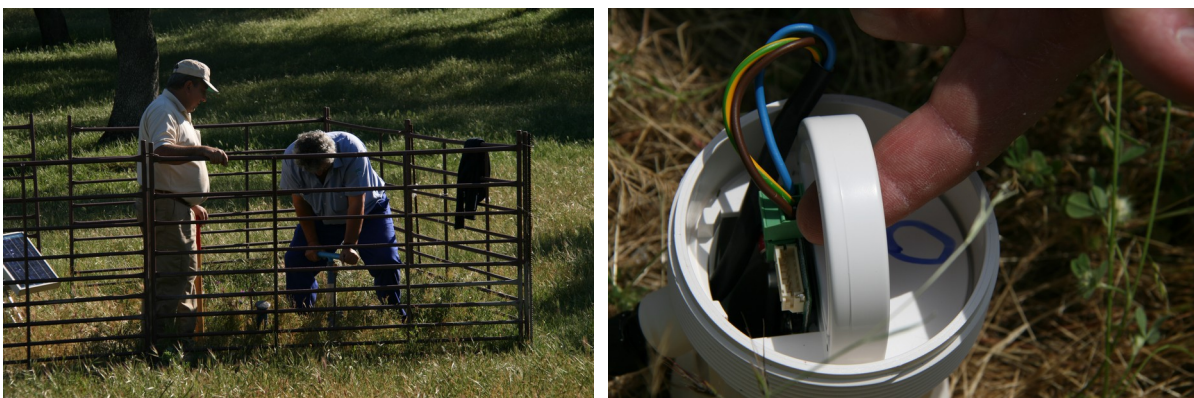


Figure 2.7: Soil humidity probes installed in Santa Clotilde study area.

Energy balance closure, a formulation of the first Law of Thermodynamics, requires that the sum of latent and sensible heat be equivalent to all other energy sinks and sources ($R_n - G = H + LE$). However, turbulent fluxes obtained by the method described are generally underestimated if the sum is compared with the available energy. Possible reasons can be found in the influence of horizontal advection, energy storage in canopies, flux divergences, photosynthesis, errors in measurements of R_n or G , frequency response of the sensors, measurement errors on turbulent fluxes, and separation of the instruments. The average error is around 20% - 30% (Twine *et al.*, 2000; Wilson *et al.*, 2002; Foken, 2008; Franssen *et al.*, 2010). Twine *et al.* (2000) compared different methods to force balance closure (BC), either keeping the Bowen ratio (ratio between H and LE) or assuming that H is measured accurately and solving LE as a residual of the energy-balance equation. In this case, even if we prefer to not close the balance because of existing uncertainties in R_n and G measurements, due to failures in the calibration of KH20 during 2013 summer period, LE values were calculated forcing the closure of the EB with the residual method, in order to be able to use the whole data series after studying the BC for the periods with all fluxes measured. This method is used when measurements of R_n , G and H are accurate (Kizer *et al.* 1990; Kelliher *et al.*, 1990; Diawara *et al.*, 1991; Mizutani *et al.*, 1997) as we consider to be the case here, due to the closure balance error obtained.

For ecosystems with tall vegetation, Foken, (2008) suggested that it would be useful to incorporate energy storage within the biomass (S), underlining that this could be a relevant flux in the total energy balance equation. S has been estimated in this ecosystem through a simple approach (Stewart and Thom, 1973; Stewart, 1978), due the difficulty of measuring it on field scale (Wilson *et al.*, 2001), as a proxy of this EB component magnitude. To determine the area that contributes most to the measured fluxes at the tower and assure sufficient fetch for remote sensing integration (Fig. 2.8), an approximate solution for the contribution to the vertical flux (Schuepp *et al.*, 1990) was computed. An additional analysis was also performed by TK3 software, using the Kormann and Meixner (2001) model, and determining the influence of the target land-use in the fluxes measured.

A meteorological station was installed inside the open grass exclusion area, which measured certain variables required by the EB model, such as solar direct radiation (Fig. 2.9b, piranometer, LP02 model, Campbell Scientific, Logan, UT), the rainfall using a pluviometer (ARG100 Tipping Bucket Raingauge, EML, UK), and grass/soil temperature (IRTS, Campbell Scientific, Logan, UT). An

infrared thermometer (SI 111, Campbell Scientific) was installed on the tower, and measured oak tree temperature continuously. Both of these temperatures were corrected for tree and grass or soil emissivity, with standard previously published values (*Campbell and Norman, 1998*). Due to the IRTS field of view (FOV), the oak canopy temperature has a slight bias caused by the part of bare soil seen from the top of the tower (<10%), although this value will vary depending on the season due to changes in oak phenology (Fig. 2.9a).



Figure 2.8: Wind components fetch of Santa Clotilde study area.

The eddy covariance instrumentation is located on a platform over an elevator that can ascend from 3 m (soil level) to 17 m (close to the top of the tower). The system leverage was checked every month on the top of the tower. Every 15 days, and coinciding with the cleaning of the system and other field measurements, the wind profile was measured at heights of 17, 12, 7 and 3 m, during the half-hour averaging period.

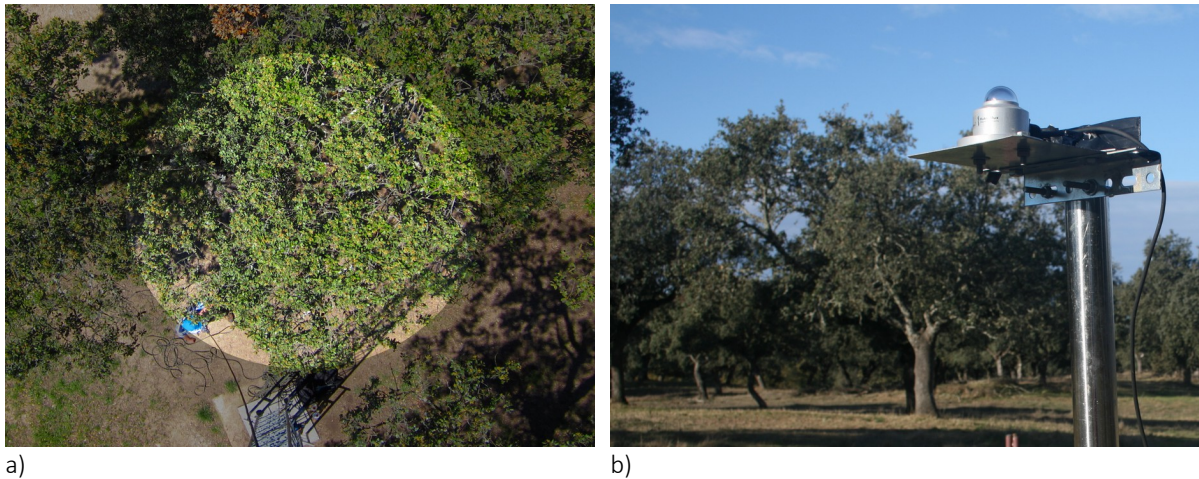


Figure 2.9: a) FOV of the SI111 installed over the oak and b) pyranometer installed in EA1.

2.2.1.2 Las Majadas del Tietar.

The second study area is located in central Spain (Boyal de Majadas del Tiétar, ES-LMa, 39°56' N; 5°46' W, 260 m a.s.l), part of FluxNet, CarboEurope network (Fig. 2.10). The ecosystem is a typical *dehesa* composed of *Quercus Ilex spp.* accompanied by a herbaceous understorey with very high species diversity, with gentle slopes (<5%). Mean oak height is around eight meters, with a mean DBH (measured in October 2006) of 0.45 m. Ten per cent of the trees are pruned every winter (in January); each tree is thus pruned approximately every 10 years. The farm is continuously grazed by cows and sheep. The mean estimated standard tree age based on a size-age empirical relationship (*Plieninger et al., 2003*) is 105 years, with a standard deviation of 23. Mean annual temperature is 16.7° C and the annual precipitation is around 530 mm. Predominant wind directions are southwest (250°) and northeast (70°), with homogeneous fetches of more than 2 km and 1.5 km respectively. Soil type is a stagnic alisol (ochric, argic, stagnig pp.9), with depths greater than 0.8 m, and a bulk density of 1.59 g/cm³. The ground fractional cover of the oaks (f_c) is 0.20.

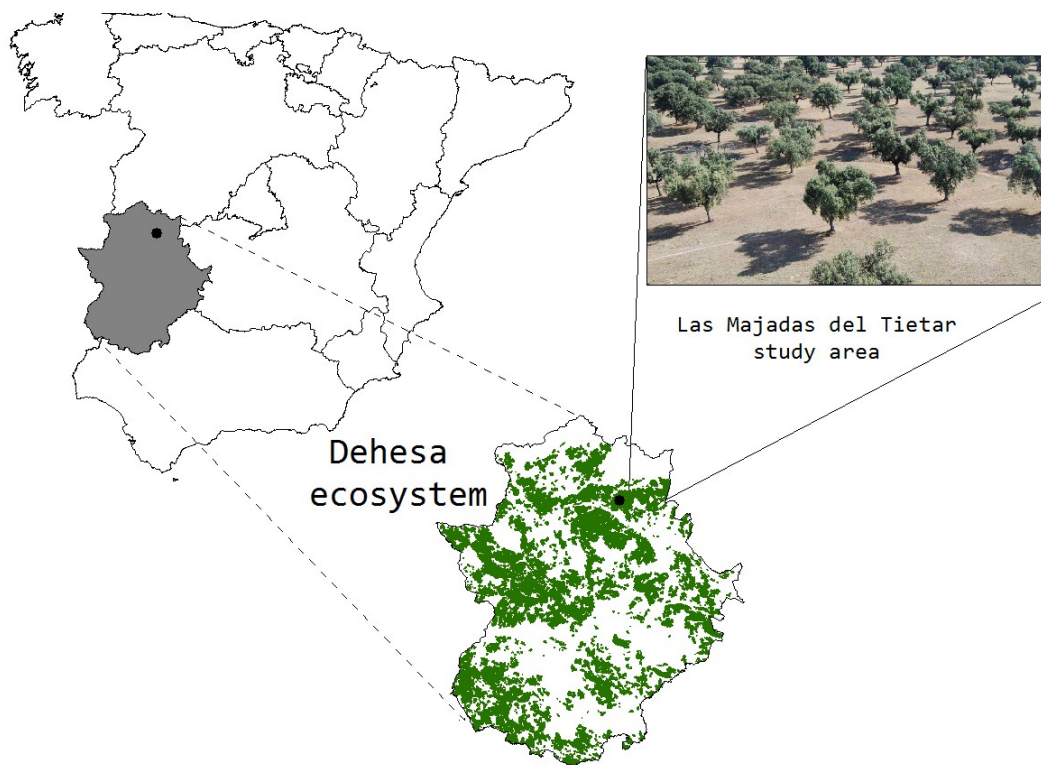


Figure 2.10: Location of site 2, Las Majadas study area and areas of dehesa system (in green), in Extremadura.

LAI field measurements were made in 2008 and 2009. Only one value was derived for trees, because this parameter was believed to be essentially constant throughout the year, while understorey measurements were made at least monthly. The LAI for the grass had significant seasonal variation, with minimum values over the summer dry season (June-September, $LAI < 0.1$) and maximum values in spring (0.9 – 2). Understorey LAI was measured by taking 12 samples of 25 x 25 cm (4 of them below the tree canopy). The samples were separated into different fractions, the green leaves being scanned, and LAI was estimated according to the ecosystem distribution. Moss lichen panicles and flowers were not included. Tree LAI was measured as the average of LAI estimations performed according to two methods. The first was based on single tree LAI estimates (measurement performed on nine trees with LAI2000 using four rings for calculation) and extrapolating this value to the whole ecosystem, assuming a canopy cover fraction of 20%. The second method was based on site-specific measurements ($SLA = 45.95 \text{ cm}^2\text{g}^{-1}$) and an estimate of foliage biomass from allometric relationships (based on DBH distribution from a survey of 244 trees in a 12.46 ha area surrounding the tower).

An eddy covariance open-path system measuring all energy balance components was installed over a tower of 15.5 m height. It is equipped with a three-dimensional sonic anemometer (SOLENT-50, Gill) and an analyzer LI-7500 IRGA (LI-COR Inc.) measuring water vapor and CO₂ fluxes; a CM-3 pyranometer, CG-3 pyrgeometer and CNR1 net radiometer (Kipp & Zonen) for measuring the different components of the radiation budget and dishes HFP-01EC (Hukseflux Thermal Sensors) for measuring the heat flux in soil. The raw data were processed using Eddylog (SC-DLO Fastcom) software, following the CarboEurope IP methodology for post-processing and flux quality checking. The energy storage within the biomass (S) was also estimated in this experimental site following *Stewart and Thom (1973)* and *Stewart (1978)*, in order to test the influence of this component on the overall energy balance. In order to determine the contributing area to measured fluxes and the match of this area with the remote data, an approximate solution for the contribution to the vertical flux (according to *Schuepp et al., 1990*) was estimated.

The air humidity and temperature needed as inputs for the model were measured with an Hygro-Thermo transmitter (Thies Clima, Goettingen, Germany) and the atmospheric pressure with a Model 276 barometric pressure sensor (Setra, Boxborough, MA, USA). Precipitation was measured with a precipitation transmitter (Thies Clima). Wind-speed (cup anemometer #40, NRG Systems Inc., Hinesburg, VT, USA) and wind direction at heights of 15, 9 and 5 meters were measured (wind vane #200P, NRG Systems Inc., Hinesburg, VT, USA) as were temperature data from the tree and the grass/soil for 2011. Data from 2011 were used to study the behavior of the wind speed profile, while data from 2008 and 2009 were used to evaluate the modified wind profile, and data from 2008 through 2011 were used to perform the statistical analysis of the Priestley-Taylor coefficient.

2.2.2 Description of the model and the modified wind speed profile versions.

The Two-Source Energy Balance (TSEB) model of *Norman et al., (1995)* has displayed good performance for a wide range of arid and partially-vegetated landscapes (*Kustas and Norman, 1997; French et al., 2005; Timmermans et al., 2007; González-Dugo et al., 2009*). For those ecosystems, dual-source models that distinguish between the soil and vegetation contributions to the radiative and turbulent fluxes are more suitable than single-source models (*Huntingford et al., 1995; Kustas and Norman, 1996; Timmermans et al., 2007; González-Dugo et al., 2009*).

The TSEB model includes two different versions according to the resistance network selected for parameterizing the energy flux exchange, which may be structured in series or in parallel (Norman *et al.*, 1995). The series version of the TSEB resistance network (Fig. 2.11) allows for interactions between soil/substrate and main canopy layer, and is useful over relatively dry and partially covered areas (Li *et al.*, 2005). In this study, the series resistance network was employed.

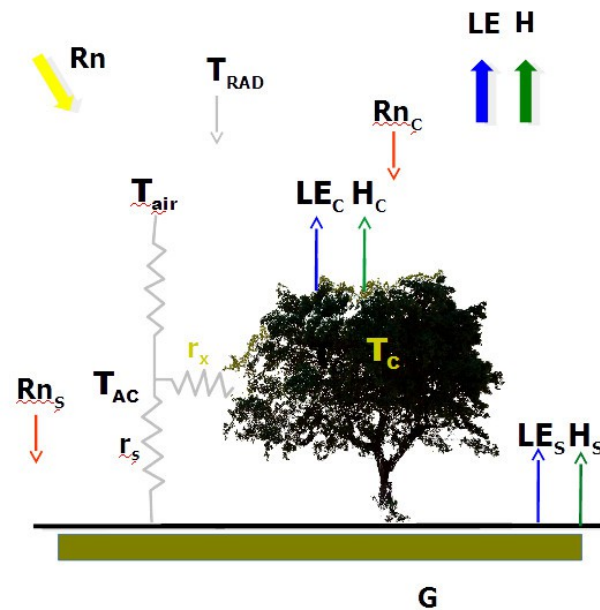


Figure 2.11: Scheme of the TSEB series version. Variables are described in this section (Figure adapted from Norman *et al.*, 1995).

Descriptions of the model are available in Norman *et al.* (1995) and Kustas and Norman (1999), but a general description is provided in the following sections, in order to provide a better understanding of how the model functions.

2.2.2.1 Two source energy balance model (TSEB)

The model used in this study is the updated version of the Two-Source Energy Balance (TSEB) model as described by Kustas and Norman (1999) and Li *et al.* (2005).

The model assumes that the surface radiometric temperature (T_{RAD}) is a combination of soil (T_s) and canopy (T_c) temperatures, weighted by the vegetation fraction:

$$T_{\text{RAD}}(\phi) = [f_c(\phi) T_c^4 + (1 - f_c(\phi) T_s^4)]^{(1/4)} \quad (2.7)$$

where f_c is affected by the sensor viewing angle (ϕ). The angular variation of directional emissivity is neglected because variations of less than 0.005 were obtained between viewing angles at nadir and 60° for most vegetated surfaces (*Anton and Ross, 1987; Kustas and Norman, 1997*).

Fractional cover was derived from field LAI measurements approximating f_c at nadir view angle (when $\phi=0$) by an exponential function as *Choudhury, (1987)* suggested:

$$f_c(0) = 1 - \exp(-k \text{LAI}) \quad (2.8)$$

where k is the leaf angle distribution function, which appears to range between 0.5 – 0.7 (*Ross, 1975*) depending on the leaves being distributed randomly ($k = 0.5$), vertically ($k < 0.5$) or horizontally ($k > 0.5$). We believe that it is possible to assumed a random distribution because the ecosystem contains erectophile grasses and planophile oak trees.

The scaled NDVI approach (*Choudhury et al., 1994*) method was used to retrieve $f_c(0)$ with remote data:

$$f_c(0) = 1 - \left[\frac{\text{NDVI}_{\text{MAX}} - \text{NDVI}}{\text{NDVI}_{\text{MAX}} - \text{NDVI}_{\text{MIN}}} \right]^p \quad (2.9)$$

where NDVI_{MAX} and NDVI_{MIN} , represent a surface fully covered by vegetation (~ 0.9) and completely bare (~ 0.08), respectively. The parameter p represents the ratio of a leaf angle distribution term (k) to canopy extinction (k'), where $p = k/k'$. k' is the damping coefficient, ranging between 0.8 and 1.3 for the NDVI (*Asrar et al., 1984; Baret and Guyot, 1991*). We used a weighted k' parameter by the area occupied by grass ($k \approx 0.8$) and oak ($k' > 1.3$) (*Kull et al., 1999*).

Pereira et al. (1995) using remote sensing information obtained the best results with the NDVI index to estimate canopy cover for oak savannas ($r^2=0.65$). *Oliveira (1998)*, using field radiometry and Landsat TM images found that NDVI produced the best performance ($r^2=0.75$). *Calvaio and*

Palmeirim (2004) identified correlations between several biophysical parameters and spectral variables from Landsat TM data, and the higher correlation for canopy cover was obtained with NDVI ($r^2=0.91$).

Apparent cover fraction at view angle ϕ is then obtained with:

$$f_c(\phi) = 1 - \exp\left(\frac{-kLAI\Omega(\phi)}{\cos\phi}\right) \quad (2.10)$$

where the directional clumping factor $\Omega(\phi)$ depends on canopy architecture. Because the model was originally developed for uniformly distributed crops, in the case of clumped canopies with partial vegetation cover such *dehesa*, the parameterizations have to be corrected by a clumping factor (Campbell and Norman, 1998) in order to take the particular distribution of the vegetation into account. This factor corrects for the reduction in the extinction of the radiation in a clumped canopy as compared to a uniformly distributed one by multiplying the LAI by a clumping factor. In this case, we estimated the clumping factor for the trees, as suggested by Campbell and Norman (1998), following the semi-empirical expression:

$$\Omega(\phi) = \frac{\Omega(0)}{\Omega(0) + [1 - \Omega(0)] \exp[-2.2(\phi_s^{p'})]} \quad (2.11)$$

where $\Omega(\phi)$ is the clumping factor at solar angle ϕ , $\Omega(0)$ is the clumping factor for a nadir solar zenith angle, and p' is an empirical expression given by:

$$p' = 3.8 - 0.46 D_p \quad (2.12)$$

where D_p is the plant height to the width ratio, given as:

$$D_p = \frac{h_c}{w_v} = \frac{h_c}{s_{ROW} f_c} \quad (2.13)$$

where h_c is the vegetation height [m] and w_v the vegetation clump width [m]. In row crops, w_v can be estimated as s_{ROW} plus f_c , where s_{ROW} [m] is the mean row spacing of the crops (estimated from a land-

use map). For forest and woodland, s_{ROW} was determined as the average distance between trees. The tree clumping factor for nadir solar zenith angle can be estimated from the total LAI observed in the field and the canopy fractional cover following *Kustas and Norman (2000)*. In the following sections, LAI from the oak was always affected by the clumped value.

Radiation scheme

The surface energy-balance equation can be formulated for the entire soil-canopy-atmosphere system, or for the soil (subfix s) and canopy (subfix c) components separately:

$$Rn_c = L E_c + H_c \quad (2.14)$$

$$Rn_s = L E_s + H_s + G \quad (2.15)$$

This partitioning considers separately the divergence of the short-wave (S_n) and long-wave radiation (L_n) following *Kustas and Norman (2000)*. Net short-wave radiation for the soil and the canopy was estimated as follows (*Campbell and Norman, 1998*):

$$S_{n_s} = (1 - \alpha_s) R_s \exp(-kLAI) \quad (2.16)$$

$$S_{n_c} = (1 - \alpha_c) R_s [1 - \exp(-kLAI)] \quad (2.17)$$

where α_c and α_s are the canopy and soil albedo respectively, and R_s the incoming solar radiation.

Net long-wave radiation was calculated as suggested by *Ross (1975)*, assuming exponential extinction law of radiation in canopy air-space:

$$L n_s = \exp(-k_L LAI) \epsilon' \sum T_{air}^4 + [1 - \exp(-k_L LAI)] \epsilon_c \sum T_c^4 - \epsilon_s \sum T_s^4 \quad (2.18)$$

$$L n_c = [1 - \exp(-k_L LAI)] (\epsilon' \sum T_{air}^4 - 2 \epsilon_c \sum T_c^4 + \epsilon_s \sum T_s^4) \quad (2.19)$$

where k_L is the extinction coefficient in the long-wave (0.7 – 0.9, depending on LAI), ϵ' is the atmospheric emissivity (following *Brutsaert, 1984*), σ is the Stefan-Boltzmann constant, ϵ_c the canopy emissivity (values of 0.99 for the tree and 0.98 for the grass were selected) and ϵ_s the soil emissivity (0.92) (*Brutsaert, 1984*). T_{air} is the air temperature above the canopy.

Since the radiation formulation follows the “layer-approach” (*Lhomme and Chehbouni, 1999*), a simple summation of the soil and canopy components yields the total flux;

$$R_n = R_{n_c} + R_{n_s} \quad (2.20)$$

$$H = H_c + H_s \quad (2.21)$$

$$LE = LE_c + LE_s \quad (2.22)$$

Soil heat flux

The soil heat flux is then estimated as a time-dependent function of the net radiation that reaches the soil, as follows:

$$G = A \cos[2\pi(t_s + C)/B] R_{n_s} \quad (2.23)$$

where t_s is the time in seconds relative to solar noon, A represents the maximum value of the ratio G/R_{n_s} , assumed to have a constant value of 0.35 (*Choudhury, 1987; Kustas and Daughtry 1990; Friedl, 1996*), C [s] is the peak in time position, supposed equal to 3600 following *Cellier et al. (1996)*, and B [s] is set equal to 74000 (*Cammalleri et al., 2010*).

Sensible heat flux

Within the series resistance scheme, the sensible heat fluxes H_c , H_s and H are expressed as:

$$H_c = \rho_a C_p (T_c - T_{AC}) / R_x \quad (2.24)$$

$$H_s = \rho_a C_p (T_s - T_{AC}) / R_s \quad (2.25)$$

$$H = H_c + H_s = \rho_a C_p (T_{AC} - T_A) / R_A \quad (2.26)$$

where T_{AC} is the air temperature in the canopy – air space (K), R_x is the resistance to heat flow of the vegetation leaf boundary layer ($s\ m^{-1}$), R_s is the resistance to the heat flow in the boundary layer above the soil ($s\ m^{-1}$), and R_A is the aerodynamic resistance calculated from the stability-corrected temperature profile equations (*Brutsaert, 1984*), using Monin-Obhukov Similarity Theory (MOST).

Resistances and wind-speed profile scheme

We present the resistance parameterizations for R_x , R_s and R_A below, following *Norman et al. (1995)* and *Kustas and Norman (1999)*.

$$R_A = \frac{[\ln(z_u - d_0 / z_{OM} - \% \Psi_M)] [\ln(z_T - d_0 / z_{OM} - \% \Psi_H)]}{k_{vk}^2 u} \quad (2.27)$$

where z_u and z_T [m] are the measurement heights for wind speed and temperature respectively, d_0 is the zero-displacement plane [m], z_{OM} is the roughness length for momentum transfer [m], k_{vk} is the Von Karman constant and Ψ_M and Ψ_H are the atmospheric stability functions.

$$R_s = \frac{1}{a' + b' u_s} \quad (2.28)$$

where the coefficients a' [$m \cdot s^{-1} \cdot K^{-1/3}$] and b' [-] are provided by *Kustas and Norman (1999)*, as used in the work of *Kondo and Ishida (1997)*:

$$a' = 0.0025 (T_s - T_c)^{(1/3)} \quad \text{and} \quad b' = 0.012 \quad (2.29)$$

The wind speed just above the soil surface, u_s [$m \cdot s^{-1}$], in Eq. (2.28) is parameterized as:

$$u_s = u_c \exp \left[-a \left(1 - \frac{z_s}{h_c} \right) \right] \quad (2.30)$$

where z_s [m] is the height above the soil where the effect of soil surface roughness becomes negligible, and is set equal to 0.1 for tall vegetation and 0.05 for short canopy.

Wind speed at the top of the canopy, u_c , is given by;

$$u_c = u \left[\frac{\ln\left(\frac{h_c - d_0}{z_{0M}}\right)}{\ln\left(\frac{z_u - d_0}{z_{0m}}\right) - \psi_M} \right] \quad (2.31)$$

and the factor a given by *Goudriaan (1977)* as:

$$a = 0.28 \text{ LAI}^{2/3} h_c^{1/3} s^{-1/3} \quad (2.32)$$

$$R_x = \frac{C'}{\text{LAI}} \left(\frac{s}{u_{d_0+z_{0M}}} \right)^{1/2} \quad (2.33)$$

C' is assumed to be equal to $90 \text{ [s}^{1/2} \cdot \text{m}^{-1}]$, following *Norman et al. (1995)*, s is the mean leaf size and $u_{d_0+z_{0M}}$ is parameterized following Eq. (2.30), but using $(d_0 + z_{0M})$ [m] as the reference height;

$$u_{d_0+z_{0M}} = u_c \exp \left[-a \left(1 - \frac{d_0 + z_{0M}}{h_c} \right) \right] \quad (2.34)$$

Roughness length and zero displacement plane

Roughness length and zero displacement plane were estimated according to *Massman (1997)* and *Massman and Weil (1999)* as describe below:

$$u(z)/u_c = e^{-n[1-\zeta(z)/\zeta(h_c)]} \quad (2.35)$$

$$\zeta(z) = \int_0^z [C_d(z') a''(z') / P_m(z')] d_0 z' \quad (2.36)$$

$$n = \frac{\zeta(h_c)}{\gamma u_c^2 / u_c^2} \quad (2.37)$$

$$u_{\text{star}}/u_c = c_1 - c_2 e^{-c_3 \zeta(h_c)} \quad (2.38)$$

$$d_0/h_c = 1 - \int_0^1 e^{-2n[1-\zeta(z)/\zeta(h_c)]} d_0 \xi \quad (2.39)$$

$$z_{0M}/h_c = (1 - d_0/h_c) e^{-k_{vk} u_c / u_{star}} \quad (2.40)$$

where $u(z)$ is the wind speed at height z , $\zeta(h_c)$ is a generalization of $C_d LAI$ (which accounts for foliage density), C_d is the drag coefficient of the foliage elements (0.2), a'' is the vertical leaf area density, which, together with P_m , the momentum shelter factor and C_d , takes into account the vertical canopy structure. $c_1=0.320$; $c_2=0.264$; and $c_3=15.1$ are model constants related to the bulk surface drag coefficient ($=2u_{star}^2/u(h_c)^2$) and to the substrate or soil drag coefficient as discussed by *Massman (1997)*, u_{star} is the friction velocity and k_{vk} is the Von Karman constant.

Due to the characteristics of the ecosystem, the *Massman (1997)* approach may not reproduce well the peculiarities of the system roughness length, and other formulations were tested, following *Choudhury and Monteith (1988)* and *Raupach (1994)*. The first approach used the second-order closure model of *Shaw and Pereira (1982)* to estimate d and Z_{0M} as:

$$d_0 = h_c \left[(1 + X^{1/6}) + 0.03 \ln(1 + X^6) \right] \quad (2.41)$$

$$Z_{0M} = z_s + 0.28 h_c X^{1/2}, \quad 0 \leq X \leq 0.2 \quad (2.42)$$

$$Z_{0M} = 0 - 3h(1 - d/h_c), \quad 0.2 \leq X \leq 2 \quad (2.43)$$

where the general expression for X is $0.2LAI$.

The latter approach, that of *Raupach (1994)*, takes into account the tree structure and is more suitable for tall woody vegetation, using observation data to fit the estimation of normalized displaced height and roughness length related to frontal area index (FAI).

$$d_0 = \left(1 - \frac{1 - e^{-\sqrt{a_1} \text{FAI}}}{\sqrt{a_1} \text{FAI}}\right) h_c \quad (2.44)$$

$$z_{0M} = (a_2 e^{-b_2 \text{FAI}^{C_2}} \text{FAI}^{d_2} + (z_{00}/h_c)) h_c, \text{ FAI} \leq 0.152 \quad (2.45)$$

$$z_{0M} = \frac{a_3}{\text{FAI}^{d_3}} [1 - e^{-b_3 \text{FAI}^{C_3}}] + f_2, \text{ FAI} > 0.152 \quad (2.46)$$

where $a_1=15.0$, $a_2=5.86$, $b_2=10.9$, $C_2=1.12$, $d_2=1.33$, $a_3=0.0537$, $b_3=10.9$, $C_3=0.874$, $d_3=0.510$ and $f_2=0.00368$ and $z_{00}/h_c=0.00086$. The value of z_{00}/h_c is the asymptotic value for bare soil. Constants were derived from a wide range of laboratory wind tunnel and field data.

FAI is calculated from the frontal area of trees (Schaudt and Dickinson, 2000), A_f as:

$$A_f = \text{FBHDBH} + \frac{1}{2} (h_c - \text{FBH}) \text{CW} \quad (2.47)$$

and the FAI is calculated by total A_f divided by the total area of the plot.

This approximations of the roughness length and zero displacement plane were compared with field measurements. The observed aerodynamic roughness length and zero-plane displacement were estimated using wind profile data. To calculate d_0 and z_{0M} , two wind speeds u_1 and u_2 (ms^{-1}) have been observed at height $z_1=15$ and $z_2=9$ (m) with cup anemometers, and friction velocity, u_{star} (ms^{-1}) at $z_U=15$ [m] has been computed with a sonic anemometer. Variables u_1 and u_2 were sampled at 20 Hz and averaged over 30 min, and u_{star} was calculated every 30 min from wind-speed data sampled at a rate of 10 Hz. d_0 and z_{0M} were computed under neutral conditions as follows (Rooney, 2001; Nakai, et al., 2008):

$$d_0 = \frac{z_2 \exp(k_{vk} u_1 / u_{\text{star}}) / \exp(k_{vk} u_2 / u_{\text{star}}) - z_1}{\exp(k_{vk} u_1 / u_{\text{star}}) / \exp(k_{vk} u_2 / u_{\text{star}}) - 1} \quad (2.48)$$

$$z_{0M} = \frac{z_1 - d_0}{\exp(k_{vk} u_1 / u_{\text{star}})} \quad (2.49)$$

In order to guarantee near-neutral conditions, only data where Z/L was lower than 0.05 and higher than zero (De Bruin and Moore, 1985) and $u_2(z_2)$ higher than u_1 were used. Roughness length was also evaluated for the Santa Clotilde area with no wind profile measurements, and assuming a constant d_0 , since the resistance calculation was less sensitive to this factor, and using the friction velocity equation under near-neutral conditions:

$$Z_{OM} = \frac{z_m - d(\text{constant})}{e^{\frac{k u}{u_{star}}}} \quad (2.50)$$

Latent heat flux

Finally, the canopy latent heat flux (LE_c) was derived, using as initial assumption a potentially transpiring canopy, following the Priestley-Taylor equation (Priestley and Taylor, 1972):

$$LE_c = \alpha_{PT} f_g \left(\frac{\Delta}{\Delta + \gamma} \right) Rn_c \quad (2.51)$$

where α_{PT} is the Priestley-Taylor coefficient, usually taken as 1.26 [-], f_g is the green vegetation fraction [-], Δ is the slope of the saturation vapor pressure versus temperature [kPa K^{-1}] and γ is the psychrometric constant [kPa K^{-1}]. If the vegetation is stressed, the Priestley – Taylor approximation, i.e. Eq. (2.51), overestimates the transpiration of the canopy and negative values of LE_s are computed by the model. This unlikely level of condensation over the soil during daytime indicates the existence of vegetation water stress, and is solved by an iteration process that reduces α_{PT} until it yields a coefficient value of 0.1, when LE_s becomes 0.

Green fraction (f_g)

The fraction of vegetation that is green and transpiring (f_g) was adjusted by means of the suggestions of Guzinski *et al.* (2013), to reflect the current phenological conditions. f_g was considered to be equal to the ratio of the fraction of photosynthetically active radiation (PAR) absorbed by the green vegetation cover, and the fraction of PAR intercepted by the total vegetation cover, and was estimated using vegetation indices (VI), as computed by Fisher *et al.* (2008), with the NDVI and the enhanced vegetation index (EVI) obtained from MODIS as:

$$f_g = 1.2 \frac{EVI}{NDVI}, 0 \leq f_g \leq 1 \quad (2.52)$$

In order to test the influence of each canopy layer on the total green fraction given by MODIS, ASD reflectance field measurements were processed to simulate MODIS bands, by averaging ASD values using the satellite distribution function for each band, in order to compute the NDVI and the EVI as:

$$EVI = G \frac{NIR - RED}{(NIR + C1)(RED - C2)(BLUE + L')} \quad (2.53)$$

where NIR and RED are the reflectances measured in both regions, L' is the canopy background adjustment that addresses the non-linear, differential NIR and RED radiant transfer through the canopy. C1 and C2 are the coefficients of the aerosol resistance term, which uses the blue band to correct the aerosol influences into the red band. The coefficients adopted are the same as in the MODIS-EVI algorithm; L'=1, C1 = 6, C2 = 7.5, and G is the gain factor equal to 2.5.

NDVI was then calculated as:

$$NDVI = \frac{NIR - RED}{NIR + RED} \quad (2.54)$$

Priestly-Taylor coefficient

The Priestley-Taylor coefficient (α_{PT}) is defined as (*Priestley-Taylor, 1972*):

$$\alpha_{PT} = \frac{E}{E_{eq}} \quad (2.55)$$

where E is the evaporation rate and E_{eq} is the equilibrium evaporation rate. Theoretically, air passing over a saturated surface will gradually decrease in saturation deficit until an “equilibrium” evaporation rate is reached (*Priestley-Taylor, 1972; Monteith and Unsworth, 1990; Raupach, 2001*). α_{PT} is a useful index for comparing evaporation rates from different sites, showing the relative significance of E to E_{eq} ,

and thus indicating the evaporative control.

There exist theoretical and experimental studies that show that the value of α_{PT} varies significantly with LAI, vapor pressure deficit (VPD) and soil moisture (e.g. *Tanner and Jury, 1976; Flint and Childs, 1991; Baldocchi, 1994; Baldocchi et al., 1997; Pereira, 2004; Baldocchi and Xu, 2007*). For natural vegetation, the optimal canopy α_{PT} coefficient assumed lower values on average and fell even further at high values of VPD (*Agam et al., 2010; Baldocchi and Xu, 2007; Galmés et al., 2007d*). This response may be related to the physiological characteristics of the natural vegetation growing in arid and semiarid environments. Although an increase in VPD enhances transpiration by producing a steeper humidity gradient between the leaf and the atmosphere, it also initiates a negative feedback on stomatal conductance, which leads to a reduction in transpiration (*Baldocchi and Xu, 2007*). The α_{PT} coefficient may also display seasonal variations (*De Bruin and Keijman, 1979*), with minimum values occurring in midsummer, when radiation inputs are at their peak, and maximum values during the spring and autumn.

Thus, adopting $\alpha_{PT} = 1.26$ would not be appropriate for the *dehesa* ecosystem, since some degree of canopy stress or reduction in LE_c could be reached before the TSEB algorithm would indicate $\alpha_{PT} < 1.26$ due to soil evaporation becoming less than zero; in other words the TSEB model could not be used in its current form to detect reduced transpiration through a reduction in α_{PT} from the widely adopted value of 1.26 (*Agam et al., 2010*) due to the plant physiology. Observational studies in forests have found that unstressed α_{PT} is significantly lower than the typical value of 1.26 (*Droppo and Hamilton, 1973; Black, 1979; Shuttleworth and Calder, 1979; Giles et al., 1985; Kelliher et al., 1992; Kanda et al., 1997; Tanaka et al., 1998; Meiresonne, 1999; Komatsu, 2005*). Thus, a lower value of input α_{PT} might be considered, reflecting the relatively conservative water-use tendencies of undomesticated natural vegetation subject to limited water supplies and frequent droughts.

A statistical process was performed to assess the α_{PT} value under the conditions of the study, applying the model to the ecosystem when only trees would be active and the understorey is dry (during the summer and winter), assuming a constant LAI for oaks (using ground-truth measurement over the area) and green fraction equal to 1 and then with f_g obtained with MODIS (< 1), evaluating the behavior of α_{PT} during 2007-2011. It was analyzed using an optimization scheme similar to that of *Agam et al., (2010)* iteratively running the TSEB with the radiometric temperature derived from the four-way radiometer (i.e. the upwelling longwave measurements),

over a range of initial α_{pT} values between 0.5 and 1.5, with increments of 0.05. After each run, the modeled LE was compared to the measured flux. The best fit was taken as the optimal α_{pT} for the canopy.

A second approach was also tested according to an analytical method to evaluate the $\alpha_{pT-BULK}$ coefficient (soil and canopy) behavior over this ecosystem (E/E_{eq}), computing E_{eq} as:

$$E_{eq} = \frac{\Delta}{\Delta + \gamma} R_n - G \quad (2.56)$$

and using the measured data from the eddy covariance tower as input. The relationship with VPD was also studied.

An attempt was made to analyze the α_{pT} , taking only the canopy into account, by assuming that during the summer the understorey grass is dry and all the latent heat flux measured by the ECT system should come from tree transpiration. For the calculation of the α_{pT} we inverted Eq. (2.51).

2.2.2.2 Wind speed profile modification and TSEB versions

The behavior of the vegetation in this ecosystem has two separate phases; when the grass, following its annual growth curve, is dry (summer and winter), and when this layer is fully growing (spring and autumn). The original TSEB model and the modified wind speed profile versions described in this section were applied and evaluated over the area during both periods.

With regard to the wind speed profile, the original TSEB uses the *Goudriaan (1977)* formulation described before, although the use of an exponential wind profile within the forest could not be appropriated (*Brutsaert, 1984*). *Shaw (1977)* found that in the lower region of the canopy, a hyperbolic-cosine profile could be more appropriate, in response to which, *Massman (1987)* suggested the following expression, assuming a uniform vertical distribution of the vegetation:

$$u_{(z)} = u_c \left[\frac{\cosh\left(\beta \frac{z}{h_c}\right)}{\cosh \beta} \right]^{(1/2)} \quad (2.57)$$

where the parameter β , similar to the extinction coefficient for *Goudriaan (1977)*, can be derived by the relationship:

$$\beta = \frac{4 C_d \text{LAI}}{0.16 \alpha_{\text{star}}^2} \quad (2.58)$$

where C_d is the drag coefficient, typically equal to 0.2 (*Goudriaan, 1977*), and α_{star} is a dimensionless coefficient that takes into account the presence of the roughness sub-layer of the underlying vegetative surface, taking values between 1.0 and 2.0 (*Raupach and Thorm, 1981*). This parameter was set to 1, following *Massman (1987)*, based on the wind profiles for different crops.

Based on wind-profile evaluation over a conifer forest, *Lalic et al. (2003)* modeled the wind profile within the canopy space as:

$$u(z) = u_c \left[\frac{\cosh \beta \left(\frac{z - z_d}{h_c} \right)}{\cosh \beta} \right]^{(7/2)}, \quad z_d < z \leq h_c \quad (2.59)$$

$$u(z) = C_c u_c, \quad z_{0s} < z < z_d \quad (2.60)$$

where z_d [m] is the crown bottom height, the factor β is equal to the one from *Massman (1987)* and the parameter C_c is defined as follows:

$$C_c = \left[\cosh \beta \left(1 - \frac{z_d}{h_c} \right) \right]^{(-7/2)} \quad (2.61)$$

z_d was set equal to 1/3 as *Cammalleri et al. (2010)* suggested, on the hypothesis that for tall canopies the foliage occupies primarily the upper 2/3 of the canopy height. These equations were used to estimate the velocity at heights of nine and five meters, above and inside the tree canopy layer, and then compared with the wind speed measurements over Las Majadas experimental site, evaluating the relative error. Best fits were then used at detail scale to evaluate the fluxes.

Assuming the hypothesis of a relatively constant behavior of trees, two different approaches for integrating the two-canopy layers were proposed and tested:

1. **TSEB Gp – TSEB Mp.** The wind speed profile following *Goudriaan (1977)* -**TSEB G** and *Massman (1987)* -**TSEB M**, were modified to include the differences in vegetation LAI, height and structure, as described below.

LAI for the tree was treated as being constant, and LAI for the understorey as variable. Total LAI was computed weighting both different leaf area indexes by the fractional cover of each canopy layer, estimated using summertime images. The oak LAI was minorate using the clumping factor computed for the trees.

Figure 2.12 displays a schema to describe the modifications in wind-speed profile following *Goudriaan (1977)*, using the same nomenclature as in equations 30, 31, 32 and 34, but with subscripts “oak” and “grass” to refer to the different canopy layers.

In this section, the modifications to the wind speed profile formulation are shown:

$$u_{d_0+z_{0M}-m} = u_{C(oak)} \exp \left[-a_{(oak)} \left(1 - \frac{d_0 + Z_{0M}}{h_{C(oak)}} \right) \right] \quad (2.62)$$

in which the wind speed at the top of the tree canopy, $u_{C(oak)}$, is given by;

$$u_{C(oak)} = u_{(z_u)} \left[\frac{\ln \left(\frac{h_{C(oak)} - d_0}{z_{0M}} \right)}{\ln \left(\frac{z_u - d_0}{z_{0m}} \right) - \psi_M} \right] \quad (2.63)$$

The wind speed just above the soil surface, u_{s-m} [$m \cdot s^{-1}$], is parameterized as in Eq. (2.30), but using 0.05 [m] as the reference height, as follows;

$$u_{s-m} = u_{C(\text{grass})} \exp \left[-a_{(\text{grass})} \left(1 - \frac{z_s}{h_{C(\text{grass})}} \right) \right] \quad (2.64)$$

$u_{C(\text{grass})}$ is equal to:

$$u_{C(\text{grass})} = u_{C(\text{oak})} \exp \left[-a_{(\text{oak})} \left(1 - \frac{h_{C(\text{oak})}}{h_{C(\text{grass})}} \right) \right] \quad (2.65)$$

and factors $a_{(\text{oak})}$ and $a_{(\text{grass})}$ are given according to *Goudriaan (1977)* as:

$$a_{(\text{oak})} = 0.28 \text{LAI}_{(\text{oak})}^{2/3} h_{C(\text{oak})}^{1/3} s_{(\text{oak})}^{-1/3} \quad (2.66)$$

$$a_{(\text{grass})} = 0.28 \text{LAI}_{(\text{grass})}^{2/3} h_{C(\text{grass})}^{1/3} s_{(\text{grass})}^{-1/3} \quad (2.67)$$

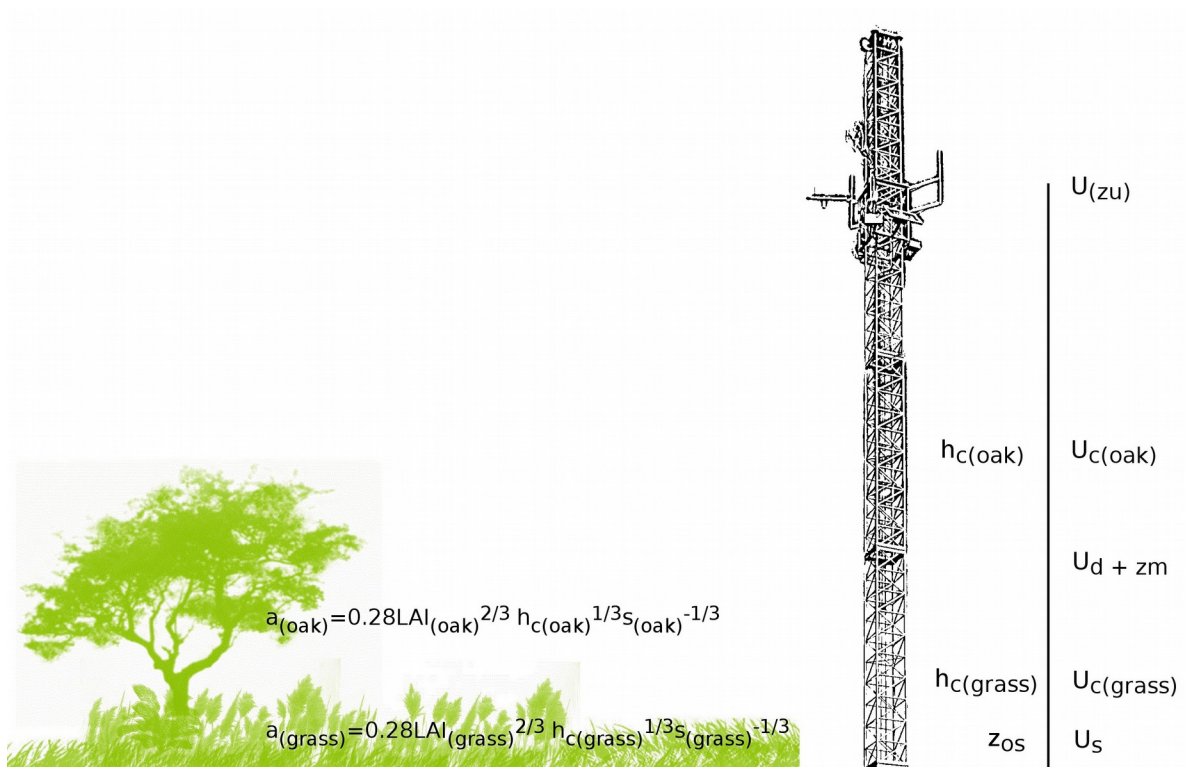


Figure 2.12: Modified *Goudriaan (1977)* wind speed profile for the different canopy layers.

Roughness length and zero displacement plane were computed separately for each canopy layer, using the measured values of LAI from the oak and the herbaceous layer respectively. Z_{OM}/d_0 for the tree was estimated according to *Raupach (1994)*, and was a constant value depending only on the oak structure. Z_{OM}/d_0 for the grass was estimated according to *Massman (1997)*, and was a function of grass LAI, which was variable during the period. Tree height was treated as a constant over the time and the understorey canopy variation of the nominal canopy height was estimated using a common growth curve, with the maximum and minimum measured heights depending on the NDVI. Leaf size was modified using a weighted average of the tree and herbaceous canopy values.

For the *Massman (1987)* formulation, an analogue reasoning was followed, with different β (extinction coefficients) for the tree and the grass. This modification of the wind profile within the vegetation, with different extinction coefficients for each canopy layer, was tested by comparing the wind speed estimated values at five meters with the measured ones over the Las Majadas experimental site. It was also tested by comparing the estimated values of wind speed measured at 12, 7 and 3 meters over the Santa Clotilde study area.

2. ***TSEB effective (TSEB eff)***. An effective LAI and height of the “total” vegetation were used, maintaining the original formulation of TSEB but deriving an effective height using the roughness length computed for tree and grass separately, inverting Eq. (2.45) or (2.46) and (2.40).

Table 2.1 presents the formulation for $d_0 - Z_{OM}$ and the wind-speed profile used in each version of the model:

Table 2.1: formulation for $d_0 - Z_{OM}$ and the wind-speed profile used for TSEB, TSEB G, TSEB M, TSEB Gp, TSEB Mp and TSEB eff

$d_0 - Z_{OM}$	TSEB	TSEB G	TSEB M	TSEB Gp	TSEB Mp	TSEB eff
<i>Massman (1997)</i>	X			X (grass)	X (grass)	x
<i>Raupach (1994)</i>		X	X	X (oak)	X (oak)	x
Wind-speed profile						
<i>Goudriaan (1987)</i>						
a	X	X				X (weighted)
a(oak) – a (grass)				X		
<i>Massman (1977)</i>						
β			X			
$\beta(\text{oak}) - \beta(\text{grass})$					X	

In order to clarify the procedure used in this study, the next scheme with present the followed temporal line:

1. Ground-based flux analysis: including the closure, footprint analyzes and estimation of energy storage within the canopy.
2. Oak clumping factor.
3. LAI behavior for trees and grass. Evaluation of constant tree LAI assumption.
4. Estimation of green fraction.
5. Roughness length evaluation and best approach selection for the estimation under the studied conditions.
6. Evaluation of wind-speed profile.
7. Priestley-Taylor analysis.
8. Statistical evaluation of the different TSEB approaches with ECT data.
 - 8.1 TSEB G
 - 8.2 TSEB M
 - 8.3 TSEB Gp
 - 8.4 TSEB Mp
 - 8.5 TSEB eff
 - 8.6 TSEB without any modification.

For the evaluation of the different versions of the model, the following statistics were used: mean difference (MD), mean absolute difference (MAD), mean absolute error (MAE), root mean square difference (RMSD), mean value (MA) and its standard deviation (SD):

$$MA = \frac{\sum_{i=1}^n (X_i)}{n} \quad (2.68)$$

$$MD = \frac{\sum_{i=1}^n (X_i - Y_i)}{n} \quad (2.69)$$

$$MAD = \frac{\sum_{i=1}^n |X_i - Y_i|}{n} \quad (2.70)$$

$$MAE = \frac{100}{MA} \left(\frac{\sum_{i=1}^n |X_i - Y_i|}{n} \right) \quad (2.71)$$

$$RMSD = \left[\frac{\sum_{i=1}^n (X_i - Y_i)^2}{n} \right]^{0.5} \quad (2.72)$$

where X_i and Y_i are the i_{th} observed or measured variable and n the sample size.

2.3 RESULTS AND DISCUSSION

2.3.1 Evaluation of the energy surface fluxes measured at the ECT sites

Direct measurement of the four energy balance components were evaluated in both study areas, yielding average closures of 80% for Santa Clotilde and 86% for Las Majadas, both within the error range found by other authors (*Foken, 2008; Franssen et al., 2010*). These quantities represent absolute errors of 49 Wm^{-2} and 40 Wm^{-2} , respectively. The observations were of better quality during the summer and winter, probably due to the lack of noise caused by rain and condensation processes, and this is reflected in the closure balance (Table 2.2). It can also be seen that low values of LE correlate with better closure balance. This could be because the uncertainties in the measurement of LE are higher than in H measurement, given that this flux was very low during the summer and the dry/cold winter period.

Table 2.2: Monthly closure balance for Santa Clotilde and Las Majadas ground ECT measurements.

	Closure balance [%]	
	Santa Clotilde	Las Majadas
January	87	82
February	74	79
March	72	77
April	80	76
May	70	77
June	81	84
July	91	90
August	90	89
September	84	94
October	82	86
November	-	82
December	69	81

Figure 2.13 compares the available energy of the ecosystem and the turbulent flux measurements for both sites.

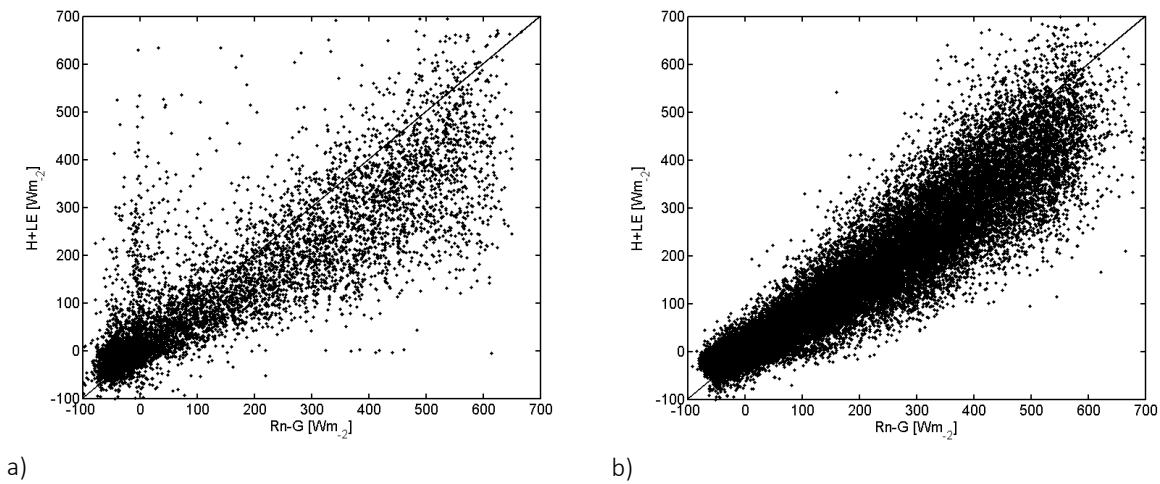


Figure 2.13: Closure balance for a) Santa Clotilde and b) Las Majadas ground-ECT measurements.

Energy storage within the biomass was estimated according to *Stewart and Thom (1973)* and *Stewart (1978)*, to test the relative importance of this component for the overall balance. The analysis revealed that the energy storage in the biomass was very low, with monthly average values ranging between 0 and less than 10 Wm^{-2} (Figs. 2.14a and 2.15a), and instantaneous maximum values around the 10% of the net radiation. Unfortunately, ground measurement of this component is difficult, and the low estimated values suggest that it may not be worth the effort under these conditions. It also can be derived that this component could be ignored in both sites without a significant loss of information. However, the situation could be different for *dehesas* with higher tree ground coverage.

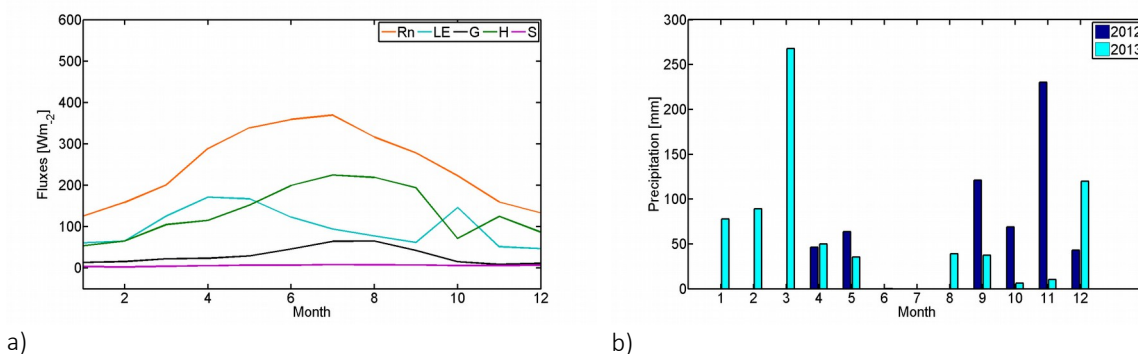


Figure 2.14: a) Annual mean fluxes and b) precipitation for Santa Clotilde study area.

It is possible to see in Figures 2.14a and 2.15a that the estimated monthly mean energy storage within the biomass is very low, ranging between 0 and less than 10 Wm^{-2} ; it could therefore be neglected under these conditions. LE has two peaks, in the spring and in autumn, related to the typical rainfall of the spring and fall/winter seasons. However, the magnitude and timing can vary significantly from year to year (Fig. 2.14b and 2.15b).

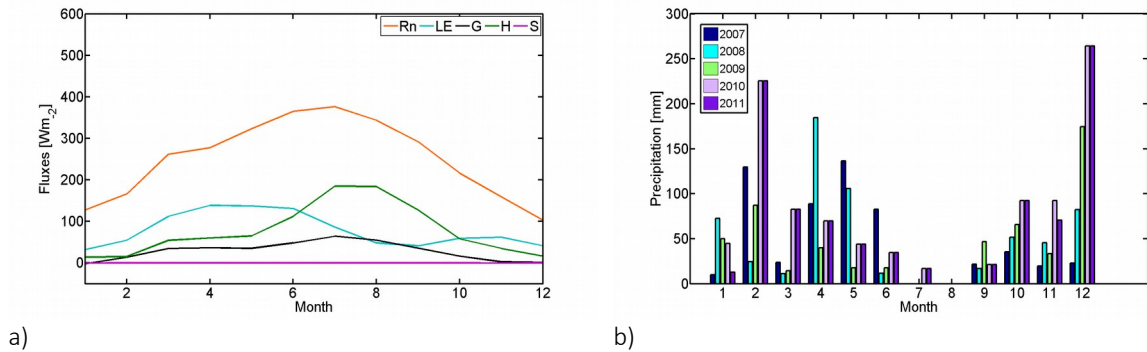


Figure 2.15: Annual mean fluxes and precipitation for Las Majadas study area.

The wind direction was analyzed in order to accurately determine the area that contributes most to the flux measurements made at the ECT. Southwest is the dominant component over Santa Clotilde with 1 km homogeneous fetch (Fig. 2.16a), with an average wind-speed of 2.5 ms^{-1} and peaks located at around noon. Maximum values over the area are around 20 ms^{-1} . The wind direction for this period over Las Majadas (Fig. 2.16b) agreed with the information provided by the personnel of the station, with southwest (250°) and northeast (70°) as the dominant components, with homogeneous fetches of more than 2 and 1.5 km respectively.

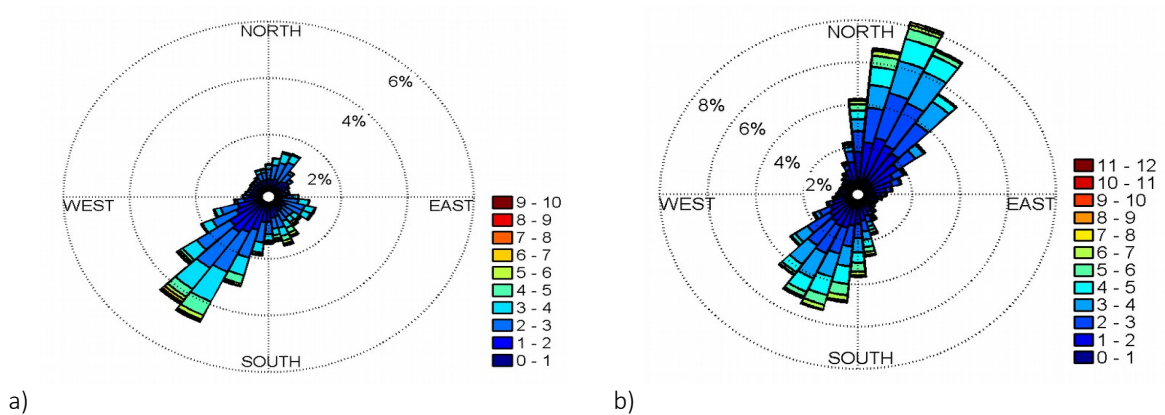


Figure 2.16: Contributing percentage of the wind speed direction for a) Santa Clotilde and b) Las Majadas.

A cumulative normalized contribution to flux measurement curve was estimated for each location as a function of distance from the measurement point, as well as the relative contribution to the measurement flux. The area that most contributed to the energy fluxes measured at the Santa Clotilde ECT using the approximate solution of *Schuepp et al., (1990)* was located with 500 meters (Fig. 2.17a), at an average distance of 110 meters from the measuring point. Sixty per cent of the flux captured by the ECT comes from the area between 0 and 500 m, reaching 80% in the first 1000 meters. According to analyses performed using the model of *Kormann and Meixer (2001)*, integrated in TK3 program, 76% of the Santa Clotilde area contributing to the energy fluxes is within the first 1000 meters, for the study period. Both formulations gave similar results.

Over the night lower contributions of the area within 1000 m have been observed. The maximum is located in the first 200 meters in Santa Clotilde.

At Las Majadas (Fig. 2.17b), the peak contribution is located within 500 meters, with 70% of the flux captured by the ECT coming from the area between 0 and 500 m, reaching almost 90% in the first 1000 meters, verifying that the footprint is large enough for the majority of the fetch of interest.

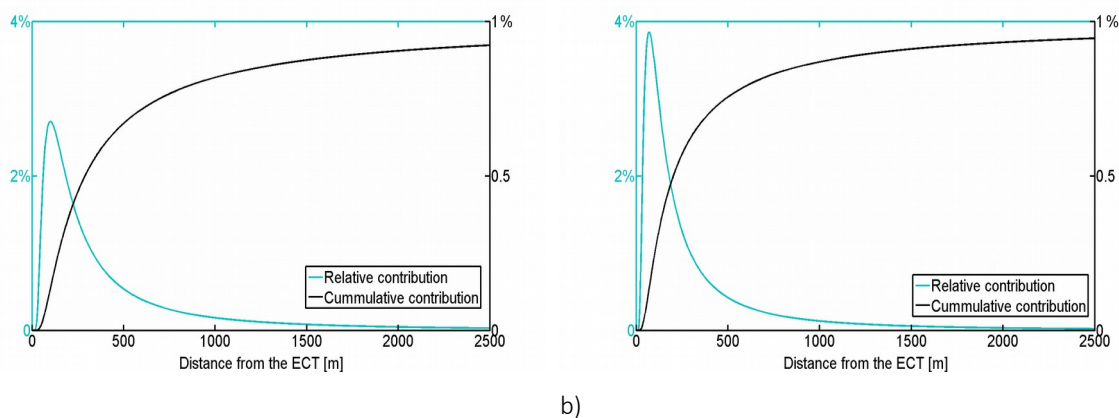


Figure 2.17: Maximum contribution to the energy fluxes measured in the ECT (Schuepp et al., 1990) for a) Santa Clotilde and b) Las Majadas.

Given these results, and considering that the same land use is extended and uniform at least 1000 meters along the principal wind directions (SW for Santa Clotilde, SW and NE for Las Majadas), no

problems of fetch might be expected taking ECT data measured over the principal wind component. In the same way it is possible to integrate information from medium-resolution (pixel size between 30 and 120 meters) and even low-resolution (250m – 1km pixel size) Earth observation satellites (Fig. 2.18).

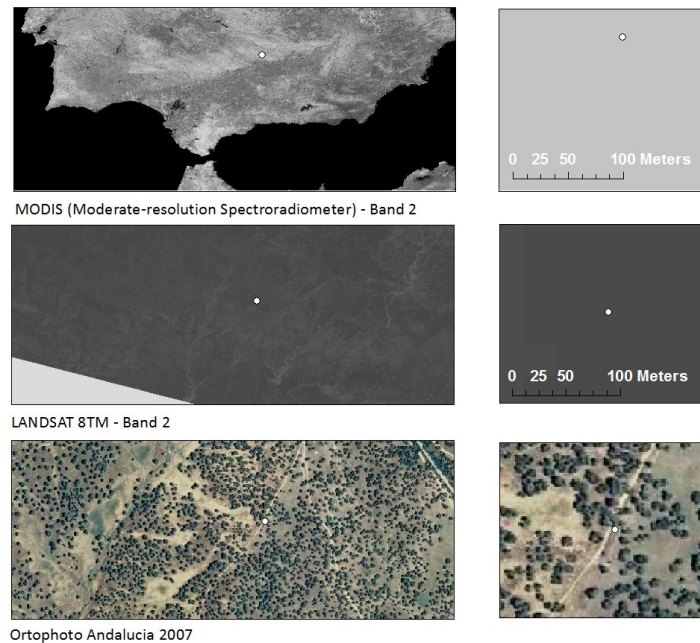


Figure 2.18: Example of the remote information spatial resolution.

The typical diurnal pattern of flux variation corresponding to semi-arid areas, with wet-cold and hot-dry periods, can be observed in Figure 2.19. In dry periods (Fig. 2.19b) sensible heat flux reaches its maximum value in the middle of the afternoon, while the soil heat flux does so earlier, to reach the minimum after dark. Latent heat increases during the day, but remains low due to the lack of available water in the soil for transpiration and/or evaporation (Fig. 2.19b). On the contrary, during wet season (Fig. 2.19a), LE is higher than H, while G values are reduced, probably due to the effect of the grass layer, that protects the top layer of soil from incoming radiation.

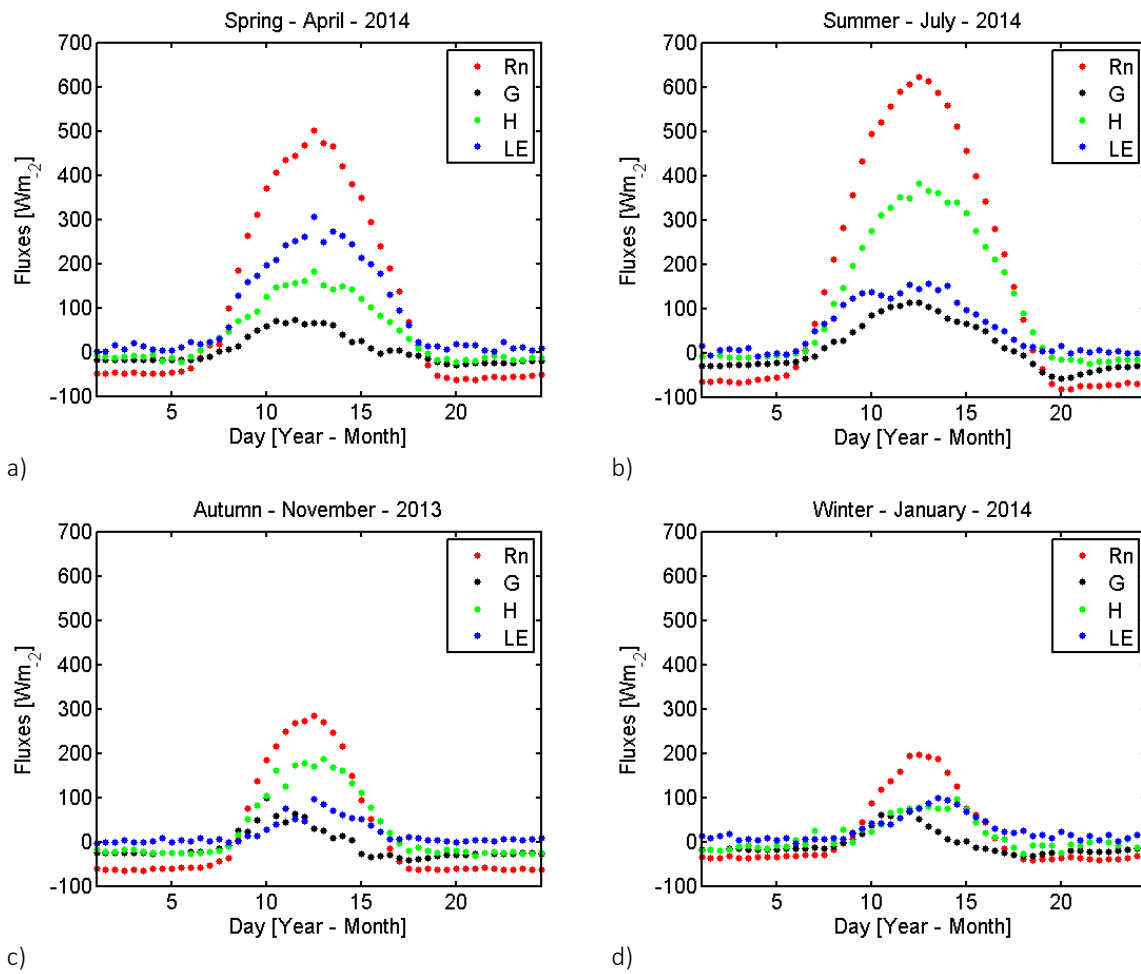


Figure 2.19: Typical measured daily fluxes for Santa Clotilde for a) spring, b) summer, c) autumn and d) winter.

Normally, due to the lesser importance of the soil heat flux compared to the other components, many studies have simplified the estimated energy balance by discarding this flux on daily scales. In these areas, however, G represents more than the 20% of the net radiation during the summer, similar to or even higher than the latent heat flux (Fig. 2.19a), with sensible heat flux reaching values higher than the 45% of Rn. Both quantities are consistent with water shortages resulting from the climatic conditions of the area, with high temperatures and lack of precipitation for long periods, during which the soil moisture powerfully influences the partitioning of available energy between the sensible and latent heat fluxes (*Entekhabi and Rodriguez-Iturbe, 1994*). During the wet season, the opposite trend is shown.

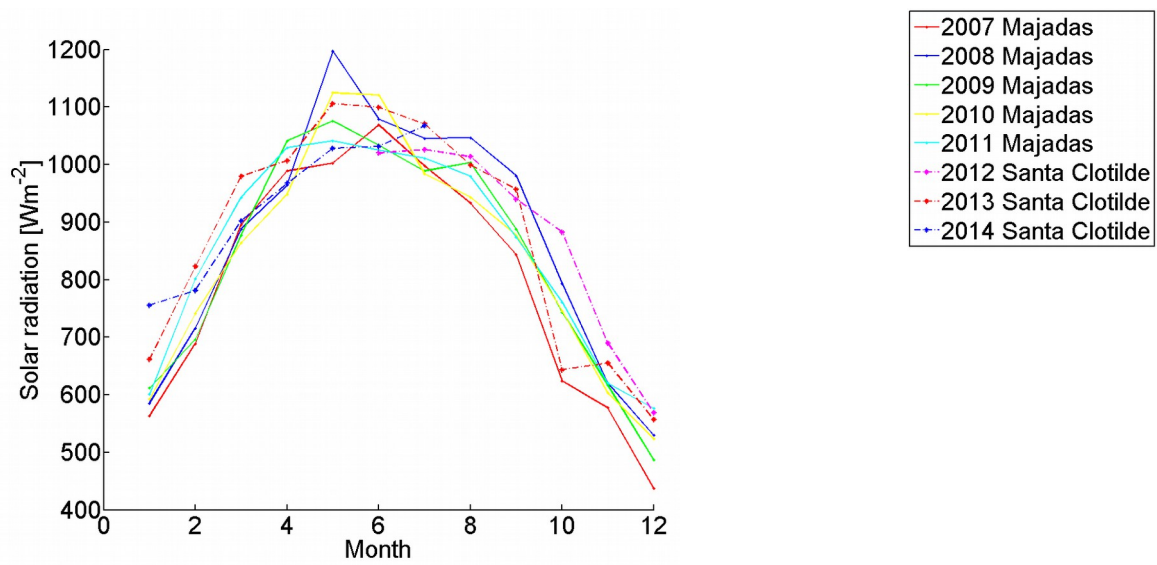
Table 2.3 presents the mean values of latent heat flux and precipitation for Las Majadas (for Santa Clotilde we do not have a complete year period). We can see that in some years (especially during

2011), the precipitation rate is lower than the LE rate, which probably means that the trees are able to reach water from deep underground sources (*Paço et al., 2009*). Precipitation may also be intercepted by vegetation surfaces, later evaporating into the atmosphere. With respect to mean rainfall values for the area, only 2010 and 2011 were outside the usual range, these being humid and dry years, respectively. For Santa Clotilde, the annual precipitation recorded in a nearby meteorological station was 522 mm in 2012, and 706 mm in 2013, the first year studied being relatively dry. Until 20th October 2014, the accumulated precipitation for 2014 has been 410 mm.

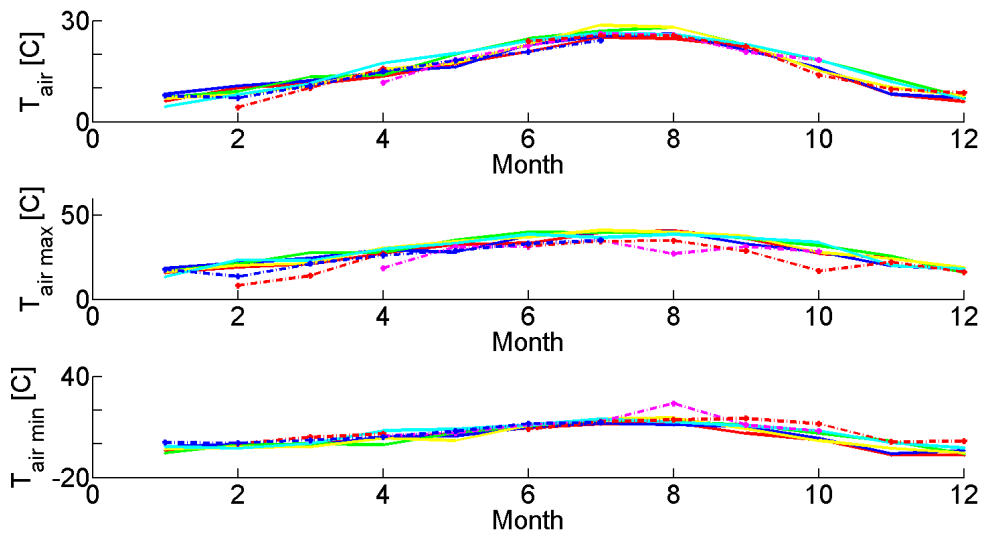
Table 2.3: Accumulate precipitation [mm] and ET [mm] for Las Majadas site.

[mm]	2007	2008	2009	2010	2011
Precipitation	570	609	548	965	374
ET	997	784	800	865	1166

Both areas, sharing the same ecosystem but located at different latitudes and longitudes, have similar conditions, as we can see in Figures 2.20a and 2.20b, which show the monthly average incoming solar radiation and the mean, maximum and minimum average monthly values for air temperature. For this reason, and because of their similar fractional cover, we believe that it is permissible to extrapolate the results from one area to the other, and probably to almost the whole *dehesa* in this region, due to the constant qualities of this particular ecosystem but taking into account the influence that existing differences in f_c and meteorological conditions could cause.



a)



b)

Figure 2.20: a) Incoming solar radiation and b) maximum, average and minimum air temperatures for Santa Clotilde and Las Majadas sites.

During the dry season, the temperature of the oaks can exceed air temperatures over these arid areas (Fig. 2.21), reaching close to the upper limit of the canopy temperature range (0-39 °C) (Baldocchi and Xu, 2007) at which enzymatic activity is inhibited (Bjorkman, 1980).

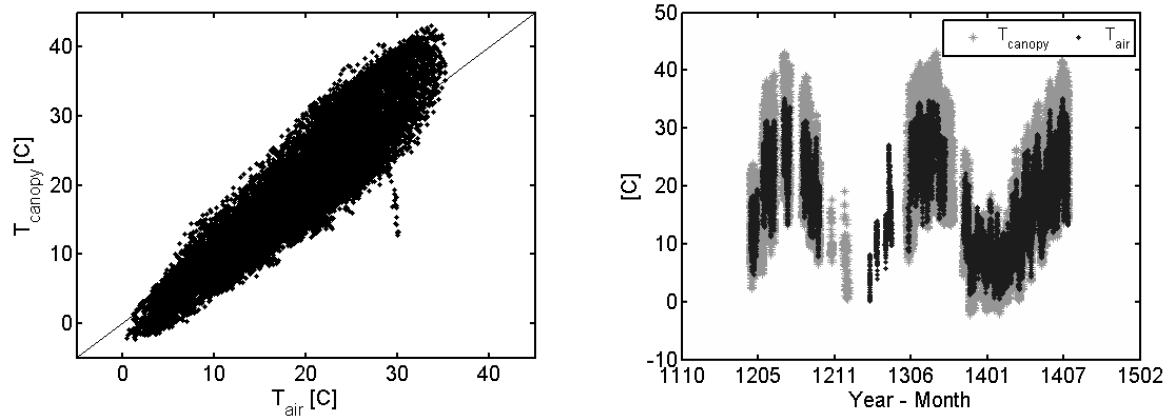


Figure 2.21: a) Canopy measured temperature vs. air temperature over Santa Clotilde.

2.3.2 Oak tree clumping factor $\Omega(0)$.

In Las Majadas, the tree LAI measured in the field was 0.34 and fractional cover, $f_c = 0.2$. If the vegetation had been randomly distributed and the leaf angle distribution approximated a spherical distribution, the canopy gap fraction from the zenith would be $\exp(-0.5LAI) \approx 0.844$. Oak *dehesa* vegetation is clumped so the field LAI corresponds to a local LAI (LAI_L) equal to $LAI/f_c \approx 1.7$. If all the leaves were randomly distributed, then the transmission of this vegetated region will be $f_c \exp(-0.5LAI_L)$. The fraction of the nadir view occupied by the soil is $f_c \exp(-0.5LAI_L) + (1-f_c) \approx 0.886$ so that $\exp(-0.5\Omega LAI) \approx 0.886$ yielding a $\Omega(0)$ for the trees of 0.71. For Santa Clotilde, the local tree LAI measured in the field was 2.6 and fractional cover, $f_c = 0.2$. $LAI = LAI_L f_c \approx 0.52$. The fraction of the nadir view occupied by the soil is $f_c \exp(-0.5LAI_L) + (1-f_c) \approx 0.854$ so that $\exp(-0.5\Omega LAI) \approx 0.854$ yielding a $\Omega(0)$ for the trees of Santa Clotilde of 0.61.

For the estimation of the clumping factor at solar zenith angle ϕ , s_{row} parameter (Eq. 2.11) was evaluated by means of GIS techniques, averaging the distance between consecutive trees over both areas, giving a mean value of 30 meters. This value in woody crops is much lower, being for example around 3 m for vineyard, and for olive trees ranging from 3 m to more than 6 m, depending on the management intensity.

2.3.3 Oak and understorey LAI variation over the year

We analyzed the variations in oak and understorey leaf area indices in the course of the year, and evaluated their effects on the model. In Figure 2.22, local herbaceous LAI values from both areas and local oak LAI in Santa Clotilde are presented. The oak LAI, although it varies slightly during the year, displays a more constant behavior than does the understorey LAI. In Santa Clotilde, the mean local oak LAI is 2.60, with a standard deviation of 0.13. The local mean grass LAI was 0.42 ($\sigma = 0.48$) and 0.62 ($\sigma = 0.69$) in Las Majadas and Santa Clotilde respectively. Both deviations showed the variation of the herbaceous index compared with the tree index.

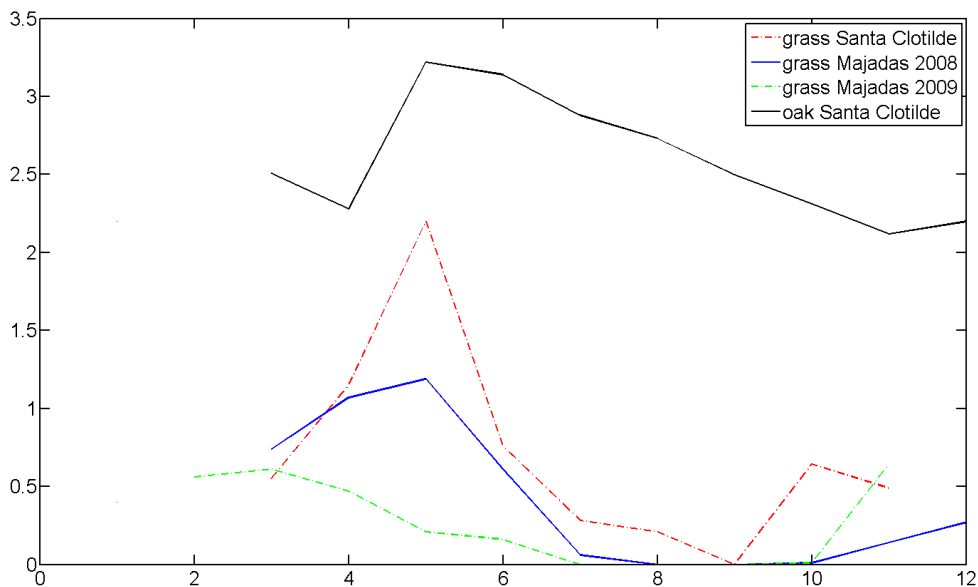
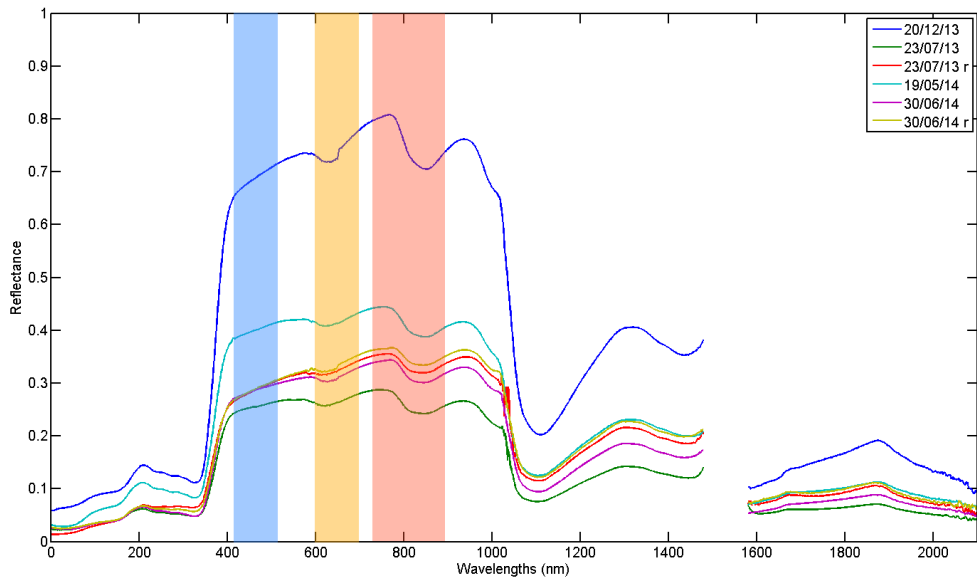


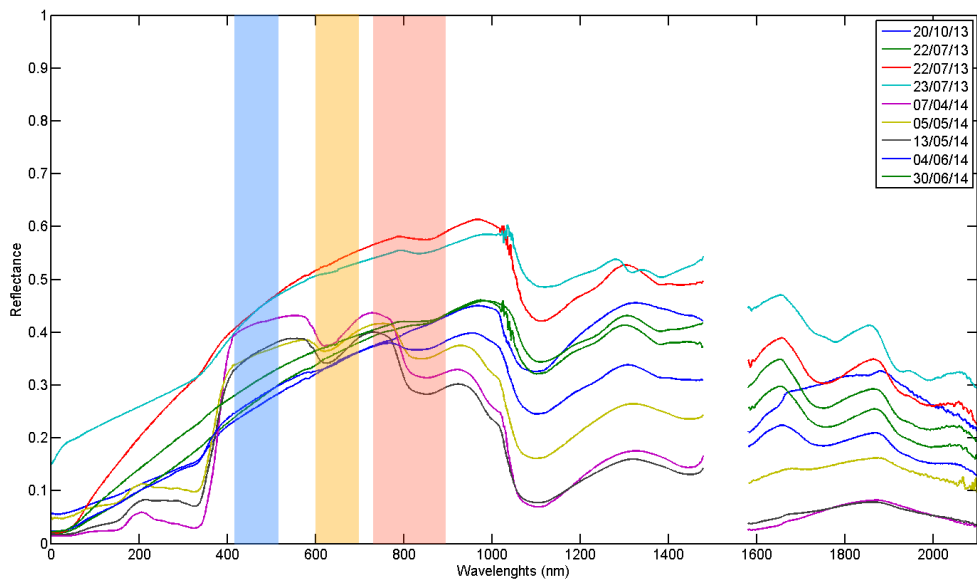
Figure 2.22: Local LAI measured in the field for Santa Clotilde and Las Majadas.

Figure 2.23a shows the oak spectra measured on different dates in 2013 and 2014 in Santa Clotilde. A small region of the spectrum ranging between 1480-1580 nanometers has been masked, due to the noise produced by the SWIR 1 InGaAs Photodiode detector of the ASD instrument. Even when the variation is perceptible over the seasons, the spectral region used to derive LAI, as a function of NDVI, remains constant, the same as those used for EVI. Observing the grass spectrum over the season (Fig. 2.23b), greater variations could be observed due to the growing cycle of this annual vegetation, which in the course of the year ranges between almost

full cover to bare soil/dry grass. Averaging the measured spectrum using MODIS spectral filter bands, the estimated local LAI value for oaks is 2.294 ($\sigma = 0.092$), and for grass, 0.64 ($\sigma = 0.82$).



a)



b)

Figure 2.23: a) Oak and b) herbaceous layer spectral information measured in the field. The blue band is marked with blue, the red band in orange and NIR band in red.

The reflectance spectrum of the collected leaves, analyzed in the laboratory is even more homogeneous (Fig. 2.24). It is probably due to the more uniform artificial light beam used for measuring reflectance in the laboratory, and to the greater homogeneity of the prepared leaf samples, compared to canopy FOV under field conditions. Differences between the average values computed using MODIS spectral filters bands, represented by blue (BLUE), orange (Red) and red (NIR) in Fig. 2.24 for the different months is less than 0.03 points.

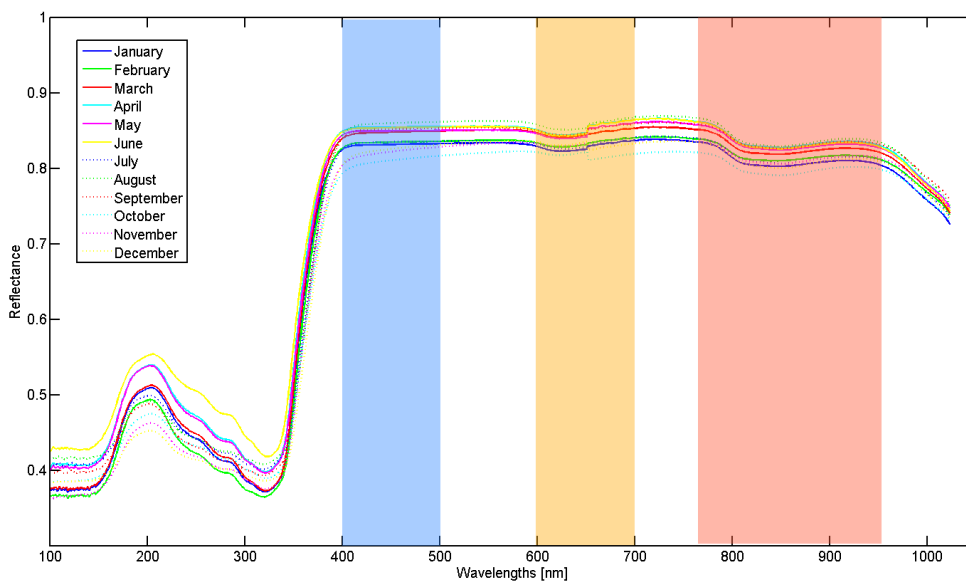


Figure 2.24: Spectrum information for oak leaves measured in the laboratory. The blue band is marked in blue, the RED band in orange and the NIR band in red.

As mentioned above, local LAI from grass and oaks were derived from field spectral information in order to determine whether the derivation of LAI using the broad bands from satellites could be used as a proxy, and supported the assumption of non-variability of the oaks' spectral properties throughout the year when extrapolating the estimates. The RMSD of the local oak LAI when the spectrometer-derived and measured indices were compared was 0.58, with 28% relative error. The RMSD for grass was 0.19, with 27% relative error and $r^2=0.9524$. Although the number of measurements is limited, the sampling design integrated a significant number of points, within different soil, substrate and canopy ranges (Table 2.4).

Table 2.4: Local LAI observed in the field and estimated with Landsat and MODIS distribution functions.

LAI_L OBSERVED			LAI_L – Landsat derived			LAI_L – MODIS derived		
Date	n*	LAI_L	Date	n*	LAI_L	Date	n*	LAI_L
Oak								
23/07/13	21	3.61	23/07/13	39	2.32	23/07/13	39	2.33
20/12/13	19	2.20	20/12/13	12	2.67	20/12/13	12	2.62
19/05/14	7	2.43	19/05/14	6	2.11	19/05/14	6	2.07
30/06/14	8	3.33	30/06/14	18	2.52	30/06/14	18	2.52
17/07/14	15	2.15	30/06/14	2	2.19	30/06/14	2	2.29
Understorey layer								
23/08/13	5	0.21	23/07/13	93	0.37	23/07/13	93	0.33
17/10/13	4	0.15	20/10/13	12	0.58	20/10/13	12	0.59
19/05/14	24	2.04	19/05/14	47	2.34	19/05/14	47	2.20
04/06/14	6	0.62	04/06/14	43	0.65	04/06/14	43	0.62
17/06/14	6	0.31	30/06/14	20	0.28	30/06/14	20	0.15

n* number of samples

The results suggest that the assumption of a constant oak LAI during the year is acceptable for the purposes of this study. Similarly, remotely sensed information for deriving vegetation indices for oaks and grasses in this ecosystem is sufficiently accurate.

2.3.4 Green fraction estimation.

A green fraction (f_g) was derived for both locations using MODIS satellite data, as suggested by *Guzinski et al., (2013)*. f_g was also derived from the spectral data collected for each canopy layer, averaging the spectral information by means of the MODIS band distribution functions. In order to integrate in a single spectral-derived index both canopy types, each estimation was weighted by the area occupied by each component within the ecosystem. This was only possible on the three days on which spectral measurements were made over both covers, in July 2013 and May and June 2014. Comparing these results (Table 2.5), no conclusion about the goodness of the adjustment of MODIS index could be drawn, due to the low number of samples, although it seems that the MODIS-derived index in summer is higher than the spectral-derived index. Observing spectral-derived f_g values, it seems that the threshold value for green/dry vegetation is close to 0.8.

Table 2.5: f_g estimated from field spectra using MODIS bands functions and f_g estimated from MODIS products.

Date	f_g from spectral information			f_g MODIS product
	oak	grass	Oak + grass	Oak + grass
23/07/13	0.73	0.75	0.75	0.81
23/07/13	0.76	--	0.75	0.81
20/10/13	--	0.78	--	0.66
20/12/13	1	--	--	--
07/04/14	--	0.94		
05/05/14	--	0.98	0.98	0.74
13/05/14	--	0.87	0.90	0.74
19/05/14	1	--		
30/06/14	0.78	0.82	0.81	0.71

As Figure 2.25 shows, even when the grass is completely dry, f_g values derived from MODIS are still high (e.g. August 2013 = 0.82). f_g derived from the satellite incorporates the effect of the evergreen vegetation along with the grass, but considering the low tree fractional cover in these ecosystems, a strong influence would not be expected. It may be that this parameter does not reflect phenological conditions during the dry period sufficiently accurately.

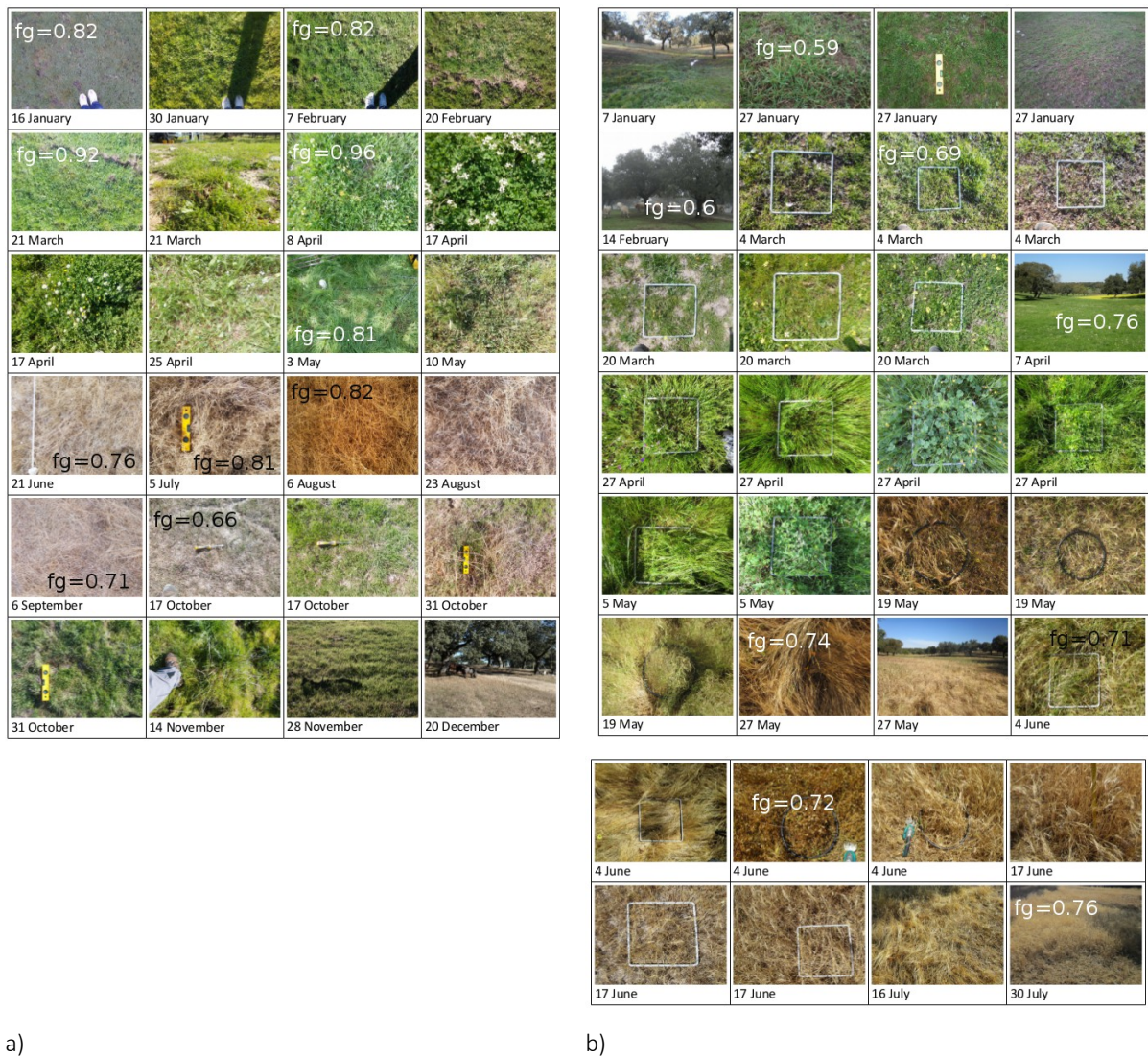


Figure 2.25: Monthly f_g parameter estimated from MODIS satellite for a) year 2013 and b) 2014 over Santa Clotilde.

2.3.5 Roughness length and zero displacement plane assessment

Real roughness length and zero displacement height were first estimated using wind and u_{star} measurements with the log profile under near-neutral conditions, as suggested by *Nakai et al. (2008)* and *Rooney (2001)*, and then estimated based on the formulations of *Massman (1997)*, *Choudury and Monteith (1988)* and *Raupach (1994)*, described in section 2.2.2.1 above.

The estimated value of the zero displacement height, d_0 was less influenced by the formulation

selected than the roughness length, with an uncertainty of 25% in the various approaches. A sensitivity analysis of d_0 was performed using the data of Las Majadas (2007-2008) with d_0 values ranging from a minimum of 1.5 to maximum of 4 m, estimated using the formulations described above. The results showed that the maximum variation in flux estimation caused by the value adopted for d_0 was less than 1 Wm^{-2} for LE and 4 Wm^{-2} for H.

For roughness length, estimates of Z_{OM} ranged from 0.1 to 1 m. Using this range in Z_{OM} in TSEB resulted in a variation of 20 Wm^{-2} (20%) in the sensible heat flux (an order of magnitude). Variations in the value of Z_{OM} affect the computation of the resistances and wind speed profile. Lower Z_{OM} would lead to a higher R_A (Eq. 2.27), and also higher R_x (Eq. 2.33), due to the higher wind speed above the canopy. This higher wind speed will result in a higher wind speed at soil level, resulting in lower R_s (Eq. 2.28). This will yield lower H values (and higher LE values). A larger H_s would result, while a higher R_A and R_x would reduce H_c . R_x is less influenced by the value of Z_{OM} than R_A or R_s , with mean differences between the resistance values resulting in $Z_{OM} = 0.1$ and $Z_{OM} = 1$ of 50 s m^{-1} for R_A , 20 s m^{-1} for R_s and less than 1 s m^{-1} for R_x . (Figure 2.26).

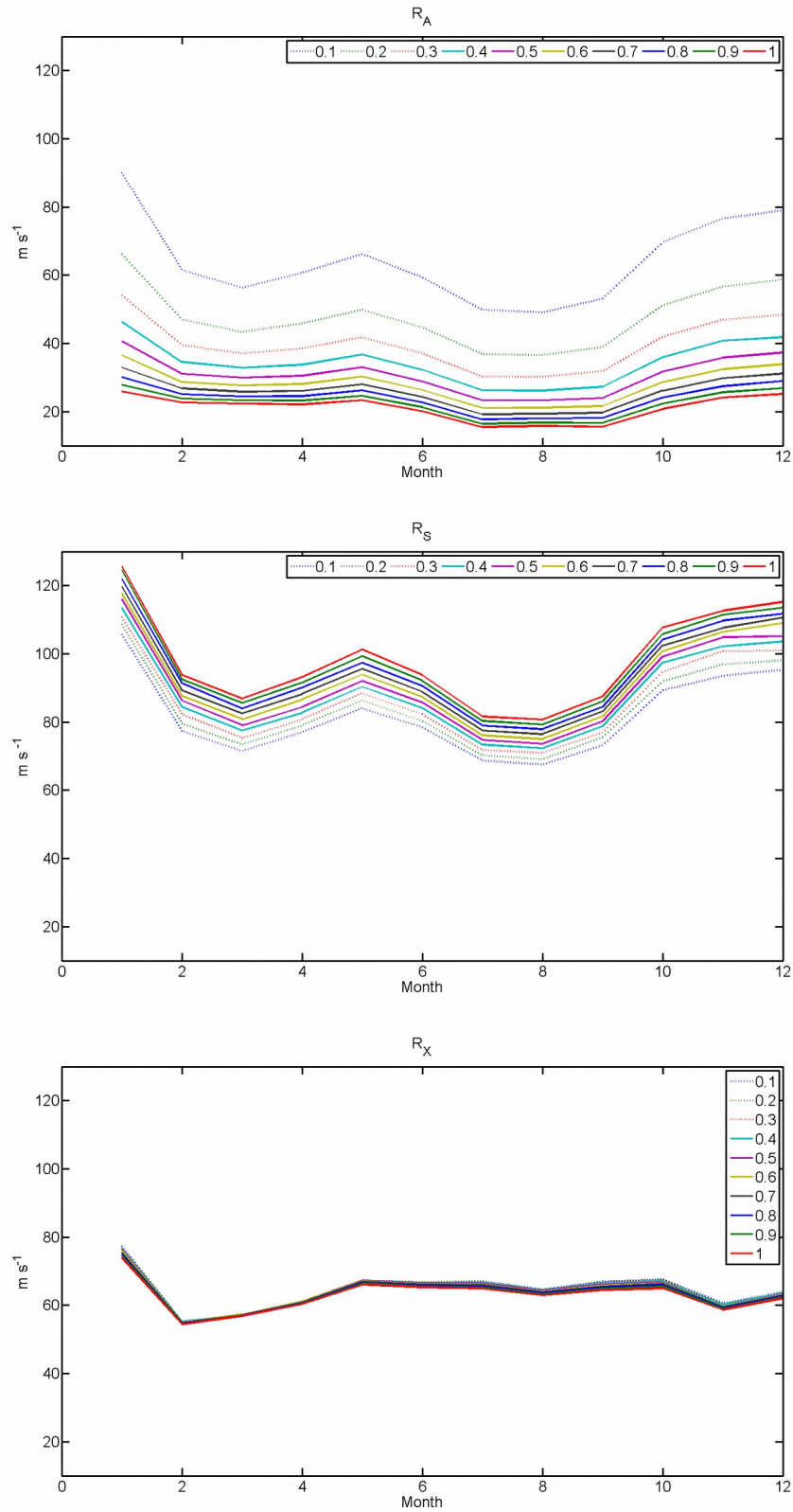
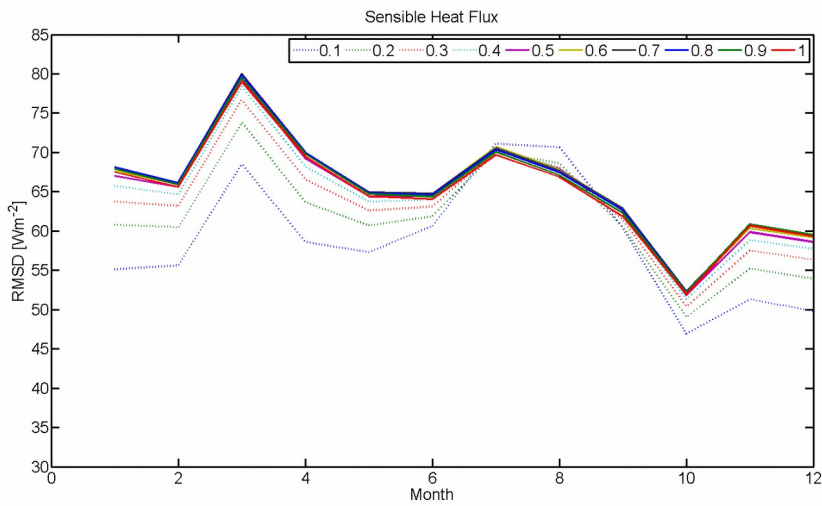
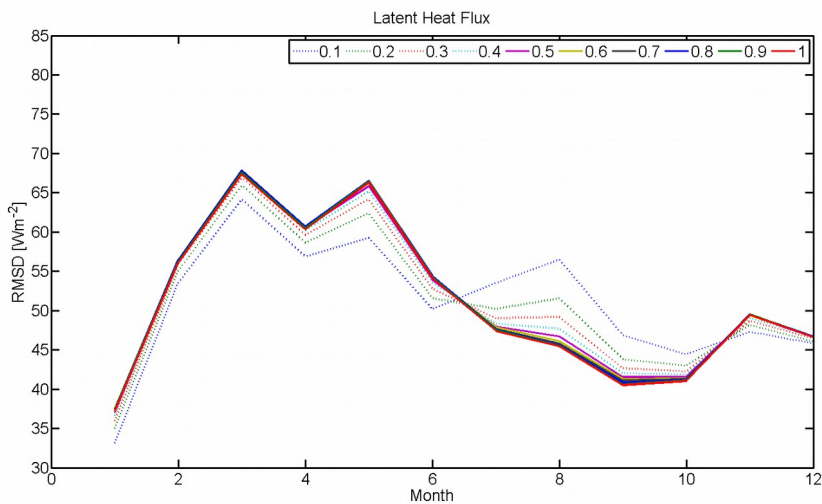


Figure 2.26: R_A , R_S and R_x monthly values with Z_{0M} values ranging from 0.1 to 1.

Figure 2.27a shows the variation in sensible heat flux RMSD for a given number of roughness length values during the year. During the summer the model appears to be less sensitive to roughness length, probably because differences between the canopy/soil and air temperatures is much larger during this season. It can also be observed that when Z_{OM} reaches a threshold value, H RMSD finds a limit and higher Z_{OM} values do not increase the errors. LE is less sensitive to changes in roughness length (Fig. 2.27b), although during the summer, higher Z_{OM} values would reduce the error. Higher Z_{OM} might facilitate the sensible heat flux transport, with a decrease in R_A at the expense of latent heat flux, improving the simulation of low LE rates over the dry season.



a)



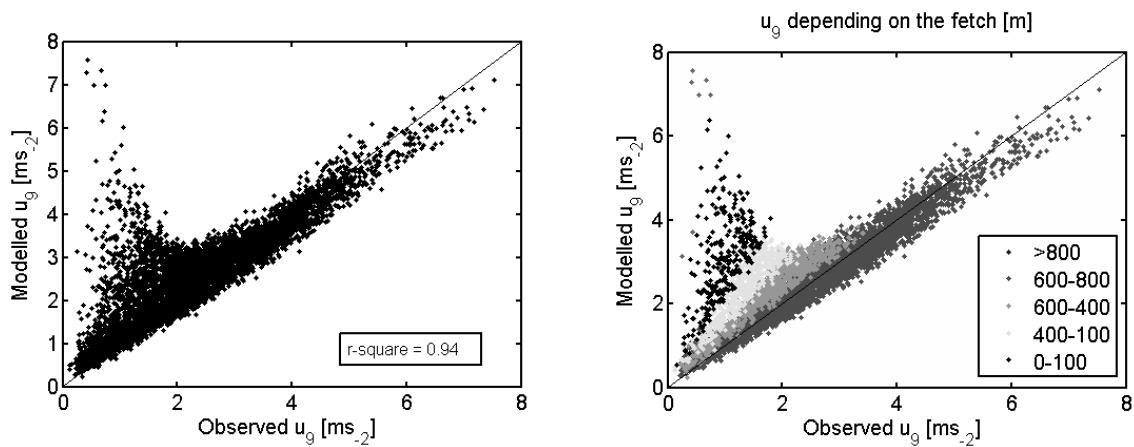
b)

Figure 2.27: a) Sensible and b) latent heat flux RMSD [Wm^{-2}] at Las Majadas, obtained for a range of roughness lengths during the year.

We found that the best adjustment for the roughness length was given by *Raupach (1994)* formulation (45% MAE), which also integrates the vertical structure of the trees. Meanwhile, *Choudhury and Monteith (1988)* gives a MAE of 125% and *Massman (1997)* of 140%. Mean “measured” roughness length is smaller ($x = 0.52$ and $\sigma = 0.3$) than the one we would have expected for this tall vegetation environment (~ 1) using the common formulations, possibly due to the low fractional cover of the oaks. The roughness length in Santa Clotilde is higher, as estimated using the friction velocity with d_0 as a constant ($d_0 = 3.5$) it gives a higher Z_{OM} value ($x = 0.7$ and $\sigma = 0.55$) than for Las Majadas, due probably to the steeper slope observed in the landscape and to a lesser extent to the slightly higher tree height (8.5 vs. 8 m). When the separate estimates of Z_{OM}/d_0 for trees and grass were needed (wind speed profile modification), we assumed the *Raupach (1994)* formulation for the oak (function of tree vertical and horizontal structure) and the *Massman (1997)* formulation for the grass (function of the LAI and the height) which presented good results in previous studies of this kind of herbaceous vegetation (*Norman et al., 1995; Kustas and Norman, 1999; Cammalleri et al., 2012*).

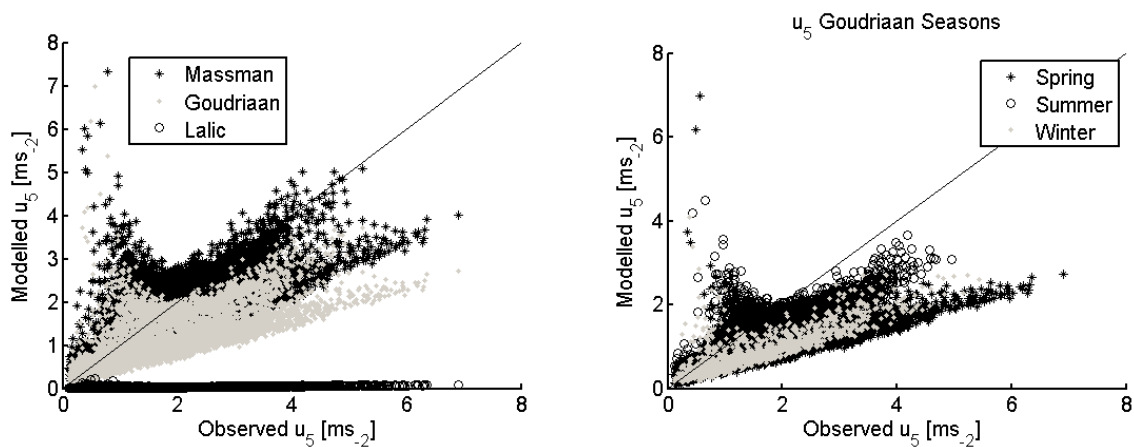
2.3.6 Wind profile analysis

As observed by *Brutsaert (1984)*, the use of an exponential wind profile inside the foliage space may not be always appropriate, especially close to the soil surface. For this reason, *Goudriaan (1977)*, *Massman (1987)* and *Lalic et al. (2003)* formulations were tested comparing the estimations with the wind speed measured at 5 meters over Las Majadas for year 2011. Estimates of wind speed at 9 meters using a logarithmic approach were also compared with the measurements. The MAE in the estimate of wind speed at 9 meters (outside the canopy layer) using a simple logarithmic approach considering stability effects was 20%, with r^2 of 0.94 (Fig. 2.28a). The errors were highly dependent on the fetch influencing the measurements (Fig. 2.28b), with significantly higher errors when the fetch was up to the first 100 meters. As the figure shows, this low fetch reflects low wind speeds and highly unstable conditions. Under these circumstances, the logarithmic profile may break down.



a) b)
 Figure 2.28: a) Wind speed estimated and measured at 9 meters on Las Majadas site and b) in relation to the fetch.

With regard to the estimates of wind speed at a height of 5 meters (within the tree canopy layer), the three formulations tested, *Massman*, *Goudriaan* and *Lalic*, yielded errors of 32%, 43% and 99% respectively (Fig. 2.29a). The *Lalic* model estimates a strong wind-speed extinction coefficient within the canopy, which yields a very low wind speed at 5 meters. In view of these results, *Lalic* model was not used for the next analyses. As Fig. 2.29b shows for the *Goudriaan* approach, differences in the slope may correspond to different seasons and consequently different leaf area indexes, with the existence and activity (dry or fully growing) of a herbaceous canopy layer influencing the relationship.



a) b)
 Figure 2.29: a) Wind speed estimated and measured at 5 m over Las Majadas. b) Wind speed estimates following *Goudriaan* related to the different seasons

When the modified wind speed profile was applied to the data (Section 2.2.2), using the *Raupach (1994)* and *Massman (1997)* formulations to estimate roughness length for the trees and grass respectively (Fig. 2.30), and then deriving an extinction coefficient for each canopy layer according to the different vegetation structures, we found that the error in the estimation of wind velocity at 5 meters was reduced to 24% using the *Massman* approach and 28% using *Goudriaan*. The LAI for the oak was always reduced by the clumping factor (0.71). This formulation takes into account for the fact that the wind speed at a height of 5 meters is only affected by tall vegetation.

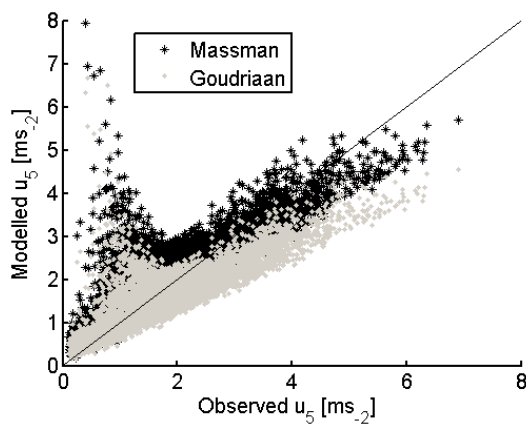


Figure 2.30: Wind speed estimated and measured at 5 meters over Las Majadas using the modified wind profile

These results encourage the consideration of the *Massman* approach as a possibility to model wind profile in TSEB, as *Cammalleri et al. (2010)* found, while the *Goudriaan* model also yielded reasonable estimates. However no measurements under the grass canopy layer were available, preventing a complete test of the assumption that separate extinction coefficients for each canopy layer might be a suitable solution for this ecosystem. Nevertheless, the use of an “oak extinction coefficient” for the wind speed estimate at a height of 5 meters seems an appropriate solution under the conditions studied.

The same procedure was employed for 14 days, during which “wind speed profile” data were collected over Santa Clotilde, when wind speed averaged 17, 12, 7 and 3 meters, displaying the same trend in the reduction of the bias, as Table 2.6 shows.

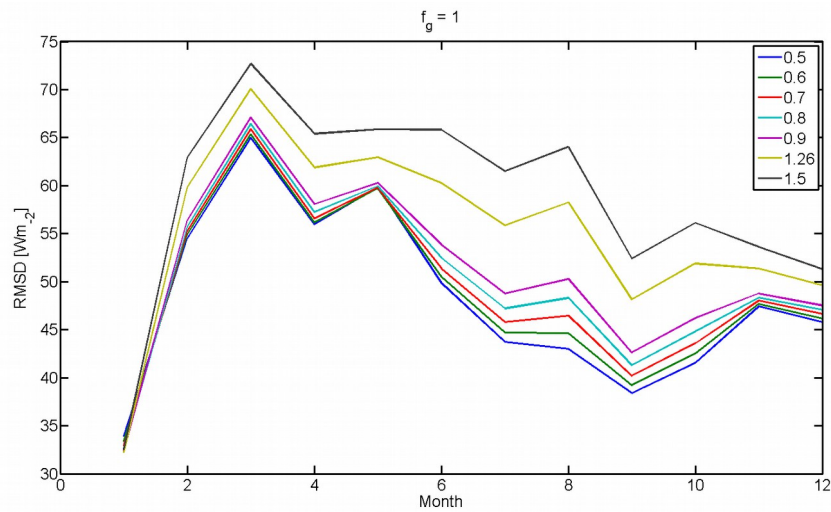
Table 2.6: MAE between measured and estimated values of wind speed at 12, 7 and 3 meters over Santa Clotilde

	Extinction coefficient for the bulk system						Different extinction coefficient for oak and grass					
	MAD u (12) m		MAD u(7) m		MAD u(3) m		MAD u (12) m		MAD u(7) m		MAD u(3) m	
	G	M	G	M	G	M	G	M	G	M	G	M
05/07/13	0.17	0.44	0.75	0.71	0.90	0.80	0.34	0.50	0.71	0.67	0.85	0.74
06/09/13	0.13	0.40	0.35	0.23	0.31	0.37	0.29	0.46	0.28	0.18	0.03	0.65
14/11/13	0.28	0.18	0.65	0.58	0.91	0.81	0.25	0.43	0.50	0.43	0.75	0.57
28/11/13	0.94	0.23	0.53	0.43	0.74	0.45	0.07	0.20	0.30	0.20	0.14	0.46
07/01/14	0.10	0.29	0.67	0.60	0.86	0.71	0.09	0.18	0.27	0.17	0.43	0.02
27/01/14	0.29	0.18	0.78	0.73	0.90	0.79	0.37	0.53	0.64	0.60	0.60	0.33
20/03/14	2.13	0.98	0.45	0.33	0.90	0.79	0.43	0.08	0.07	0.06	0.52	0.19
07/04/14	3.37	1.76	0.46	0.35	0.93	0.85	0.87	0.41	0.03	0.11	0.60	0.32
25/04/14	1.97	0.88			0.65	0.26	0.40	0.05			0.55	1.64
05/05/14	2.34	1.11	0.59	0.50	0.89	0.77	0.30	0.02	0.27	0.17	0.33	0.14
19/05/14	0.34	0.14	0.52	0.42	0.80	0.59	0.19	0.39	0.33	0.23	0.45	0.07
04/06/14	1.33	0.53	0.45	0.34	0.38	0.30	0.60	0.20	0.29	0.19	0.34	1.28
17/06/14	0.52	0.03	0.41	0.30	0.22	0.58	0.19	0.10	0.32	0.23	0.22	1.07
30/06/14	1.80	0.91	0.44	0.71	0.21	0.58	1.29	0.73	0.62	0.85	0.15	0.96
MAE	111%	58%	54%	48%	69%	62%	41%	31%	36%	31%	43%	60%

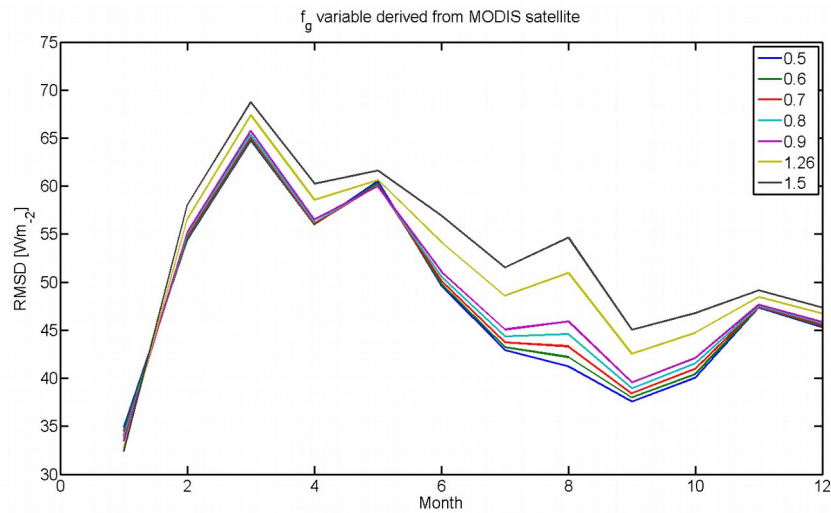
2.3.7 Priestly-Taylor coefficient analysis

The Priestley-Taylor coefficient was analyzed using an optimization scheme similar to *Agam et al. (2010)*, iteratively running the TSEB with the radiometric temperature derived from the four-way radiometer installed at Las Majadas over a range of initial values ranging from 0.1 to 1.5, using five years of data (2007-2011). After each run, modeled and observed ET values were compared. Because the available energy remains constant, it is necessary to study the RMSD of the sensible heat flux in parallel.

Initially, a constant measured LAI for oak trees, with a constant clumping factor of 0.71 and f_g equal to 1 was assumed, subsequently incorporating f_g as a variable, in order to analyze the influence of the different vegetation conditions. The selection of a P-T coefficient value for oak trees focused on data collected during the summer and winter. However, it is interesting to examine the results of the interaction in the course of the year (Fig. 2.31), even when for long periods, mainly during the autumn and spring, values corresponded to the co-existence of two contrasting vegetation layers, in this case oak trees and grasses.



a)

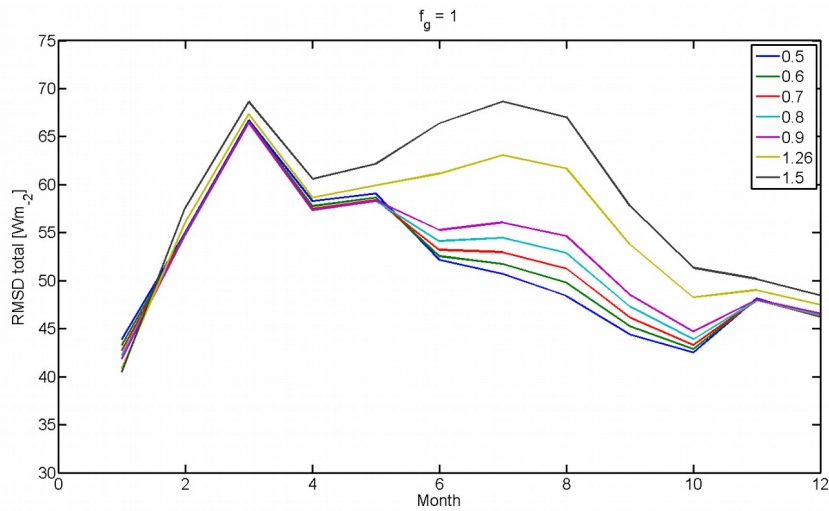


b)

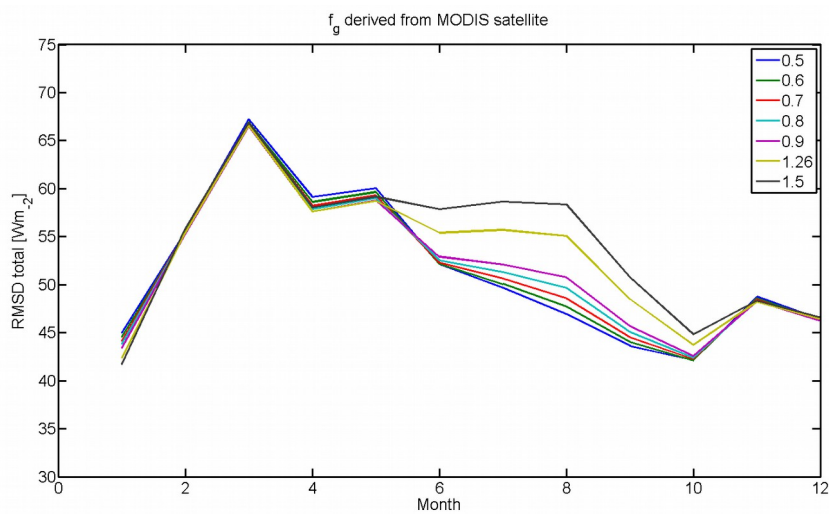
Figure 2.31: Latent heat flux RMSD [Wm^{-2}] modifying the Priestley-Taylor coefficient from 0.5 to 1.5 with a) constant f_g and b) variable f_g , for Las Majadas

This analysis confirmed that the Priestley-Taylor coefficient also displays seasonal variations (*De Bruin and Keijman, 1979*), with minimum values occurring in mid-summer, when radiation inputs were at their peak, and maxima during the spring and autumn. During the winter, the error found for LE with both applications was similar for every Priestley-Taylor coefficient selected. During the summer, less error on LE was found, with the lowest value of α_{PT} with $f_g=1$ and for f_g variable. Up to $\alpha_{\text{PT}} = 0.9$, errors during the summer remain low, and large differences could not be found in the interval 0.5-0.9, but when the standard value $\alpha_{\text{PT}} = 1.26$ is selected errors rose around 10 Wm^{-2}

with $f_g=1$ and slightly less with f_g variable. The best fit for LE in summer corresponded to a $\alpha_{PT} = 0.5$, even taking into account the green fraction that in this case is not low enough to constrain LE rates over the dry season. However, the difference in TSEB performance varies little with α_{PT} ranging from 0.5 to 0.9. During the winter, the best fit was when $\alpha_{PT} = 1.08$.



a)



b)

Figure 2.32: Average RMSD [Wm^{-2}] for LE and H, modifying the Priestley-Taylor coefficient from 0.5 to 1.5 with a) constant f_g and b) variable one, at Las Majadas

Attending to the RMSD incorporating sensible heat flux with variable f_g , presented in Fig. 2.32b, we can see that during almost all the winter, when there is no grass layer, the best fit P-T

coefficient is greater than 1, although the range of error is low. In summer, $\alpha_{pT} = 0.5$ still has the best fit. It can be seen that P-T coefficient value does not greatly influence the overall error except during the summer period, when values higher than 0.9 result in errors of more than 10 Wm^{-2} .

P-T bulk coefficient estimation with the equilibrium ET and its relationship with vapor pressure deficit (VPD)

α_{pT} bulk estimation displayed average values of 0.57. Usually LE in the equilibrium is higher than or equal to LE (Fig. 2.33), so the coefficient may vary between 0 and 1. In forest environments, this approach has been adopted in order to take into account the P-T coefficient (Komatsu, 2005), but in this case with the low tree fractional cover, is not possible to isolate the influence of the soil. As Figure 2.34 shows, the P-T coefficient displayed an indirect relationship with the VPD as suggested by Agam et al. (2010) and Baldocchi and Xu (2007). In this ecosystem, VPD could reach peak values of more than 6 mb during the dry season.

The estimation of α_{pT} for summer season with no grass in the field, using the net radiation reaching the canopy displayed an average value of 1.03, with wide variation (± 0.6).

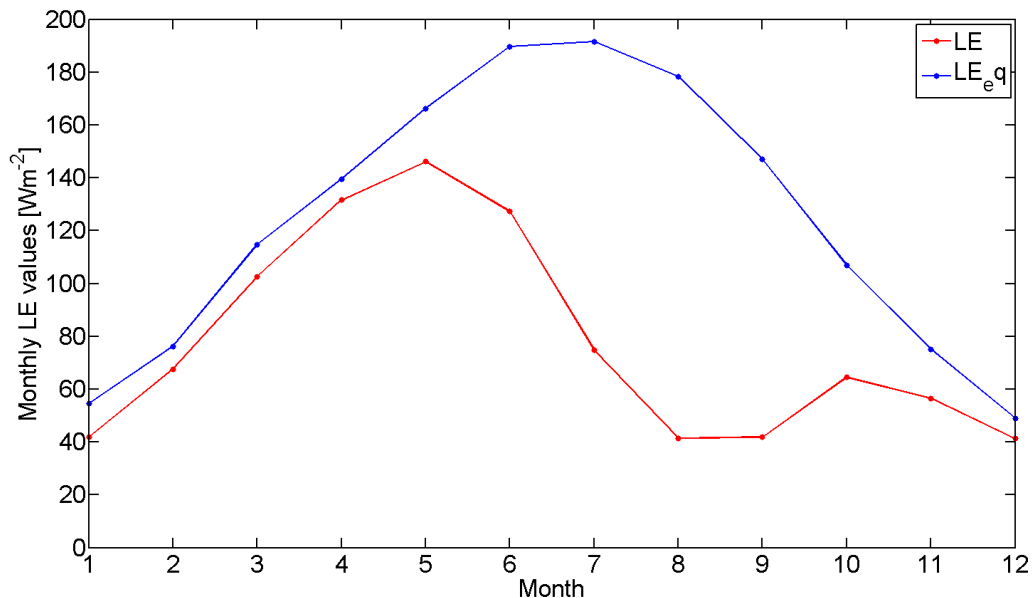


Figure 2.33: Le_{eq} and LE [Wm^{-2}] measured over Las Majadas for 2007-2011 period.

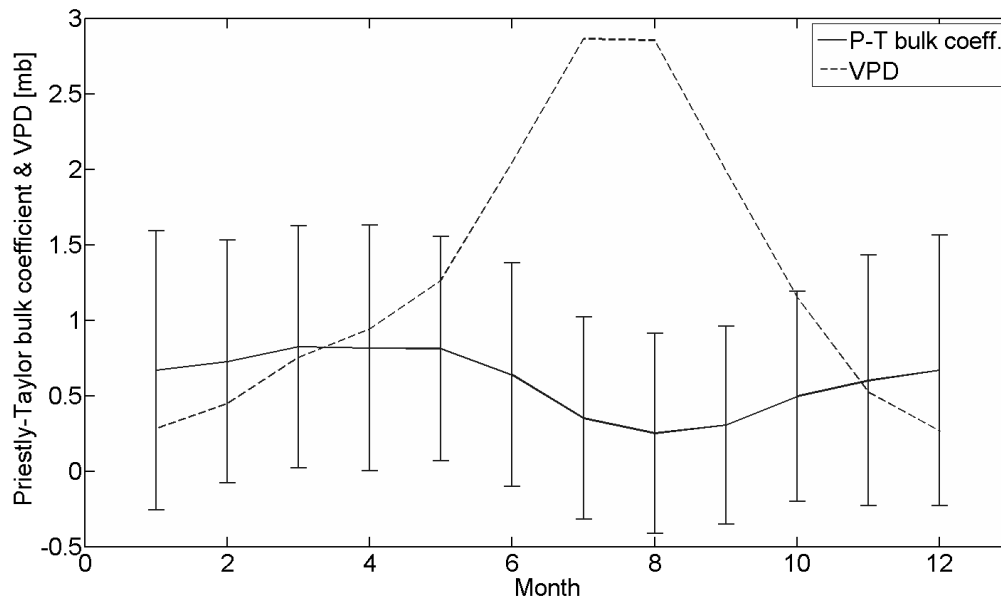


Figure 2.34: α_{PT} bulk estimations vs. VPD over Las Majadas for 2007-2011 period.

Baldocchi and Xu (2007) found that the maximum value of α_{PT} for a similar ecosystem with dry grass and at full leaf and soil moisture was about 0.9, 30% less than the values associated with evaporation from green, well-irrigated and fertilized crops such as wheat (*Baldocchi and Xu, 2007; Priestly-Taylor, 1972*). In forest, observational studies found that unstressed α_{PT} associated with canopy is significantly lower than the typical value of 1.26. Some of the values found for temperate broad-leaf evergreen forest were 0.99 (*Droppo et al., 1973*), 0.65 (*Kelliher et al., 1992*), 0.93 (*Kanda et al., 1997*), 0.61 (*Tanaka et al., 1998*), 0.64 (*Meiresonne et al., 1999*) and 0.72 (*Black, 1979, Shuttleworth and Calder, 1979, Giles et al., 1985*). *Komatsu (2005)* found for temperate broad-leaved forest a mean value of 0.82 ± 0.16 . In general, on the basis of all these studies we can conclude that natural vegetation displays a value of α_{PT} that is lower than the standard for crops, reflecting the relatively conservative water-use tendencies of undomesticated plants. Taking into account these previous studies and the results presented in this section, we decided to modify the Priestly-Taylor coefficient value to 0.9 for this ecosystem, related to the fact that values higher than that result in errors of more than 10 Wm^{-2} in the summer period.

2.3.8 Detail-scale evaluation of TSEB integrating the parameter analysis (Z_{OM}/d_0 and P-T coefficient) and the wind profile modifications (TSEB G, TSEB M, TSEB Gp, TSEB Mp, TSEB ef)

Figure 2.35 compares estimated and observed fluxes for different applications of TSEB versions. In order to be more accurate, and to test the assumption of a constant oak LAI and variable grass LAI we used the LAI measured at Las Majadas during 2008 and 2009, with a clumping factor over nadir view of 0.71. As model input (air temperature and humidity, solar incoming radiation and wind speed) and validation data (four surface energy fluxes) we used the data-set collected over the same period by the eddy covariance tower. The Priestley-Taylor coefficient finally selected was 0.9, with f_g estimated using MODIS remote information, as described in section 2.2.2.1. The roughness length formulation selected for the application of TSEB with *Goudriaan (1977)* and *Massman (1987)* wind profiles with the common formulation of the extinction coefficient (TSEB G and TSEB M) was that of *Raupach (1994)*. When separate estimates of Z_{OM}/d_0 for the trees and grasses were required, because an extinction coefficient for each canopy layer was calculated (TSEB Gp and TSEB Mp), we employed the *Raupach (1994)* formulation for the oak (function of tree vertical and horizontal structure) and the *Massman (1997)* formulation for the grass (function of the LAI and the height). Table 2.7 presents RMSD values for every version, including the TSEB with a P-T coefficient equal to 1.26.

In both Figure 2.35 and table 2.7, we can see that all the modified versions outperformed the direct application of TSEB. TSEB G and TSEB M showed less dispersion, but differences between the modified wind speed profiles versions are hardly noticeable. R_n is almost invariant as well as G in all simulations. All versions (TSEB G, TSEB Gp, TSEB M, TSEB ef) except the *Massman* modified wind speed profile (TSEB Mp) that calculates an extinction coefficient for each canopy layer, tended to overestimate LE for low-medium values showing the opposite trend for H , possibly because even integrating the green fraction and reducing the α_{PT} coefficient, during the dry periods without available water LE flux is so low as to approach zero. Original TSEB overestimate LE during the whole year, specially in summer.

Table 2.7: RMSD for Rn, G, H and LE from the application of TSEB and the different versions with T_{RAD} derived from the 4-way radiometer (ECT).

RMSD [Wm^{-2}]	TSEB $\alpha_{PT} = 1.26$	TSEB G	TSEB M	TSEB Gp
Rn	27	27	28	30
G	28	28	28	28
H	50	48	46	55
LE	60	46	46	48

After the modifications, RMSD between estimated and observed values for the energy fluxes are within the limits found by other authors for more uniform and homogeneous canopies (*Norman et al., 1995; Kustas and Norman, 1999; Timmermans et al., 2007; Sánchez et al., 2008; González-Dugo et al., 2009*), and the uncertainties of the measurement technique ($\sim 40 Wm^{-2}$). It is worth noting that all the modified wind profile versions that account for the existence of different canopy layers, with different extinctions coefficients displayed similar deviations, without a significant improvement using them. The *Massman* model yielded reasonable estimates of both fluxes, with lower discrepancies than the *Goudriaan* approach. *Cammalleri et al. (2010)* found for a similar sparse woody crop (olive orchard) RMSD for H and LE of 40 and 43 Wm^{-2} respectively following *Goudriaan*, and 32 and 40 Wm^{-2} with the *Massman* approach. The RMSD for net radiation displayed almost the same differences for both formulations, 28 Wm^{-2} , as the ones we found here. However, soil heat flux RMSD is lower (17 – 16 Wm^{-2}), in this application influencing the differences between modeled and observed values in the turbulent fluxes. TSEB without any modification ($\alpha_{PT} = 1.26$ & Z_{OM}/d_0) showed the highest error for latent heat flux, and the effective version had slightly better results for H and LE fluxes than the modified wind-profile ones.

The discrepancy between the measured and observed values of net radiation is over 14%, being almost 50% for the soil heat flux. The turbulent fluxes had a relative error of 35% for LE and 30% for H. During the dry period, the relative error of LE greatly increased, due to the small rate of measured LE. It can be derived from these results that a revision of the net radiation scheme, to account for the existence of a double canopy layer, and leading to the change in the available energy, might be a further advance in the modelling of turbulent fluxes under these conditions. Due to the magnitude of the soil heat flux in this semi-arid ecosystem and its influence on the total available energy, further research is also needed to improved the accuracy of G estimations.

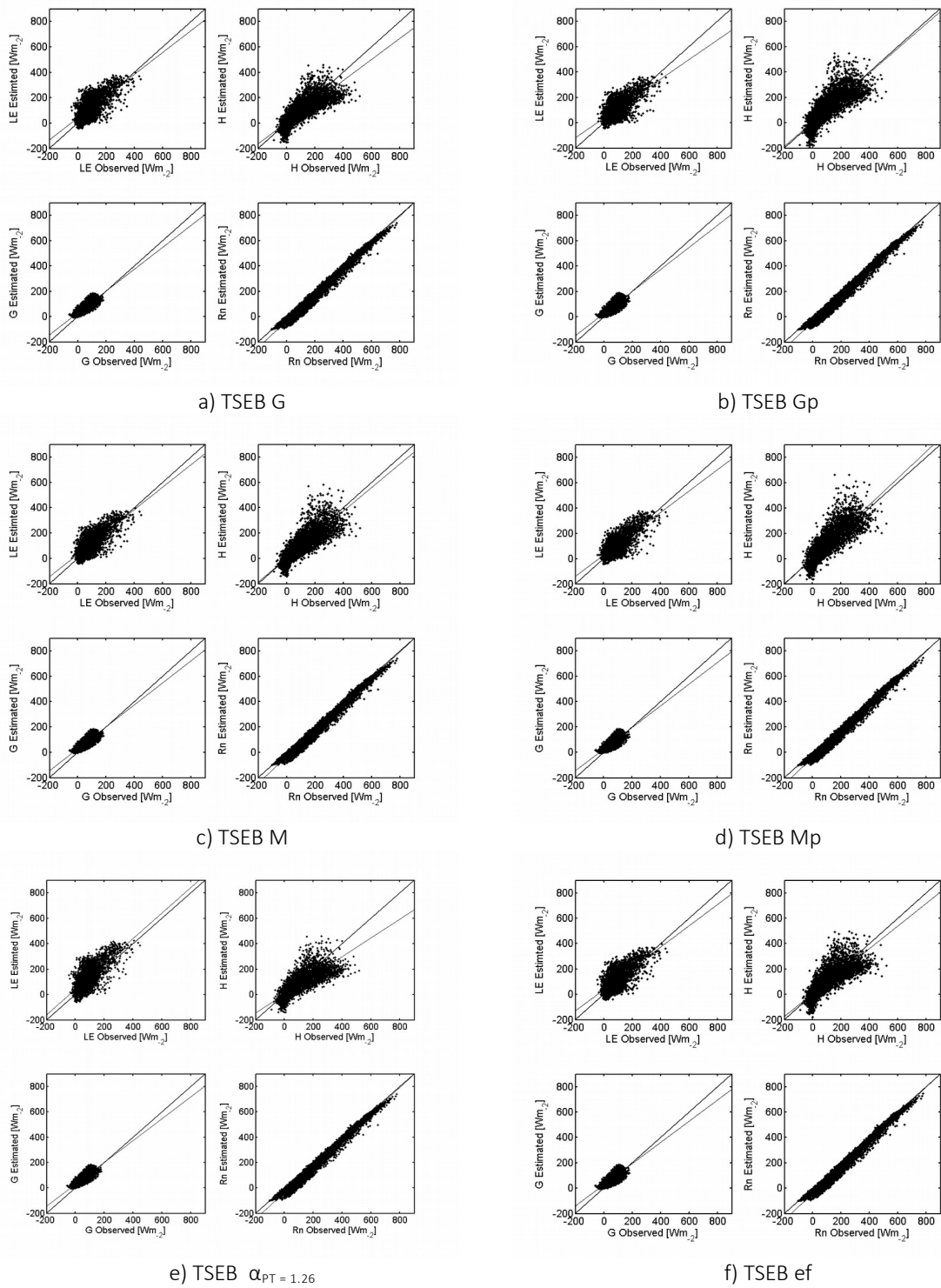


Figure 2.35. Estimated values for LE, H, G and Rn for TSEB and the different version using T_{RAD} derived from the ECTs vs. the observed values measured in the ECTs.

However, the accuracy in the estimation of LE and sensible heat for a natural cover vegetation structure as complex as the *dehesa* using the TSEB is adequate and encourages future applications. Given the results obtained in this section, the model version selected for the distributed application in a *dehesa*-type ecosystem in the following chapter 3 was a TSEB model with the simple *Goudriaan* formulation for the wind speed profile, a Priestley-Taylor coefficient of 0.9 and clumping factors over nadir of 0.71 (Las Majadas) and 0.62 (Santa Clotilde), with *Raupach* (1994) roughness length formulation.

2.5. SUMMARY AND CONCLUSIONS

Concerning the ground-truth data used to analyze the influence of complex vegetation in energy fluxes exchange modelling, the data collected by means of eddy covariance techniques, showed an average closure within the error range found by other authors (*Foken, 2008; Franssen et al., 2010*) which was suitable for evaluation/validation. The analysis of the contributing area at both ECTs indicated that the area within 500 meters contributed most to the energy fluxes measured, with 80% of the fluxes coming from the area between 0 and 1000 m. In view of these results, and considering that the same land use is extended and uniform for at least 1 km along the principal wind directions (SW at Santa Clotilde, SW and NE at Las Majadas), no problems of fetch were to be expected for ECT data measured over this wind component. Both areas sharing the same ecosystem, have similar conditions and fractional cover, making possible the extrapolation of results from one area to the other.

The energy storage within the biomass at both locations was estimated (*Stewart and Thom, 1973; Stewart, 1978*), and it was found that it could reach values greater than 10% of the net radiation, although monthly mean S values ranged between 0 and less than 10 Wm^{-2} , and could therefore be neglected under these conditions. In *dehesa* ecosystems with more dense canopies than the usual values ($f_c \sim 0.2$), integrating biomass energy storage into the surface energy balance could improve the balance closure and the further applications.

A separate analysis of the leaf area index of oaks and grasses enabled us to take into account separately the effect of each canopy layer, which differs in phenology and physiology, on the radiative and turbulent exchanges. Based on the analysis performed using local field LAI measurement and spectra information, the assumption of a constant oak LAI during the year is

acceptable for the purposes of this study. Similarly, the use remotely sensed vegetation indexes for oaks and grasses LAI estimations in this ecosystem is sufficiently accurate. The clumping factor was estimated and integrate into TSEB reducing local oak LAI, following *Kustas and Norman (2000)*, and showing values of 0.71 and 0.61 for Las Majadas and Santa Clotilde, respectively, in accordance with the ecosystem structure. Green fraction index, which was also integrate into the TSEB calculations and derived as *Guzinski et al. (2013)* suggested, may not reflect phenological conditions during the dry period with sufficient accuracy, as the comparison between that value and f_g derived from spectra information showed, and the direct comparison with photography where the phenology of the canopy layers was captured.

The roughness length and zero displacement plane parameters, used in the resistances to the heat flux transfer formulations, showed that the estimated value of d_0 was less influenced by the formulation selected than roughness length. The results of the sensitivity analysis showed that the maximum variation in flux estimation caused by the value adopted for d_0 was less than 1 Wm^{-2} for LE and 4 Wm^{-2} for H, with the variation caused by Z_{OM} being an order of magnitude greater ($\sim 20 \text{ Wm}^{-2}$). We found that the best adjustment for the roughness length was provided by the *Raupach (1994)* formulation (45% MAE), which also integrated the vertical structure of the trees. Mean “measured” roughness length was smaller (~ 0.52) than what would have been expected for this tall vegetation environment (~ 1) using the common formulations, possibly due to the low fractional cover of the oaks. The roughness length at Santa Clotilde was higher (~ 0.7) than at Las Majadas, possibly due to the steeper slope observed in the landscape and to a lesser extent to the slightly higher tree height (8.5 vs. 8 m).

The Priestley-Taylor coefficient constant value of 1.26, which influences the calculation of the canopy latent heat flux used by TSEB as the first estimation of the iteration process was revised, with a similar optimization scheme as *Agam et al. (2010)* finding that during the summer, a smaller RMSD for LE was found with the lowest values of α_{PT} . Up to $\alpha_{PT} = 0.9$, errors remained low, and larger differences could not be found in the interval 0.5-0.9, but when the standard value $\alpha_{PT} = 1.26$ was selected errors emerged at around 10 Wm^{-2} with $f_g=1$ and slightly less with f_g variable. It can be seen that the P-T coefficient value does not greatly influence the overall error, except during the summer, when values higher than 0.9 resulted in errors of more than 10 Wm^{-2} . The α_{PT} bulk estimation displayed average values of 0.57, because LE in the equilibrium is usually higher than or equal to LE, so the bulk coefficient may range between 0 and 1. In this case, the low tree

fractional cover makes it impossible to isolate the influence of the soil in this bulk coefficient. The results showed that α_{PT} bulk has an indirect relationship with the VPD, as suggested by *Agam et al. (2010)* and *Baldocchi and Xu (2007)*. The estimates of α_{PT} in summer with no grass in the field, using the net radiation reaching the canopy had an average value of 1.03, with wide variation ($\sigma = 0.6$). On the basis of the previous analysis, we decided to select value of α_{PT} equal to 0.9 from this system, in accordance with the results of *Baldocchi and Xu (2007)*, who found this value for a similar ecosystem with dry grass and at full leaf and soil moisture. In general, on the basis of our own analysis and other studies of forest and similar landscapes (*Droppo et al., 1973; Kelliher et al., 1992; Kanda et al., 1997; Tanaka et al., 1998; Meiresome, 1999; Komatsu, 2005*) we can conclude that natural vegetation displays a lower value of α_{PT} than the standard for crops, reflecting the relatively conservative water-use tendencies of undomesticated plants.

With regard to the wind-speed profile, the use of an exponential wind profile within the forest could not be appropriated in oak savanna ecosystem (*Brutsaert, 1984*) and other formulations were tested besides the one directly integrated into TSEB (*Goudriaan, 1977; Massman, 1987; Lalic et al., 2003*). The relative error in the estimates of wind speed at a height of nine meters (i.e. outside the canopy layer) assuming a logarithmic approach and taking stability effects into account was 20%, with r^2 of 0.94, which is accurate enough for this application. The errors were highly dependent on the fetch influencing the measurements, related to highly unstable conditions under which the logarithmic profile may break down. With regard to the estimates of wind speed at a height of five meters (within the tree canopy layer), the three formulations tested, *Massman*, *Goudriaan* and *Lalic*, yielded relative errors of 32%, 43% and 99% respectively. The *Lalic* model estimated a strong wind-speed extinction coefficient within the canopy, which yielded a very low wind speed at five meters. In view of these results, the *Lalic* model was not used for the subsequent analysis. The differences in the slope of the relationship between measured and estimated values of wind speed at five meters may correspond to different seasons, and consequently to different existences and activity of a herbaceous layer influencing the relationship.

When the modified wind speed profile was applied to the data, taking into account this double canopy layer by deriving an extinction coefficient for each layer, we found that the error in the estimation of wind velocity at 5 meters was reduced to 24%, when we adopted the *Massman* approach and 28% using *Goudriaan*. These results encourage us to consider *Massman* approach as

a possibility to model wind profile in TSEB under this conditions, as *Cammalleri et al. (2010)* suggested for olive groves, while the *Goudriaan* model also yields reasonable estimates. However no measurements under the grass canopy layer were available, which prevented a complete test of the assumption that separation of the extinction coefficients for each canopy layer might be a suitable solution for this ecosystem. The use of an “oak extinction coefficient” for the wind speed estimate at a height of 5 meters seems an appropriate solution under the conditions studied.

Assuming constant behavior of the oak LAI, the approaches proposed to integrate the two-canopy layers were tested, by modifying the wind-speed profile formulations to include the differences in the vegetation layers. RMSD values from the application of this different TSEB modified wind-speed profile versions, as well as TSEB with α_{PT} equal to 0.9 and Z_{OM}/d_0 computed following Raupach (1994) and TSEB with $\alpha_{PT} = 1.26$ and Z_{OM}/d_0 *Massman (1997)* are within the limits found by other authors ($\sim 20 \text{ Wm}^{-2}$ - $\sim 50 \text{ Wm}^{-2}$) for more uniform and homogeneous canopies (*Norman et al., 1995; Kustas and Norman, 1999; Timmermans et al., 2007; Sánchez et al., 2008; González-Dugo et al., 2009*), and the uncertainties of the measurement technique ($\sim 40 \text{ Wm}^{-2}$). It is worth noting that all the modified wind-speed profile versions (TSEBGp, TSEBMp, TSEBef) displayed similar deviations between each other.

The accuracy of the estimates of LE and sensible heat flux for a natural vegetation cover structure as complex as the *dehesa*, using the TSEB with an adjusted α_{PT} and a Z_{OM}/d_0 formulation that takes into account the tree structure is adequate and encourages future applications of the model on a regular basis to assist management actions over this ecosystem.

Acknowledgments. We would like to thank Arnaud Carrara and the group managing the experimental site of Las Majadas for the ground-truth ECT measurements and the additional data. We also would like to thank Bill Kustas for his critically reviewing, which led to a greatly improvement of this chapter.

This work has been funded by the Andalusian Institute for Agricultural and Fisheries Research and Training (IFAPA, Consejería de Agricultura, Pesca y Desarrollo Rural de la Junta de Andalucía) and the European Social Fund Operational Programme 2007-2013, in the field of priority Axis 3 (Improving human capital), in an 80%. The work was partly supported by grant AGL2011-30498 (Ministerio de Economía y Competitividad of Spain, co-funded by FEDER)

2.6. REFERENCES

- Agam, N., Kustas, W.P., Anderson, M.C., Norman, J.M., Colaizzi, P.D., Howell, T.A., Prueger, J.H., Meyers, T.P., & Wilson, T.B. (2010). Application of the Priestley-Taylor Approach in a Two-Source Surface Energy Balance Model. *Journal of Hydrometeorology*, 11, 185-198
- Alameda, D., Villar, R., & Iriondo, J.M. (2010). Spatial pattern of soil compaction: Trees footprint on soil physical properties. *Forest Ecology and Management*, 283, 128-137
- Anton, J.A., & Ross, J.K. (1987). Emissivity of the vegetation-soil system (in Russian with English summary). *Soviet Journal of Remote Sensing*, 5, 49-55
- Asrar, G., Fuchs, M., Kanemasu, E.T., & Hatfield, J.L. (1984). Estimating Absorbed Photosynthetic Radiation and Leaf Area Index from Spectral Reflectance in Wheat. *Agron. J.*, 76, 300-306
- Baldocchi, D. (1994). A comparative study of mass and energy exchange over a closed C3 (wheat) and an open C4 (corn) canopy: I. The partitioning of available energy into latent and sensible heat exchange. *Agricultural and Forest Meteorology*, 67, 191-220
- Baldocchi, D.D., Vogel, C.A., & Hall, B. (1997). Seasonal variation of energy and water vapor exchange rates above and below a boreal jack pine forest canopy. *Journal of Geophysical Research: Atmospheres*, 102, 28939-28951
- Baldocchi, D.D., & Xu, L. (2007). What limits evaporation from Mediterranean oak woodlands - " The supply of moisture in the soil, physiological control by plants or the demand by the atmosphere? *Advances in Water Resources*, 30, 2113-2122
- Baldocchi, D.D., Xu, L., & Kiang, N. (2004). How plant functional-type, weather, seasonal drought, and soil physical properties alter water and energy fluxes of an oak grass savanna and an annual grassland. *Agricultural and Forest Meteorology*, 123, 13-39
- Baret, F., & Guyot, G. (1991). Potentials and limits of vegetation indices for LAI and APAR assessment. *Remote Sensing of Environment*, 35, 161-173
- Bassett, I.E., Simcock, R.C., & Mitchell, N.D. (2005). Consequences of soil compaction for seedling establishment: Implications for natural regeneration and restoration. *Austral Ecology*, 30, 827-833
- Bjorkman, O. (1980). *The response of photosynthesis to temperature*. Oxford, UK: Blackwell
- Black, T.A. (1979). Evapotranspiration from Douglas fir stands exposed to soil water deficits. *Water Resources Research*, 15, 164-170
- Brasier, C.M. (1993). *Phytophthora cinnamomi* as a contributory factor on European oak declines. In A.V. N Luisi (Ed.), *Recent advances in Studies on Oak Decline*. (pp. 49-58)
- Brutsaert, W. (1984). *Evaporation into the Atmosphere: Theory, History and Applications*. Dordrecht/Boston/Lancaster: D. Reidel Publishing Company
- Calvao, T., & Palmeirim, J.M. (2004). Mapping Mediterranean scrub with satellite imagery: biomass estimation

- and spectral behavior. *International Journal of Remote Sensing*, 25, 3113-3126
- Cammalleri, C., Anderson, M.C., Ciraolo, G., D'Urso, G., Kustas, W.P., La Loggia, G., & Minacapilli, M. (2010). The impact of in-canopy wind profile formulations on heat flux estimation in an open orchard using the remote sensing-based two-source model. *Hydrol. Earth Syst. Sci.*, 14, 2643-2659
- Campbell, G.S., & Norman, J.M. (Eds.) (1998). *An introduction to Environmental Biophysics*
- Campos, I., Villodre, J., Carrara, A., & Calera, A. (2013). Remote sensing-based soil water balance to estimate Mediterranean holm oak savanna (dehesa) evapotranspiration under water stress conditions. *Journal of Hydrology*, 494, 1-9
- Carreiras, J.M.B., Pereira, J.M.C., & Pereira, J.S. (2006). Estimation of tree canopy cover in evergreen oak woodlands using remote sensing. *Forest Ecology and Management*, 223, 45-53
- Cellier, P., Richard, G., & Robin, P. (1996). Partition of sensible heat fluxes into bare soil and the atmosphere. *Agricultural and Forest Meteorology*, 82, 245-265
- Coelho, C.O.A., Ferreira, A.J.D., Laouina, A., Hamza, A., Chaker, M., Naafa, R., Regaya, K., Boulet, A.K., Keizer, J.J., & Carvalho, T.M.M. (2004). *Changes in land use and land management practices affecting land degradation within forest and grazing ecosystems in the Western Mediterranean*. Catena Verlag, Reiskirchen, Germany: Advances in GeoEcology
- Choudhury, B.J. (1987). Relationships between vegetation indices, radiation absorption, and net photosynthesis evaluated by a sensitivity analysis. *Remote Sensing of Environment*, 22, 209-233
- Choudhury, B.J., Ahmed, N.U., Idso, S.B., Reginato, R.J., & Daughtry, C.S.T. (1994). Relations between evaporation coefficients and vegetation indices studied by model simulations. . *Remote Sensing of Environment*, 50, 1-17
- Choudhury, B.J., & Monteith, J.L. (1988). A four-layer model for the heat budget of homogeneous land surfaces. *Quarterly Journal of the Royal Meteorological Society*, 114, 373-398
- David, T.S., Ferreira, M.I., Cohen, S., Pereira, J.S., & David, J.S. (2004). Constraints on transpiration from an evergreen oak tree in southern Portugal. *Agricultural and Forest Meteorology*, 122, 193-205
- De Bruin, H.A.R., & Keijman, J.Q. (1979). The Priestley-Taylor Evaporation Model Applied to a Large, Shallow Lake in the Netherlands. In, *Journal of Applied Meteorology* (pp. 898-903): American Meteorological Society
- De Bruin, H.A.R., & Moore, C.J. (1985). Zero-plane displacement and roughness length for tall vegetation, derived from a simple mass conservation hypothesis. *Boundary-Layer Meteorology*, 31, 39-49
- Diawara, A., Loustau, D., & Berbigier, P. (1991). Comparison of two methods for estimating the evaporation of a *Pinus pinaster* (Ait.) stand: sap flow and energy balance with sensible heat flux measurements by an eddy covariance method. *Agricultural and Forest Meteorology*, 54, 49-66
- Diaz, M., Campos, P., & Pulido, F.J. (1997). *The Spanish dehesas: a diversity in land-use and wildlife*. San Diego: Pain, D. J. and Pienkowsky, M. W.
- Droppo, J.G., & Hamilton, H.L. (1973). Experimental Variability in the Determination of the Energy Balance in a Deciduous Forest. In, *Journal of Applied Meteorology* (pp. 781-791): American Meteorological Society

- Entekhabi, D., & Rodriguez-Iturbe, I. (1994). Analytical framework for the characterization of the space-time variability of soil moisture. *Advances in Water Resources*, 17, 35-45
- Fisher, J.B., Tu, K.P., & Baldocchi, D.D. (2008). Global estimates of the landsat atmosphere water flux based on monthly AVHRR and ISLSCP-II data, validated at 16 FLUXNET sites. *Remote Sensing of Environment*, 112, 901-919
- Flint, A.L., & Childs, S.W. (1991). Use of the Priestley-Taylor evaporation equation for soil water limited conditions in a small forest clearcut. *Agricultural and Forest Meteorology*, 56, 247-260
- Foken, T. (2008). The Energy Balance Closure Problem: an overview. *Ecological Applications*, 18, 1351-1367
- Foken, T., Wimmer, F., Mauder, M., Thomas, C., & Liebethal, C. (2006). Some aspects of the energy balance closure problem. *Atmos. Chem. Phys.*, 6, 4395-4402
- Franssen, H.J.H., Stockli, R., Lehner, I., Rotenberg, E., & Seneviratne, S.I. (2010). Energy balance closure of eddy-covariance data: A multisite analysis for European FLUXNET stations. *Agricultural and Forest Meteorology*, 150, 1553-1567
- French, A.N., Jacob, F., Anderson, M.C., Kustas, W.P., Timmermans, W., Gieske, A., Su, Z., Su, H., McCabe, M.F., Li, F., Prueger, J., & Brunsell, N. (2005). Surface energy fluxes with the Advanced Spaceborne Thermal Emission and Reflection radiometer (ASTER) at the Iowa 2002 SMACEX site (USA). *Remote Sensing of Environment*, 99, 55-65
- Friedl, M.A. (1996). Relationships among Remotely Sensed Data, Surface Energy Balance, and Area-Averaged Fluxes over Partially Vegetated Land Surfaces. In, *Journal of Applied Meteorology* (pp. 2091-2103): American Meteorological Society
- Fuchs, M., & Tanner, C.B. (1967). Evaporation from a Drying Soil. In, *Journal of Applied Meteorology* (pp. 852-857): American Meteorological Society
- Galmés, J., Medrano, H., & Flexas, J. (2007d). Photosynthetic limitations in response to water stress and recovery in Mediterranean plants with different growth forms. *New Phytologist*, 175, 81-93
- Giles, D.G., Black, T.A., & Spittlehouse, D.L. (1985). Determination of growing season soil water deficits on a forested slope using water balance analysis. *Canadian Journal of Forest Research*, 15, 107-114
- Godefroid, S., & Koedam, N. (2004). The impact of forest paths upon adjacent vegetation: effects of the path surfacing material on the species composition and soil compaction. *Biological Conservation*, 119, 405-419
- Gonzalez-Dugo, M.P., Neale, C.M.U., Mateos, L., Kustas, W.P., Prueger, J.H., Anderson, M.C., & Li, F. (2009). A comparison of operational remote sensing-based models for estimating crop evapotranspiration. *Agricultural and Forest Meteorology*, 149, 1843-1853
- Goudriaan, J. (1977). Crop micrometeorology : a simulation study. In. Wageningen: Pudoc
- Grove, A.T., & Rackham, O. (2003). *The Nature of Mediterranean Europe. An Ecological History*. New Haven: Yale University Press
- Guzinski, R., Anderson, M.C., Kustas, W.P., Nieto, H., & Sandholt, I. (2013). Using a thermal-based two source energy balance model with time-differencing to estimate surface energy fluxes with day-night MODIS

- observations. *Hydrol. Earth Syst. Sci.*, 17, 2809-2825
- Huntingford, C., Allen, S.J., & Harding, R.J. (1995). An intercomparison of single and dual-source vegetation-atmosphere transfer models applied to transpiration from sahelian savannah. *Boundary-Layer Meteorology*, 74, 397-418
- Joffre, R., & Rambal, S. (1993). How Tree Cover Influences the Water Balance of Mediterranean Rangelands. *Ecology*, 74, 570-582
- Kaimal, J.C., & Finnigan, J.J. (1994). *Atmospheric boundary layer flows: Their structure and measurement*. New York
- Kanda, M., Moriwaki, R., Takayanagi, Y., Yokoyama, H., & Hamada, T. (1997). Environmental effect of Meiji Shrine Forest as a sink for atmospheric energy and pollutants. (I) Field observation in summer 1996. . *Tenki*, 44, 713-722
- Kelliher, F.M., Kastner, B.M.M., Hollinger, D.Y., Byers, J.N., Hunt, J.E., McSeveny, T.M., Meserth, R., Weir, P.L., & Schulze, E.D. (1992). Evaporation, xylem sap flow, and tree transpiration in a New Zealand broad-leaved forest. *Agricultural and Forest Meteorology*, 62, 53-73
- Kelliher, F.M., Whitehead, D., McAneney, K.J., & Judd, M.J. (1990). Partitioning evapotranspiration into tree and understorey components in two young pinus radiata D. Don stands. *Agricultural and Forest Meteorology*, 50, 211-227
- Kizer, M., Elliott, R., & Stone, J. (1990). Hourly ET Model Calibration with Eddy Flux and Energy Balance Data. *Journal of Irrigation and Drainage Engineering*, 116, 172-181
- Komatsu, H. (2005). Forest categorization according to dry-canopy evaporation rates in the growing season: comparison of the Priestley–Taylor coefficient values from various observation sites. *Hydrological Processes*, 19, 3873-3896
- Kondo, J., & Ishida, S. (1997). Sensible Heat Flux from the Earth's Surface under Natural Convective Conditions. *Journal of the Atmospheric Sciences*, 54, 498-509
- Kormann, R., & Meixner, F. (2001). An Analytical Footprint Model For Non-Neutral Stratification. *Boundary-Layer Meteorology*, 99, 207-224
- Kull, O., Broadmeadow, M., Kruijt, B., & Meir, P. (1999). Light distribution and foliage structure in an oak canopy. *Trees*, 14, 55-64
- Kustas, W.P., & Daughtry, C.S.T. (1990). Estimation of the soil heat flux/net radiation ratio from spectral data. *Agricultural and Forest Meteorology*, 49, 205-223
- Kustas, W.P., & Norman, J.M. (1996). Use of remote sensing for evapotranspiration monitoring over land surfaces. *Hydrological Sciences Journal*, 41, 495 - 516
- Kustas, W.P., & Norman, J.M. (1997). A two-source approach for estimating turbulent fluxes using multiple angle thermal infrared observations. *Water Resources Research*, 33, 1495-1508
- Kustas, W.P., & Norman, J.M. (1999). Evaluation of soil and vegetation heat flux predictions using a simple two-source model with radiometric temperatures for partial canopy cover. *Agricultural and Forest*

Meteorology, 94, 13-29

- Kustas, W.P., & Norman, J.M. (2000). A Two-Source Energy Balance Approach Using Directional Radiometric Temperature Observations for Sparse Canopy Covered Surfaces. *Agron. J.*, 92, 847-854
- Lalic, B., Mihailovic, D.T., Rajkovic, B., Arsenic, I.D., & Radlovic, D. (2003). Wind profile within the forest canopy and in the transition layer above it. *Environmental Modelling & Software*, 18, 943-950
- Lee, X., Massman, W.J., & Law, B. (2004). *Handbook of Micrometeorology: A Guide for Surface Flux Measurement and Analysis*.
- Lhomme, J.P., & Chehbouni, A. (1999). Comments on dual-source vegetation-atmosphere transfer models. *Agricultural and Forest Meteorology*, 94, 269-273
- Li, F., Kustas, W.P., Prueger, J.H., Neale, C.M.U., & Jackson, T.J. (2005). Utility of Remote Sensing Based Two-Source Energy Balance Model under Low- and High-Vegetation Cover Conditions. *Journal of Hydrometeorology*, 6, 878-891
- Massman, W. (1987). A comparative study of some mathematical models of the mean wind structure and aerodynamic drag of plant canopies. *Boundary-Layer Meteorology*, 40, 179-197
- Massman, W.J. (1997). An Analytical one-dimensional model of momentum transfer by vegetation of arbitrary structure. *Boundary-Layer Meteorology*, 83, 407-421
- Massman, W.J. (1999). A model study of kBH-1 for vegetated surfaces using a localized near-field Lagrangian theory. *Journal of Hydrology*, 223, 27-43
- Massman, W.J., & Weil, J.C. (1999). An Analytical one-Dimensional Second-Order Closure Model of Turbulence Statistics and the Lagrangian Time Scale Within and Above Plant Canopies of Arbitrary Structure. *Boundary-Layer Meteorology*, 91, 81-107
- Mauder, M., & Foken, T. (2013). *Documentation and Instruction Manual of the Eddy-Covariance Software Package TK3*: Universitaet Bayreuth
- Meiresonne, L., Nadezhdin, N., Cermak, J., van Slycken, J., & Ceulemans, R. (1999). Measured sap flow and simulated transpiration from a poplar stand in Flanders (Belgium). *Agricultural and Forest Meteorology*, 96, 165-179
- Mizutani, K., Yamanoi, K., Ikeda, T., & Watanabe, T. (1997). Applicability of the eddy correlation method to measure sensible heat transfer to forest under rainfall conditions. *Agricultural and Forest Meteorology*, 86, 193-203
- Monteith, J.L., & Unsworth, M. (1990). *Principles of Environmental Physics*. London
- Montoya, J.M. (1998). *Método de ordenación silvopastoral. La dehesa, aprovechamiento sostenible de los recursos naturales*. Madrid: Editorial Agrícola Española
- Moore, C.J. (1986). Frequency response corrections for eddy correlation systems. *Boundary-Layer Meteorology*, 37, 17-35
- Moran, M.S., Peters-Lidard, C.D., Watts, J.M., & McElroy, S. (2004). Estimating soil moisture at the watershed scale with satellite-based radar and land surface models. *Canadian Journal of Remote Sensing*, 30, 805-

- Morillas, L., Garcia, M., Nieto, H., Villagarcia, L., Sandholt, I., Gonzalez-Dugo, M.P., Zarco-Tejada, P.J., & Domingo, F. (2013). Using radiometric surface temperature for surface energy flux estimation in Mediterranean drylands from a two-source perspective. *Remote Sensing of Environment*, 136, 234-246
- Nakai, T., Sumida, A., Daikoku, K.i., Matsumoto, K., van der Molen, M.K., Kodama, Y., Kononov, A.V., Maximov, T.C., Dolman, A.J., Yabuki, H., Hara, T., & Ohta, T. (2008). Parameterisation of aerodynamic roughness over boreal, cool- and warm-temperate forests. *Agricultural and Forest Meteorology*, 148, 1916-1925
- Norman, J.M., Kustas, W.P., & Humes, K.S. (1995). A two - source approach for estimating soil and vegetation energy fluxes in observations of directional radiometric surface temperature. *Agricultural and Forest Meteorology*, 77, 263-293
- Oliveira, T.M. (1998). *Cartografia Quantitativa de Formaço es Arbustivas Empregando Dados de Detecção Remota*. Universidade Tecnica de Lisboa, Instituto Superior de Agronomia, Lisbon, Portugal.
- Paço, T.A., David, T.S., Henriques, M.O., Pereira, J.S., Valente, F., Banza, J., Pereira, F.L., Pinto, C., & David, J.S. (2009). Evapotranspiration from a Mediterranean evergreen oak savannah: The role of trees and pasture. *Journal of Hydrology*, 369, 98-106
- Papanastasis, V.P. (2004). *Vegetation degradation and land use changes in agrosilvopastoral systems*. Catena Verlag, Reiskirchen, Germany: Advances in GeoEcology
- Pereira, A.R. (2004). The Priestley Taylor parameter and the decoupling factor for estimating reference evapotranspiration. *Agricultural and Forest Meteorology*, 125, 305-313
- Pereira, J.M.C., Oliveira, T.M., & Paul, J.C.P. (1995). Satellite-Based Estimation of Mediterranean Shrubland Structural Parameters *EARSEL ADVANCES IN REMOTE SENSING*, 4, 14-20
- Plieninger, T., Pulido, F.J., & Konold, W. (2003). Effects of land-use history on size structure of holm oak stands in Spanish dehesas: implications for conservation and restoration. *Environmental Conservation*, 30, 61-70
- Plieninger, T., & Schaar, M. (2008). Modification of Land Cover in a Traditional Agroforestry System in Spain: Processes of Tree Expansion and Regression *Ecology and Society*, 13, 25
- Plieninger, T., & Wilbrand, C. (2001). Land use, biodiversity conservation, and rural development in the dehesas of Cuatro Lugares, Spain. *Agroforestry Systems*, 51, 23-34
- Priestley, C.H.B., & Taylor, R.J. (1972). On the assessment of surface heat flux and evaporation using large scale parameters. *Weather Revision*, 100, 81-92
- Pulido, F.J., & Diaz, M. (2005). Regeneration of a Mediterranean oak: a whole cycle approach. *Ecoscience*, 12, 92-102
- Quero, J.L., Villar, R., Marañón, T., Zamora, R., & Poorter, L. (2007). Seed-mass effects in four Mediterranean Quercus species (Fagaceae) growing in contrasting light environments. *American Journal of Botany*, 94, 1795-1803
- Quero, J.M., & Villar, R. (2009). *Parques Naturales de Sierra de Cardeña y Montoro*: Publicaciones Comunitarias, Grupo Hercules,

- Rambal, S. (1993). The differential role of mechanisms for drought resistance in a Mediterranean evergreen shrub: a simulation approach. *Plant, Cell & Environment*, 16, 35-44
- Raupach, M.R. (1994). Simplified expressions for vegetation roughness length and zero-plane displacement as functions of canopy height and area index. *Boundary-Layer Meteorology*, 71, 211-216
- Raupach, M.R. (2001). Combination theory and equilibrium evaporation. *Quarterly Journal of the Royal Meteorological Society*, 127, 1149-1181
- Raupach, M.R., & Thom, A.S. (1981). Turbulence in and above Plant Canopies. *Annual Review of Fluid Mechanics*, 13, 97-129
- Rooney, G.G. (2001). Comparison Of Upwind Land Use And Roughness Length Measured In The Urban Boundary Layer. *Boundary-Layer Meteorology*, 100, 469-485
- Ross, J.K. (1975). *Radiative transfer in plant communities*. London: Academic Press.
- Sánchez, J.M., Kustas, W.P., Caselles, V., & Anderson, M.C. (2008). Modelling surface energy fluxes over maize using a two-source patch model and radiometric soil and canopy temperature observations. *Remote Sensing of Environment*, 112, 1130-1143
- Sánchez, M.E., Caetano, P., Ferraz, J., & Trapero, A. (2002). Phytophthora disease of *Quercus ilex* in south-western Spain. *Forest Pathology*, 32, 5-18
- Schaudt, K.J., & Dickinson, R.E. (2000). An approach to deriving roughness length and zero-plane displacement height from satellite data, prototyped with BOREAS data. *Agricultural and Forest Meteorology*, 104, 143-155
- Schnabel, S., & Ferreira, A. (2004). *Prologue*. Catena Verlag, Reiskirchen, Germany: Advances in GeoEcology
- Schotanus, P., Nieuwstadt, F.T.M., & De Bruin, H.A.R. (1983). Temperature measurement with a sonic anemometer and its application to heat and moisture fluxes. *Boundary-Layer Meteorology*, 26, 81-93
- Schuepp, P.H., Leclerc, M.Y., MacPherson, J.I., & Desjardins, R.L. (1990). Footprint prediction of scalar fluxes from analytical solutions of the diffusion equation. *Boundary-Layer Meteorology*, 50, 355-373
- Shakesby, R.A., Coelho, C.O.A., Schnabel, S., Keizer, J.J., Clarke, M.A., Lavado Contador, J.F., Walsh, R.P.D., Ferreira, A.J.D., & Doerr, S.H. (2002). A ranking methodology for assessing relative erosion risk and its application to dehesas and montados in Spain and Portugal. *Land Degradation & Development*, 13, 129-140
- Shaw, R.H. (1977). Secondary Wind Speed Maxima Inside Plant Canopies. In, *Journal of Applied Meteorology* (pp. 514-521): American Meteorological Society
- Shaw, R.H., & Pereira, A.R. (1982). Aerodynamic roughness of a plant canopy: A numerical experiment. *Agricultural Meteorology*, 26, 51-65
- Shuttleworth, W.J., & Calder, I.R. (1979). Has the Priestley-Taylor Equation Any Relevance to Forest Evaporation? In, *Journal of Applied Meteorology* (pp. 639-646): American Meteorological Society
- Stewart, J.B. (1978). A micrometeorological investigation into the factors controlling the evaporation from a forest. In,

- Stewart, J.B., & Thom, A.S. (1973). Energy Budgets in pine forest. *Quarterly Journal of the Royal Meteorological Society (Q J ROY METEOR SOC)*, 99, 154-170
- Tanaka, K., Kosugi, Y., Ohte, N., Kobashi, S., & Nakamura, A. (1998). Model of CO₂ flux between a plant community and the atmosphere, and simulation of CO₂ flux over a planted forest. *Japanese Journal of Ecology*, 48, 265-268
- Tanner, B.D., Swiatek, E., & Green, J.P. (1993). Density fluctuations and use of the krypton hygrometer in surface flux measurements. In R.G.a.N. Allen, C. M. U. American Society of Civil Engineers (Ed.), *Management of Irrigation and Drainage Systems: Integrated Perspectives. National Conference on Irrigation and Drainage Engineering*. (pp. 105-112). Park City, UT.ASCE, New York
- Tanner, C.B., & Jury, W.A. (1976). Estimating Evaporation and Transpiration from a Row Crop during Incomplete Cover1. *Agron. J.*, 68, 239-243
- Timmermans, W.J., Kustas, W.P., Anderson, M.C., & French, A.N. (2007). An intercomparison of the Surface Energy Balance Algorithm for Land (SEBAL) and the Two-Source Energy Balance (TSEB) modelling schemes. *Remote Sensing of Environment*, 108, 369-384
- Twine, T.E., Kustas, W.P., Norman, J.M., Cook, D.R., Houser, P.R., Meyers, T.P., Prueger, J.H., Starks, P.J., Wesely, M.L (2000). Correcting eddy-covariance flux underestimates over a grassland. *Agric. For. Meteor.*, 103, 279–300
- Vickers, D., & Mahrt, L. (1997). Quality control and flux sampling problems for tower and aircraft data. . *Journal of Atmospheric Oceanic Technology*, 14, 512-526
- Webb, E.K., Pearman, G.I., & Leuning, R. (1980). Correction of flux measurements for density effects due to heat and water vapour transfer. *Quarterly Journal of the Royal Meteorological Society*, 106, 85-100
- Wilczak, J., Oncley, S., & Stage, S. (2001). Sonic Anemometer Tilt Correction Algorithms. *Boundary-Layer Meteorology*, 99, 127-150
- Wilson, K., Goldstein, A., Falge, E., Aubinet, M., Baldocchi, D., Berbigier, P., Bernhofer, C., Ceulemans, R., Dolman, H., Field, C., Grelle, A., Ibrom, A., Law, B.E., Kowalski, A., Meyers, T., Moncrieff, J., Monson, R., Oechel, W., Tenhunen, J., Verma, S., & Valentini, R. (2002). Energy Balance Closure at FLUXNET Sites. *Agric. For. Meteor.*, 113, 223-243
- Wilson, K.B., Hanson, P.J., Mulholland, P.J., Baldocchi, D.D., & Wullschleger, S.D. (2001). A comparison of methods for determining forest evapotranspiration and its components: sap-flow, soil water budget, eddy covariance and catchment water balance. *Agricultural and Forest Meteorology*, 106, 153-168
- Woodward, F.I. (1987). *Climate and plant distribution*. Cambridge:: Cambridge University Press

Chapter 3: Application and evaluation of TSEB over a dehesa ecosystem integrating remote sensing information from medium and low spatial resolution sensors

The main results of this chapter are been prepared for publication in a peer review journal. Partial results have been previously presented at:

Andreu, A., Kustas, W. P., Polo, M. J., Anderson, M. C., González-Dugo, M. P., 2013. Modelling surface energy fluxes over a dehesa ecosystem using a two-source energy balance model and medium resolution satellite data. Proc. SPIE 8887, Remote Sensing for Agriculture, Ecosystems, and Hydrology XV, 888717 (16 October 2013); doi: [10.1117/12.2029235](https://doi.org/10.1117/12.2029235)

Andreu, A., W. P. Kustas, M. C. Anderson, A. Carrara and M. P. González-Dugo. *Seguimiento de los flujos de energía en superficie en una dehesa integrando datos térmicos en un modelo de doble fuente. (Monitoring surface energy fluxes in a dehesa with the integration of thermal data in a two-source model.* Asociación Española de Teledetección, Madrid, 2013.

González-Dugo, M. P., A. Andreu and M. J. Polo. *Remote sensed monitoring of dehesa ecosystem evapotranspiration and water stress.* Environmental Workshops 2013: Oak forest coping with global change: ecology and management, UNIA, Baeza, 2013.

González-Dugo, M. P., Andreu, A., Carpintero, E., Gómez-Giraldez, P. and Polo, M. J., 2014. Vegetation water stress monitoring with remote sensing-based energy balance modelling. Geophysical Research Abstracts, Vol. 16, EGU2014-13298, 2014, EGU General Assembly 2014.

3.1 INTRODUCTION

Mediterranean evergreen oak woodlands in Southern Spain (*dehesas*), Portugal (*montados*) and Greece are savanna-type ecosystems with widely-space trees (*Quercus ilex*, *Quercus suber*, *Quercus pyrenaica* and *Quercus rotundifolia*) combined with a sub-canopy of crops, annual grassland and shrubs. They are widely distributed over Europe (≈ 3 million hectares) and Mediterranean-type climate areas (e.g. California and South Africa), being recognized as an example of sustainable land use that depends upon human maintenance (*Habitats Directive 92/43/EEC*), forming a multiple agroforestry land use system (*Diaz et al., 1997; Plieninger and Wilbrand, 2001; Grove and Rackham, 2003; Papanastasis, 2004; Carreiras et al., 2006*). The climate of these areas is highly seasonal and variable, with wet winters and hot dry summers, when natural droughts are frequent. The intensity and duration of these events is increasing, aggravated by the intensification of use and global warming (*Pulido and Díaz, 2005; Miranda et al., 2006*).

A better understanding of the processes that drive the functioning of these ecosystems and how they respond to these changes could therefore improve their management and conservation. In these water-controlled ecosystems there are many interactions between climate, soil and vegetation, with evaporation (ET) being a key indicator of woodland health (*Moran et al., 2004*), connecting the energy and water budgets. As these ecosystems comprise several layers of vegetation that differ in physiology and phenology (*Baldocchi et al., 2004; Baldocchi and Xu, 2007*) and areas with bare soil, they cannot be treated as a single spatially uniform system for energy and water exchanges (*Paço et al., 2009*). These ecosystems, located in rainfall transition areas, are well adapted to the extreme and variable weather conditions, and have evolved control mechanisms to deal with water-stress conditions.

In this context, regional estimation of ET using thermal-based EB models which distinguish soil/substrate and vegetation contributions to the radiative temperature and radiation/turbulent fluxes such as TSEB (*Norman et al., 1995; Kustas and Norman, 1999*), can be more precise than single-source approaches (*Timmermans et al., 2007; Gonzalez-Dugo et al., 2009*). Moreover, TSEB has a more robust physical basis than other models and allows for adaptation to the specific characteristics of the ecosystem, modifying some aspects of the EB in order to take into account

the particular physiological, phenological and meteorological conditions of this ecosystem. The model has largely been validated over agricultural areas (*Kustas and Norman, 1997; French et al., 2005; Timmermans et al., 2007; Gonzalez-Dugo et al., 2009*), while studies of woody natural vegetation or woody crops are less common (*Cammalieri et al., 2010; Guzinski et al., 2013; Morillas et al., 2013*). Although further research is required, mapping ET on this regional scale is currently possible by integrating earth observation techniques, using distributed information as model input to describe the current surface status. This provides a better representation of ecosystem heterogeneity and takes to a certain degree local meteorological conditions into account.

In this study, a TSEB model that integrates satellite remote-sensing images was evaluated in two areas of *dehesa* ecosystem Western and Southern Spain. Instant LE values [Wm^{-2}] and the associated daily ET values [mm] were derived on a regional scale and compared with ECT measurements, this last value being more useful for agricultural and hydrological purposes than the one directly provided by the model at the time of the satellite overpass. Distributed ET over Andalusian *dehesa* was mapped as an approach to monitor the ecosystem status on a regular basis. This procedure might permit early detection of droughts and the determination of ecosystem health, by examining whether the vegetation is operating adequately, maintaining its optimal activity and structure over the time, or is water-stressed, what reduces its capability to produce quality commodities and provide services to society (*Moran, 2003*).

3.2. MATERIALS AND METHODS

Details of two study areas, the input meteorological data (air temperature, wind velocity, solar incoming radiation and relative humidity) and the ground-truth data for validation are described in Chapter 2, sections 2.2.1 and 2.3.1. One site is located in Southern Spain (Santa Clotilde, Andalucía, 39°56' N; 5°46' W, 736 m a.s.l), and the other in the Southwestern (Boyal de Majadas del Tiétar, Extremadura, ES-LMa, 39°56' N; 5°46' W, 260 m a.s.l). Both study sites are *dehesa*-type ecosystems, with homogeneous landscapes and smooth topographies, gentle slopes and Mediterranean climate. Ground fractional cover of the oaks (f_c) is around 20%, determined during the period with maximum spectral contrast between the overstorey and the understorey (*Carreiras et al., 2006*). Significant parameters for the description of the canopy structure, such as

leaf area index (LAI), tree height or leave size have been assessed in the field.

All energy balance components used to evaluate the behavior of the model were measured directly with eddy covariance towers (ECT), the closure balance error being 20% and 14% for Santa Clotilde and Las Majadas respectively, both values within the range found by other authors (Foken, 2008; Franssen et al., 2010). A cumulative normalized contribution to the flux measurement curve was estimated for each area as a function of the distance from the measurement point, as well as the relative contribution to the measured flux (Schuepp et al., 1990). The area that contributed most to the energy fluxes measured at both ECT was within 500 meters, with 80% of the fluxes captured by the ECT coming from the area between 0 and 1000 m. Principal wind direction is SW for Santa Clotilde, with 1 km fetch, and SW and NE for Las Majadas, with 1.5 km and 2 km fetches respectively.

Both areas share the same ecosystem, and although they are located 250 kilometers apart they have similar conditions and fractional cover, making it possible to assume the extrapolation of the results from one area to the other. Since both of them can be regarded as representative of the *dehesa* ecosystem, the results should be useful for the whole region and other savanna areas with similar conditions.

The TSEB model was evaluated in chapter 2 with the radiometric temperature derived from the ECT data, to refine the formulation, and the behavior of some key parameters was also analyzed, finding that the application of the TSEB was accurate enough to continue with the distributed application. In this study, the TSEB model was employed, and was compared using MODIS (*Moderate Resolution Imaging Spectroradiometer*) images at both study sites, testing the scale-dependance of the model outputs. Daily ET [mm] was derived from MODIS images for both study sites and compared with the measurements of the ECTs. TSEB was also evaluated using Landsat-7 ETM+ and Landsat-8 OLI images, with higher spatial resolution, for the Santa Clotilde site.

After validation of the model on different scales, an example of a potential regional monitoring procedure extended over time was proposed and discussed. TSEB was employed over the whole Andalusian *dehesa*, covering around 1.2 million hectares (10 – 15 % of the region) using MODIS images and meteorological maps captured in 2014. For this first application some days of the current year during the winter, spring and summer season were selected and analyzed, with the

idea of extending the study using daily MODIS images, that might provide more continuous monitoring of the ecosystem depending on the cloud coverage. The *dehesa* over this region extends primarily along the Sierra Morena mountains (Biosphere Reserve), where it displays a high degree of geographical continuity, and to a lesser extent around Cádiz and Málaga. The most important *dehesa* ecosystems are located over the Sierra de Aracena y Picos de Aroche, Sierra Norte de Sevilla, Sierra de Hornachuelos, Sierra de Cardena y Montoro, Sierra de Andújar, Los Alcornocales and Sierra de Grazalema Natural Parks. Figure 3.1 shows *dehesa* ecosystem and the Andalusian Natural Parks, being 7 of them located at *dehesa* ecosystem.

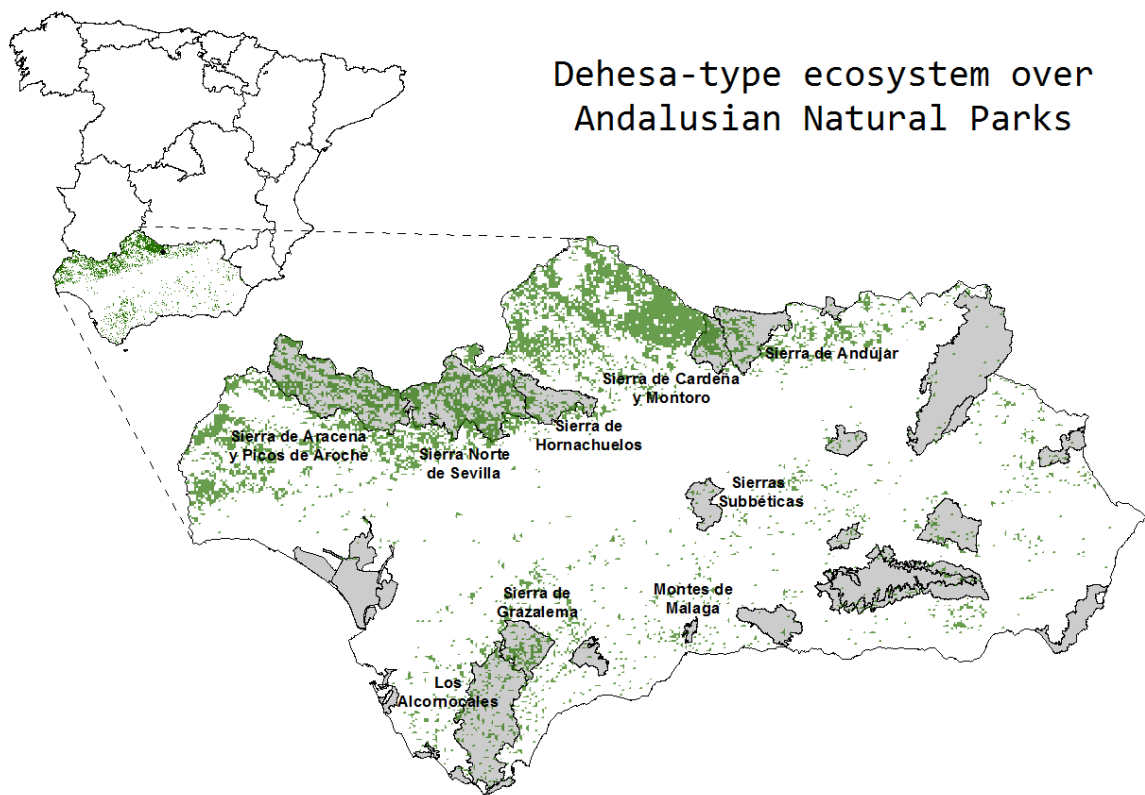


Figure 3.1: *Dehesa*-type ecosystem located over Andalusia (in green) and Natural Parks of the region (marked in grey).

3.2.1 Remote sensing data: surface radiometric temperature and vegetation indexes

Two satellite sensors with different spatial and temporal resolutions were used as a source of surface radiometric temperature (T_{RAD}) values: MODIS (*Moderate Resolution Imaging Spectroradiometer*) and Landsat 7ETM+ and 8OLI. The first sensor has daily coverage, with 250 meters and 1 km spatial resolution for the visible and the thermal bands respectively. The thermal product MYD11A1, which supplies T_{RAD} with the atmospheric and emissivity effects corrected was used. For Las Majadas, 40 days in 2008 and 2011 were analyzed and for Santa Clotilde site 65 days between 2012 and 2014. Eleven cloudless Landsat 7ETM + & 8OLI images (path 201 and row 33) coincident with the study period and the series of data from the Santa Clotilde ECT without gaps were also acquired and processed (DOY 124 for 2012 and 110, 182, 190, 198, 206, 214, 310, 318, 342, 350 for 2013). The images were already geo-referenced, with spatial resolutions of 30 m in the shortwave bands and 60/100 m in the thermal band, depending on whether the satellite was 7ETM+ or 8OLI. Atmospheric and surface emissivity effects were corrected by an atmospheric radiative transfer model MODTRAN4 (*Berk et al., 1998*). The lack of available atmospheric data required for an *in-situ* atmospheric characterization led us to use MODIS satellite-derived atmospheric profiles of air temperature and humidity (MOD07 product) which, according to *Jimenez-Muñoz et al. (2010)*, provides an RMSE of 0.6 K in radiometric temperature estimates compared to locally measured profiles. The followed procedure is described in detail in Annex I.

The dates used in the analyses have been selected from the data series from both ECT, discarding days according to the following criteria: (a) periods with gaps due to instrument failure, (b) lacking thermal information in the ECT pixel of the image due to clouds, (c) unsuitable footprint. The selection was made in an attempt to capture the seasonal variability of *dehesa*; the dates are shown in Table 3.1. However, in Santa Clotilde the first data series collected by the ECT had several gaps, mainly due to the set-up and different tests performed on the tower and the instruments, and it was not always possible to capture an image every month. Nevertheless, the data collected was distributed as homogeneously as possible, taking into account these imitations.

Table 3.1: MODIS selected dates for Santa Clotilde and Las Majadas study sites.

Year	Month	Day	Year	Month	Day	Year	Month	Day	Year	Month	Day
Santa Clotilde site			Santa Clotilde site			Santa Clotilde site			Las Majadas site		
2012	6	21	2013	7	31	2014	6	4	2008	8	3
2012	7	21	2013	8	1	2014	6	9	2008	8	13
2012	7	23	2013	8	2	2014	6	26	2008	8	27
2012	7	28	2013	8	3	2014	6	29	2008	9	7
2012	7	29	2013	8	13	2014	7	9	2008	11	1
2013	3	15	2013	8	25	2014	7	17	2008	12	2
2013	6	13	2013	8	27	Las Majadas site			2008	12	12
2013	6	26	2013	8	28	2008	1	4	2008	12	22
2013	7	5	2013	8	30	2008	1	20	2008	12	25
2013	7	6	2013	9	1	2008	1	30	2011	3	22
2013	7	7	2013	9	3	2008	3	18	2011	3	31
2013	7	8	2013	9	6	2008	3	21	2011	4	7
2013	7	12	2013	9	8	2008	3	23	2011	4	10
2013	7	13	2013	9	12	2008	4	6	2011	5	20
2013	7	15	2014	1	7	2008	4	27	2011	6	29
2013	7	16	2014	1	20	2008	4	29	2011	7	29
2013	7	17	2014	2	2	2008	5	3	2011	8	8
2013	7	20	2014	3	4	2008	5	17	2011	10	17
2013	7	21	2014	3	6	2008	6	6	2011	11	6
2013	7	22	2014	3	21	2008	6	12	2011	11	17
2013	7	24	2014	4	7	2008	6	25	2011	11	26
2013	7	26	2014	4	30	2008	7	6	2011	12	3
2013	7	29	2014	5	10	2008	7	16	2011	12	6
2013	7	30	2014	5	25	2008	7	31	2011	12	19

For the estimation of NDVI and the derivation of the leaf area index and the fractional cover, red and near infrared (NIR) bands were used, as well as blue band for the green fraction (Table 3.2), following the same procedure as described in Chapter 2, section 2.2.2.1.

Table 3.2: MODIS and Landsat-7 ETM+ and -8 OLI wavelengths intervals for Blue, Red, NIR and TIR bands

	MODIS	Landsat 7TM	Landsat 8TM
Blue	B3 (0.459-0.479 μm)	B1 (0.441-0.514 μm)	B1 (0.452-0.512 μm)
Red	B1 (0.620 – 0.670 μm)	B3 (0.631-0.692 μm)	B4 (0.636-0.673 μm)
NIR	B2 (0.841 – 0.876 μm)	B4 (0.772-0.898 μm)	B5 (0.851-0.879 μm)
TIR	B31 (10.78 – 11.28 μm)	B6 (10.31 – 12.36 μm)	B10 (10.60 – 11.19 μm)
	B32 (11.77 – 12.27 μm)		B11 (11.50 – 12.51 μm)

When the MODIS satellite was used, the NDVI for the first period (2012 and part of 2013) over Santa Clotilde was derived from the separate red and NIR bands daily reflectance data. For the

following periods and for Las Majadas, after testing, the behavior of the MODIS product MOD13Q1 with 250 m of resolution and fifteen days of frequency was regarded as accurate enough for our requirements (Figure 3.2). This product select an NDVI representative of the 15-day period, as the average of the two days with maximum NDVI and higher-quality information. For that reason, MOD13Q1 data are always higher than daily derived NDVI (Fig. 3.2). However, the similarity of the pairs of data, with RMSD between the estimated NDVI and that provided by MODIS equal to 0.03, with a relative error of 6% and the continuous nature of changes in NDVI, led to the decision to use the MOD13Q1 product directly, facilitating the process.

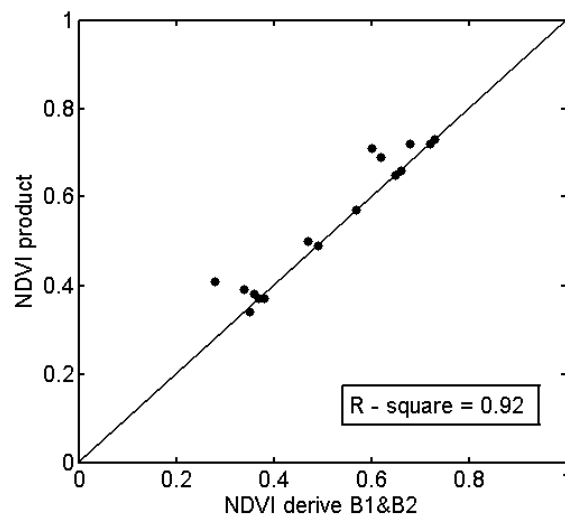


Figure 3.2: Comparison between NDVI derived from reflectance MODIS product and NDVI from MOD13Q1 product.

Landsat-7 ETM+ suffered a technical problem on 31st May 2003, related to the scan-line corrector, since when it has been operating without this instrument functioning properly. The sensor images the surface in a “zig-zag” pattern, resulting in some areas not being scanned. These areas are approximately 22% of a Landsat-7 scene (Storey *et al.*, 2005), with the effect being greater on the east and west sides, with no missing values over the central line. In this case, Santa Clotilde is on the east part of the image, with losses due to this effect that could be visible on the results. No gap-filling techniques have been used.

For the example of a potential regional monitoring procedure extended over time, the same

MODIS images for 2014 over the Iberian Peninsula, listed in Table 3.1 were selected, to apply TSEB over the Andalusian *dehesa*.

3.2.2 Derivation of the oak LAI and total ecosystem LAI from remote-sensing data

In order to isolate the effect of the tree layer from the understorey component and to study its variability in the course of the year, the local LAI of the trees was derived from MODIS data for both locations, taking into account that the LAI index thus derived integrated the clumping effect. This was done for the period when the herbaceous layer was dry, assuming that the reflectance registered by the sensor corresponded only to the oaks. The estimated oak LAI results from Santa Clotilde were compared with field measurements of LAI in order to study the accuracy of the estimation. Seven days were analyzed following this procedure (21st June, 23rd July and 23rd August 2013, 4th June, 17th June, 30th June and 17th July, 2014). During the period with an active grass layer, with local LAI field measurements of both oaks and grass, an “average ecosystem LAI” weighted by the surface occupied by each component was derived and then compared with the MODIS-estimated index. Dates available for the analysis were 15th and 21st May, 8th April, 20th September, 17th and 31st October and 14th of November in 2013, and in 2014, 25th April and 19th May.

3.2.3 Footprint analysis

In order to validate the model estimates, it is necessary to determine the area which is contributing to the ECT measurements. As we showed in Chapter 2 it is possible to integrate information from low spatial resolution sensors (pixel size $\sim 10^3$ m) directly along the principal component of the wind due to the homogeneous fetch of that area. For satellites with medium spatial resolution and lower temporal resolution, such as Landsat (pixel size of 60 and 120 meters, temporal resolution of 15 days) a weighted integration of the pixels inside the contributing area was calculated, in order to validate these estimates against ground-truth measurements even when the wind direction was not the predominant one. The method used to calculate the footprint was described by *Timmermans et al, (2009)*.

A three-dimensional footprint model that calculates the source strength, F_{xy} of a single

observation point was used as follows:

$$F_{x',y'} = \frac{F_{x'}}{\sqrt{2\pi\alpha_{y'}}} e^{-(y'^2/2\alpha_{y'}^2)} \quad (3.1)$$

where $\alpha_{y'}$ is the cross-wind spread in the direction y' perpendicular to the wind direction (x') and $F_{x'}$ is the relative contribution per running meter along the wind direction, as:

$$F_{x'} = \frac{u}{u_{star}} \frac{z_m}{k_{vk} x'^2} e^{-(u/u_{star})(z_m/k_{vk} x')} \quad (3.2)$$

where k_{vk} is the von Karman constant and z_m the measuring height. The footprint model, described in detail in *Soegaard et al. (2003)*, was then combined with a weighting function to obtain the relative contribution of each pixel to the tower measurements.

For the net radiation sensor, 99% of the observations originate from a circle whose diameter is 10 times the sensor height (170 meters), corresponding approximately to a thermal Landsat pixel. However, since a re-sampling of the T_{RAD} images to 30 meters as the visible spatial resolution bands was performed, a window of 5 x 5 pixels was taken, as well as for the soil heat flux, in an attempt to integrate the heterogeneity of this flux.

3.2.4 Daily evapotranspiration estimation

An integrated value of the latent heat flux over the day is more useful for agriculture and hydrological applications than the instantaneous values provided by the energy balance models at the time of the satellite overpass. In this case, the extrapolation was performed assuming that the energy partition among the balance components, expressed by the evaporative fraction (F_{evap}), remains constant over the day (*Shuttleworth et al., 1989; Crago and Brutsaert, 1996*). However, some authors (*Crago, 1996; Lhomme and Elguero, 1999; Gentine et al., 2007*) have found that the F_{evap} calculated in mid-days hours produced an underestimate of ET, because F_{evap} daily- curve has a convex shape with a minimum around noon. *Anderson et al. (1997)* found differences of around 10% between estimated and daily fluxes for instantaneous values computed at around the Landsat overpass time. For the same time of

day, Gonzalez-Dugo et al. (2009) found an optimal adjustment using measured fluxes with a correction coefficient of 1.1. We used an evaporative fraction given by:

$$F_{\text{evap}} = 1.1 \frac{LE}{Rn - G} \quad (3.3)$$

3.2.5 Distributed evaluation of energy fluxes over Andalusian *dehesas*

For this application of the model to the entire *dehesa* region, we selected 10 MODIS images from 2014 (2nd February, 6th March, 21st March, 7th April, 30th April, 25th May 9th June, 26th June, 9th July and 17th July) with the lowest cloud coverage and distributed over the winter, spring and summer seasons. Meteorological variables used as model input, including air temperature and humidity, wind speed and solar incoming radiation were spatially interpolated with the inverse of distance algorithms, using half hourly data registered by 29 meteorological stations in the regional agroclimatic network (RIA, Fig. 3.3). The stations were selected to integrate the variability between the different areas of *dehesa*, in an attempt to capture the heterogeneity of the *Andalucía* region.

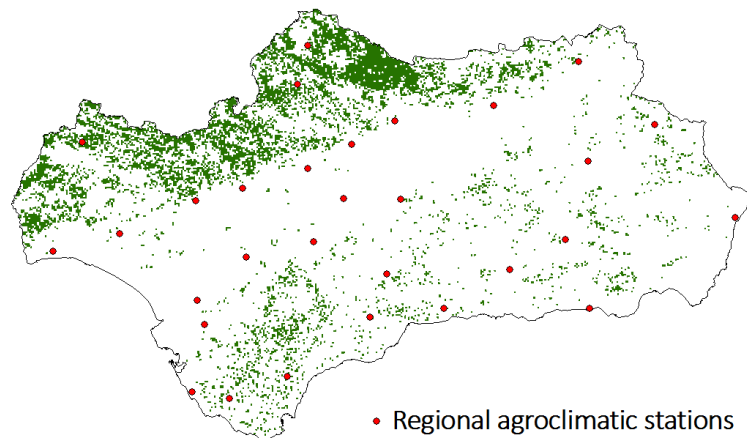


Figure 3.3: Location of the regional meteorological stations selected.

Because the fluxes from the *dehesa* need to be estimated above the woodland turbulent layer, the spatial meteorological information must be measured at greater heights than is usual (2 m). Under non-neutral conditions the air flow will be affected by the transfer of sensible heat and water vapor. However, in the lower part of the atmospheric boundary layer (dynamic layer) the water vapor and the sensible heat may be regarded as passive mixtures, and the effects of density stratification resulting from humidity and temperature gradients will be negligible. Under these circumstances (with near-neutral atmospheric conditions), the upscaling of the wind speed, air temperature and humidity with a logarithmic profile can be accurate. Given the location of the meteorological stations over open areas with bare soil and/or short grass ($h_c < 0.2$ m, Fig. 3.4), the assumption that the heights ranging from 2 to 17 m are within the dynamic sublayer can be considered accurate enough.

However, under high stable or unstable conditions the logarithmic profile may break down. Such conditions can occur (a) when the vertical motion of air is suppressed by thermal stratification (stable condition), a situation that typically occur at night when H is negative ($T_{air} > T_{RAD}$) and (b) when H is positive (the surface is warmer than the air) and mixing is enhanced (unstable condition). The first situation was not studied here, because more unstable conditions can be expected due to the time of the estimates ($\sim 13:00$ hr), which are determined by the satellite overpass. These unstable conditions produces lower wind speeds than under neutral conditions, due to strong vertical air motions which prevent significant increases in wind speed.

Highly unstable conditions are associated with low wind speeds ($< 2 \text{ ms}^{-1}$), high levels of incoming solar radiation ($> 600 \text{ Wm}^{-2}$) and steep gradients between $T_{air} < T_{RAD}$. The parameters used to estimate atmospheric stability (Obukhov length or the Richardson number) usually require measurements of heat and momentum fluxes or temperature at two different levels (Arya, 2001). The regional meteorological stations do not offer these data, and no stability corrections were therefore made for the extrapolation of wind speed following the logarithmic approach. Nevertheless, distributed maps of the gradient between T_{air} and T_{RAD} , together with wind speed and solar radiation maps were analyzed for each day, in an attempt to study the stability of the individual zones. Areas were classified into 5 classes using Pasquill (1961) scheme for each period: very unstable, unstable, near-neutral, stable and very stable. Roughness length and zero-displacement height were taken to be equal to $1/8 h_c$ and $2/3 h_c$, respectively, for the wind speed extrapolation.

To extrapolate the individual air temperature and humidity measurements provided by the meteorological stations additional information about the sensible heat flux density are needed. Therefore, taking into account the small roughness length of the area and the fact that the magnitude gradient becomes smaller far from the surface, we have assumed a constant value for these two variables.



Figure 3.4: Location of selected meteorological stations form RIA network (Source: IFAPA, *Consejería de Agricultura, Pesca y Desarrollo Rural*)

3.3 RESULTS AND DISCUSSION

3.3.1 Comparison between MODIS estimated and measured LAI. Derivation of the oak constant LAI

The RMSD between observed and estimated local oak LAI values for Santa Clotilde was 0.12, which suggests an error of 16% (Fig. 3.5). For the average LAI of the complete ecosystem, taking into account the changes in the pasture layer, the RMSD was 0.45, which yielded a 30% error. As we can see in Figure 3.5, the measured ecosystem LAI was in general lower than its estimated value. This could be caused by a mismatch in the comparison procedure. Constant values of oak and grass ground fraction coverage were assumed for every measurement day, without considering the possible existence of bare soil. This fraction is difficult to assess accurately in the field on a large scale, given its high spatial variability. However, satellite-estimated LAI suggests that this influence produces lower and more

spatially variable LAI values. During the study period, the mean estimated local LAI for the oaks (integrating a constant 0.2 f_c for the trees and estimated during summer) with MODIS over Santa Clotilde was 3.17, with a standard deviation of 0.09, and for Las Majadas was 3.37 with similar σ value.

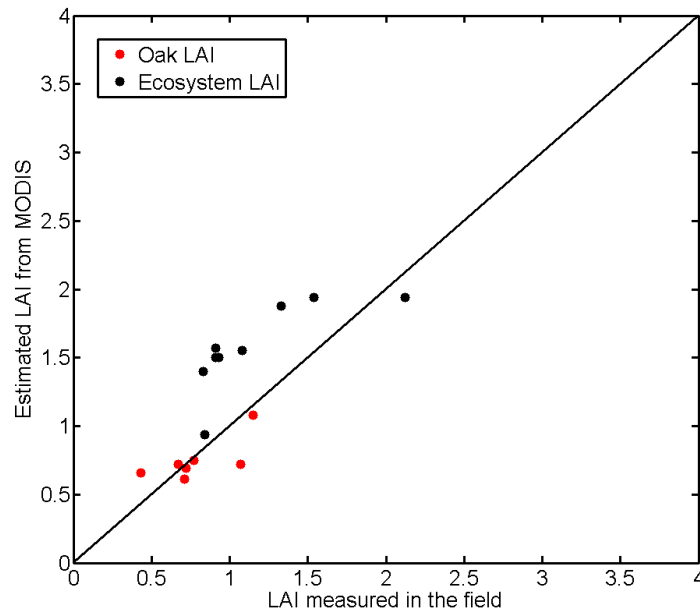


Figure 3.5: Comparison between effective LAI observed in the field (following the ecosystem structure with a constant f_c for trees and grasses) and MODIS-estimated LAI.

The variability of the effective LAI estimated with MODIS during the year is higher, because it integrates the herbaceous layer phenology, making it difficult to provide an average LAI value for the season. Effective total LAI values of 1.06 ($\sigma = 0.65$) and 1.26 ($\sigma = 0.49$) were estimated for Santa Clotilde and Las Majadas respectively, with higher deviation than oak LAI, caused by the grass influence.

3.3.2 Distributed application using MODIS images over Las Majadas and Santa Clotilde

The TSEB model was utilized and evaluated over both areas, finding that the RMSD values for the energy fluxes (Table 3.3) are within the range found by other authors (*Norman et al., 1995; Kustas and Norman, 1999; Timmermans et al., 2007; Sánchez et al., 2008; González-Dugo et al., 2009*) and consistent with typical uncertainties derived for the flux measurement system ($\sim 40 \text{ Wm}^{-2}$) (e.g.

Twine et al., 2000). Norman et al. (1995) found values of H RMSD ranging from 30 to 60 Wm^{-2} and from 40 to 55 Wm^{-2} for LE, over a semiarid rangeland and a subhumid environment, applying the original formulation of TSEB with radiometric surface temperature data measured in the field. Kustas and Norman (1999) found for a furrowed sparsely vegetated cotton crop located over central Arizona, a RMSD for Rn and G $\sim 20 \text{ Wm}^{-2}$ and 23 Wm^{-2} and 42 Wm^{-2} for H and LE, respectively, applying TSEB with ground-truth and airborne-based radiometric temperatures (Kustas, 1990). Later Kustas and Norman. (2000) integrated into the model the effect of the clumping value and found for the same location a RMSD value of 25 Wm^{-2} for H and 37 Wm^{-2} for LE. Sánchez et al. (2008) applied a TSEB patch version with ground-based surface radiometric temperature over a maize (corn) crop in Maryland, over the growing season with different fractional covers, yielding RMSD of 13 Wm^{-2} , 38 Wm^{-2} , 19 Wm^{-2} and 48 Wm^{-2} for Rn, G, H and LE respectively. Gonzalez-Dugo et al. (2009) found, when they applied the model integrating Landsat images over a rainfed corn and soybean crops located over Iowa, RMSDs of 25 Wm^{-2} for the turbulent fluxes.

Cammalleri et al. (2010b) found in a similar sparse, semi-arid ecosystem (olive orchard) as the *dehesa*, RMSD values for Rn of 28 Wm^{-2} , for G of 17 Wm^{-2} , and 40 and 43 Wm^{-2} for H and LE, respectively. It can be derived from the comparison with Cammalleri et al. (2010b) results, that an important source of error might be the higher soil heat flux error found in the *dehesa* application, as this directly influences the available energy of the system. Morillas et al. (2013) found in a much more arid environment (almost a desert) RMSD values for Rn of 58 Wm^{-2} , 64 Wm^{-2} for H and 105 for LE Wm^{-2} , with canopy and soil radiometric temperatures ground data.

Table 3.3: TSEB-MODIS RMSD of the surface energy fluxes for Las Majadas and Santa Clotilde.

	Las Majadas		Santa Clotilde	
	RMSD [Wm^{-2}]	MAE [%]	RMSD [Wm^{-2}]	MAE [%]
Rn	24	5	26	5
G	30	37	33	31
H	62	36	61	21
LE	44	28	47	35

LE relative error increases during the summer, due to the low rates of the daily flux over this semi-arid ecosystem. Differences in the Rn and turbulent fluxes magnitudes (Fig. 3.6 and 3.7) between both locations are due to the different periods/seasons selected. At Santa Clotilde (Fig. 3.7), a large number of days during the dry summer period were analyzed, with LE values being more concentrated and less

dispersed than at Las Majadas (Fig. 3.6).

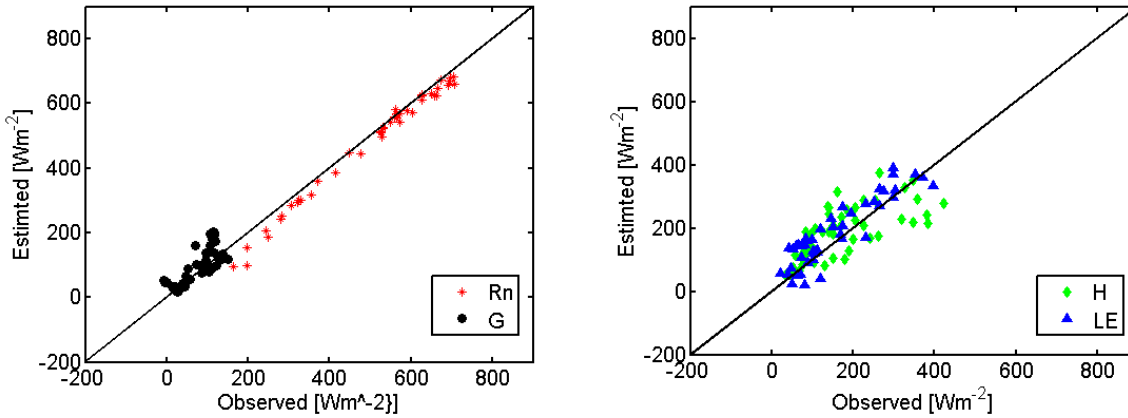


Figure 3.6: TSEB-MODIS estimated values and ECT observed values of energy fluxes over Las Majadas site during 2008 and 2011.

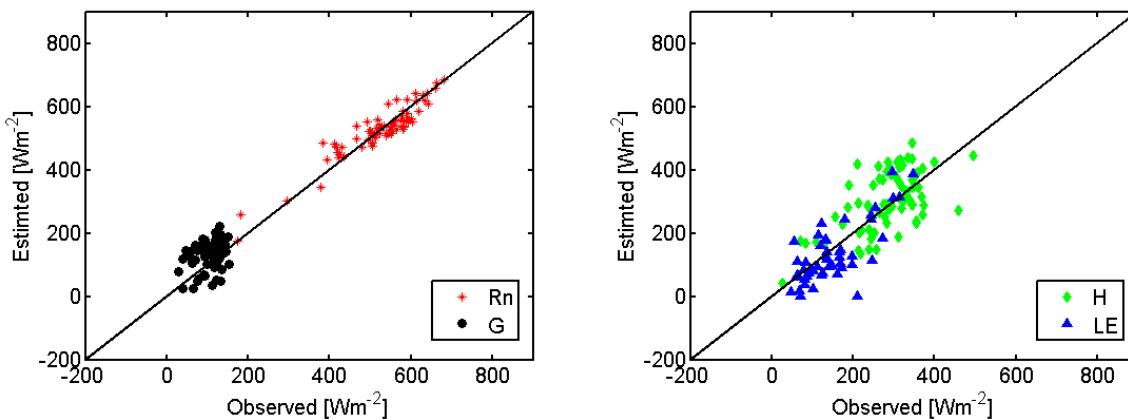


Figure 3.7: TSEB-MODIS estimated values and ECT observed values of energy fluxes over Santa Clotilde site during 2012- 2014.

3.3.3 Distributed application using LANDSAT images over Santa Clotilde area

To compare the turbulent fluxes results with the measurements it is necessary to weight the pixels that contribute to the ECT measurements. In this case the footprint analysis was made following the procedure described by *Timmermans et al. (2009)*. On 80% of the days analyzed using Landsat images, the wind direction corresponded to the predominant one (SW). A high wind speed also means a larger

footprint, and this needs to be incorporated in the validation. After studying the homogeneity of the area when no predominant wind direction was observed, we selected the days where a comparison of the ECT measurements and the TSEB estimation was possible.

Figure 3.8 shows the observed and estimated values of the energy fluxes, showing a RMSD of 64 Wm^{-2} for LE (38% absolute difference), 51 Wm^{-2} for H (26% absolute difference), and 44 (7%) and 40 (36%) Wm^{-2} for Rn and G respectively, somewhat higher than the errors found for the MODIS application but still within a similar range. Absolute discrepancies applying the model with the radiometric temperature derived from the four-way radiometer (Chapter 2, section 2.3.8) showed slightly higher values than the distributed application, particularly for Rn and G. That result might be due to the average T_{RAD} provided by the satellite, which better integrates the heterogeneity of the source area. Estimates of the G as a function of Rn reaching the soil and the time of the day may be not adequately modeled. Even when it integrates the seasonal variation of net radiation over the year, the ratio between G/Rn might not be the same along the dry/wet period (Norman *et al.*, 1995). Due to the disposition of the sensors registering G in the field, located in the EA1 and EA2 grazing areas, the measurements might be not representative of the surrounding areas. The partition between the net radiation reaching the soil and the vegetation, influenced by the two different layers of canopy (i.e. understory vegetation) might be not accurate enough in this type of ecosystem.

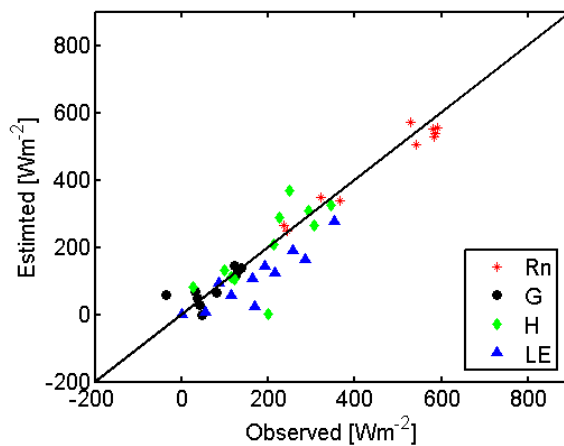


Figure 3.8: TSEB-Landsat estimated values and ECT observed values of energy fluxes over Santa Clotilde site during 2012- 2013.

Figure 3.9 shows an example of the distributed fluxes estimated over Santa Clotilde. Results derived from Landsat-7 ETM+ T_{RAD} images present unscanned areas visible as no-data lines. It can be seen that

in summer the H over the area is high compared with the LE, and the trend is inverted during wet periods (May) with maximum values of LE, as expected. However, during the winter, both turbulent fluxes are low, probably due to the low values of available energy and the lack of precipitation during the days studied. Spatial quantification of these variables, together with their evolution under different circumstances, in the context of climate change effects such as droughts, waterlogging or heat waves, could help to monitor the functioning of the ecosystem and its response to these extreme events.

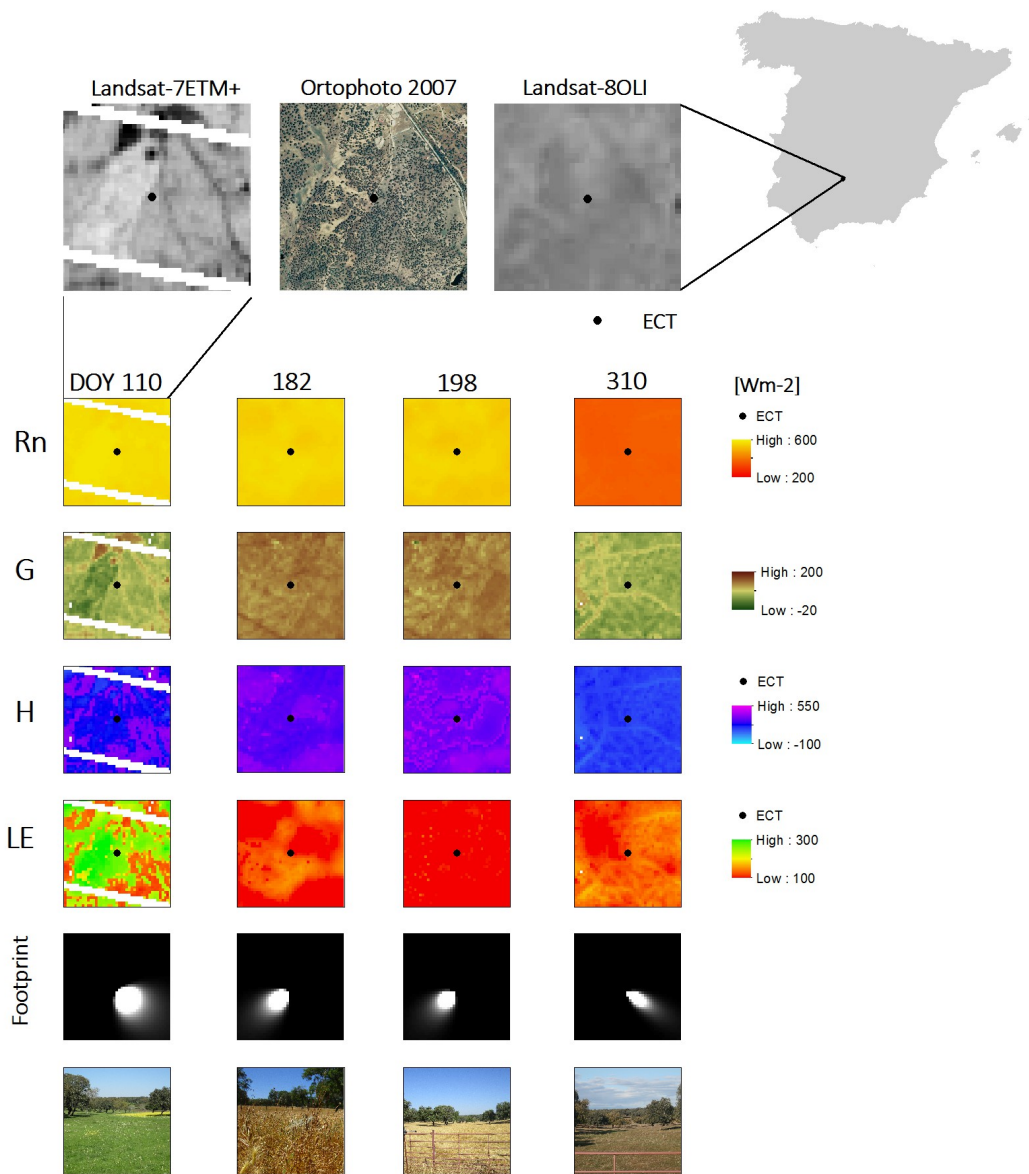


Figure 3.9: TSEB-Landsat energy fluxes distributed estimations for Santa Clotilde experimental site.

3.3.4. Temporal evaluation of daily ET

Daily estimations of ET integrating MODIS data (Fig. 3.10 and Fig. 3.11) were compared to the ground-truth measurements yielding a RMSD of 1 mm day⁻¹ for Las Majadas and 0.9 mm day⁻¹ for Santa Clotilde. Although the extrapolation to daily ET using $1.1F_{\text{evap}}$ (Eq. 3.3) during the day might contribute to the discrepancies of estimated and observed values, this accuracy was regarded as being good enough for management purposes and similar to values found by other authors for more homogeneous crops (*Kustas et al., 2013*) and similar woody sparse semi-arid crops as vineyards (*Gonzalez-Dugo et al., 2012*). However, further research of the F_{evap} daily-curve of this particular ecosystem (i.e. analyzing F_{evap} with ECTs data) is needed, particularly during stress conditions (*Lhomme and Elguero, 1999*). These results are also within the range of previous studies of this system using a different approach based on water balance and vegetation index-derived crop coefficients. *Campos et al. (2013)* found an RMSD for daily ET of 0.55 mm day⁻¹. This agreement may encourage further studies to integrate the two approaches, taking advantage of the opportunities of coupling both methodologies.

Daily ET data derived from remote sensing would allow the ecosystem to be monitored on a constant basis, and thus enable the degree of water stress that the vegetation is enduring to be assessed by comparing actual with potential ET values. Figure 3.10 shows how in Las Majadas (2008) after the end of June (around DOY 175), the curves of actual ET and reference ET (ET_0) display opposing trends, which means that the transpiration rate is drastically reduced during the summer. This is due to the reduction in green grass vegetation on the one hand and the reduction of oak transpiration caused by soil water deficit on the other. As Figure 3.11 shows, given the low rates of actual ET during the summer, the reproduction of ET values is difficult during this dry period. During 2014, the ET_0 and ET curves were similar until they reached DOY 150, when they displayed a turning point as the evaporative demand started to be higher than the capability of the ecosystem, for the given water conditions.

Although days with data points are joined up in Figure 3.10 and 3.11 by a dotted line to illustrate the evolution of ET values, the interpolation between dates is not linear and sharp changes may be expected, specially after rainfall. This limitation can be overcome to some extent using MODIS data, which can provide frequent surface radiometric temperature data, depending on the cloud coverage.

When the temporal resolution of the satellites or cloud coverage does not permit continuous monitoring, the coupling between water and energy balance models might present a good solution, using the information derived from the EB as a real proxy of the ecosystem water status to be incorporated in the continuous water-balance approach.

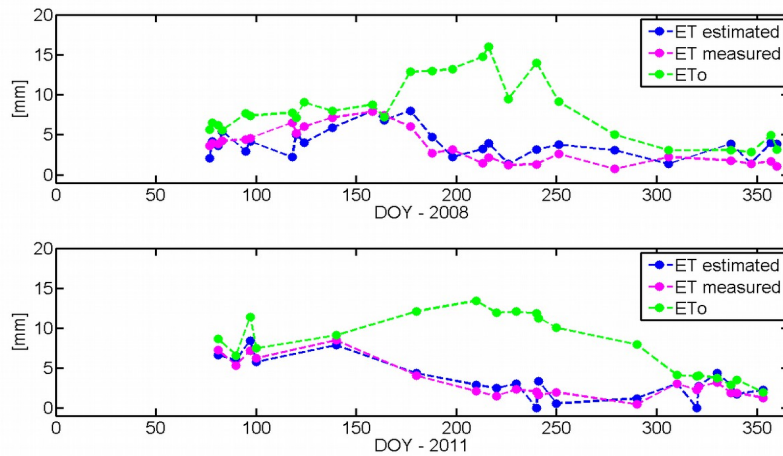


Figure 3.10: TSEB-MODIS daily estimated ET and daily measured ET (ECTs) and ET_0 for Las Majadas (2008 and 2011).

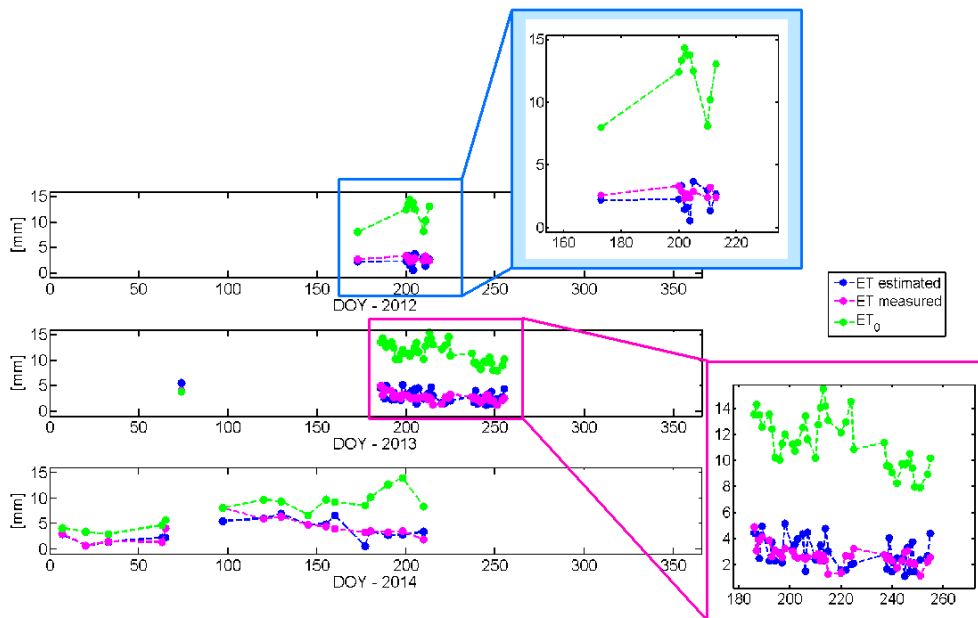


Figure 3.11: TSEB-MODIS daily estimated ET and daily measured ET (ECTs) and ET_0 for Santa Clotilde (2012-2014).

3.3.5 Evaluation of distributed energy fluxes over Andalusian *dehesas*

For this first attempt to evaluate the energy fluxes over Andalusian *dehesas*, 10 days of the current year within winter, spring and summer were selected and analyzed, with the objective of evaluating a future extension of the study using daily MODIS images, depending on the cloud coverage. Distributed maps of meteorological variables were used as input to study the heterogeneity of the region, where the differences in orographic, meteorological, abiotic and biotic conditions (Fig. 3.12) create different Mediterranean subtypes (*bioclimatic levels*).

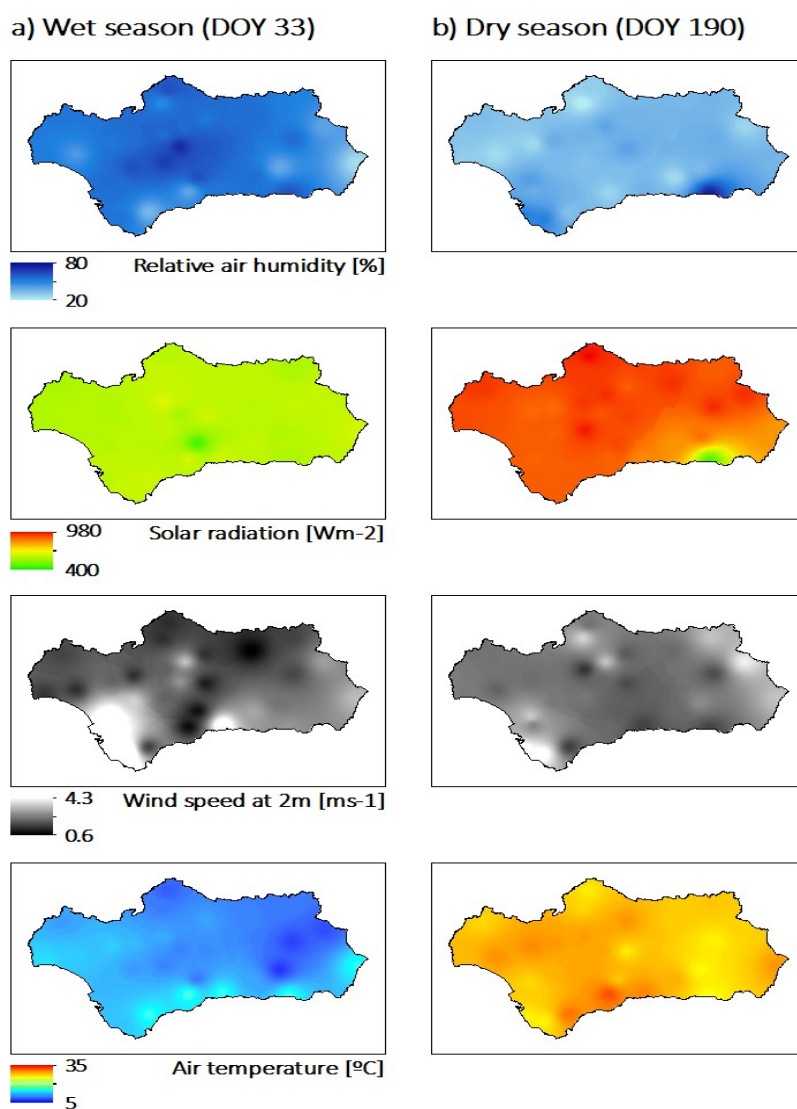


Figure 3.12: Example of the meteorological maps used as an input for TSEB-MODIS *dehesa* application.

The fractional coverage of the vegetation of the entire region is also shown for the wet and dry seasons (Fig. 3.13), and we can observe the differences between zones caused by climate and landuse variability. The densest coverages are located over the natural parks in the Cádiz region (zone 1) and lower coverages over the north of *Andalucía* (zone 2). In the *Cardeña y Montoro* natural park (zone 3) the average values of f_c are shown. We selected these zones as examples to provide some insights in the behavior of surface energy fluxes throughout the year.

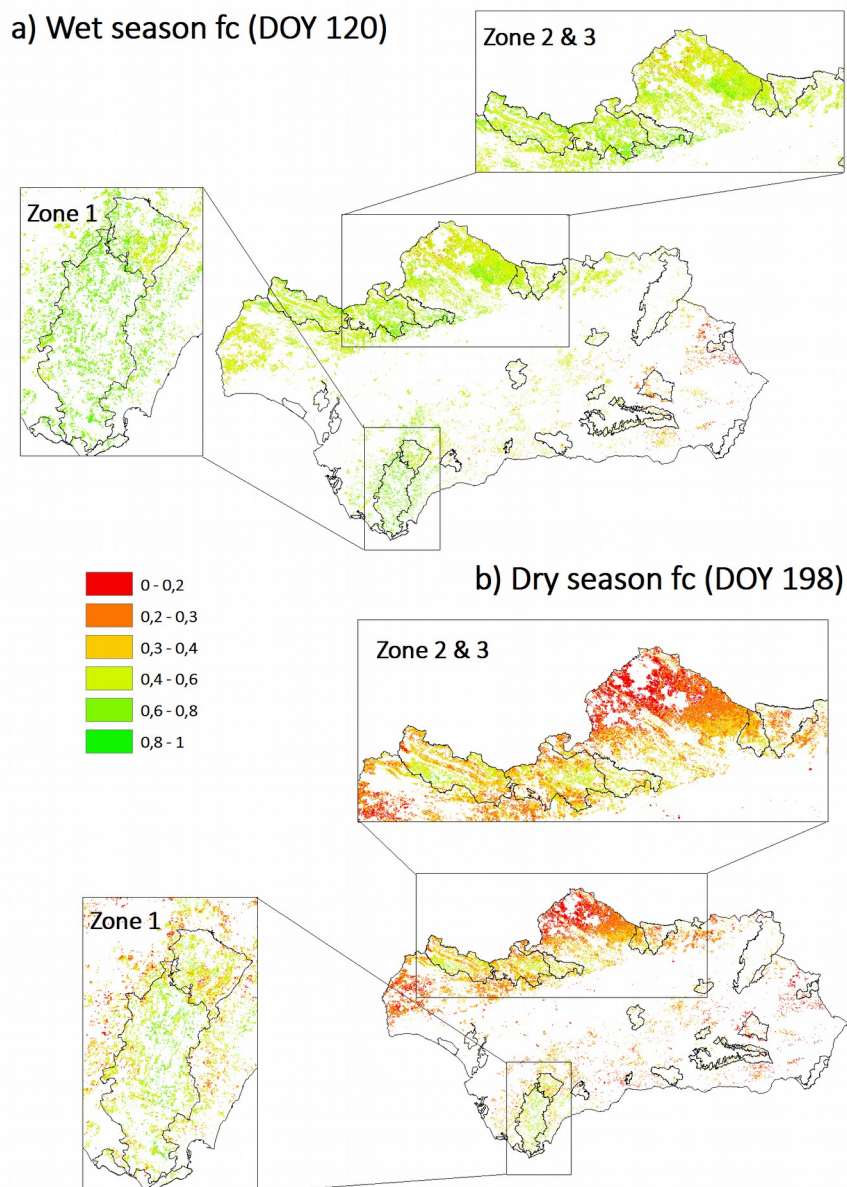


Figure 3.13: MODIS-estimated fractional cover for Andalusian dehesa for the a) wet and b) dry seasons.

The most dense forested areas are located over zones with higher annual mean precipitation and a moderate Mediterranean climate, due to the proximity to the sea that reduces annual temperature oscillations (Fig. 3.14). The mountains of *Grazalema* and *Los Alcornocales* natural parks mountains offer a topographic wall to the Atlantic ocean's water-saturated winds. As a result rainfall events are very intense, with some points registering the highest rates in Spain with more than 2200 mm per year. (Fig. 3.14).

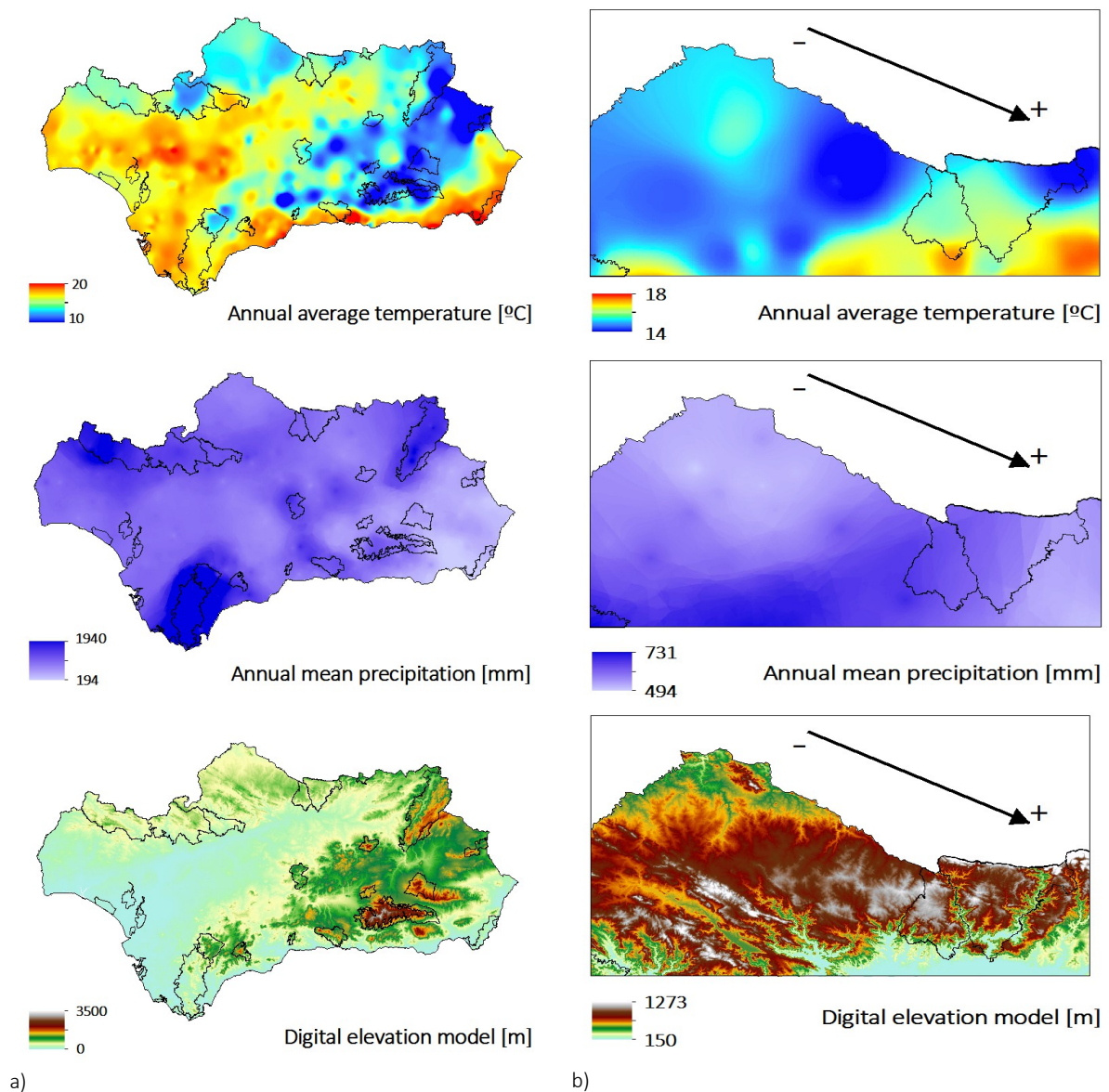


Figure 3.14: Annual mean values for temperature and precipitation for a) the entire Andalusian region and b) the zones 2 & 3.

Due to the differences in these conditions compared to other areas of *dehesa*, other species occur more frequently than *Quercus Ilex*; these include *Quercus suber* and *Quercus faginea*, and to a lesser extent *Quercus pyrenaica*. The variety of wild olive tree, commonly known as *acebuche* (*Olea europaea* var. *sylvestris*), is also widely distributed throughout all *dehesa* ecosystems. During the dry season when the sub-canopy layer is not active, the fractional cover values derived from the remotely sensed information are due only to the oaks. In Figure 3.13 we can see that $f_c = 0.2$ for almost the entire *dehesa* area except zone 1, where woodlands are dense. As Figure 3.14 shows, between zones 2 and 3 there is a rising gradient for precipitation and air temperature, in southwesterly direction, that results in the different canopy and soil conditions.

Stability effects may be an important source of error for these large-scale estimates when strongly unstable conditions are observed (sunny days with high temperature gradients) and the logarithmic profile assumption may break down. Maps of the temperature gradient between air and surface were analyzed together with wind speed and radiation maps (Fig. 3.15), finding a higher gradient over zone 3 during the summer, for which more unstable conditions are likely, than in zones 1 and 2, which presented lower gradients. In zone 1, high wind speed values are frequently registered. Heat transport in the very unstable areas may be overestimated, due to the lower values of wind speed caused by unstable conditions.

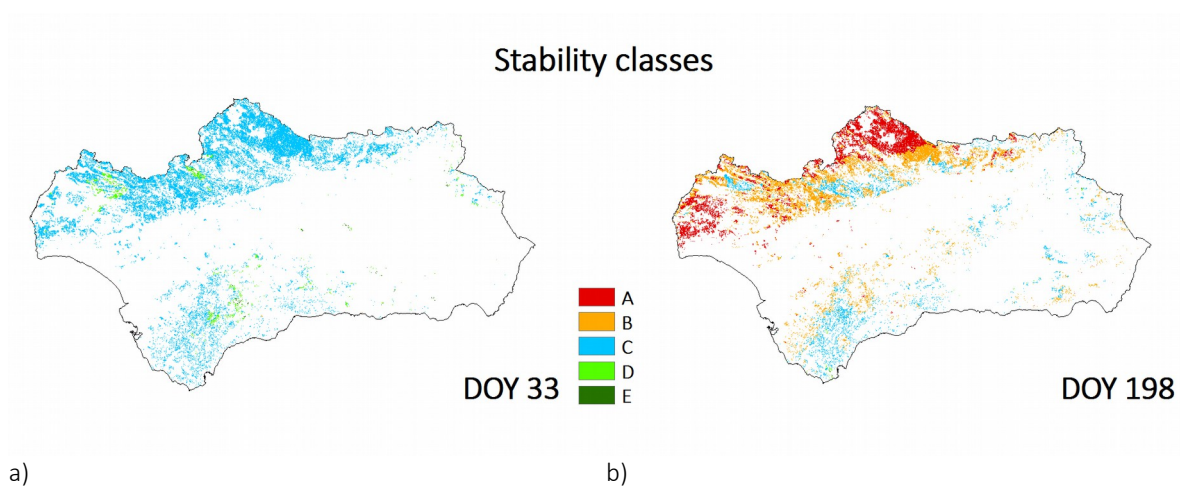


Figure 3.15: Stability classes (A-very unstable, B-unstable, C-near-neutral, D-stable, E-very stable) derived from air-surface temperatures gradient, wind speed and solar incoming radiation for a) wet and b) dry season.

As expected, during the dry season (Fig. 3.16) LE showed the lowest values, due to water scarcity and the summer meteorological conditions. Nevertheless, over zone 1 (Fig 3.16) it was still possible to observe relatively high values of this flux ($\sim 300 \text{ Wm}^{-2}$), due to the particular characteristics of the area. Higher water availability conditions may be ascribed to summer fogs and mists, known as “*barbas de levante*”, moisturizing the environment. The strong winds of the area, due to the proximity of the *Strait of Gibraltar* and the topography of the mountains, have similar effects, bringing humidity from the sea. These factors create a special micro-climate similar to subtropical areas.

The H (Fig. 3.17) and G (Fig. 3.18) showed lower values during the winter, as expected, and higher values during the dry season, when the surface temperature rose. Throughout the year, *dehesa* located in zone 2 displayed the lowest values of ET, due to the low annual mean precipitation together with a stronger arid climate and low vegetation fractional coverage. Over these areas, it is likely that one of the canopy mechanisms that enable *dehesa* to adapt to the harsh environment conditions is reducing the ecosystem fractional cover, as we can see in Figure 3.13. Rn showed higher values during the dry season, as expected (Fig. 3.19).

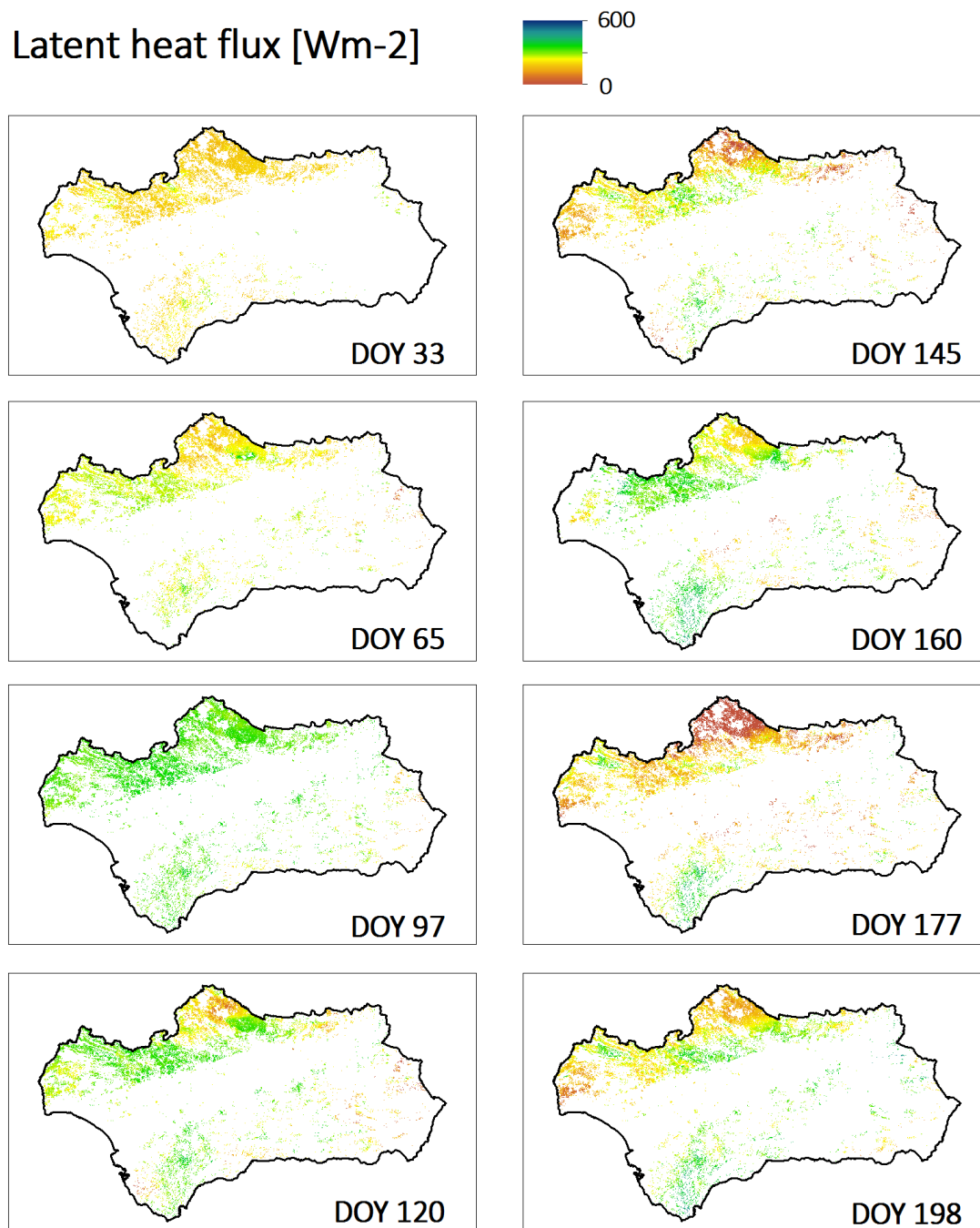


Figure 3.16: TSEB-MODIS estimated LE distributed over Andalusian dehesa for 2014. Other landuses different of *dehesa* were masked (white area)

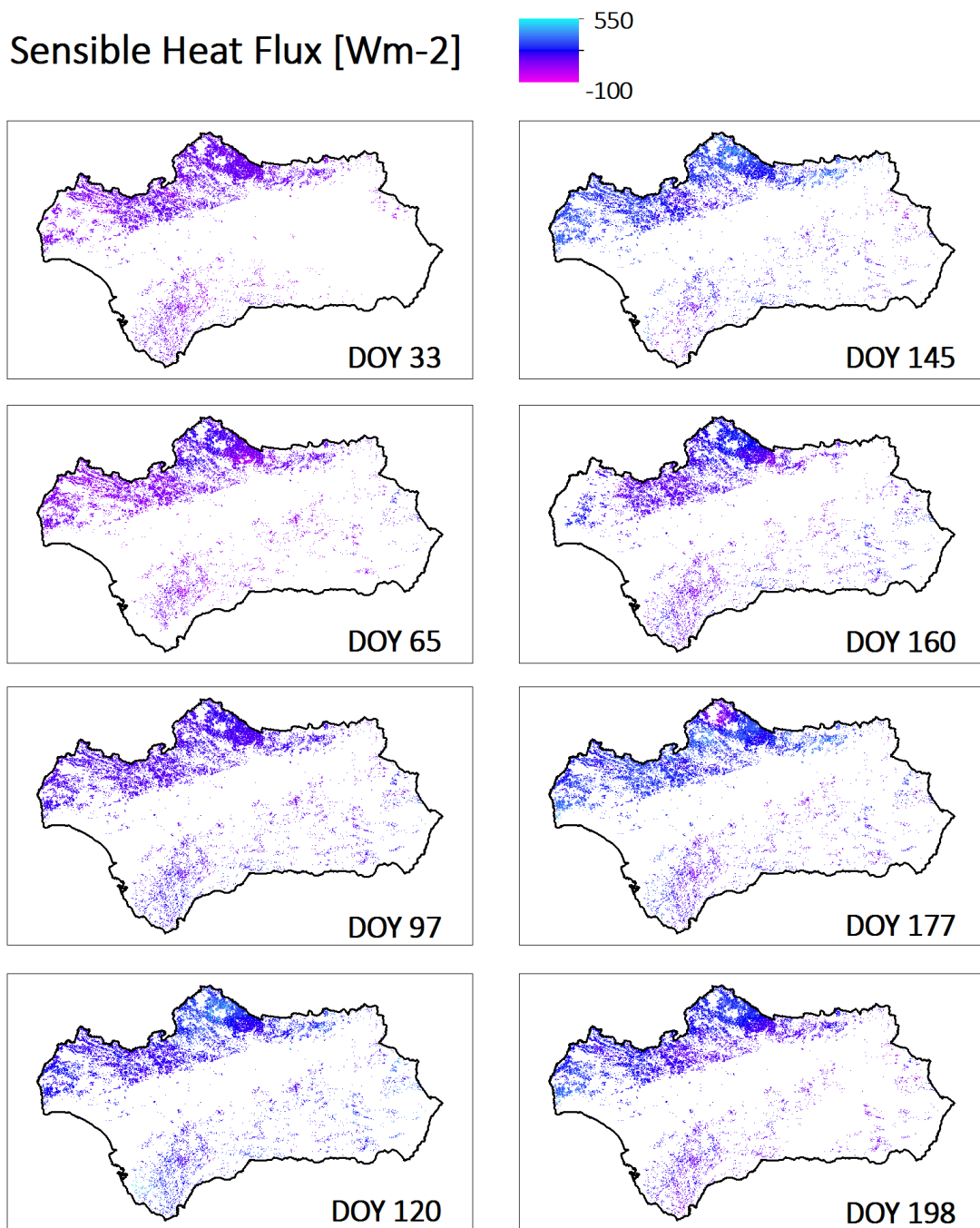


Figure 3.17: TSEB-MODIS estimated H distributed over Andalusian dehesa for 2014. Other landuses different of *dehesa* were masked (white area)

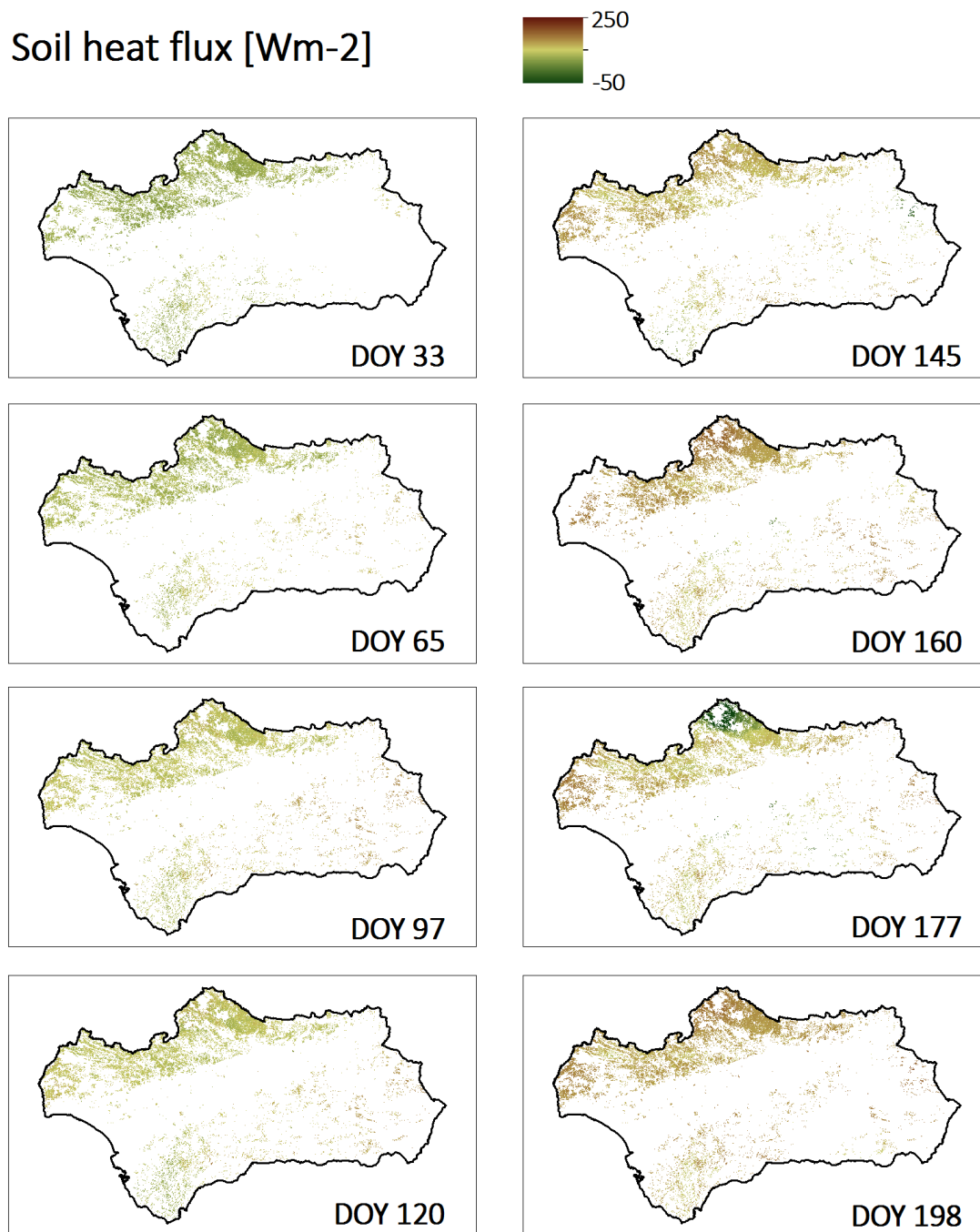


Figure 3.18: TSEB-MODIS estimated G distributed over Andalusian dehesa for 2014. Other landuses different of *dehesa* were masked (white area)

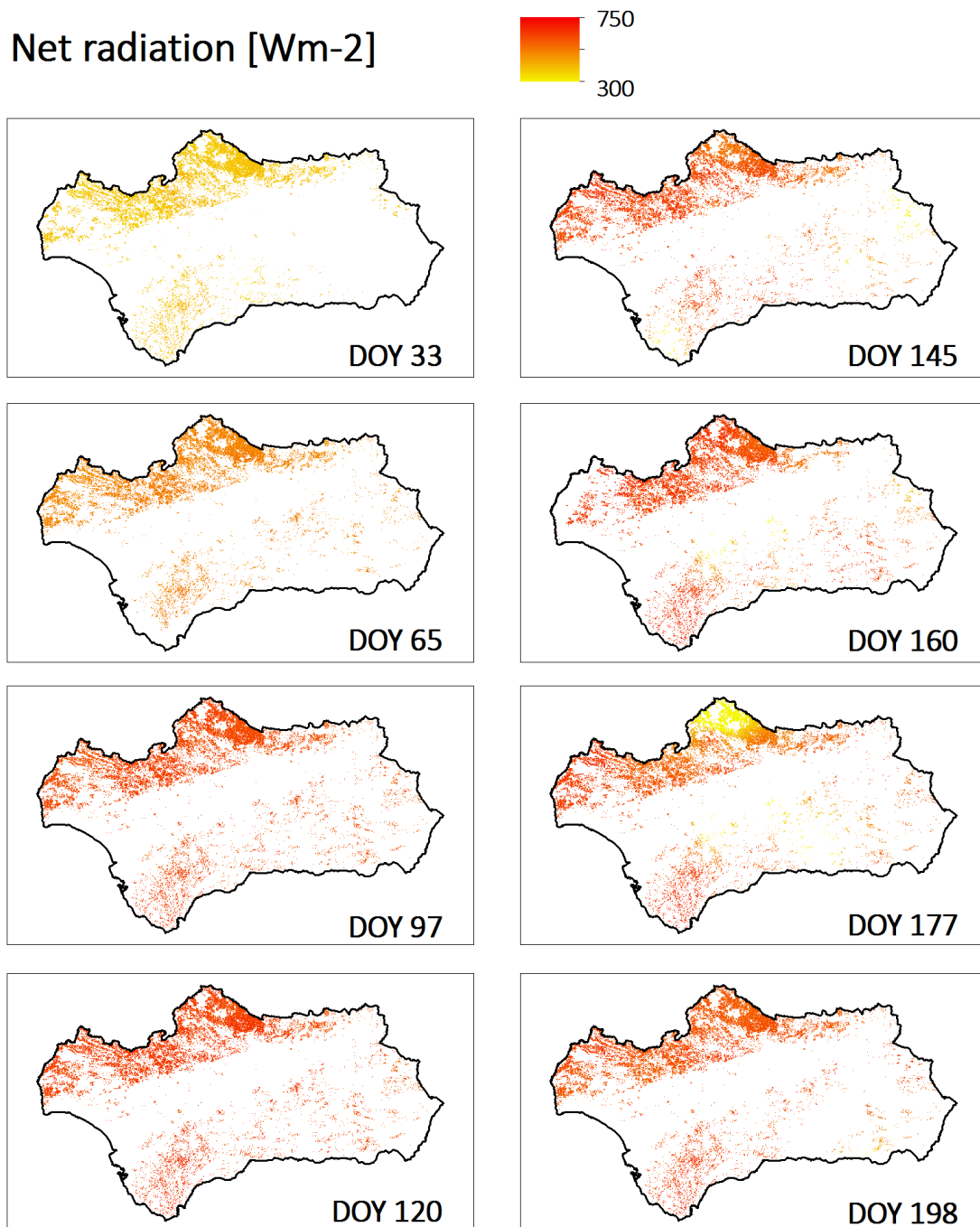


Figure 3.19: TSEB-MODIS estimated R_n distributed over Andalusian dehesa for 2014. Other landuses different of *dehesa* were masked (white area)

We can observe the spatial gaps in the results due to the existence of clouds in the images used as input data, resulting in some loss of information. March 21st was analyzed but not integrated into the final series. It is shown in Figure 3.20, compared with April 7th as an example of how the quality and number of observations can affect the final estimates. The meteorological inputs may be re-scaled by using physical approaches, by (a) utilizing logarithmic profiles as we did but analyzing the stability effects based on Richardson number and correct the wind speed, (b) by using MODIS atmospheric temperature and humidity profiles or (c) ALEXI approach, which estimates air temperatures operating in differential mode using information obtained twice a day from geostationary satellites (*Anderson et al., 2010*). This last approach is less sensitive to absolute errors in surface radiometric temperature. Topographic corrections could be applied to the solar radiation and temperature data with the interpolation algorithms, using the procedure described by *Aguilar et al. (2010)*, to avoid the limitations of the conventional spatial interpolation over areas with high slopes. Nevertheless, no steep gradients are observed in the landscapes with *dehesa* ecosystem.

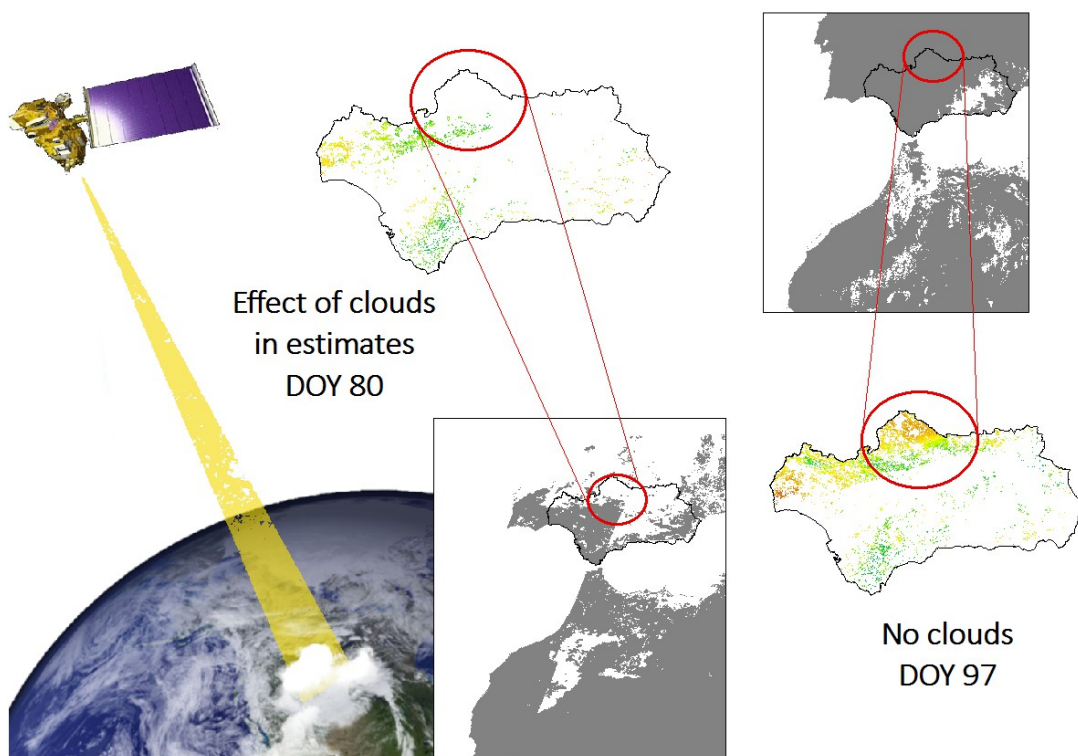


Figure 3.20: Example of the gaps caused in the TSEB-MODIS LE estimates by the cloud coverage, for March 21st (DOY 80) and April 7th (DOY 97).

3.4. SUMMARY AND CONCLUSIONS

Our evaluation of the TSEB model estimates of the energy fluxes integrating medium and low resolution satellite images over *dehesa* ecosystem leads us to consider that the model is sufficiently accurate for it to be employed for management purposes on a regular day-to-day basis.

Considering the footprint analysis made in Santa Clotilde and Las Majadas sites, since the same land use is extended and uniform at least 1000 m along the principal wind directions (SW for Santa Clotilde, SW and NE for Las Majadas), no problems of fetch should be expected from taking ECT data measured over this wind component, making it possible to integrate information from medium-resolution (pixel size between 30 and 120 meters) and even low-resolution (250-1 km pixel size) Earth observation satellites.

With the TSEB application using MODIS images, the RMSD values found for the net radiation ($\sim 25 \text{ Wm}^{-2}$), soil heat flux ($\sim 30 \text{ Wm}^{-2}$), sensible heat flux ($\sim 60 \text{ Wm}^{-2}$) and latent heat flux ($\sim 45 \text{ Wm}^{-2}$) are within the range founded by other authors (Norman *et al.*, 1995; Kustas and Norman, 1999; Timmermans *et al.*, 2007; Sánchez *et al.*, 2008; Gonzalez-Dugo *et al.*, 2009) and consistent with typical uncertainties derived for the flux measurement system ($\sim 40 \text{ Wm}^{-2}$) (e.g. Twine *et al.*, 2000). With regard to the application using higher-resolution information, a 3D footprint analysis was been previously performed to integrate images where the ECT ground-truth data were not registered along the prevailing wind direction. The RMSD for this application was also consistent with the values found by other authors (RMSD $\sim 40 \text{ Wm}^{-2}$ - $\sim 60 \text{ Wm}^{-2}$). An important source of error in the experimental sites could be due to the higher soil heat flux error found in the *dehesa* application, which directly influenced the available energy of the system. Nevertheless, this flux is difficult to measure on field scale, due to the heterogeneity of the experimental areas and the difficulties involved in locating sensors distributed throughout the zone, due to the type of extensive livestock farming that is typical of this region. Discrepancies between observed and estimated fluxes might also be due to the existence of a subcanopy layer with a different phenology than that of the oaks. This requires further research, which should attempt to integrate this behavior not only into the wind speed profile (Chapter 2), but also over the radiation budgets, with different extinction coefficients depending on the individual canopy layers.

Although further research of the daily evaporative fraction variation (i.e. analyzing ECT fluxes), daily estimates of ET integrating MODIS yield a RMSD of $\sim 1 \text{ mm day}^{-1}$, the accuracy being good enough for management purposes and similar to the values found by other authors for more homogeneous crops (reviewed by *Kustas et al., 2013*), and similar woody sparse semi-arid crops such as vineyards (*Gonzalez-Dugo et al., 2012*). These results also lie within the range of studies of this system that took a different approach based on water balance and vegetation index derived crop coefficient (*Campos et al., 2013*). This agreement may encourage further studies to integrate both approaches, taking advantage of the opportunities offered by coupling methodologies. Daily ET data derived from remote sensing would allow the ecosystem stress to be monitored on a regular basis and on a distributed scale. This would help to monitor the functioning of the *dehesa*, and its responses to climate change and extreme events such as droughts.

An initial attempt was made to evaluate evapotranspiration over the Andalusian *dehesas* in 2014, with the objective of assessing a future extension of the study using a constellation of satellites, which would provide information with various spatial and temporal resolutions. The analysis showed that integrating spatially distributed remotely sensed data and meteorological maps make it possible to estimate the energy fluxes on a regional scale. This would be more useful for management purposes, noticing the different behavior of each *dehesa* zone and taking into account vegetation heterogeneity, individual fractional covers and local meteorological conditions.

The gaps caused by the existence of clouds might be solved by coupling EB techniques with water balance approaches. The information provided by such a distributed approach could allow early detection of droughts and the determination of the status of the entire ecosystem thus providing an indication of whether the vegetation is under stress. Correct operation of the system enable us to maintain the forestry, agricultural and livestock production of the *dehesa*, as well as the services related to the community and to society as a whole.

Acknowledgments. We would like to thank Arnaud Carrara and the group managing the experimental site of Las Majadas for the ground-truth ECT measurements and the additional data. We also would like to thank Bill Kustas for his critically reviewing, which led to a greatly improvement of this chapter.

This work has been funded by the Andalusian Institute for Agricultural and Fisheries Research and

Training (IFAPA, Consejería de Agricultura, Pesca y Desarrollo Rural de la Junta de Andalucía) and the European Social Fund Operational Programme 2007-2013, in the field of priority Axis 3 (Improving human capital), in an 80%. The work was partly supported by grant AGL2011-30498 (Ministerio de Economía y Competitividad of Spain, co-funded by FEDER)

3.5. REFERENCES

- Aguilar, C., Herrero, J., & Polo, M.J. (2010). Topographic effects on solar radiation distribution in mountainous watersheds and their influence on reference evapotranspiration estimates at watershed scale. *Hydrol. Earth Syst. Sci.*, 14
- Anderson, M.C., Kustas, W.P., & Norman, J.M. (2007). *Upscaling flux observations from local to continental scales using thermal remote sensing*. Madison, WI, ETATS-UNIS: American Society of Agronomy
- Anderson, M.C., Kustas, W.P., Norman, J.M., Hain, C.R., Mecikalski, J.R., Schultz, L., González-Dugo, M.P., Cammalleri, C., d'Urso, G., Pimstein, A., & Gao, F. (2010). Mapping daily evapotranspiration at field to global scales using geostationary and polar orbiting satellite imagery. *Hydrol. Earth Syst. Sci. Discuss. HESSD*, 7, 5957 – 5990
- Anderson, M.C., Norman, J.M., Diak, G.R., Kustas, W.P., & Mecikalski, J.R. (1997). A two-source time-integrated model for estimating surface fluxes using thermal infrared remote sensing. *Remote Sensing of Environment*, 60, 195-216
- Arya, S.P. (2001). Introduction to Micrometeorology. In A. Press (Ed.), *International Geophysics Series*. Cornwall, UK
- Baldocchi, D.D., & Xu, L. (2007). What limits evaporation from Mediterranean oak woodlands - “ The supply of moisture in the soil, physiological control by plants or the demand by the atmosphere? *Advances in Water Resources*, 30, 2113-2122
- Baldocchi, D.D., Xu, L., & Kiang, N. (2004). How plant functional-type, weather, seasonal drought, and soil physical properties alter water and energy fluxes of an oak grass savanna and an annual grassland. *Agricultural and Forest Meteorology*, 123, 13-39
- Berk, A., Bernstein, L.S., Anderson, G.P., Acharya, P.K., Robertson, D.C., Chetwynd, J.H., & Adler-Golden, S.M. (1998). MODTRAN Cloud and Multiple Scattering Upgrades with Application to AVIRIS. *Remote Sensing of Environment*, 65, 367-375
- Cammalleri, C., Agnese, C., Ciraolo, G., Minacapilli, M., Provenzano, G., & Rallo, G. (2010a). Actual evapotranspiration assessment by means of a coupled energy/hydrologic balance model: Validation over an olive grove by means of scintillometry and measurements of soil water contents. *Journal of Hydrology*, 392, 70-82

- Cammalleri, C., Anderson, M.C., Ciraolo, G., D'Urso, G., Kustas, W.P., La Loggia, G., & Minacapilli, M. (2010b). The impact of in-canopy wind profile formulations on heat flux estimation in an open orchard using the remote sensing-based two-source model. *Hydrol. Earth Syst. Sci.*, *14*, 2643-2659
- Campos, I., Villodre, J., Carrara, A., & Calera, A. (2013). Remote sensing-based soil water balance to estimate Mediterranean holm oak savanna (dehesa) evapotranspiration under water stress conditions. *Journal of Hydrology*, *494*, 1-9
- Carreiras, J.M.B., Pereira, J.M.C., & Pereira, J.S. (2006). Estimation of tree canopy cover in evergreen oak woodlands using remote sensing. *Forest Ecology and Management*, *223*, 45-53
- Crago, R., & Brutsaert, W. (1996). Daytime evaporation and the self-preservation of the evaporative fraction and the Bowen ratio. *Journal of Hydrology*, *178*, 241-255
- Crago, R.D. (1996). Conservation and variability of the evaporative fraction during the daytime. *J. Hydrology*, *180*, 173-194
- Diaz, M., Campos, P., & Pulido, F.J. (1997). *The Spanish dehesas: a diversity in land-use and wildlife*. San Diego: Pain, D. J. and Pienkowsky, M. W.
- Foken, T. (2008). The Energy Balance Closure Problem: an overview. *Ecological Applications*, *18*, 1351-1367
- Franssen, H.J.H., Stockli, R., Lehner, I., Rotenberg, E., & Seneviratne, S.I. (2010). Energy balance closure of eddy-covariance data: A multisite analysis for European FLUXNET stations. *Agricultural and Forest Meteorology*, *150*, 1553-1567
- French, A.N., Jacob, F., Anderson, M.C., Kustas, W.P., Timmermans, W., Gieske, A., Su, Z., Su, H., McCabe, M.F., Li, F., Prueger, J., & Brunsell, N. (2005). Surface energy fluxes with the Advanced Spaceborne Thermal Emission and Reflection radiometer (ASTER) at the Iowa 2002 SMACEX site (USA). *Remote Sensing of Environment*, *99*, 55-65
- Gentine, P., Entekhabi, D., Chehbouni, A., Boulet, G., & Duchemin, B.t. (2007). Analysis of evaporative fraction diurnal behaviour. *Agricultural and Forest Meteorology*, *143*, 13-29
- Gonzalez-Dugo, M.P., González-Piqueras, J., Campos, I., Andreu, A., Balbotin, C., & Calera, A. (2012). *Evapotranspiration monitoring in vineyard using satellite-based thermal remote sensing*. In E. Remote Sensing for Agriculture, and Hydrology XIV (Ed.), SPIE
- Gonzalez-Dugo, M.P., Neale, C.M.U., Mateos, L., Kustas, W.P., Prueger, J.H., Anderson, M.C., & Li, F. (2009). A comparison of operational remote sensing-based models for estimating crop evapotranspiration. *Agricultural and Forest Meteorology*, *149*, 1843-1853
- Grove, A.T., & Rackham, O. (2003). *The Nature of Mediterranean Europe. An Ecological History*. New Haven: Yale University Press
- Guzinski, R., Anderson, M.C., Kustas, W.P., Nieto, H., & Sandholt, I. (2013). Using a thermal-based two source energy balance model with time-differencing to estimate surface energy fluxes with day-night MODIS observations. *Hydrol. Earth Syst. Sci.*, *17*, 2809-2825
- Jimenez-Muñoz, J.C., Sobrino, J.A., Mattar, C., & Franch, B. (2010). Atmospheric correction of optical imagery

- from MODIS and Reanalysis atmospheric products. *Remote Sensing of Environment*, 114, 2195-2210
- Kustas, W.P. (1990). Estimates of Evapotranspiration with a One- and Two-Layer Model of Heat Transfer over Partial Canopy Cover. In, *Journal of Applied Meteorology* (pp. 704-715): American Meteorological Society
- Kustas, W.P., Anderson, M.C., Cammalleri, C., & Alfieri, J.G. (2013). Utility of a Thermal-based Two-source Energy Balance Model for Estimating Surface Fluxes over Complex Landscapes. In, *Four Decades of Progress in Monitoring and modelling of Processes in the Soil-Plant-Atmosphere System: Applications and Challenges* (pp. 224-230)
- Kustas, W.P., Anderson, M.C., Cammalleri, C., & Alfieri, J.G. Utility of a Thermal-based Two-source Energy Balance Model for Estimating Surface Fluxes over Complex Landscapes. In, *Four Decades of Progress in Monitoring and modelling of Processes in the Soil-Plant-Atmosphere System: Applications and Challenges* (pp. 224-230)
- Kustas, W.P., & Norman, J.M. (1997). A two-source approach for estimating turbulent fluxes using multiple angle thermal infrared observations. *Water Resources Research*, 33, 1495-1508
- Kustas, W.P., & Norman, J.M. (1999). Evaluation of soil and vegetation heat flux predictions using a simple two-source model with radiometric temperatures for partial canopy cover. *Agricultural and Forest Meteorology*, 94, 13-29
- Kustas, W.P., & Norman, J.M. (2000). A Two-Source Energy Balance Approach Using Directional Radiometric Temperature Observations for Sparse Canopy Covered Surfaces. *Agron. J.*, 92, 847-854
- Lhomme, J.P., & Elguero, E. (1999). Examination of evaporative fraction diurnal behaviour using a soil-vegetation model coupled with a mixed-layer model. *Hydrol. Earth Syst. Sci.*, 3, 259-270
- Miranda, P.M.A., Valente, M.A., Tome, A.R., Trigo, R., Coelho, M.F.E.S., Aguiar, A., & Azevedo, E.B. (2006). O clima de Portugal nos seculos XX e XXI. In F.D. Santos, Miranda, P. (Ed.), *Alteracoes Climaticas em Portugal. Cenarios, Impactes e Medidas de Adaptacao*. (pp. 45–113). Gradiva, Lisboa
- Moran, M.S. (2003). Thermal infrared measurement as an indicator of plant ecosystem health. In D.A.Q.a.J. Luvall (Ed.), *Thermal Remote Sensing in Land Surface Processes* (pp. 257-282). Philadelphia, Pa: Taylor and Francis
- Moran, M.S., Peters-Lidard, C.D., Watts, J.M., & McElroy, S. (2004). Estimating soil moisture at the watershed scale with satellite-based radar and land surface models. *Canadian Journal of Remote Sensing*, 30, 805-826
- Morillas, L., Garcia, M., Nieto, H., Villagarcia, L., Sandholt, I., Gonzalez-Dugo, M.P., Zarco-Tejada, P.J., & Domingo, F. (2013). Using radiometric surface temperature for surface energy flux estimation in Mediterranean drylands from a two-source perspective. *Remote Sensing of Environment*, 136, 234-246
- Norman, J.M., Kustas, W.P., & Humes, K.S. (1995). A two - source approach for estimating soil and vegetation energy fluxes in observations of directional radiometric surface temperature. *Agricultural and Forest Meteorology*, 77, 263-293
- Paço, T.A., David, T.S., Henriques, M.O., Pereira, J.S., Valente, F., Banza, J., Pereira, F.L., Pinto, C., & David, J.S.

- (2009). Evapotranspiration from a Mediterranean evergreen oak savannah: The role of trees and pasture. *Journal of Hydrology*, 369, 98-106
- Papanastasis, V.P. (2004). *Vegetation degradation and land use changes in agrosilvopastoral systems*. Catena Verlag, Reiskirchen, Germany: Advances in GeoEcology
- Pasquill, F. (1961). *The estimation of the dispersion of windborne material*.
- Plieninger, T., & Wilbrand, C. (2001). Land use, biodiversity conservation, and rural development in the dehesas of Cuatro Lugares, Spain. *Agroforestry Systems*, 51, 23-34
- Pulido, F.J., & Diaz, M. (2005). Regeneration of a Mediterranean oak: a whole cycle approach. *Ecoscience*, 12, 92-102
- Fernandez-Rebollo, P., Carbonero-Muñoz, M.D, García-Moreno, A. (2009). Control y seguimiento de los Programas Agroambientales en la Comunidad Autónoma Andaluza. El estado de los recursos en la dehesa y el papel de las medidas agroambientales. *Documento Técnico. Consejería de Agricultura y Pesca, Junta de Andalucía*.
- Sánchez, J.M., Kustas, W.P., Caselles, V., & Anderson, M.C. (2008). Modelling surface energy fluxes over maize using a two-source patch model and radiometric soil and canopy temperature observations. *Remote Sensing of Environment*, 112, 1130-1143
- Schuepp, P.H., Leclerc, M.Y., MacPherson, J.I., & Desjardins, R.L. (1990). Footprint prediction of scalar fluxes from analytical solutions of the diffusion equation. *Boundary-Layer Meteorology*, 50, 355-373
- Shuttleworth, W.J., Gurney, R.J., Hsu, A.Y., & Ormsby, J.P. (1989). *FIFE: the variation in energy partition at surface flux sites*.
- Soegaard, H., Jensen, N.O., Boegh, E., Hasager, C.B., Schelde, K., & Thomsen, A. (2003). Carbon dioxide exchange over agricultural landscape using eddy correlation and footprint modelling. *Agricultural and Forest Meteorology*, 114, 153-173
- Storey, J., Scaramuzza, P., Schmidt, G., & Barsi, J. (2005). Landsat 7 scan line corrector-off gap-filled product development. . In ASPRS (Ed.), *Pecora 16 "Global Priorities in Land Remote Sensing"*
- Timmermans, W., Su, Z., & Olioso, A. (2009). Footprint issues in scintillometry over heterogeneous landscapes. *Hydrol. Earth Syst. Sci.*, 13, 2179-2190
- Timmermans, W.J., Kustas, W.P., Anderson, M.C., & French, A.N. (2007). An intercomparison of the Surface Energy Balance Algorithm for Land (SEBAL) and the Two-Source Energy Balance (TSEB) modelling schemes. *Remote Sensing of Environment*, 108, 369-384
- Twine, T.E., Kustas, W.P., Norman, J.M., Cook, D.R., Houser, P.R., Meyers, T.P., Prueger, J.H., Starks, P.J., Wesely, M.L (2000). Correcting eddy-covariance flux underestimates over a grassland. *Agric. For. Meteorol.*, 103, 279-300

Chapter 4: Influence of thermal component derivation for dual source energy flux estimates over a drip-irrigated vineyard using TSEB.

Chapter 4 was submitted to Acta Geophysica for publication and is currently under review:

Andreu, A., Timmermans, W. J., Skokovic, D., González-Dugo, M. P., 2014. Influence of thermal component derivation for dual source energy flux estimates over a drip-irrigated vineyard. Submitted to Acta Geophysica.

Partial results of this chapter have been previously presented at:

Corbari C., Timmermans W., Andreu A.. *Intercomparison of surface energy fluxes estimates from the FEST-EWB and TSEB models over the heterogeneous REFLEX 2012 site (Barrax, Spain)*. Accepted on Sep 23, 2014 in Acta Geophysica.

Timmermans, W. J. et al., 2014. An overview of the Regional Experiments For Land-atmosphere Exchanges 2012 (REFLEX12) Campaign. Accepted on Sep 23, 2014 in Acta Geophysica.

Andreu. A., Timmermans, W. J., Skokovic, D., González-Dugo, M. P., 2014. Influence of thermal component derivation for dual source energy flux estimates over a drip-irrigated vineyard. 4th International Symposium Recent Advances in Quantitative Remote Sensing, 22 – 26th September 2014, Torrent (Valencia), Spain.

Andreu,A., W. Timmermans, J. Timmermans, C. Van der Tol, S. Zhongbo. *Influence of thermal component derivation in dual source energy flux estimates results from the REFLEX 2012 Campaign*. ESA living Planet Symposium 2013, Edinburgh, 2013.

ABSTRACT

A two-source model (TSEB) for deriving surface energy fluxes and their soil and canopy components was evaluated using multi-angle airborne observations (*Norman et al., 1995; Kustas and Norman, 1999*). In the original formulation (TSEB1) a single temperature observation, a Priestley-Taylor parameterization and the vegetation fraction are used to derive the component fluxes. When temperature observations are made from different angles, soil and canopy temperatures can be extracted directly. Two dual angle model versions are compared versus TSEB1; one incorporating the Priestley-Taylor parameterization (TSEB2I) and one using the component temperatures directly (TSEB2D), for which data from two airborne campaigns over an agricultural area in Spain are used. Validation of TSEB1 versus ground measurements showed RMSD values of 28 Wm^{-2} and 10 Wm^{-2} for sensible and latent heat fluxes respectively. Reasonable agreement between TSEB1 and TSEB2I were found, and lower correlation between TSEB1 and TSEB2D was observed. The TSEB2D estimates appear to be more realistic under the given conditions.

Key words: Two Source Energy Balance (TSEB) model, component temperatures, resistance schemes, available energy.

4.1 INTRODUCTION

Quantification of the spatial and temporal variability in hydrological processes and land surface states is of interest on several different disciplines, including agriculture, hydrology, meteorology and climatology. Interconnections and feedbacks between hydrological variables and regional hydrometeorology have led to an increase in the use of satellite remote sensing to determine the water and energy budgets at the earth's surface. The partitioning of available energy into sensible and latent heat fluxes largely depends on the composition of the observed area, specifically, whether it is vegetated or bare. Due to the heterogeneity of the earth's surface at most scales, energy-balance models that distinguish between soil/substrate and vegetation contributions to the radiative temperature and radiation/turbulent fluxes have proven to be most reliable. A proper partitioning in component fluxes is of importance, not only for its practical consequences, such as the determination of the water-use efficiency of plants but also because it is important for climate change issues, since

the transpiration component shows a strong correlation with carbon sequestration (Scott *et al.*, 2006). During the last few decades these physically based models have evolved into an operational mode. In particular, the two-source energy balance model (TSEB) of Norman *et al.* (1995) has been shown to be robust for semi-arid sparse canopy-cover landscapes. Although it has a strong physical basis, still a number of assumptions and tabulated input parameters, which are neither easily available nor measured at an operational basis are required, and their influence on model output over a variety of landcover units needs to be evaluated. Such models tend to use resistance schemes in which the turbulent sensible (latent) heat fluxes are determined by the ratio of a temperature (vapor pressure) difference between the overlaying air and the surface, whether soil or canopy, over an aerodynamic resistance to heat (vapor) transport. Since operational remote-sensing observations of vapor pressure are not readily available, the models are usually designed to utilize observations of temperature rather than vapor pressure. As a result the resistance schemes used to derive sensible heat fluxes and latent heat fluxes are then calculated as a rest-term in the energy balance. In an operational mode, the soil surface temperature, T_s , and canopy temperature, T_c , are usually derived from a single observation of directional radiometric temperature, T_{RAD} , in combination with an estimate of the fractional vegetation cover, f_c .

In the TSEB model, T_{RAD} is calculated from the brightness temperature, which is directly measured by the radiometer, thereby assuming a single directional emissivity that represents soil and vegetation combined. Deriving the soil and canopy component temperatures from f_c and a single T_{RAD} observation requires an iterative process, where it is uncertain whether the proper solution is obtained in terms of component temperatures and hence in terms of properly parameterized resistances. Numerous validation studies have shown a good performance of the TSEB model flux output versus flux observations (French *et al.*, 2005; Gonzalez-Dugo *et al.*, 2009; Kustas and Norman, 1997; Timmermans *et al.*, 2007), which are usually “lumped-together” observations of total H and LE fluxes. Less is known about the validity of the internal model parameters, these being the component temperatures, resistances and the component flux output. This limits our understanding of the physical processes involved and thus limits model portability (Colaizzi *et al.*, 2012a; Kalma *et al.*, 2008).

However, when T_{RAD} observations made from multiple angles are available, the component temperatures can be derived directly (Kustas and Norman, 1997), thereby offering the possibility to assess the validity of the parameterizations used. Some studies have tested the TSEB model by using component temperatures (Colaizzi *et al.*, 2012a; Kustas and Norman, 1997; Morillas *et al.*, 2013).

However, a key assumption of the TSEB model, and also of other dual source models, is that the effective source/sink for turbulent flux exchange for the entire canopy, as well as for the soil/substrate, can be described by a bulk canopy, or bulk soil/substrate, temperature and resistance, (Colaizzi et al., 2012a). Even so, large local differences in observed temperature exist for sunlit and shaded leaves and soil, old and young leaves, and transpiring and non-transpiring leaves (Timmermans et al., 2008a). When locally measured component temperatures such as in Colaizzi et al. (2012a) or Morillas et al. (2013), or ground-based multiple viewing angle observations such as in Kustas and Norman (1997) are used they may not represent the bulk canopy and bulk soil temperatures used in the parameterization scheme. Moreover, a significant mismatch between the spatial resolution of the temperature measurements and the size of the flux footprint can cause significant discrepancies between modeled and measured fluxes (Kustas and Norman, 1997). Therefore in the current contribution we preferred to use airborne imagery acquired from very different viewing angles at a resolution that is low enough to obtain “observations” of the representative bulk component temperatures but high enough to capture within-field variation. As such, this study focuses more on inter-model output differences than on absolute validation.

The objective of this study was to determine how physically based retrieval of the representative bulk soil and canopy component temperatures, which are used in the model parameterization, influences estimates of the turbulent fluxes, their components and model parameters. To achieve this goal, the first step is the validation of the TSEB model, as it is commonly used (Anderson et al., 1997; French et al., 2005; Norman et al., 1995), against ground-truth observations of radiation and energy fluxes over the current area. The second step involved the extraction of soil and canopy component temperatures from dual angle airborne observations, which were then used in the dual angle version of TSEB (Colaizzi et al., 2012a; Kustas and Norman, 1997). The third step was to compare the output produced by the different versions of the model. Finally, an attempt has been made to explain the differences in model output.

4.2 MATERIALS AND METHODS

4.2.1. Description of the two source energy balance model

The dual-source model used in this study is the well-established Two-Source Energy Balance (TSEB)

model of *Norman et al. (1995)* which has shown good performance over a wide range of arid and partially-vegetated landscapes (*French et al., 2005; Gonzalez-Dugo et al., 2009; Kustas and Norman, 1997; Timmermans et al., 2007*). Under such circumstances, a dual source model that distinguishes between the soil and vegetation contribution to the turbulent fluxes has clear and well-known advantages over simpler single-source models that treat these contributions in a lumped manner (*Huntingford et al., 1995; Kustas et al., 1996*). The TSEB model presents two different versions, according to the assumed resistance network for parameterizing the energy flux exchange, being either in series or in parallel (*Norman et al., 1995*). The series version of the TSEB resistance network allows interactions between soil/substrate and main canopy layer and is therefore particularly useful over relatively dry but relatively densely vegetated areas. Because the vineyard area under study is characterized by just these conditions, use here is made of the series approach only. Although descriptions of the model are available in *Norman et al. (1995)* and *Kustas and Norman (1997)*, the following sections offer a detailed description of the several steps involved in the different versions. This is considered relevant in view of the specific differences in their output, see section 4.3.2.

4.2.1.1. Single-angle model

The single-angle model is the updated version of the Two-Source Energy Balance (TSEB) model (*Norman et al., 1995*), as described by *Kustas and Norman (1999)* and *Li et al. (2005)*. From here on this scheme will be referred to as TSEB1.

The model assumes that the surface radiometric temperature (T_{RAD}) is a combination of soil (T_s) and canopy (T_c) temperatures, weighted by the vegetation fraction (f_c):

$$T_{\text{RAD}}(\phi) = [f_c(\phi) T_c^4 + (1 - f_c(\phi)) T_s^4]^{(1/4)} \quad (4.1)$$

where f_c is affected by the sensor viewing angle (ϕ). Note that the angular variation of directional emissivity is neglected because variations of less than 0.005 are obtained between viewing angles at nadir and 60° for most vegetated surfaces (*Anton and Ross, 1987; Kustas and Norman, 1997*).

The surface energy-balance equation can be formulated for the entire soil-canopy-atmosphere system, or for the soil and canopy components separately:

$$Rn_c = LE_c + H_c \quad (4.2)$$

$$Rn_s = LE_s + H_s + G \quad (4.3)$$

Original formulations for Rn , Rn_c , Rn_s and G can be found in *Norman et al. (1995)* and *Kustas and Norman (1999)*. The spatial variation in the horizontal direction is mainly regulated by fractional vegetation cover and in the vertical (radiation extinction within the canopy) by LAI. Since the radiation formulation follows the so-called “layer-approach” (*Lhomme and Chehbouni, 1999*), a simple summation of the soil and canopy components yields the total flux;

$$Rn = Rn_c + Rn_s \quad (4.4)$$

$$H = H_c + H_s \quad (4.5)$$

$$LE = LE_c + LE_s \quad (4.6)$$

The model was originally developed for uniformly distributed crops. In the case of clumped canopies with partial vegetation cover, such as vineyards and orchards, the parameterizations are corrected by a so-called clumping factor (*Anderson et al., 2005*). This factor corrects for the reduction in the extinction of the radiation in a clumped canopy as compared to a uniformly distributed one, by multiplying the LAI by the clumping factor. The soil heat flux is then estimated as a time-dependent function of the net radiation reaching the soil:

$$G = c_g Rn_s \quad (4.7)$$

where c_g is slightly variable with time. Details of the original determination can be found in (*Kustas et al., 1998*). Here it is calibrated against local observations using the measurements from the test sites.

Within the series resistance scheme, the sensible heat fluxes H_c , H_s and H are expressed as:

$$H_c = \rho_a C_p (T_c - T_{AC}) / R_x \quad (4.8)$$

$$H_s = \rho_a C_p (T_s - T_{AC}) / R_s \quad (4.9)$$

$$H = H_c + H_s = \rho_a C_p (T_{AC} - T_{air}) / R_A \quad (4.10)$$

where T_{AC} is the air temperature in the canopy – air space [K], R_x is the resistance to heat flow of the vegetation leaf boundary layer [$s\ m^{-1}$], R_s is the resistance to the heat flow in the boundary layer above the soil [$s\ m^{-1}$], and R_A is the aerodynamic resistance calculated from the stability-corrected temperature-profile equations (*Brutsaert, 1982*), using Monin-Obhukov Similarity Theory (MOST), and T_{air} is the air temperature. The procedure to derive T_{AC} is provided in the Appendix of *Norman et al. (1995)*.

For the sake of completeness and to facilitate the discussion of model results, we present the resistance parameterizations for R_x , R_s and R_A below, following *Norman et al. (1995)* and *Kustas and Norman (1999)*;

$$R_A = \frac{[\ln(z_u - d_0 / z_{0M} - \psi_M)][\ln(z_T - d_0 / z_{0M} - \psi_H)]}{k_{vk}^2 u} \quad (4.11)$$

$$R_x = \frac{C'}{LAI} \left(\frac{s}{u_{d_0+z_{0M}}} \right)^{1/2} \quad (4.12)$$

$$R_s = \frac{1}{a' + b' u_s} \quad (4.13)$$

where C' is taken equal to $90\ s^{1/2}\ m^{-1}$, following *Norman et al. (1995)* and $u_{d_0+z_{0M}}$ is given by;

$$u_{d_0+z_{0M}} = u_c \exp \left[-a \left(1 - \frac{d_0 + z_{0M}}{h_c} \right) \right] \quad (4.14)$$

in which the wind speed at the top of the canopy, u_c , is given by;

$$u_c = u \left[\frac{\ln \left(\frac{h_c - d_0}{z_{0M}} \right)}{\ln \left(\frac{z_u - d_0}{z_{0m}} \right) - \psi_M} \right] \quad (4.15)$$

and the factor a given by *Goudriaan (1977)* as:

$$a = 0.28 LAI^{2/3} h_c^{1/3} s^{-1/3} \quad (4.16)$$

The wind speed just above the soil surface, u_s [$m s^{-1}$], in Eq. (4.13) is parameterized following Eq. (4.14), but using 0.05 m as the reference height, as follow;

$$u_s = u_c \exp \left[-a \left(1 - \frac{z_s}{h_c} \right) \right] \quad (4.17)$$

Coefficients a' [$m s^{-1} K^{-1/3}$] and b' [-] in Eq. (4.13) are provided by *Kustas and Norman (1999)*, as used in the work of *Kondo and Ishida (1997)*:

$$a' = 0.0025 (T_s - T_c)^{(1/3)} \quad \text{and} \quad b' = 0.012 \quad (4.18)$$

The canopy latent heat flux is derived using as an initial assumption a potentially transpiring canopy, following the Priestley-Taylor equation (*Priestley and Taylor, 1972*):

$$LE_c = \alpha_{PT} f_g \left(\frac{\Delta}{\Delta + \gamma} \right) Rn_c \quad (4.19)$$

where α_{PT} is the Priestley-Taylor coefficient, usually taken as 1.26 [-], f_g is the green vegetation fraction [-], Δ is the slope of the saturation vapor pressure versus temperature [$kPa K^{-1}$] and γ is the psychrometric constant [$kPa K^{-1}$].

In practice all conductive fluxes, i.e. Rn , Rn_c , Rn_s and G , are calculated once, following the formulations as given by (*Norman et al., 1995*), and remain constant thereafter. When only one radiometric temperature image is available the next step is then to derive H_c from Eq. (4.2). A first approximation of T_c , i.e. the average of air temperature T_{air} and radiometric temperature T_{RAD} , is used to derive T_s from Eq. (4.1). In the series approach, which was used here, a linear approximation of T_c is calculated following the procedure described in the Appendix of *Norman et al. (1995)*, using H_c and T_s to arrive at the within-canopy air temperature, T_{AC} . T_{AC} is then used for a first estimation of H_s using Eq. (4.9). LE_s is

finally derived from Eq. (4.3). If the vegetation is stressed, the Priestley-Taylor approximation, i.e. Eq. (4.11), overestimates the transpiration of the canopy and negative values of LE_s are computed. This improbable condensation over the soil during daytime indicates the existence of vegetation water stress and it is solved by reducing α_{PT} . An updated, lower, estimate of LE_c is obtained which yields an updated, higher, estimate of H_c through the use of Eq. (4.2). Next, Eq. (4.8) provides a new, higher, estimate of T_c , which in turn yields a, lower, estimate of T_s through Eq. (4.1), resulting in a, lower, updated estimate of H_s . Through the use of Eq. (4.3) an updated, higher estimate of LE_s is obtained. This iteration process is continued until $LE_s > 0$.

At this moment all the fluxes, radiative, conductive and turbulent, and their components, soil and canopy are known, as well as the “equilibrium” soil and canopy component temperatures. However, when multiple viewing angle observations of T_{RAD} are available, the soil and canopy temperatures may be derived directly from the observations. These provide the opportunity to estimate the component sensible heat fluxes from Eq. (4.8) and (4.9), thereby avoiding the need of the above iteration process and as such a check on the physical realism of the model.

4.2.1.2. Dual-angle model

In the dual-angle approach, a version also described by *Kustas and Norman (1997)*, T_{RAD} observations at different viewing angles provide soil and canopy component temperatures. The physical framework of the model remains identical to the single-angle version of TSEB. However, the mathematical framework to determine the turbulent fluxes is slightly different. The radiative and conductive fluxes, Rn_s , Rn_c and G , are estimated following the same parameterization as in TSEB1 and they remain constant during the steps necessary to derive the component turbulent fluxes. Still, different approaches can be followed to arrive at H_s , H_c , LE_s and LE_c . Two fundamentally different approaches are described in detail in the following sections.

Dual-angle iteration approach

In what it is referred to as the dual-angle iteration approach, TSEB2I, the first step concerns the estimation of LE_c and H_c following Eq. (4.2) and (4.19) as in TSEB1. H_c is used in combination with T_c to obtain the within-canopy temperature, T_{AC} , as in TSEB1. Since T_s is known from the observations, it is used with T_{AC} in Eq. (4.9) to estimate H_s . LE_s is then calculated as a rest-term from Eq. (4.3). If negative

values of LE_s are computed, this problem is solved by reducing α_{PT} , as in TSEB1. An updated, lower, estimate of LE_c is obtained which yields an updated, higher, estimate of H_c through the use of Eq. (4.2). The updated H_c is again used in combination with T_c to derive an update of T_{AC} , which in turn is used in conjunction with T_s in Eq. (4.9), to produce a new estimate of H_s . Again, through the use of Eq. (4.3) a new estimate of LE_s is obtained. This iteration process is continued until $LE_s > 0$.

Dual-angle component approach

In the dual angle component approach, TSEB2D, neither the Priestley-Taylor approximation nor any other iteration process is used. Instead the within-canopy temperature, T_{AC} , is estimated directly from the known component temperatures and the resistances, as follow:

$$T_{AC} = \frac{\frac{T_{air}}{R_A} + \frac{T_s}{R_s} + \frac{T_c}{R_x}}{\frac{1}{R_A} + \frac{1}{R_s} + \frac{1}{R_x}} \quad (4.20)$$

The component sensible heat fluxes, H_c and H_s , are then calculated directly from Eq. (4.8) and (4.9). Note that the formulation of Eq. (4.20) is equal to the general expression of the aerodynamic temperature in two-source models (*Shuttleworth and Gurney, 1990; Merlin and Chehbouni, 2004*).

The component latent heat fluxes, LE_c and LE_s , are simply calculated as rest-term from Eq. (4.2) and (4.3). If LE_c or LE_s is below 0, then it is set to 0, and H_c or H_s is calculated as a rest-term from Eq. (4.2) or Eq. (4.3) respectively. Basically, the TSEB2D approach is the same as the 2ANGLE model described by *Kustas and Norman (1997)*.

4.2.2. Methodology

In order to ensure the proper extraction of the bulk soil and canopy component temperatures from dual-angle observations, some minimum difference in viewing angle of these observations is needed. The optimum viewing-angle difference, usually between nadir and a particular zenith viewing angle, depends among other things on pixel resolution, local vegetation cover and geometry, as well as on component temperature differences. For practical application, differences of some 40 to 60 degrees

are generally desirable (Vining and Blad, 1992; Kustas and Norman, 1997; Merlin and Chehbouni, 2004; Colaizzi et al., 2012a).

Airborne data that fulfill these requirements were obtained during two campaigns over a vineyard in an agricultural test-site near Barrax, Spain. This concerns the EODIX and REFLEX campaigns. The first, carried out in June 2011, was specifically designed to obtaining imagery with large differences in viewing angle. Unfortunately, during this campaign no detailed flux and component temperature observations were collected, which made it difficult to validate the model results. Over the vineyard the only data available for validation was the water flux measured by a weighing lysimeter. Therefore data from the REFLEX campaign, which was flown in July 2012 over exactly the same vineyard and was designed specifically to advance our understanding of land-atmosphere interaction processes, were then used to validate the model output for surface energy fluxes.

The approach was first to validate the model performance for several different land cover units at the Barrax site, using data from the REFLEX-2012 campaign to ensure that the model was providing reliable output for this area, and the vineyard in particular. The results are shown in section 4.3.1. Secondly, data from the EODIX campaign were used to extract bulk canopy and soil component temperatures for the vineyard, which is located at the center of the site. The procedure is outlined in section 4.2.3.2 and the results are shown in section 4.3.2.1. At the time of the campaigns the vineyard is characterized by dry soils and drip-irrigated grape stands. The drip irrigation system was not located directly on the soil, but some cm above it, watering the surface along the tube. As a consequence, to some degree grass was growing under the vine stands and at some locations also in the corridors. The vineyard can best be described as relatively sparse; grape stands ranging in height from 1.0 to 2.5 meter are planted in rows at about 3 meter intervals, but having a relatively dense canopy. This makes the site particularly suitable to test the TSEB series model parameterization, which was specifically designed for this type of landcover (Norman et al., 1995). This is done by comparing model output from the single-angle and dual-angle TSEB versions using the data of the EODIX campaign. Since for all TSEB versions the net radiation and soil heat flux parameterizations are identical, the focus in the comparison study is on the turbulent flux output only. The results are provided in section 4.3.2.2 and 4.3.2.3.

A brief description of the observations and processing done for the input to and validation of the TSEB model is provided below. For a more complete description of the campaign observations see

Timmermans et al. (2014) and *Van der Tol et al. (2014)* for the REFLEX campaign and *Mattar et al. (2014)* for the EODIX campaign.

4.2.3. Observations and data processing

4.2.3.1. REFLEX 2012 Campaign

Ground-truth data

Reference meteorological data were recorded at two permanent meteorological stations in the area. During the campaign, which took place from 16 to 28 of July 2012, three eddy covariance (EC) towers and a large aperture scintillometer (LAS) were installed over different landcover units as well. Apart from the turbulent H and LE fluxes, the flux towers measured standard meteorological parameters at three different heights, see *Van der Tol et al. (2014)* for a detailed description of these observations. Required meteorological model inputs concern incoming shortwave radiation and air temperature, relative humidity and wind speed at a certain reference level. Since some crop and tree heights in the area were greater than the measurement level at the reference stations, the required meteorological model input was obtained by the average of the three EC stations at a reference height of 5 meter. Although a certain spatial variability in these variables is known to influence flux estimations over such heterogeneous sites (*Timmermans et al., 2008b*) this spatial average (the standard deviation of air temperature was 0.9 degrees, and 0.09 ms⁻¹ for wind speed) was considered to be representative of the area with respect to the current model validation.

In addition to the standard meteorological observations, the components of the surface energy balance (Rn, G, H and LE) were measured continuously for the duration of the campaign. The EC towers were installed over the camelina field, vineyard and the reforestation area, and the LAS was installed over a large wheat-stubble field, see Figure 4.1. Typical site characteristics, such as representative canopy, or stand, heights and average fractional cover for each site are provided in Table 4.1.

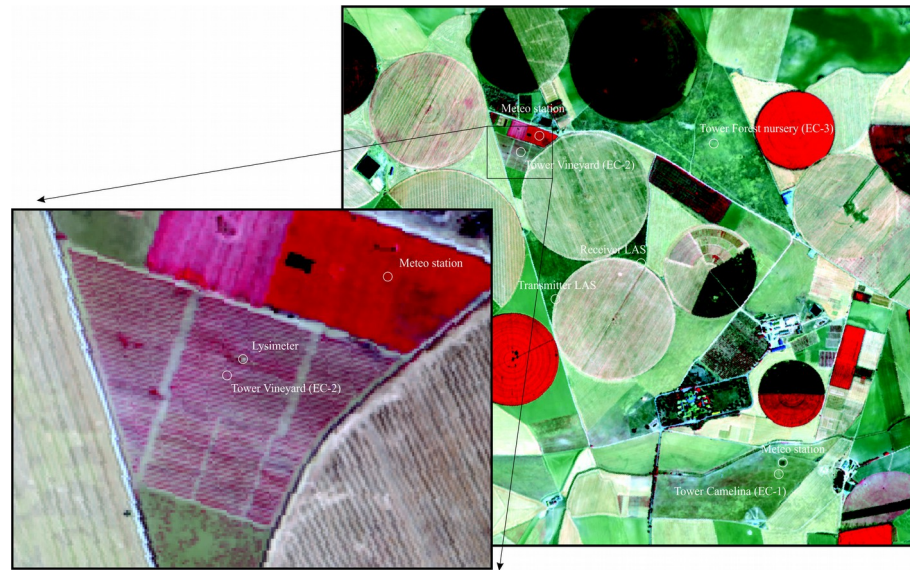


Figure 4.1: Site overview with reference stations and flux tower sites. The zoom shows details of the vineyard site with a W-NW to E-SE crop row orientation, and lysimeter and flux tower positions.

Table 4.1. Site characteristics.

Canopy	Canopy height [m]	Fractional cover [%]
Camelina	0.5	2.25 (\pm 0.9)
Vineyard	2	13.45 (\pm 1.1)
Reforestation area	1	4.03 (\pm 1.2)
Wheat-stubble	0.15	4.78 (\pm 1.2)

Net radiation was measured at the vineyard and camelina sites using a 4-component radiometer. At the forest nursery and wheat stubble sites local surface-temperature observations were used to estimate outgoing longwave radiation, while incoming longwave and shortwave radiation were assumed to be constant over the whole area. An estimate of reflected shortwave radiation for these sites was obtained by using albedo estimates from the airborne overpasses. It goes without saying that this approach prevents a proper ground-based validation of the net radiation at these two sites.

The soil heat flux measurements at the individual sites were taken at depths of a few centimeters and needed to be corrected for storage in the soil layer above the sensors. Over the vineyard, one measurement was taken below the vine stand and another one in between the stands, such as to obtain representative observations for this particular site. Soil moisture and soil temperature

observations were taken at different depths for the post-processing of the soil heat fluxes following the methodology described in *Van der Tol (2012)*. Unfortunately, these additional measurements were not taken at all four sites. However, following *de Vries (1963)* the soil heat flux may be described by:

$$G(z,t) = A(0) e^{-z/D} \sqrt{\omega B D c \lambda} \sin \left[\omega t - \frac{z}{D_{dd}} + \frac{\pi}{4} \right] \quad (4.21)$$

where z [m] is depth from the surface, t is time [unit the same as ω], $A(0)$ is the amplitude of the temperature wave at the surface [K], ω is the period of the soil heat flux (here taken as one day, unit taken in hours), ρ is the soil density [kg m^{-3}], c the soil specific heat [$\text{kJ kg}^{-1} \text{K}^{-1}$], λ the soil thermal conductivity [$\text{Wm}^{-1} \text{K}^{-1}$] and D_{dd} the so-called damping depth [m]. The corrections made at the camelina site were used in combination with Eq. (4.13) to derive D_{dd} and the time delay of the temperature wave between 2 different depths. Assuming that soil properties in the area were homogeneous, these were then used to correct soil heat flux measurements taken at the other sites.

A detailed discussion of the turbulent flux observations is provided in *Van der Tol et al. (2014)*, which includes a discussion of the well-known closure problem. For validation purposes, a correction procedure is sometimes followed whereby the residual is distributed according to the Bowen ratio to the sensible and latent heat flux (*Foken, 2008*). However, due to the indirect procedure employed to obtain ground observation of net radiation for the forest nursery and wheat stubble site, combined with the uncertainties in the net radiation measurement over the vineyard and the small number of soil heat flux observations at most of the sites (*Timmermans et al., 2014*), the energy balance was not closed.

Detailed footprint analysis were performed for each site at the time of the airplane overpass in order to enable a comparison between the remote sensing-based turbulent flux estimates and the corresponding ground measurements to be made. The procedure outlined in *Timmermans et al. (2009)*, originally developed for LAS observations, but easily adaptable for EC observations, was used for all four sites. Observations from these sites were then used for the validation of TSEB1 over the Barrax site.

Remote sensing data

Required remote sensing-based model inputs covered broadband surface albedo, normalized difference vegetation index and surface temperature. These were obtained from optical airborne data acquired with the Airborne Hyperspectral Scanner (AHS), a sensor mounted on the Spanish Instituto Nacional de Técnica Aeroespacial (INTA) aircraft platform. Acquisitions were made on two consecutive days in order to cover a full daily cycle (*Timmermans et al., 2014*). However, for the current contribution, an overpass at 09:28 UTC on the 25th July 2012 was used.

At-surface georeferenced reflectances (level 2b), resampled to a 4 meter pixel size, were provided by the INTA Remote Sensing Laboratory that was in charge of post-processing the airborne acquisitions. The at-surface reflectance was validated against field spectroscopy acquired *in situ* over a variety of landcover units, that showed good overall agreement. Details of these observations and post-processing steps are provided in *De Miguel et al. (2014)*.

Broadband surface albedo and NDVI were then derived from the surface reflectance in specific Red and Near Infrared (NIR) bands of the AHS sensor, following the same procedure as described in *Timmermans et al. (2011)*.

At-sensor radiances (level 1b) from the thermal AHS channels were processed by the Global Change Unit at the Faculty of Earth Physics at the University of Valencia, Spain and validated against ground observations performed over several different landcovers. Land surface temperature and emissivity were retrieved simultaneously using the Temperature-Emissivity-Separation algorithm of *Gillespie et al. (1998)*, adapted for use with the AHS data as described in *Sobrino et al. (2009)*.

4.2.3.2. EODIX 2011 Campaign

Ground-truth data

The necessary meteorological model input data were obtained from the lysimeter station located inside the vineyard, see zoom Figure 4.1. The meteorological observations were acquired at a height of 4 meter. They consisted of 15-minute averages of incoming shortwave radiation and 1-hour averages of air temperature, relative humidity and wind speed. The hourly averages were then interpolated to

acquire estimates at the airborne overpass time. The lysimeter station records hourly actual evaporation rates, which are interpolated for the overpass time of the airplane. The observation was used as an indication of the model performance, testing to which degree the estimations of LE fluxes were realistic and physically meaningful. The average fractional cover over the vineyard obtained in the EODIX 2011 campaign was 39% (± 0.02).

Remote-sensing data

Airborne optical imagery used to analyze the performance of the different model versions was also obtained from the Airborne Hyperspectral Scanner (AHS) operated by INTA. Two parallel flight lines acquired at 09:00 and 09:20 UTC on the 12th June 2011 were utilized for this purpose. The flight lines were chosen such that they were parallel to each other and also parallel to the row orientation of the vineyard, in order to minimize potential local differences in shadowing effects due to differences in viewing azimuth. The campaign was specifically designed to obtain large differences in viewing angle. In order to achieve view zenith angles close to 60°, a wedge was placed under the sensor, to tilt it during the flight (*Mattar et al., 2014*). This produced a nadir viewing angle over the vineyard for the flight line acquired at 09:00 and a zenith viewing angle of 57° over the vineyard for the flight line obtained at 09:20.

Required general model inputs, broadband surface albedo, NDVI and surface temperature were obtained from the nadir flight in exactly the same manner as for the REFLEX 2012 campaign and are therefore not described here again. In addition, the dual-angle model versions require bulk soil and canopy component temperature observations. These were obtained from the two parallel flight lines, which were characterized by viewing zenith angle differences over the vineyard of around 57°.

The soil and canopy component temperatures were obtained from the simultaneous solution of two equations containing two unknowns, where f_{c1} and f_{c2} and $T_{RAD}(\phi_1)$ and $T_{RAD}(\phi_2)$ are the fractional covers and the radiometric surface temperatures at the first viewing angle, ϕ_1 , and second viewing angle, ϕ_2 . Eq. (4.1) was used for the two flight lines to derive the component soil and canopy temperatures, following:

$$T_S = \left(\frac{f_{C2} T_{RAD}^4(\phi_1) - f_{C1} T_{RAD}^4(\phi_2)}{f_{C2} - f_{C1}} \right)^{1/4} \quad (4.22)$$

$$T_C = \left(\frac{T_{RAD}^4(\phi_1) - (1 - f_{C1}) T_S^4}{f_{C1}} \right)^{1/4} \quad (4.23)$$

In order to take the small time difference of 20 minutes between the two successive flight lines into account, a correction of T_{RAD} was made, using the ratio of $T_{RAD}(\phi_1) / T_{RAD}(\phi_2)$ taken from a homogeneously vegetated area (dense grass cover) just north of the vineyard. However, the differences obtained were almost negligible.

As can be seen in the zoom of Figure 4.1, two corridors exist in the vineyard, characterized by a very low fractional cover. As they were oriented perpendicularly to the flight lines, the difference in fractional cover between the two flight lines was minimal. Since this difference is in the denominator of Eq. (4.13) the determination of T_S can become very sensitive to errors. These pixels were therefore excluded from the analysis.

4.3 RESULTS AND DISCUSSION

4.3.1 Validation of single-angle model over Barrax (REFLEX 2012 Campaign)

TSEB model output for R_n , G , H and LE as derived from the AHS overpass at 09:28 UTC on 25th July, 2012, was validated against ground observations. For this purpose the so-called field-of-view of the local sensors needs to be determined. This is especially important when dealing with high-resolution imagery as is the case in the underlying study.

For the net radiation sensor, 99% of the observations originate from a circle whose diameter is 10 times the sensor height (i.e. 5 meter), although ground surfaces closer to the sensor have a higher weighting. A window of 10 x 10 pixels (i.e. 40 x 40 m) was selected around the location of the observation. The same was done for the soil heat flux observations, which are characterized by a high spatial variation. To at least take this effect into account we chose a similar window as for the net radiation observations. For the turbulent fluxes a different strategy is followed. The “field-of-view”, or footprint (Vesala *et al.*, 2008), of these sensors depend on terrain characteristics, wind speed and wind

direction. The procedure outlined in *Timmermans et al. (2009)* is used to calculate the footprints of the observation towers at the moment of airborne overpass. Footprint-weighted averages of the model output for H and LE were then compared to the ground observations. Results for the individual sites for all four fluxes are shown in Figure 4.2.

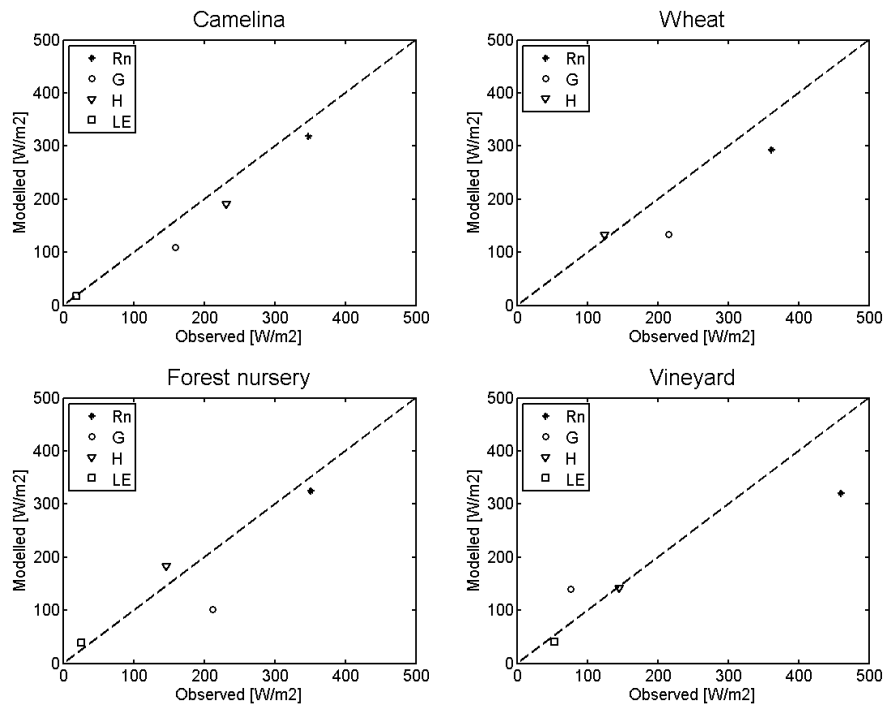


Figure 4.2: Observed versus estimated fluxes with the TSEB model over the Barrax site for 25th July 2012 (REFLEX campaign).

Model performance was evaluated using difference statistics comprising of the mean absolute difference (MAD), the mean absolute error (MAE) and the root mean square difference (RMSD), Table 4.2.

Table 4.2. Difference statistics for the four observation sites.

	H	LE	G	Rn
MAD [Wm ⁻²]	22.5	8.7	85.0	51.5
MAE [%]	13.9	29.4	51.2	13.6
RMSD [Wm ⁻²]	28.0	10.0	87.2	58.3

Although only a limited ground observations were available for this particular study, a general good agreement between observed and modelled fluxes is noted from Table 4.2 although performance for R_n and G is less than what is observed in other studies (*French et al., 2005; Timmermans et al., 2007*). Despite that the focus of the current contribution is on the turbulent fluxes, we explain the results for all four fluxes below.

Generally, modelled net radiation estimates are slightly lower than the observed values. However, the somewhat high difference between observed and modelled net radiation estimates is mainly due to the difference over the vineyard site. This is attributed to the position of the sensor relative to the geometry of the vineyard. At a sensor height of 5 m over a row crop of 2 m height and a sensor field of view of 150° the canopy will be more dominant than it is in the airborne observations. This phenomenon has a greater effect in the shortwave region than in the longwave region under the circumstances during the overpass. Therefore the, locally observed lower albedo resulted in a higher local observation of net radiation. Leaving out this observation results in a far better match between modelled and observed radiation values, that is comparable to previous studies ($MAD=36.3 \text{ Wm}^{-2}$; $MAE=10.3\%$; $RMSD=37.4 \text{ Wm}^{-2}$).

As mentioned before, soil heat flux quantities may be spatially highly variable. Despite the attempt to position the limited number of available soil heat flux plates at representative locations, this makes validation slightly difficult. Moreover, local calibration of the model coefficient c_g in Eq. (4.7) linked the model soil heat flux estimates to the model estimates of net radiation, which may reach up to 50% thereof in semi-arid ecosystems like the study area. Although this results in a slight underestimate of the soil heat fluxes, the effect on the available energy (i.e. net radiation minus soil heat flux) is partially cancelled out by this phenomenon.

The results for the turbulent fluxes show a good similarity to local observations, with RMSD for H and LE equal to 28 Wm^{-2} ($MAE 14\%$) and 10 Wm^{-2} ($MAE 29\%$) respectively. The relatively high value of MAE for the LE fluxes is due to the low absolute magnitude of this flux. In this semi-arid climate during the summer, over non-irrigated areas, this flux will rarely exceed 5% to 10% of net radiation rates. Not surprisingly, the vineyard observations of LE show the highest values of the observation sites, which is reflected by the model results. However, observations at this location are influenced by the neighbouring fields. During the overpass, the prevailing wind direction was from the South-East. For the camelina, nursery and wheat stubble sites, the footprint analysis revealed that observed fluxes

originated almost solely from the land cover where the observations were made. For the vineyard site however, 64.9% of the observed flux originated from the nearby dry barley stubble field. For validation purposes this effect is taken into account, but “pure” vineyard rates for LE will be higher than those observed by the flux tower.

Model estimates for sensible heat flux show very good agreement with local observations for all sites. When compared with the error obtained by other studies ($\sim 30 \text{ Wm}^{-2}$) for relatively homogeneous canopies (French *et al.*, 2005; Gonzalez-Dugo *et al.*, 2009; Kustas and Norman, 1997; Timmermans *et al.*, 2007) the results obtained over the current area are even more favorable. Therefore, we regard the overall model performance of TSEB1 with respect to the estimation of both radiative and especially turbulent fluxes over the heterogeneous Barrax site as reliable.

4.3.2. Comparison between single-angle and dual-angle model (EODIX 2011 Campaign)

4.3.2.1. Soil and canopy component temperatures

Bulk soil and canopy component temperatures obtained from the dual angle airborne observations showed average values of 310.6 and 300.7 K respectively, with standard deviations of 0.62 for the soil and 0.30 for the canopy. Although these “observed” temperatures are actually derived from Eq. (4.22) and (4.23), and as such are not actual observations of T_s and T_c , they will be referred to as “observed” from here onwards, to differentiate them from soil and canopy temperatures as modelled by TSEB1. The soil temperatures ranged from 303.8 to 318.1 K, while observed canopy temperatures were between 298.0 and 302.6 K. Unfortunately, during the EODIX 2011 campaign, no detailed ground observations of soil and leaf component temperatures were available. However, given an observed air temperature of 296.5 K and a vapor pressure deficit of 1.2 kPa the observations are in agreement with theoretical limits as defined by Jackson *et al.* (1981) and Gardner *et al.* (1992), or more recently, by Colaizzi *et al.* (2012b). They report that typical values for foliage temperatures under these circumstances may range from 1.5 K below air temperature for potentially transpiring crops to 5.0 K above air temperature for non-transpiring crops, although it is stated that measurements may occasionally exceed these limits.

Similar observations were made by *Timmermans et al. (2008a)* during the Sen2Flex campaign over the Barrax vineyard. Apart from measuring sunlit and shaded soil temperature, they used contact probes to measure individual leaf temperatures of sunlit and shadowed, old and young leaves, at different heights in the canopy. They found within-canopy differences in leaf temperature ranging from 5 K below air temperature to 6 K above air temperature in late morning and reported standard deviations as large as 3.1 K for soil and 1.3 K for the canopy component temperatures, within a 5 m radius.

The canopy temperatures observed in the study are obviously biased towards the upper theoretical limit with respect to air temperature. This may indicate that, though irrigated, the crops are transpiring at a sub-potential rate.

A comparison of the component temperatures with the modelled values of soil and canopy temperatures obtained from TSEB1 is provided in Figure 4.3. For a large part of the vineyard the modelled values of T_c are lower than observations (298.7 K vs. 300.7 K on average respectively) and in much of the vineyard the values of modelled T_s are higher than observed (312.1 K vs. 310.6 K on average respectively). Apart from this the spread of the modelled values of both T_c and T_s is smaller than for the observations. Observed T_c shows a standard deviation of 0.30 K versus a standard deviation of 0.20 K for the modelled values. For T_s the standard deviations for observations and modelled values are 0.62 K and 0.49 K respectively.

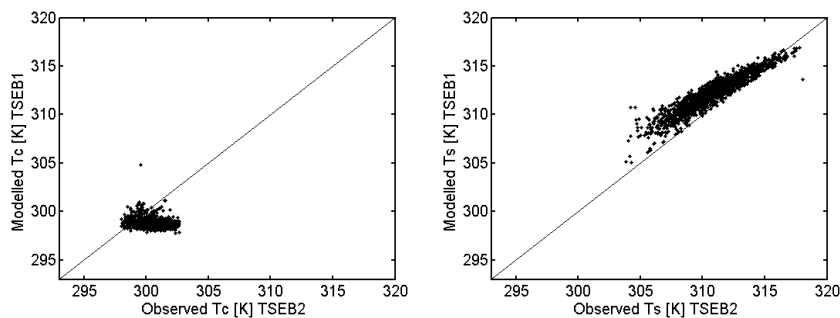


Figure 4.3: Observed versus estimated component temperatures for 12th, June 2011.

4.3.2.2. Single-angle (TSEB1) and dual-angle iteration approach (TSEB2)

Model output from TSEB1 is plotted versus TSEB2 output for the turbulent fluxes in Figure 4.4.

Although a reasonable agreement and clear correlation, R , between the two model versions (R is equal to 0.91 for LE and 0.82 for H) is noted in this figure, there are also clear differences. A general under-estimation of sensible heat flux by TSEB2I with respect to TSEB1 output is noted and a similar over-estimate of latent heat flux by TSEB2I with respect to TSEB1 can be seen. An explanation for this is found by a closer examination of the component flux outputs of both model versions, which are shown in Figure 4.5. Model output statistics, including those from the TSEB2D model version, are presented in Table 4.3.

Table 4.3. Model output statistics for TSEB1 and TSEB2I: mean (\bar{x}) and standard deviation (σ).

	H		H_c		H_s		LE		LE_c		LE_s	
	\bar{x}	σ										
TSEB1	102	4.0	5	2.7	97	3.7	185	6.8	97	6.8	88	4.2
TSEB2I	68	7.7	3	4.2	66	7.0	219	10.8	100	7.5	119	7.0
TSEB2D	142	5.2	69	10.0	73	6.6	145	5.7	34	8.8	112	6.7

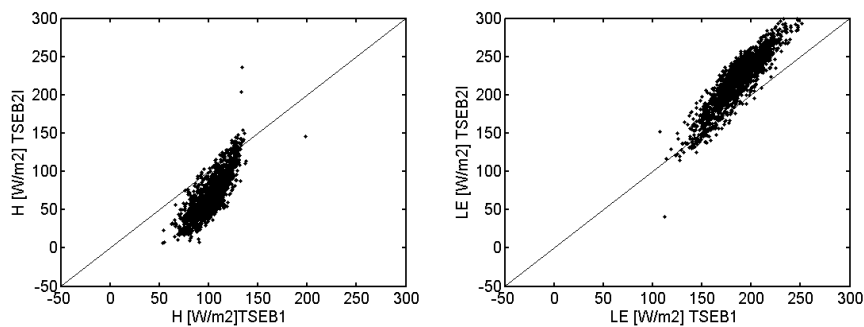


Figure 4.4: Turbulent fluxes from TSEB1 vs. TSEB2I, left panel for sensible heat flux, right panel for latent heat flux.

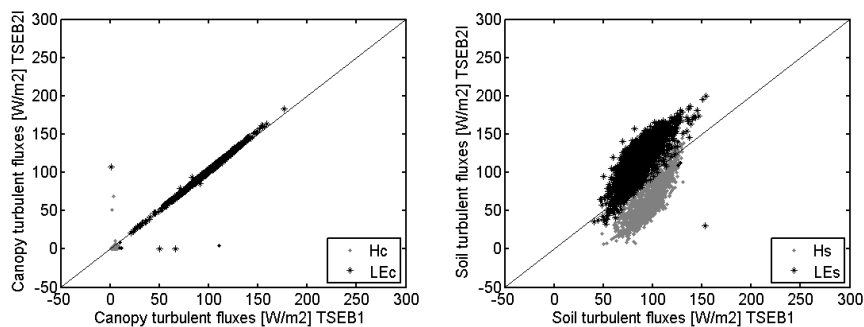


Figure 4.5: Component turbulent fluxes from TSEB1 vs. TSEB2I, left panel for the canopy, right panel for soil.

In the left panel of Figure 4.5 the canopy component fluxes of TSEB1 are plotted against those of TSEB2I, and in the right panel the soil components are shown.

The canopy component fluxes of TSEB1 and TSEB2I are identical for almost all pixels in the vineyard. This is due to the Priestley-Taylor iteration procedure that was used here in both versions of the model. If the first estimates of T_s , in TSEB1, or observations of T_s , in TSEB2I, yield an H_s that is smaller than $R_{n_s}-G$, then the first estimate of $LE_s > 0$. This is the situation for nearly all points, which means that the two versions yield the same values for LE_c and H_c fluxes under these circumstances.

Since for almost all pixels the canopy component fluxes are identical for the two versions of the model and LE_s is determined as a rest-term, the differences for H and LE are entirely regulated by the differences for H_s . The TSEB2I model output for H_s is almost everywhere smaller than in the TSEB1 version, see Figure 4.5 right panel. Examination of Eq. (4.9) reveals that differences in H_s may be invoked by differences in T_{AC} , in R_s or in different values for T_s .

Many of the observed values of T_c are larger than the TSEB1 model output for T_c , see Figure 4.3. Eq. (4.1) shows that for T_s the opposite then must hold true, which is confirmed in the right panel of Figure 4.3. Lower values of T_s in TSEB2I potentially yield lower values for H_s . Model differences for R_s are mainly regulated by differences in the coefficient a' in Eq. (4.13) and defined in Eq. (4.18). Larger T_c values in TSEB2I, and thus lower T_s values, result in lower values for a' and thus in higher R_s values, since wind speed values do not differ significantly between model versions. Higher R_s values potentially yield lower values for H_s in TSEB2I as well.

Within canopy air temperature, T_{AC} , is obtained by rewriting Eq. (4.8) to:

$$T_{AC} = T_c - \frac{H_c R_x}{\rho_a C_p} \quad (4.24)$$

Since values for R_x , mainly driven by wind speed, and H_c are similar in both versions of the model, higher values of T_c in TSEB2I also yield higher values of T_{AC} in TSEB2I. Larger values of T_{AC} potentially yield lower values of H_s in TSEB2I as compared to TSEB1.

The model differences for R_s and T_{AC} described above are illustrated in Figure 4.6. Using the original R_s formulation, where a' in Eq. (4.18) is equal to 0.004 and independent of $T_s - T_c$ reduced differences for R_s , but did not significantly influence model differences for H_s (the difference between H_s from TSEB1 and TSEB2I-D with the original R_s formulation and the one temperature dependent was less than 20 Wm^{-2}). Resuming, larger values of observed T_c as compared to modelled T_c in TSEB1 for all three parameters that have a direct influence on H_s yield lower values of H_s . On the other hand, if lower values of T_c were observed than for TSEB1-modelled T_c this would yield higher values of H_s in TSEB2I than in TSEB1. Since many of the observed values of T_c were higher than those of the modelled T_c the dual angle model output for H_s , and thus for H , is lower.

4.3.2.3. Single-angle (TSEB1) and dual-angle component approach (TSEB2D)

The model output from TSEB1 is plotted versus TSEB2D output for the turbulent fluxes in Figure 4.7. Agreement between the two models is less than in the case of TSEB1 versus TSEB2I, with the correlation, R , between the two model versions equal to 0.55 for LE and 0.30 for H. Once again, an explanation is found by a closer examination of the component flux outputs of both model versions, as shown in Figure 4.8

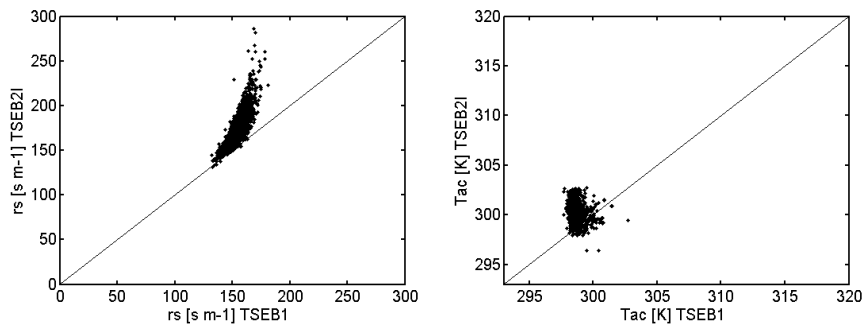


Figure 4.6: Left panel R_s , right panel T_{AC} .

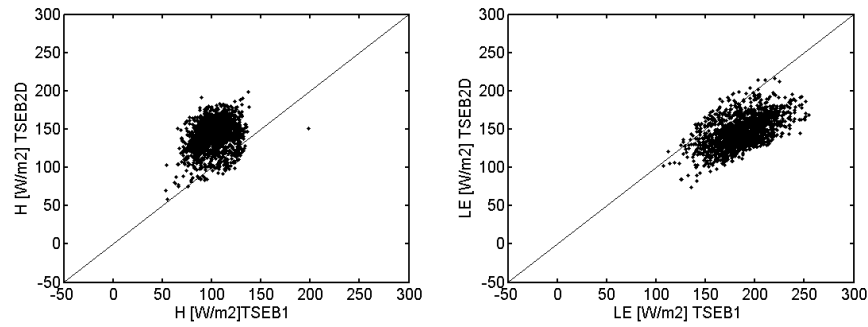


Figure 4.7: Turbulent fluxes from TSEB1 versus TSEB2D, left panel for H, right panel for LE.

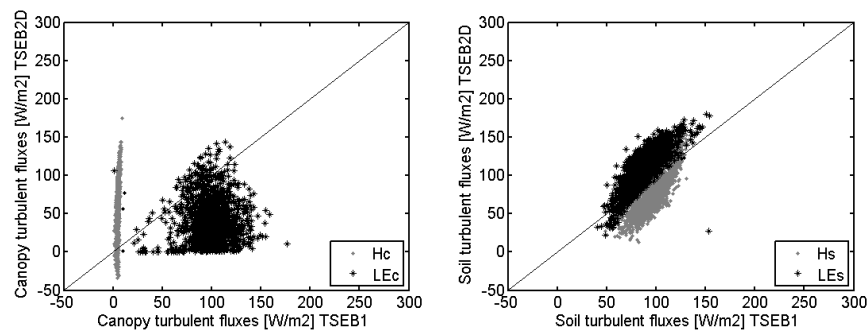


Figure 4.8: Component turbulent fluxes from TSEB1 versus TSEB2D, left panel for canopy, right panel for soil.

For the soil component fluxes, shown in the right panel of Figure 4.8, a similar reasoning may be followed as described in the last paragraph of section 4.3.2.2. Therefore the right panel of Figure 4.8 is very similar to the right panel of Figure 4.5.

However, a striking difference between the two model versions can be observed with respect to the canopy component fluxes. In the TSEB2D approach, values for H_c range from -35 to 175 Wm^{-2} . However, in the TSEB1 approach, for almost the entire vineyard, the canopy is transpiring at the potential rate, resulting in negligible values for H_c under the current circumstances.

In the absence of senescent vegetation, the first estimate of the partitioning of R_{nc} into LE_c and H_c in TSEB1 is determined entirely by the slope of the saturation vapor pressure, Δ , which depends solely on air temperature. In the temperature range between 25 and $35 \text{ }^\circ\text{C}$, which are typical summertime values at this latitude, the first estimate of the portion of R_{nc} that is consumed by latent heat exchange ranges from 95 to 105% . This leaves only negligible amounts of energy available for sensible heat

exchange between the canopy and the air. Under TSEB1 these first estimates will not change as long as the first estimate of the soil component of the sensible heat flux, H_{S-1} , is smaller than the available amount of energy for the soil, i.e. Rn_s-G . In other words, these first estimates will not change as long as LE_{S-1} is larger than 0. This is the case for almost all pixels in the vineyard.

Following Eq. (4.24), negligible sensible flux over the canopy results in a within-canopy air temperature very similar to the canopy temperature. One could reason that in such a case the sensible heat flux over the soil is driven by the difference between T_s and T_c . Given that the first estimate of T_c in TSEB1 is the average between air temperature and radiometric surface temperature, this means that the first estimate of H_s is driven by the difference between air and radiometric surface temperature as a function of fractional canopy cover, f_c , over the surface resistance, following:

$$H_{S-1} = \frac{\rho_a C_p}{R_s} \left[\left(\frac{\left(T_{RAD}^4 - f_c \left(\frac{T_{RAD} + T_A}{2} \right)^4 \right)^{1/4}}{1 - f_c} \right) - \left(\frac{T_{RAD} + T_A}{2} \right) \right] \quad (4.25)$$

The first estimate of LE_s is then given by:

$$LE_{S-1} = (1 - c_g) \left(Rn \exp \left(-0.45 \left(-2 \ln(1 - f_c) \right) \right) \right) - H_{S-1} \quad (4.26)$$

Substituting Eq. (4.25) in Eq. (4.26) provides a simple first check whether given conditions will predict water-stressed canopy conditions. Under the current conditions, LE_{S-1} is positive everywhere, meaning no lowering of α_{PT} in Eq. (4.29) occurred at any location. Hence the canopy sensible heat flux estimates in TSEB1 are negligible (Table 4.3). This is remarkable, given that the observed canopy component temperatures are “biased towards the upper theoretical limit with respect to air temperature”, indicating potentially relatively high canopy sensible heat fluxes.

TSEB2D estimates for canopy sensible heat fluxes, that range from -35 to 175 Wm^{-2} , are on average 69 Wm^{-2} and show a standard deviation equal to 10.0 Wm^{-2} . This relatively large range is also observed by *Kustas and Norman (1997)* who state that in general an approach that uses the component temperatures directly produces considerable scatter. Of course we do not have component flux

observations at the scale of individual vines, but given the observed range in canopy temperatures a certain scatter in canopy sensible heat fluxes may be expected. Locally even stable conditions may occur, given the nature of the vineyard where hot bare corridors alternate with drip-irrigated vines. On the other hand also relatively stressed vines may exist within the vineyard, since the irrigation scheme is rather irregular at this experimental test farm. The last irrigation registered on the lysimeter was 20 mm on the 7th June, five days before the airborne overpass. This relatively small amount may not have reached the depth where the vineyard roots are, especially given the presence of grass in between the vine stands. The relatively high LE from the soil, or substrate, can be partly attributed to this phenomenon. In addition, dew is recorded by the lysimeter almost all mornings in the period of the campaign, typically a few hours before the flight. Vaporization of this dew will also contribute to the soil, or substrate, component of LE. Although no individual canopy flux observations are available, the range in TSEB2D model output seems realistic. The larger rate of latent heat from the soil could be related with the dew registered also on the lysimeter.

In TSEB2D, the canopy sensible heat fluxes were estimated following Eq. (4.8), where ρ_a , C_p and T_c are observed parameters and R_x and T_{AC} are estimated following Eq. (4.12) and (4.20) respectively. Since the latter depend on observed air and component temperatures as well as on the resistances, Eq. (4.11-4.13), the different resistance parameterizations are of crucial importance for obtaining accurate component flux estimates. Validation of these parameterizations for the current study would have involved further experimental observations of within- and above-canopy wind, temperature and flux profiles. However, this is beyond the scope of the current study, whose objective was merely to investigate the effect of using observed component temperatures instead of model-derived component temperatures on model output.

All in all, using the observed component temperatures in TSEB2D results in higher values for H, and lower values for LE, as compared to TSEB1 under current conditions.

An indication of the model performance may be obtained from Table 4.4, where TSEB1, TSEB21 and TSEB2D model outputs for LE are compared with the lysimeter measurements. The best fit corresponds to the TSEB2D output, although the agreement with TSEB1 is still within accurate ranges.

Table 4.4: LE model results for TSEB1, TSEB2I and TSEB2D versus the lysimeter observation.

Latent heat flux [Wm ⁻²]	Lysimeter	TSEB1	TSEB2I	TSEB2D
	124	163	201	125

4.4 SUMMARY AND CONCLUSIONS

Validation of the widely used single-angle model, TSEB1, over a very heterogeneous agricultural area in a semi-arid environment showed good results that are comparable to previous validation work done for the model. Reliable results were obtained for both conductive and turbulent fluxes, where a slight under performance for the conductive fluxes is attributed to the nature of the ground observations rather than to model malfunctioning. Turbulent flux exchanges, especially over the vineyard, showed a particularly good fit with respect to ground observations.

Dual-angle measurements yielded “observations” of soil and canopy component temperatures that showed a larger spread than modelled values for T_s and T_c . No ground observations of component temperatures were made during the overpass but values showed very similar responses compared to observations made during previous and comparable campaigns and were within theoretical limits. Values obtained for canopy temperature indicated relatively stressed vegetation stands. This was not confirmed by results of the TSEB1 model, which generated values for T_c that were generally lower than observations and T_s that were generally higher than observations.

The output of two types of the dual angle version of TSEB, comparable to those described in (*Kustas and Norman, 1997*) and (*Colaizzi et al., 2012a*), was compared with the output of the single-angle model version. The first version, TSEB2I, contains a similar iteration procedure to that of the single-angle version, invoking a step-wise lowering of the Priestley-Taylor coefficient. The second version, TSEB2D, without iteration procedure, utilizes the “observed” component temperatures to estimate component sensible heat fluxes directly.

Reasonable agreement and correlations between TSEB1 and TSEB2I model outputs for the turbulent fluxes were found. TSEB1 generates slightly lower values for LE and slightly higher values for H than TSEB2I. This is entirely regulated by the soil component of the fluxes, since the canopy flux estimates

of both model versions are similar due to the iteration procedure used in both model versions. This procedure yields a potentially transpiration canopy in over almost the entire vineyard under the current conditions. The higher values for T_s obtained in TSEB1 as compared to observed values for T_s always result in higher estimates of H_s in the current parameterization. LE_s is calculated as a rest-term, so TSEB1 estimates are lower than estimates of TSEB2I. TSEB1 results for H are therefore higher than for TSEB2I and TSEB1 results for LE are lower than for TSEB2I.

There is less agreement between the TSEB1 and TSEB2D model outputs. Since the soil components are estimated in a similar manner as for TSEB2I, the reason for the lower agreement lies in the estimation of the canopy component fluxes. Under the current conditions, TSEB1 predicts potential transpiration rates for the entire vineyard, which yields negligible H_c estimates overall. However, using “observed” T_c in TSEB2D to directly estimate H_c yields values that range from -35 to 175 Wm^{-2} . Even though no ground observations are available for these component fluxes, these values seem to be more realistic under the given conditions.

Acknowledgments. The research leading to these results was funded by the European Community's 7th Framework Programme (FP7/2008-2013) under EUFAR contract n° 227159, Cost Action ES0903-EUROSPEC and ESA Grant D/EOP/rp/2012/48. The work of A. Andreu was partly supported by grant AGL2011-30498 (Ministerio de Economía y Competitividad of Spain, co-funded by FEDER).

We would like to thank Christiaan van der Tol, Wout Verhoef and Zhongbo Su for their critical and helpful comments and suggestions. We also thank Jose Sobrino of the Global Change Unit at the Department of Earth Physics, University of Valencia, Spain for providing the remote sensing data and Fernando de la Cruz of the Instituto Tecnico Agronomico Provincial de Albacete (ITAP), Spain for the ground meteorological observations of the EODIX Campaign. We also would like to thank Bill Kustas for critically reviewing, which led to substantial improvement of this contribution.

4.5 REFERENCES

- Anderson M. C., Norman J. M., Diak G. R., Kustas W. P. and J. R. Mecikalski (1997) A two-source time-integrated model for estimating surface fluxes using thermal infrared remote sensing. *Remote Sensing of Environment* 60, 195-216.
- Anderson M. C., Norman J. M., Kustas W. P., Li F., Prueger J. H. and J. R. Mecikalski (2005) Effects of vegetation clumping on two-source model estimates of surface energy fluxes from an agricultural landscape during SMACEX. *Journal of Hydrometeorology* 6, 892-909.
- Anton J. A. and J. K. Ross (1987) Emissivity of the vegetation-soil system (in Russian with English summary). *Sov. J. Remote Sens.* 5, 49-55.
- Brutsaert W. (1982) Evaporation into the atmosphere. *Reidel, Dordrecht, The Netherlands*, 299.
- Colaizzi P. D., Kustas W. P., Anderson M. C., Agam N., Tolck J. A., Evett S. R., Howell T. A., Gowda P. H. and S. A. O'Shaughnessy (2012a) Two-source energy balance model estimates of evapotranspiration using component and composite surface temperatures. *Advances in Water Resources* 50, 134-151. 10.1016/j.advwatres.2012.06.004
- Colaizzi P. D., O'Shaughnessy S. A., Evett S. R. and T. A. Howell (2012b) Using plant canopy temperature to improve irrigated crop management. *Proceedings of the 24th Annual Central Plains Irrigation Conference, Colby, Kansas, February 21-22, 2012*, 203-223.
- De Miguel E., Jimenez M., Perez I., Gutierrez de la Camara Ó., Munoz F. and J. A. Gomez-Sánchez (2014) Image processing methods and results for the REFLEX airborne remote sensing campaign. *Acta Geophysica* In review.
- De Vries D. A. (1963) Thermal properties of soils. In: *W.R. van Wijk (ed.) Physics of plant environment. North Holland, Amsterdam*, 210-233.
- Foken T. (2008) The energy balance closure problem: an overview. *Ecological Applications* 18, 1351-1367.
- French A. N., Jacob F., Anderson M. C., Kustas W. P., Timmermans W. J., Gieske A., Su Z., Su H., McCabe M. F., Li F., Prueger J. and N. Brunzell (2005) Surface energy fluxes with the Advanced Spaceborne Thermal Emission and Reflection Radiometer (ASTER) at the Iowa 2000 SMACEX site (USA). *Remote Sensing of Environment* 99, 55-65.
- Gardner B. R., Nielsen D. C. and C. C. Shock (1992) Infrared thermometry and the Crop Water Stress Index. I. History, theory, and baselines. *Journal of Production Agriculture* 5, 462-466.
- Gillespie A., Rokugawa S., Matsunaga T., Cothorn J. S., Hook S. and A. B. Kahle (1998) A temperature and emissivity separation algorithm for Advanced Spaceborne Thermal Emission and Reflection Radiometer (ASTER) images. *IEEE Transactions on Geoscience and Remote Sensing* 36, 1113-1126.
- Gonzalez-Dugo M. P., Neale C. M. U., Mateos L., Kustas W. P., Prueger J. H., Anderson M. C. and F. Li (2009) A comparison of operational remote sensing-based models for estimating crop evapotranspiration.

- Agricultural and Forest Meteorology* 149, 1843-1853. doi: 10.1016/j.agrformet.2009.06.012
- Goudriaan J. (1977) Crop Micrometeorology: A simulation study. Center for Agricultural Publication and Documentation, Wageningen.
- Huntingford C., Allen S.J. and R. J. Harding (1995). An intercomparison of single and dual-source vegetation-atmosphere transfer models applied to transpiration from Sahelian savannah. *Boundary-Layer Meteorol.*, 74, 397-418.
- Jackson R. D., Idso S. B., Reginato R. J. and P. J. Pinter (Jr) (1981) Canopy temperature as a crop water stress indicator. *Water Resources Research* 17, 1133-1138.
- Kalma J. D., McVicar T. R. and M. F. McCabe (2008) Estimating Land Surface Evaporation: A Review of Methods Using Remotely Sensed Surface Temperature Data. *Surveys in Geophysics* 29, 421-469. doi.org/10.1007/s10712-008-9037-z.
- Kondo J. and S. Ishida (1997) Sensible heat flux from the Earth's surface under natural convective conditions. *Journal of Atmospheric Sciences* 54, 498-509.
- Kustas W. P., Stannard D.I., K. J. Allwine (1996) Variability in surface energy flux partitioning during Washita '92: Resulting effects on Penman-Monteith and Priestley-Taylor parameters, *Agricultural and Forest Meteorology*, 82 (1-4), 171-193, doi.org.medina.uco.es/10.1016/0168-1923(96)02334-9.
- Kustas W. P. and J. M. Norman (1997) A two-source approach for estimating turbulent fluxes using multiple angle thermal infrared observations. *Water Resources Research* 33, 1495-1508.
- Kustas W. P., Zhan X. and T. J. Schmugge (1998) Combining optical and microwave remote sensing for mapping energy fluxes in a semiarid watershed. *Remote Sensing Environment* 64, 116-131.
- Kustas W. P. and J. M. Norman (1999) Evaluation of soil and vegetation heat flux predictions using a simple two-source model with radiometric temperatures for partial canopy cover. *Agricultural and Forest Meteorology* 94, 13-29.
- Lhomme J. P. and A. Chehbouni (1999) Comments on dual-source vegetation-atmosphere transfer models. *Agricultural and Forest Meteorology* 94, 269-273.
- Li F., Kustas W. P., Prueger J. H., Neale C. M. U. and T. J. Jackson (2005) Utility of remote sensing based two-source energy balance model under low and high vegetation cover conditions. *Journal of Hydrometeorology* 6, 878-891.
- Mattar C., Franch B., Sobrino J. A., Corbari C., Jimenez-Munoz J. C., Olivera-Guerra L., Skokovic D., Soria G., Oltra-Carrio R., Julien Y. and M. Mancini (2014) Angular effects on actual evapotranspiration estimated by S-SEBI model over an agricultural area: Part 1, influences of the broad-band albedo. *Remote Sensing of Environment* 147, 23-42.
- Merlin O. and A. Chehbouni (2004) Different approaches in estimating heat flux using dual angle observations of radiative surface temperature. *International Journal of Remote Sensing* 25, 275-289.
- Morillas L., García M., Nieto H., Villagarcia L., Sandholt I., Gonzalez-Dugo M. P., Zarco-Tejada P. J. and F. Domingo (2013) Using radiometric surface temperature for surface energy flux estimation in Mediterranean

- drylands from a two-source perspective. *Remote Sensing of Environment* 136, 234–246.
- Norman J. M., Kustas W. P. and K. S. Humes (1995) Source approach for estimating soil and vegetation energy fluxes in observations of directional radiometric surface temperature. *Agricultural and Forest Meteorology* 77, 263-293.
- Priestley C. H. B. and R. J. Taylor (1972) On the assessment of surface heat flux and evaporation using large-scale parameters, *Mon. Weather Rev.*, 100, 81–92.
- Scott R. L., Huxman T. E., Cable W. L. and W. E. Emmerich (2006) Partitioning of evapotranspiration and its relation to carbon dioxide exchange in a Chihuahuan Desert shrubland. *Hydrological Processes* 20, 3227–3243.
- Shuttleworth W. J. and R. J. Gurney (1990) The theoretical relationship between foliage temperature and canopy resistance in sparse crop. *Quart. J. R. Meteor. Soc* 116, 497-519.
- Sobrino J. A., Jimenez-Munoz J. C., Zarco-Tejada P. J., Sepulcre-Canto G., Miguel E. d., Soria G., Romaguera M., Julien Y., Cuenca J., Hidalgo V., Franch B., Mattar C., Morales L., Gillespie A., Sabol D., Balick L., Su Z., Jia L., Gieske A., Timmermans W. J., Olioso A., Nerry F., Guanter L., Moreno J. and Q. Shen (2009) Thermal remote sensing from Airborne Hyperspectral Scanner data in the framework of the SPARC and SEN2FLEX projects: an overview. *HESS* 13, 2031-2037.
- Timmermans W. J., Kustas W. P., Anderson M. C. and A. N. French (2007) An Intercomparison of the Surface Energy Balance Algorithm for Land (SEBAL) and the Two-Source Energy Balance (TSEB) modelling Schemes. *Remote Sensing of Environment* 108, 369-384.
- Timmermans J., Tol C. v. d., Verhoef W. and Z. Su (2008a) Contact and directional temperature measurements of sunlit and shaded land surface components during the SEN2FLEX 2005 campaign. *International Journal of Remote Sensing* 29, 5183-5192.
- Timmermans W. J., Bertoldi G., Albertson J. D., Olioso A., Su Z. and A. S. M. Gieske (2008b) Accounting for atmospheric boundary layer variability on flux estimation from RS observations. *International Journal of Remote Sensing* 29, 5275-5290. doi:10.1080/01431160802036383
- Timmermans W. J., Su Z. and A. Olioso (2009) Footprint issues in scintillometry over heterogeneous landscapes. *Hydrol. Earth Syst. Sci.* 13, 2179-2190.
- Timmermans W. J., Jiménez-Muñoz J. C., Hidalgo V., Richter K., Sobrino J. A., d’Urso G., Mattia F., Satalino G., De Lathauwer E. and V. R. N. Pauwels (2011) Estimation of the spatially distributed surface energy budget for AgriSAR 2006, Part I: Remote sensing model intercomparison. *JSTARS-IEEE* 4, 465-481.
- Timmermans W., Tol C. v. d., Timmermans J., Ucer M., Chen X., Alonso L., Moreno J., Carrara A., Lopez R., Tercero F. d. I. C., Corcoles H. L., Miguel E. d., Sánchez J. A. G., Pérez I., Franch B., Muñoz J.-C. J., Skokovic D., Sobrino J., Soria G., MacArthur A., Vescovo L., Reusen I., Andreu A., Burkart A., Cilia C., Contreras S., Corbari C., Calleja J. F., Guzinski R., Hellmann C., Herrmann I., Kerr G., Lazar A.-L., Leutner B., Mendiguren G., Nasilowska S., Nieto H., Pachego-Labrador J., Pulanekar S., Raj R., Schikling A., Siegmann B., Bueren S. v. and Z. B. Su (2014) An overview of the Regional Experiments For Land-atmosphere Exchanges (REFLEX)

2012 Campaign. *Acta Geophysica* In review.

Van der Tol C. (2012) Validation of remote sensing of bare soil ground heat flux. *Remote Sensing of Environment* 121, 275-286.

Van der Tol C., Timmermans W., Corbari C., Carrara A., Timmermans J. and Z. Su (2014) An analysis of turbulent heat fluxes and the energy balance during the REFLEX campaign. *Acta Geophysica* In review.

Vesala T., Kljun N., Rannik U., Rinne J., Sogachev A., Markkanen T., Sabelfeld K., Foken T. and M. Y. Leclerc (2008) Flux and concentration footprint modelling: State of the art. *Environmental Pollution* 152, 653-666. doi: 10.1016/j.envpol.2007.06.070

Vining R. C. and B. L. Blad (1992) Estimation of sensible heat flux from remotely sensed canopy temperatures. *Journal of Geophysical Research* 97, 18951–18954. doi: 10.1029/92JD01626

Chapter 5: Conclusions and future research lines

This work has addressed the modelling of the energy balance, integrating thermal infrared data into TSEB model, over two extended and valuable Mediterranean ecosystems, as the *dehesa* and the vineyard. Both exist under arid or semi-arid climatic conditions, sharing important structural characteristics with other typical woody ecosystems (e.g. olive orchards) also adapted to this water-limited environments. These complex landscapes usually comprise several layers of vegetation that differ in physiology and phenology (e.g. evergreen sclerophyll trees, shrubs and annual herbs) that have evolved control mechanism to deal with these variable weather conditions. That context have been taken into account for the regional estimation of ET, analyzing some aspects affecting the EB.

In particular, over the *dehesa* we have studied some aspects such as the co-existence of two vegetation layers and their effect over the wind-speed profile, the structure of the vegetation and its impact on the overall balance, the tree/vegetation separate leaf area index behavior and its variability along the year, and the oak evaporative control. Over the vineyard the TSEB model produced accurate turbulent flux estimations when compared to ECT ground observations. We used this ecosystem, where the partition between soil and canopy is especially important, to gain insights into the TSEB component turbulent fluxes estimations (LE_s , LE_c and H_s , H_c).

The accuracy on the estimates of the energy fluxes for a natural woody cover such as *dehesa* by means of TSEB model, with an adjusted Priestley-Taylor coefficient reflecting the relatively conservative water-use tendencies of this undomesticated semi-arid vegetation and a roughness length formulation which

takes into account the tree structure and the low fractional covers, is adequate and encourages future application. Further research is still needed to integrate the different canopy covers into the ecosystem. Meanwhile it can be assumed a constant oak leaf area index, the herbaceous layer with an annual cycle, presenting a local leaf area index which ranges from 0 (dry period) until a threshold value similar to the tree (wet period). Although the hypothesis that a separately wind-speed extinction coefficient for each layer has not been completely addressed, it seems that for the oak this approach is more precise than taken a bulk system coefficient. Nevertheless, it is necessary to integrated the different layers not only into the wind-speed profile, but also into the radiation budged, which limits the energy available for the turbulent fluxes.

Mapping ET on a regional scale has been possible integrating earth observation techniques and meteorological distributed information into TSEB model input, better representing the ecosystem heterogeneity and local meteorological conditions. Instantaneous LE values and the associated daily ET values were derived using MODIS images, with 1 km spatial resolution and daily temporal frequency (depending on the cloud coverage) for both study sites (Las Majadas and Santa Clotilde), and later compared with ECTs measurements. The difference between estimated and observed values is consistent with typical uncertainties derived for the flux measurement system, being sufficiently accurate to be employed in a distributed way and on a more regular basis. TSEB was also evaluated using a higher spatial resolution satellite (30/120 m), Landsat-7 ETM+ and Landsat-8 OLI for the Santa Clotilde site with similar accuracy. An important source of error could be due to the measurement and modelling of G. The soil heat flux directly influence the system available energy, limiting the energy used in the evapotranspiration and air heating processes. However, this flux is difficult to measure at this field scale, due to the heterogeneity of the experimental areas and the difficulties involved in a distributed sensors location, due to the type of extensive livestock farming that is typical in the region. Discrepancies between observed and estimated fluxes might also be due to the sub-canopy layer existence, with a different phenology and physiology than that of the oaks. All these aspects requires further research and an attempt should be done to integrate this behavior not only into the wind speed profile, but also into the radiation budgets.

Distributed LE over Andalusian dehesa was mapped as a first approach to monitor the ecosystem status on a regular basis with the objective of assessing a future extension of the study. As we showed, it has been possible to derived LE values that reflected the local conditions and micro-climates and the evolution of the vegetation covers along the seasons. The gaps caused by the existence of clouds might

be solved in a future by coupling EB techniques with water balance approaches, together with the use of various satellites with different spatial and temporal resolutions. The re-scalation of the meteorological maps to precisely estimate the energy fluxes over the *dehesa* above the canopy layer could be done by means of logarithmic profiles but a better analysis of the stability effects, by using ALEXI approach or MODIS atmospheric temperature and humidity profiles is required.

The partition of the turbulent fluxes into soil and canopy components, provided by TSEB, produces an estimation of the vegetation transpiration. It has been studied in this work over a vineyard system, by means of directional T_{RAD} observations at different viewing-angles that allows direct estimates of T_s and T_c and therefore, of the separate component turbulent fluxes. The soil and canopy temperatures derived from the directional radiometric surface temperature showed a larger scatter than the ones modelled by TSEB, although no ground observations of component temperatures were available. Values obtained with dual-angle TSEB model indicated some degree of stress over the vegetation stands, which was not confirmed by the results of TSEB, where the crop was transpiring always potentially. Nevertheless, and given the importance of producing separate estimations of transpiration and evaporation components, especially in irrigated systems, and the difficulties of directly measuring it in the field, sensor supplying high-resolution temperature data (in the order of few centimeters) may allow the obtention of bulk canopy and soil temperature, providing new insights of turbulent fluxes partition.

Annexe I: Correction of Landsat images

In this section we will explain the procedure followed to correct the Landsat images used in the analysis (Red, TIR, NIR). Landsat products contain a number of bands, each of them in a particular range of the electromagnetic spectrum. The reflectance is registered from visible to reflected infrared, with a spatial resolution of 30 meters, from band 1 to 5&7 for Landsat 7 and 1 to 7 for Landsat 8. TIR information is registered by L7 with a resolution of 60 meters in band 6, and 100 meters in bands 10 and 11 for L8. The temporal resolution is 15 days, but the using of both satellites reduces the temporal frequency to eight days. The electromagnetic radiance recorded by the sensors is transmitted through the atmosphere, which is both an absorbing, emitting and dispersing medium that modifies the energy by via these processes. Even though the satellites function in the atmospheric windows where these processes are minimized (Chapter 1), the influence of the atmosphere cannot be neglected, and post-processing of the data is necessary. Absorption is due almost completely to water vapor, whose atmospheric concentration is extremely variable. Part of the radiation emitted and reflected by the surface is absorbed by the vapor, which distorts the final signal arriving at the sensor.

Landsat satellites do not provide an operative product for reflectance or T_{RAD} , and the values measured by the sensor must be corrected to obtain the effective values. Different procedures are followed according to the part of the spectrum of interest. Images are geo-referenced, with each pixel located within a coordinate system and it is not necessary to perform a geometric correction. It is necessary to prepare the data directly provided by the U.S. government, converting the numerical values into radiance. This first step is the radiometric calibration, the conversion of raw numerical values into radiance values [$\text{Wm}^{-2} \text{sr}^{-1} \mu\text{m}^{-1}$]. The minimum and maximum radiance values measured in each band are known (depending on the sensor), with their corresponding numerical values, so it is only necessary to linearly re-scale the image (*Chander et al., 2009*).

$$L_{\text{sensor}} = G \cdot DN + B \quad (\text{A.1})$$

where L_{sensor} is the spectral radiance derived from the sensor [$\text{Wm}^{-2} \text{sr}^{-1} \mu\text{m}^{-1}$], DN the digital number obtained directly from the sensor, G is the gain and B the offset. After this calibration, the effect of the interference caused by atmospheric particles on the radiance must be corrected for the visible and thermal bands separately. To correct the visible bands, an ENVI module called Fast Line-of-sight Atmospheric Analysis of Spectral Hypocubes (FLAASH, Spectral Sciences, Inc.,) was used. This tool, which integrates MODTRAN4 (Berk et al., 1989) radiative transfer model, corrects wavelengths in the visible through near-infrared and shortwave infrared regions, up to 3 μm . You can choose any of the standard MODTRAN model atmospheres (that will depend on the latitude and season) and aerosol types to characterize the scene. The manual describing the process followed can be found at:

http://www.exelisvis.com/portals/0/pdfs/envi/Flaash_Module.pdf

If we wish to use data from an area with steep slopes we need to make a topographic correction after the atmospheric correction, due to the differences in the light conditions caused by the irregularities of the landscape (Teillet et al., 1982; Minnaert et al., 1941, Colby, 1991). Nevertheless, no steep gradients are observed in Santa Clotilde *dehesa* experimental site. In Figure A.1 the different corrections that we should apply over the visible part of a Landsat image are shown.

The study of electromagnetic radiation transmission through a medium is based on the equation of radiative transfer. As a hypothesis, we assume that the atmosphere is free of aerosols, so the dispersion process is not relevant, is in thermodynamic equilibrium and is stratified in parallel layers. Surface spectral radiance is the sum of two components; surface emissions and the fraction reflected by the atmosphere to the surface. The equation of radiative transfer in the sensor can be written as:

$$L_{\text{sensor}} = (\epsilon L_S(T_{\text{surface}}) + (1 - \epsilon)L_{\uparrow}) \zeta + L_{\downarrow} \quad (\text{A.2})$$

where L_{sensor} is the radiance measured at satellite level [$\text{Wm}^{-2} \text{sr}^{-1} \mu\text{m}^{-1}$], ϵ is the surface emissivity, L_S the radiance measured if the surface had been be a black body at surface radiometric temperature (T_{surface}), ζ is the atmospheric transmissivity, L_{\uparrow} [$\text{Wm}^{-2} \text{sr}^{-1} \mu\text{m}^{-1}$] the upwelling radiance (solar radiance) and L_{\downarrow} the radiance added by the atmosphere [$\text{Wm}^{-2} \text{sr}^{-1} \mu\text{m}^{-1}$]. To estimated the radiometric surface temperature from the sensor temperature, the Eq. (A.2) should be inverted, and the values of the

surface radiance, the atmospheric parameters (atmospheric transmissivity, atmospheric radiance and solar radiance) and the emissivity need to be known. Atmospheric parameters are computed using MODTRAN 4 (*Berk et al., 1999*) model. To evaluate the emitted radiance by the atmosphere we need to consider the vertical variations in atmospheric transmissivity, which are dependent on the water vapor, it being necessary to characterize the atmosphere in the study site in terms of its temperature and water vapor profiles. These can be obtained with a weather probe or by using MODIS satellite-derived atmospheric profiles (MOD07 product) which, according to *Jimenez-Muñoz (2010)*, provide an RMSE of 0.6 K in radiometric temperature estimates compared to locally measured profiles.

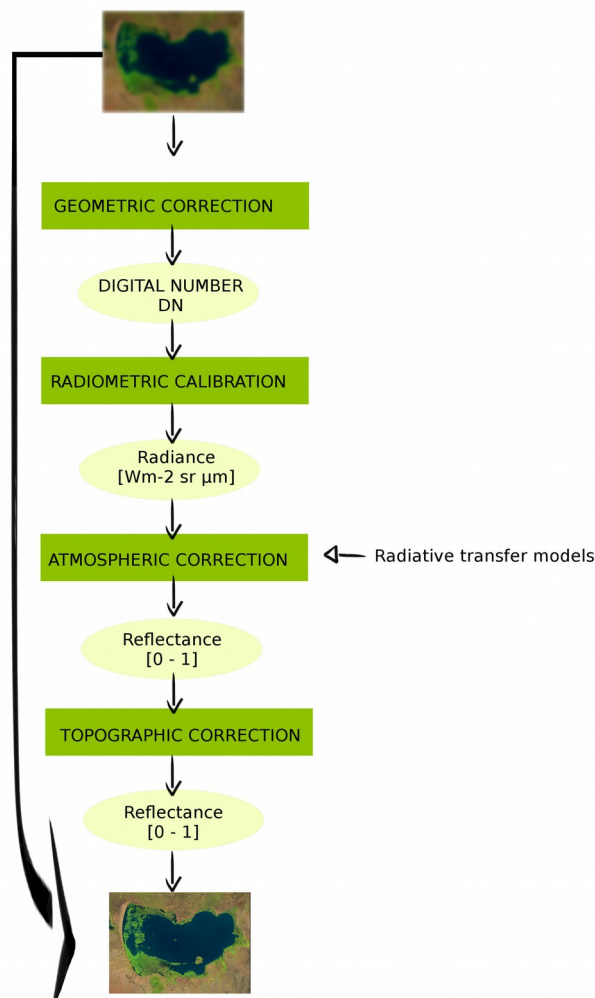


Figure A.1: Landsat correction process (Image based on the report “Corrección de Imágenes Landsat” from *Rafael Pimentel and Javier Herrero, 2012*)

The emissivity could be obtained as:

$$\varepsilon \approx \varepsilon_v f_c + (1 - f_c) \varepsilon_s \quad (\text{A.3})$$

where ε_v is vegetation emissivity and ε_s is soil emissivity.

The radiance measured by the sensor can be converted to brightness temperature (T_b), assuming that the Earth's surface is a black body, and incorporating atmospheric effects (absorption and emissions along the path). It is necessary to use the prelaunch calibration constants given by Landsat, which depend on the sensor (Chandler *et al.*, 2009). The conversion formula is:

$$T_b = \frac{k_2}{\ln\left(\frac{k_1}{L_S(T_{surface})} + 1\right)} \quad (\text{A.4})$$

where k_1 [$\text{Wm}^{-2}\text{sr}^{-1}\mu\text{m}^{-1}$] and k_2 [K] are the calibration constants.

REFERENCES of Annexe I

- Berk, A., Bernstein, L.S., Anderson, G.P., Acharya, P.K., Robertson, D.C., Chetwynd, J.H., & Adler-Golden, S.M. (1998). MODTRAN Cloud and Multiple Scattering Upgrades with Application to AVIRIS. *Remote Sensing of Environment*, 65, 367-375
- Colby, J.D. (1991). Topographic normalization in rugged terrain. *Photogrammetric Engineering and Remote Sensing*, 57, 531-537
- Chander, G., Markham, B.L., & Helder, D.L. (2009). Summary of current radiometric calibration coefficients for Landsat MSS, TM, ETM+, and EO-1 ALI sensors. *Remote Sensing of Environment*, 113, 893-903
- Jimenez-Muñoz, J.C., Sobrino, J.A., Mattar, C., & Franch, B. (2010). Atmospheric correction of optical imagery from MODIS and Reanalysis atmospheric products. *Remote Sensing of Environment*, 114, 2195-2210
- Minnaert, M. (1941). The reciprocity principle in lunar photometry. *Astrophysical Journal*, 93, 403-410
- Teillet, P.M., Guindon, B., & Goodenough, D.G. (1982). On the Slope-Aspect Correction of Multispectral Scanner Data. *Canadian Journal of Remote Sensing*, 8, 84-106

